Overland flow:
interfacing models with measurements

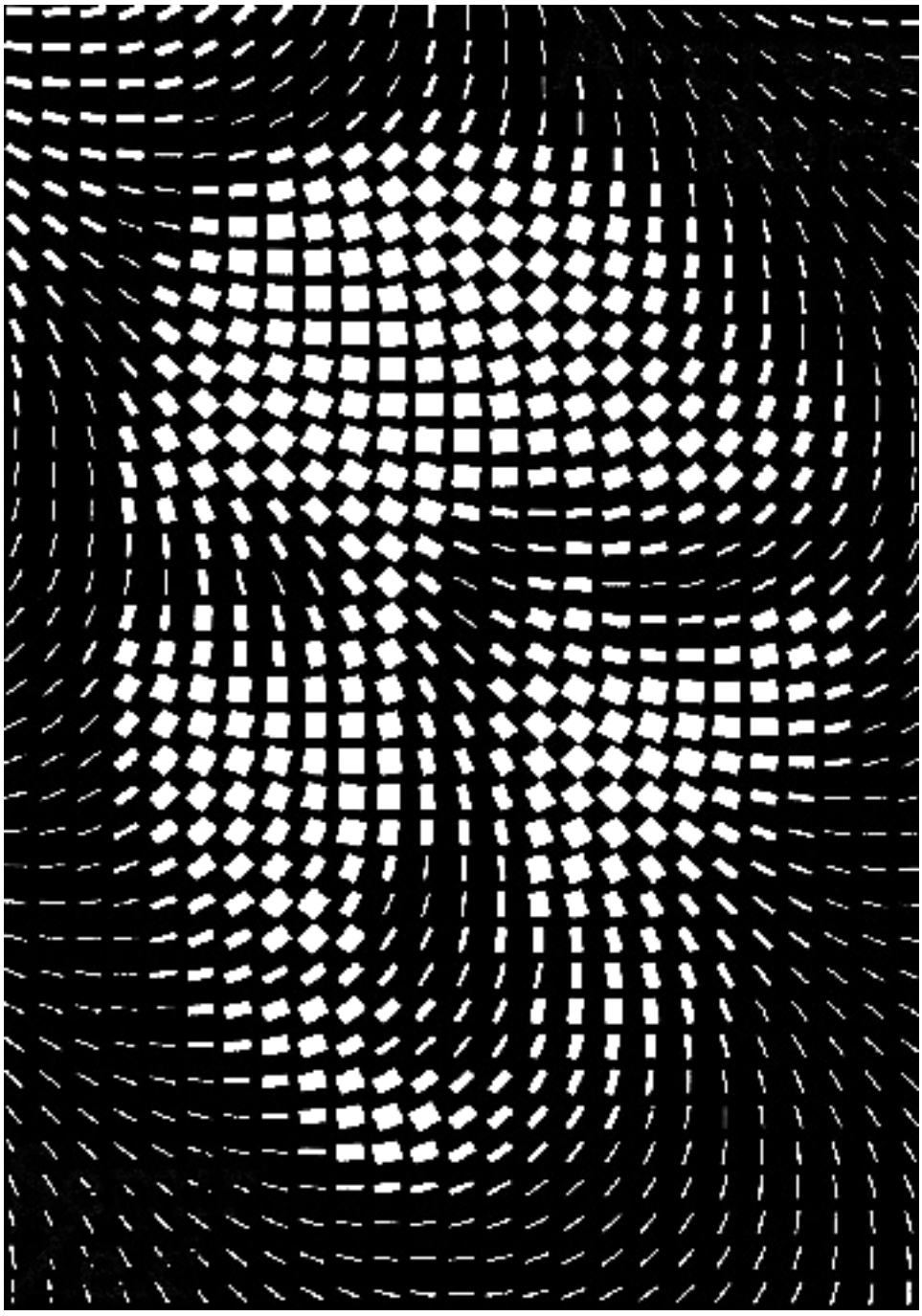

E. E. van Loon

Promotor: prof. dr. ir. L. Stroosnijder
hoogleraar Erosie en Bodem &
Waterconservering

Co-promotor: dr. ir. K. J. Keesman
universitair hoofddocent bij de leerstoelgroep Meet-,
Regel- en Systeemtechniek

Samenstelling promotiecommissie:
prof. dr. A. Bagchi, Universiteit Twente
prof. dr. M. J. Hall, IHE Delft
dr. V. G. Jetten, Universiteit Utrecht
prof. dr. ir. P. A. A. Troch, Wageningen Universiteit

Overland flow:
interfacing models with measurements

E. E. van Loon

Proefschrift
ter verkrijging van de graad van doctor
op gezag van de rector magnificus
van Wageningen Universiteit,
prof. dr. ir. L. Speelman
in het openbaar te verdedigen
op maandag 4 februari 2002
des namiddags te vier uur in de Aula

CIP-gegevens Koninklijke Bibliotheek, Den Haag

Van Loon, E. E., 2001

Overland flow: interfacting models with measurements / E. E. van Loon
Thesis Wageningen University - with ref. - with summaries in English and Dutch.
ISBN 90-5808-558-9
Subject headings: hydrology, system identification

Abstract

Van Loon, E. E., 2001. *Overland flow: interfacing models with measurements.* PhD thesis, Wageningen University, The Netherlands. 185 pp, 75 figs, 39 tables, 5 appendices.

This study presents new techniques to identify scale-dependent overland flow models and use these for ensemble-based predictions. The techniques are developed on the basis of overland flow, rain, discharge, soil, vegetation and terrain observations that were collected over a three year period in two tropical catchments. The merits of the identification technique are its robustness with regard to unknown errors, the ability to adjust model resolution in response to data availability, and to interpret the entities of the identified model structures physically. Compared to a static regression model and a dynamic distributed model the predictive performance of the scale-dependent overland flow models is good, especially when using model ensembles. Further analysis of the scale-dependent models shows that rainfall largely determines overland flow when modelled at coarse resolutions, whereas soil moisture drives overland flow when defined at fine resolutions. Interestingly, the number of model parameters remains constant over the different resolutions. The use of the scale-dependent models for predictive purposes is demonstrated by applying Tikhonov regularization for recursive state as well as parameter estimation.

Additional index words: overland flow, catchment scale, system identification, ensemble simulations.

Voorwoord

Dit onderzoek vindt zijn oorsprong bij het idee van Leo Stroosnijder om schaal problemen bij erosie-voorspelling zowel experimenteel als theoretisch te onderzoeken. Samen werkten we in 1995 aan een AIO-voorstel waarmee ik enthousiast en heel voorspoedig van start ging. Eén van de doelstellingen was om de unieke mogelijkheden die beide veld-stations van de universiteit (de 'steunpunten' in Burkina Faso en Costa Rica) boden te benutten en op beide plaatsen experimenteel werk uit te voeren. Terwijl door Leo Eppink de eerste contacten in Costa Rica werden gelegd, werd in Burkina het experimentele onderzoek opgestart onder leiding van Leo Stroosnijder. In deze begin-fase schoof Karel Keesman als begeleider aan en bezocht ik de 'scaling workshop' in Krumbach. Deze workshop sterkte mij in de overtuiging dat de keus om te werken met schaal-afhankelijke modellen de juiste was. Terwijl ik zelf gedurende een verblijf van ruim een jaar en diverse korte bezoeken het veldwerk in Costa Rica organiseerde en uitvoerde, namen anderen onder leiding van Leo het leeuwendeel van het veldwerk in Burkina op zich. Bij terugkomst uit Costa Rica boekte ik eerst maar langzaam vooruitgang bij het oplossen van diverse theoretische en computer-technische problemen. Maar plotseling raakte het onderzoek in een stroomversnelling toen ik er eind 1998 in slaagde om met een genetisch algoritme modellen te creëeren die nog werkten ook. De vele mogelijkheden die de nieuwe modelleer-techniek bood heb ik in de daarop volgende jaren toegepast op de gegevens uit de twee stroomgebieden. Terwijl ik gaandeweg steeds weer nieuwe oplossingen bedacht voor hetzelfde probleem - een enkele keer een nieuw probleem bij een bestaande oplossing - hebben Leo en Karel er voor gezorgd dat ik de oorspronkelijke doelstellingen niet uit het oog verloor en dat we zo veel mogelijk concrete resultaten boekten. De periode van dit onderzoek was een fijne tijd waarin ik veel geleerd heb en met studenten en collega's heel prettig heb samengewerkt. Met pijn in het hart sluit ik 'm af ... om met frisse moed en op soortgelijke voet weer verder te gaan. Maar niet voordat ik nog wat mensen heb bedankt.

Zoals uit de voorgaande korte geschiedenis blijkt heb ik het erg getroffen met mijn promotor, Leo Stroosnijder. In de eerste plaats heeft hij mij bijzonder plezierig en efficiënt begeleid. Daarnaast heeft Leo mij, zoals al zijn AIO's, niet alleen aangespoord van mijn wetenschappelijke vrijheid te profiteren maar daartoe ook ruimschoots de middelen verstrekt en ondersteuning geboden waar dat nodig was. Het was bijzonder waardevol om intensief veldwerk uit te voeren, een kans die maar weinig andere AIO's kregen de afgelopen decennia. Ook met Karel Keesman heb ik de afgelopen jaren intensief en heel prettig samenwerkt. Hij heeft het theoretische basismateriaal en veel kennis aangedragen voor mijn verdere werk en heeft altijd zeer enthousiast maar niet minder nauwgezet en kritisch geholpen bij het uitwerken van mijn ideeën. Leo & Karel: onze samenwerking was bijzonder inspirerend en we kunnen die hopelijk nog lang voortzetten! Iets recenter heeft zich ook een nauwe samenwerking met Peter Troch voltrokken. Hoewel deze zich officieel niet toespitste op het onderzoek van dit proefschrift, is er toch wat van onze samenwerking binnen geslopen via het laatste hoofdstuk. Zijn enthousiasme, brede en grondige hydrologische kennis hebben er toe bijgedragen dat ik ook met frisse moed en hernieuwde interesse naar de fysische achtergrond van hydrologische processen ben gaan kijken. De collega's van de leerstoelgroep doe ik tekort met een eenvoudig dankjewel voor de fijne periode en de prettige samenwerking. We hebben elkaar geholpen, samengewerkt met het opzetten van diverse proefjes, het voorbereiden en uitvoeren van practica en gediscussieerd over elkaars wetenschappelijke en (bij tijd en wijle)

politieke ideeën. Bedankt Lenny van Alphen, Leo Eppink, Gerda de Fauw, Trudy Freriks, Jan de Graaff, Fred de Klerk, Martina Mayus, Dirk Meindertsma, Max Rietkerk, Jacquelijn Ringersma, Wim Spaan, en Geert Sterk! Ik heb met alle studenten die ik begeleidde bij een afstudeeronderzoek of stage bijzonder prettig samengwerkt. Zij hebben zich erg ingezet voor mijn ondezoek en hebben er gezamenlijk voor gezorgd dat mijn veldwerk succesvol verlopen is. Hartelijk bedankt voor jullie inzet: Erik Boerrigter, Alex Hekman, Annemarie Klaasse, Floris Groesz, Tirza Molengraaf, Doekele Rienks, Jeroen Sleijffers, Corné van der Sande, Robbert van der Steeg, Carlo Vromans, en Rutger Wierikx! Iets meer op de achtergrond maar niet minder onmisbaar waren er ook de collega-onderzoekers en de staf van de steunpunten in Burkina Faso en Costa Rica. Roel Dijksma, Willem Hoogmoed, Henny van Lanen, Abdulaye Mando, Nico de Ridder en Tjeerd-Jan Stomph: bedankt voor de samenwerking, het mede-begeleiden van studenten en voor het harde werken aan de gegevens-verzameling in Kaibo. Dezelfde dank ook voor alle staf van het steunpunt in Ouagadougou, velen hebben mij met allerhande dingen bijgestaan. Teunis van Rheenen komt een ereplaats toe. Zonder hem was ik waarschijnlijk nooit aan het veldwerk in Burkina Faso begonnen, zijn huis stond altijd open en hij zorgde er voor dat het steunpunt als het er op aan kwam daadwerkelijk steun bood - niet alleen aan mij maar aan alle studenten en onderzoekers ter plaatse. De staf van het steunpunt in Guapiles (Costa Rica), onder leiding van Hans Jansen, ben ik dankbaar voor de goede hulp en inzet. Ik wil in het bijzonder Fernando Cambronero hartelijk bedanken voor zijn inspanningen om al mijn zaken in Guapiles en San José te behartigen. In Liberia, zo'n 400 km van Guapiles en slechts 30 km van mijn veldwerk in Horizontes, waren er Sandra Bot, Omar Campo en Oscar Cid die in het kader van het MAG-FAO project mijn studenten nog een plezierig laatste deel van hun stage bezorgden als ze licht vermoeid en ontredderd Horizontes verlieten. Ook Mario en Norma van de UCR in Liberia bedank ik hartelijk voor het ter beschikking stellen van het laboratorium en alle hulp bij het analyseren van de monsters en begeleiden van studenten. Carlos Elizondo van het IGN in San José bedank ik hartelijk voor het speciaal voor mijn onderzoek beschikbaar stellen van gedetailleerde topografische kaarten; en Rafael Chacon van het hydrologisch kantoor van het ICE in San José bedank ik heel hartelijk voor het bewerken en digitaal ter beschikking stellen van ICE's hydrologische en meteorologische gegevens van Guanacaste. Het zou wat te ver voeren de halve middenstand van Liberia te bedanken voor hun diverse hand- en spandiensten, maar de smid Bayardo kan ik niet overslaan. Hij heeft veel bijgedragen aan mijn onderzoek met zijn goede ideeën en de snelle en de goedkope hulp bij allerhande constructies. Op Horizontes waren er Marielos Molina en David Morales die mijn onderzoek geweldig hebben ondersteund. Pattrick Spittler bedank ik heel hartelijk voor onze vriendschappelijke samenwerking tijdens ons gezamenlijk verblijf op Horizontes. Alle andere mensen op Horizontes en Santa Rosa waren altijd gastvrij en hebben mij en mijn studenten een fijne tijd bezorgd. In Wageningen hebben nog een aantal personen aan mijn onderzoek bijgedragen. Bert Boerrigter heeft gezorgd dat de administratie van het Costa Rica project op orde bleef, en nog wat meer op de achtergrond was er Johan Bouma die het voorstel om hydrologisch veldwerk in Guanacaste op te starten vanaf het eerste moment steunde. Alfred Stein begeleidde altijd enthousiast en kundig het AIO-klasje waarvan ik deel uit maakte. Paul Torfs fungeerde als vraagbaak en klankbord voor premature gedachten - hij kan als geen ander de wiskundige vinger op de gevoelige plek leggen van een wiskundig (soms bestuurlijk) probleem. Marjolein de Vette heeft de fraaie voorkant van mijn proefschrift gemaakt. Allemaal hartelijk bedankt.

Tot slot nog mijn lieve Jantsje, Welmoed, Reinaart & Hedwig. Zij komen normaliter op de eerste plaats, maar moesten mijn werk wel eens voor laten gaan de afgelopen jaren. Bedankt voor jullie niet aflatende steun!

Contents

1 Introduction

1.1 Why a face?

You can't tell a book by it's cover. Especially when there is, on the face of it, no clear connection between illustration and title. Yet, the cover of this book provides a number of leads to introduce the issues that are dealt with in this study and does in this way tell surprisingly much about it's contents.

Characteristic for the cover image is that one knows what it represents, and that one can simultaneously sense it by a simple glance though the eyelashes. This very combination, knowing what (on earth) to expect and being able to check it effortless, is the dream of every earth scientist. The reality, as one can already anticipate, is the opposite: every piece of the earth brings new surprises, if not by the heterogeneity of nature itself, it is through the diversity and unpredictability of human activities. And to complete the terror: there are very few tools at our disposal to observe this heterogeneity. Still, in spite of these difficulties, an earth scientist desires to understand certain aspects of the natural phenomena surrounding us. Hereto simplified representations of the phenomena are often made, such as maps which may in fact look very similar to the cover image. For that matter, the cover image would make an exemplary map, displaying e.g. both height and direction of overland flow. It is the construction of such an overland flow map for a given area which is the object of study in this dissertation.

The cover image is made up of two building blocks: width (or intensity) and direction. The variation of these two parameters over a regular grid of 25×37 elements gives all that is required to recognize the essential attributes of the image. It demonstrates that with only a pair of parameters and a rather coarse discretization a view may be obtained which contains unexpected detail. The question arises whether more detail can be recovered if the grid is refined while keeping width and direction of the elements unchanged. Or to what extent width and direction have to be altered in order to enhance the image at all at the finer grid. This line of thought leads sooner or later to the question what information is actually required to determine the width and direction of the elements at the finer resolution and how this information can be obtained. These are important questions here, but then pertaining to the problem of imaging overland flow.

The translation of reality into some sort of model generally requires several levels of abstraction. In the earth sciences such levels are e.g. geographic, conceptual, mathematical, and computer-coded abstractions. In other words, earth scientists often derive models from models. This is adequately illustrated by the cover image, which is a generalization of some copy (model) of the real Mona Lisa, which is again a model of a real person (who stood model for Da Vinci). This analogy makes clear that it is probably the first step, from the real person to the canvas, which is most critical. Any deviation from reality at that stage can not be corrected anymore. The other models can still be inter-compared and hence adjusted, be it at the cost of a return trip to the Louvre. This last points underlines the vital importance of carefully collecting, checking, re-checking, maintaining, storing, making accessible and documenting field observations in the earth sciences. The concern for the quality of these activities cannot be over-emphasized.

Finally the cover image is a tribute to Da Vinci, who, among many other activities, extensively investigated the nature of surface water. This reference is more than just a curiosity, it were the

passages and the sketches in his Codex Arundel that invoked the idea of investigating overland flow by simple visual inspection. And, as will be shown later, it are especially these observations that turn out be very valuable for successful overland flow prediction.

1.2 What is overland flow and why is it important?

Nature accommodates some contrasts that seduce us to believe that it is in many ways discontinuous. Our language provides a rich repertoire for the distinct boundaries that we observe in nature: a coast separates land from sea, the horizon the earth from the atmosphere and sunset separates day from night. Yet a closer look at these boundaries shows us that they are ambiguous and quite dynamic. A similar situation exists in hydrologic terminology where many words seem to refer to some distinct part of the hydrosphere or a particular flux, such as stream flow, percolation, storage, through fall. All these terms, even when explained and exemplified, are not easily defined not to mention measured. The subject of this thesis itself, overland flow, is an example of a such a term. *Overland flow* is that part of the surface water that moves over the soil surface, while not being concentrated in channels of a given size. When overland flow concentrates in these channels it is called *channel flow*. The point where overland flow ends and channel flow starts, spatially as well as temporally, can only be defined subjectively and approximately. The combination of overland flow and channel flow is called *surface flow*. An elaborate review on this topic is found in Hogg (1982). Overland flow may originate from saturation of the soil either from above or below. When saturated from above, the quantity of rain and water from upslope areas exceeds the soil's infiltration capacity and when saturated from below the matrix pressure of the soil is positive due to pressure from soil water in situ or from upslope soil volumes. The former mechanism is called *infiltration excess* or the *Horton* mechanism while the latter is called *saturation excess* or the *Dunne* mechanism. The term *surface runoff* is distinct from overland flow in that it refers to a flux at a point in space, whereas overland flow refers to a spatially distributed phenomenon. Overland flow on natural surfaces is by definition very heterogeneous. In these conditions it displays a great variety of flow depths (ranging approximately from 1 to 100 *mm*) within a small area (say 100 m^2) and is nearly always unsteady. On surfaces with little vegetation rain and wind may have a considerable impact on flow velocities whereas on vegetated surfaces the hydraulic resistance of plants and plant debris is a dominant factor (de Lima, 1989).

Knowledge of overland flow is important because it is the main determinant for sediment transport by water (Kiepe, 1995; Lane et al., 1997), the transport and fate of nutrients and (agro)chemicals which reside on the soil surface (Jolánkai and Rast, 1999), and the size and the shape of flood peaks (Troch et al., 1994). Nearly all surface flow starts as overland flow in the upper reaches of a catchment and travels some distance before reaching a rill or channel (Emmett, 1970).

In spite of the important role overland flow plays in various instances, it has hardly ever been observed over areas larger than a few hectares through direct measurements, and also qualitative field observations of overland flow occurrence are scarce. Even renown field studies like those of Dunne and Black (1970) do not cover more than a single slope. This situation is partly due to the distributed nature of overland flow, and partly to ignorance and low appreciation of field observations. Before the computer-era (till the early seventies) the distributed nature of overland flow was a serious impediment since the (mobile) equipment was not available to observe and store the relatively large amounts of information. From the seventies onwards the relative appreciation of model studies has marginalized the attention for field observations, a situation which continues to exist in spite of the various notions since the eighties that there is an increasing need for good field observations (e.g Klemeš, 1986; National Research Council (NRC), 1991). The relative confidence that has been placed on model concepts and results is illustrated by the way in which overland flow processes have invariably been incorporated in mathematical models, as a

uniform sheet of water over a plane surface, and the fact that the value of predictions by distributed hydrological models has not been seriously questioned until the mid-eighties (Beven, 1985). This historical perspective explains the paradox that overland flow is often recognized as one of the key processes in several environmental problems, while it has nevertheless hardly been observed and quantified over areas beyond the plot scale.

1.3 Mathematical description of overland flow

Having a reason for studying overland flow, it is now appropriate to consider the state of knowledge about overland flow processes. There are several excellent reviews on overland flow hydraulics and models of overland flow (Moore and Foster, 1990; Parsons and Abrahams, 1992) as well as on infiltration (Beven, 1991; Morel-Seytoux, 1989), therefore it is superfluous to give an elaborate overview on these topics here. However, to understand the issues that will be treated in subsequent chapters, some relevant aspects will explained. This is done via a system-theoretic model classification which is explained in the next subsection. Thereafter the classification is applied to overland flow models.

General model classification framework

Before a discussion of mathematical overland flow models is possible, a clear definition is required to distinguish between a fundamental hydrodynamic concept (such as the Richards or diffusive wave equations) which is based on physical principles (generally momentum and mass conservation) and a concept that can be implemented in e.g. the form of a simulation model.

Following Beck (1987) the first type of model will be called a class I model and the second type a class II model. A class I model would have the following form.

$$\frac{\partial \mathbf{x}(t,\mathbf{r})}{\partial t} = \mathbf{f}\left\{\nabla^2\mathbf{x}, \nabla\mathbf{x}, \mathbf{x}, \mathbf{u}, \theta_1; t, \mathbf{r}\right\} \tag{1.1}$$

Here $\mathbf{x}$ is the state vector, $\mathbf{u}$ is a vector of known inputs, θ_1 a vector of model parameters, t is time and $\mathbf{r}$ is a vector representing the three spatial directions. A class I model is an abstraction of observed natural behaviour which admittedly includes simplifications, and in appropriate laboratory settings it can (at least partially) be validated, but in a natural setting it can not. This is caused by the heterogeneity encountered in nature in combination with the available observations and the applicable methods to find an appropriate system representation. For these reasons a description according to equation 1.1 has to be simplified in order to formulate a solvable problem. In practice this means a redefinition of the state vector so that it represents a discrete space system in one or two dimensions (having a limited number of state-variables) and the application of either a finite element or finite difference approximation. The thus obtained class II model can e.g. be formulated as

$$\frac{d\mathbf{x}_l(t)}{dt} = \mathbf{f}\left\{\mathbf{x}_l, \mathbf{u}_{k,l}, \theta_2; t\right\} + \xi(t) \tag{1.2}$$

in combination with an observation equation

$$\mathbf{y}(t_k) = \mathbf{h}\left\{\mathbf{x}_l, \mathbf{u}_{k,l}, \theta_2; t_k\right\} + \eta\left(t_k\right) \tag{1.3}$$

where now θ_2 is the vector of model parameters in this lumped model (θ_2 may vary with time), $\mathbf{y}$ is the vector of observed output variables, ξ is a vector of unmeasured, possibly random, input disturbances, and η is a vector of random observation errors. The subscripts k and l indicate the restriction that inputs and observations are only known at discrete time instants and discrete points in space respectively. Due to the heterogeneity of nature it is impossible to translate all aspects

contained in a class I model straight-away: a number of assumptions and approximations (such as discretization in space and time, numerical solution techniques) have to be made. Class II models are normally formulated such that these approach the structure of class I models. Note that this class covers both parameter distributed models and lumped models. A third class of models contains so-called input/output model representations, here described by a discrete-time non-linear difference equation.

$$\mathbf{y}(t_k) = \mathbf{f}\{\mathbf{y}(t_{k-1}), \ldots, \mathbf{y}(t_{k-n}), \mathbf{u}(t_{k-1}), \ldots, \mathbf{u}(t_{k-n}), \omega(t_{k-1}), \ldots, \omega(t_{k-n}), \theta_3\} \tag{1.4}$$

where θ_3 is the model parameter vector and ω contains all errors from the modelling and measurement process. The class III model aims primarily at finding the best possible relation between input and output observations or aims at testing a particular hypothesis, without strict limitations on model structure. In practice the class I model can be seen as a formalized archive and a class III model as a tool for data analysis and hypothesis testing. Clearly, when seeking an understanding of the system's observed behaviour, a class III model is not a satisfactory end point to the analysis. It should lead to the revision of inadequate hypotheses by recourse to the archive of hypotheses associated with a class I model. In this interplay the class II model has the central role as intermediary between the two other classes. Class II models do, in spite of their aggregated form, contain hypotheses about those phenomena thought to govern the system behaviour, but can on the other hand provide numerical solutions. In practice a feed through of results obtained with class III models to class II and I models appears to be difficult, and alternatively, a translation of a class I model to (a number of) class III models in order to learn more from observations is also quite uncommon. There is thus a challange to extend the available techniques for system analysis and modelling to allow such model-translations. This challenge has been part of the motivation for this study.

Application to overland flow models

The class I models in the study of overland flow are formed by the hydrodynamic equations and the Richards equation (Dingman, 1994). The hydrodynamic (St. Venant) equations comprise the continuity and momentum equations. For a one-dimensional problem the continuity equation can be written as

$$\frac{\partial q(x,t)}{\partial x} + \frac{\partial h(x,t)}{\partial t} = p(x,t) - i(x,t) \tag{1.5}$$

with initial conditions $h(x,0) = h_{i0}(x)$, $q(x,0) = q_{i0}(x)$ and boundary conditions $h(0,t) = h_{b0}(t)$, $q(0,t) = q_{b0}(t)$, $h(L,t) = h_{bL}(t)$, $q(L,t) = q_{bL}(t)$, and where $q(x,t)$ is the rate of overland flow per unit width, $h(x,t)$ is the depth of overland flow, $p(x,t)$ the rain rate, $r(x,t)$ infiltration rate, t is time and x is horizontal distance. The momentum equation is given by

$$\frac{1}{g}\frac{\partial u(x,t)}{\partial t} + \frac{\partial h(x,t)}{\partial x} + \frac{u(x,t)}{g}\frac{\partial u(x,t)}{\partial x} = \beta - \beta_f - \frac{q(x,t)}{g h(x,t)^2}\left(p(x,t) - r(x,t)\right) \tag{1.6}$$

where g is acceleration due to gravity, $u(x,t)$ is the velocity of overland flow, β is the slope of the plane, and β_f is the friction slope. Though the continuity equation is linear in q and h, the momentum equation is highly nonlinear.

The Richards equation, which is a result of combining the Darcy equation with the continuity equation (Richards, 1931), is given by

$$\nabla(K_s K_r(x,t)\nabla(\psi(x,t) + z)) = C\frac{\partial \psi(x,t)}{\partial t} \tag{1.7}$$

with initial conditions $\psi(x,0) = \psi_{i0}(x)$, $K_r(x,0) = K_{i0}(x)$ and boundary conditions $\psi(0,t) = \psi_{b0}$, $K(0,t) = K_{b0}$, $\psi(L,t) = \psi_{bL}$, $K(L,t) = K_{bL}$, and where ∇ is the Laplace operator, K_s is saturated hydraulic conductivity, $K_r(x,t)$ is the relative hydraulic conductivity, z is height above the water table or the height of the water layer h ($\psi + z$ is the hydraulic head), C is specific moisture capacity and $\psi(x,t)$ is the soil matric head. Both K and ψ are highly nonlinear functions of soil moisture (w) and these $K(w)$ and $\psi(w)$ relationships are normally analytically described via parameters representing saturated hydraulic conductivity, porosity and soil geometry (Brooks and Corey, 1966; van Genuchten, 1980). Equations 1.5 and 1.6 are linked to equation 1.7 via the $\psi(w)$ relationship and infiltration i, which equals by definition the flux in the vertical direction as calculated by equation 1.7 (i.e. $r := \frac{\partial w(x,t)}{\partial z}\Big|_{z=0}$). Briefly one could state that the St. Venant equations describe surface as well as fast subsurface transport while the Richards equation describes infiltration and slow water displacement through the soil.

The class I models based on the hydrodynamic and the Richards equations have been combined and simplified in class II models in many different ways. All of these class II models can be categorized into one of three approaches; those that: 1) neglect one of the two processes, routing or infiltration; 2) represent one of the processes by an external forcing such as terrain features or duration of rainfall; 3) link the two processes functionally (one is input or boundary condition to the other).

Obviously the three approaches are of an increasing complexity. Typical cases where infiltration is omitted are those were the study area is nearly impervious or saturated; and typical for the omission of overland flow routing are cases where either rain or terrain data are not available at the appropriate (fine) resolution or the area is relatively flat. For the second group of models, in the list above, typical external forcings that have been applied to routing are local slope and terrain roughness; and forcings applied to infiltration are duration after the start of rain, initial soil moisture content of the top soil, and soil (surface) characteristics (e.g. Moore and Foster, 1990; Scoging, 1992a,b). The last approach is not often applied because the characteristic time of the routing and infiltration processes differs under most circumstances by two orders of magnitude (it is a so-called stiff system), which makes the solution of the system cumbersome. An example of a study where the latter approach has been applied in three dimensions is found in Binley and Beven (1992), and for two dimensions examples are found in Bronstert and Palte (1997) and Freeze (1980).

An application of a class III models to a distributed overland flow problem has not been found so far, so one could say that overland flow is generally studied with class II models. The typical class II overland flow models are called *(catchment scale) parameter distributed models.* Parameter distributed models are finite difference or finite element models that handle spatial interaction by dividing an area into smaller geographical units on which computations are made. This implies that for each geographical unit a set of parameters is required, hence the term 'parameter distributed'. There exists a huge variety of parameter distributed models that incorporate a description of overland flow in some way. The structure and assumptions of these models and the overland flow component therein are best understood when considering their development in a historical context. This historical development of overland flow modelling (as part of parameter distributed hydrological modelling) is sketched in the next section.

1.4 Overland flow described by catchment scale parameter distributed models

The parameter distributed model concept can be traced back to the mid-60's when both the availability of computers and the development of conceptual models in unit hydrograph theory cre-

ated the conditions necessary for its conception and implementation (Crawford and Linsley, 1966; Dooge, 1973; Dawdy and O'Donnell, 1965). From the beginning overland flow has been a major component in many hydrological catchment models. Most current physically-based distributed models are still based on the simplified mathematical (class II) formations of Freeze and Harlan (Freeze and Harlan, 1969; Singh, 1995). The routing in almost all models that have been developed and applied since then is either based on a two-dimensional regular grid or one-dimensional cascades of plane elements, linked to a stream network. Both routing concepts typically treat overland flow as broad, laminar sheet flow which is solved through either the kinematic or diffusive wave approximation to the hydrodynamic equations (Equations 1.5 and 1.6), and do thus not imply different assumptions about the system. The treatment of infiltration and movement of water in the soil in one or two dimensions is, on the other hand, underlain by different assumptions about sub-surface system behaviour. One-dimensional approximations to the Richards equation (Equation 1.7) treat unsaturated soil water flow as a principally vertical process forming a link between surface and saturated subsurface hydrologic components, whereas two and three-dimensional approximations allow lateral redistribution of soil water. The second type of model (i.e. with two and three-dimensional approximations of the flow process) is required when the downslope flow components of partially saturated near-surface soils may be important. The one-dimensional forms of the infiltration process are used in most catchment models, examples are the Water Erosion Prediction Project (WEPP), Soil and Water Assessment Tool (SWAT) and the Système Hydrologique Européen (SHE) models (Abbott et al., 1986; Arnold and Allen, 1992; Flanagan and Nearing, 1995). THALES and the Institute of Hydrology Distributed Model (IHDM) are examples of the second style of model where the subsurface system is approximated by a two dimensional, vertical slice (Beven et al., 1988; Grayson et al., 1992a). Both modelling approaches allow to simulate the hydrology of large catchments, although the physical interpretations of the effective parameters remains difficult and it is generally not possible to derive a unique value for most parameters by an objective calibration procedure (Beven, 1989; Grayson et al., 1992b). Due to these problems and stimulated by the growing availability of digital elevation data since the mid-eighties, the idea to use topography to derive a steady-state approximation to kinematic flow Beven and Kirkby (1979) has gained large popularity. Many of the applications which couple terrain information to a hydrologic model utilize (some of) the original TOPMODEL concepts (Beven, 1984, 1997; Robson et al., 1993; Zhang and Montgomery, 1994).

All of the modelling approaches mentioned above handle spatial variability by dividing a catchment into smaller geographical units on which hydrological model computations are made, and by aggregating the results to provide a simulation for the basin as a whole. Commonly used geographic units are sub-catchments, land use or cover classes, or elevation zones. In all cases, modelling is simplified because areas of the catchment within these units are assumed to behave similarly in terms of their hydrological response. In the late eighties the question arose when to stop the process of division of a basin into ever smaller units. As a possible answer to this question, the concept of a representative elementary area (REA) was introduced (Wood et al., 1988). The REA is the smallest area for which the pattern of local heterogeneity is relatively unimportant in the sense that heterogeneities can be treated statistically without regard to the exact spatial pattern of the heterogeneity. The ultimate utility of the REA concept to the science of catchment hydrology remains to be determined. A number of papers highlighted some difficulties with the REA and presented some refinements to the concept (Blöschl and Sivapalan, 1995), but the concept has never been applied extensively in practice - possibly due to its empirical nature. Recently, the idea to treat catchments as basic units has regained interest through the progress that has been made with a theoretical approach to derive catchment-scale balances of mass, momentum, energy and entropy (Reggiani et al., 2000, 1999, 1998).

To date the establishment of the appropriate size of spatial and temporal model units, the model

resolution, and the appropriate mathematical description of processes at that resolution on the basis of measurements made over much smaller units - essentially at points - are unresolved problems in catchment modelling. Solving the problem of defining effective hydrologic relationships at one resolution and translating these to other resolutions appears to require much more than only scaling parameters or advanced statistical interpolation techniques (Kim et al., 1996), and is since the mid-eighties an area of active research (Beven, 1989, 1993; Beven and Wood, 1993).

1.5 An anatomy of the problem

At this point it is appropriate to discuss the concepts of identification, parameterization, calibration, identifiability, well-posedness, ill-posedness and regularization. These terms are closely associated with the key problems in catchment scale overland flow modelling as described in the previous section. *Identification* is the process of constructing a mathematical model of a dynamic system from observations and prior knowledge (Norton, 1986). Dynamic means in this context that the model behaviour depends on the history, not only the present inputs as in a static system. In the geophysical disciplines prior knowledge comprises the relations describing the balances of mass, momentum and sometimes entropy (see equations 1.5 and 1.6), in combination with constants (like g in Equation 1.6), parameter ranges (e.g. for the factor K_s in Equation 1.7) and empirical relations between different system components (e.g. a stage-discharge equation to relate q and h in Equation 1.5, or between ψ and w in Equation 1.7). *Parameterization*, as a distinct step in the identification phase, refers to the establishment of relationships between (spatially distributed) system components (coefficients) through a limited number of external variables and parameters. For the case of stage-discharge relationships which are generally of the form $q(x,t) = \alpha h(x,t)^{\gamma}$ (where α and γ are the the spatially variable coefficients) this means that α and γ are related to a limited number of observed variables such as topography and vegetation type by only a few parameters: $\alpha = f(topog, veg; params)$. For the case of a soil moisture-matric head relationship, which may be of the form $\psi = \psi_s \left(\frac{w}{w_s}\right)^{-1/m}$ for $\psi < \psi_s$ (where w_s, ψ_s and m are the spatially variable coefficients), w_s, ψ_s and m are often related to texture (Clapp and Hornberger, 1978). A parameterization is generally considered appropriate if the coefficients are well predicted by the chosen variables via a limited set of parameters which are constant in space and time. Once a certain relation between coefficients and parameters is established, it can be fine-tuned by collecting extra observations and re-estimating the parameter values. This step is part of the *calibration* process. When there is enough information available, through both prior knowledge and observations, so that it is possible to derive a unique parameter estimate, the system is called (structurally) *identifiable* (Bellman and Åström, 1970; Sorooshian and Gupta, 1985). The term *well-posedness* applies to both *parameterization* and *calibration*, in this context it means that a unique set of 'best' parameter values can be determined from the data for a given measure of goodness (such as the $2-$ or $\infty-$norms). Its antithesis is the term *ill-posedness*, implying that there is a lack of prior information or observations (or both) in a parameterization or a calibration problem. *Regularization* refers to the process of adding prior information to an ill-posed problem in a mathematically well-organised way so that it becomes well-posed (Hansen, 1998).

In spite of the contributions to catchment scale overland flow modelling that have been described in section 1.4, various problems in computing the relevant hydrological fluxes in catchments have not been solved at all, f.i. model identifiability and the incorporation of observations and process descriptions over small spatial and temporal units into models that use larger units. These problems have been expounded elsewhere (e.g Beck et al., 1995; Beven and Wood, 1993; Grayson et al., 1992b; Loague and Gander, 1990). The limitations inherent in using data on catchment "inputs" (i.e. measurements of rain, temperature, wind speed, etc.) and on catchment "out-

puts" (i.e. discharge at a catchment outlet) to estimate the model parameters have been appreciated for quite some time (Clarke, 1973). Although progress has been made in finding "optimal" parameter estimates (Duan et al., 1992; Pickup, 1977), there is a fundamental limitation set by the amount of information in the available hydrological observations, e.g. on how many parameters can be estimated (Jakeman and Hornberger, 1993). It also has been pointed out that parameters in many of these models are dependent on the climate during the calibration period (Gan and Burges, 1990). Because of these limitations parameter distributed descriptions of overland flow will remain highly subjective and specific to a certain geographical areas. A way to measure the parameters independently of input-output data still has to be found.

In this study the problem of catchment scale overland flow prediction will be anatomized different as it has been done previously in e.g. Hornberger and Boyer (1995); Jakeman et al. (1994) by concentrating in the first place on practical aspects and secondly on the mathematical aspects rather than the physical aspects of predicting overland flow at the catchment scale. In practice three *phases* can be distinguished when quantifying overland flow at the catchment scale: a phase where the relations governing the system and the appropriate problem resolution are unknown ('identification'), a phase where the governing relations and resolution are known and model output is of direct importance ('prediction'), and a phase where the system is known but outputs are only relevant in combination with generated or speculative information ('projection'). A normal sequence, when encountering a new hydrologic prediction or design problem, is to move through the sequence of identification, prediction and projection, as shown in Figure 1.1. It illustrates that in the case of model identification the collection of observations is (or should be) dependent on previous identification results. This aspect has received only scant attention in hydrologic problems. Note that the term 'prediction' is here not defined as normally done in the systems and control discipline, where it means that only input data are available from $t = t_0$ into the future, to make model calculations starting at t_0. In this study it is used to indicate that the model structure is fixed but that both input and output data may be available. In the prediction phase the output data may be used to fine tune a few parameters (re-calibration) or for state estimation (filtering or smoothing), but the model structure is furthermore fixed. An example where re-calibration or state-estimation is desired is when a model is identified for a research catchment while predictions are required for a different catchment. In the projection phase additional processing of either input or output data is often required, i.e. the spatial or temporal units at which the model outputs are obtained have to be redefined or not all model inputs are available (e.g. long-term rain sequences) so that these have to be generated.

From the above it is clear that with regard to the requirement of observations the three phases are different. For identification of overland flow models the required quantity and types of observations are largely unknown and therefore a set of observations should comprise as much different quantities over different integration periods and areas as possible. For prediction, on the other hand, it is known *a priori* which observations are required, so that specific types of observations can be collected at a known number of locations and time period. In the case of projection problems observations are often not available and have to be generated. Also with regard to predictive uncertainty the three phases (identification, prediction and projection) are distinct. In model identification prediction error (i.e. the difference between observed and predicted outputs) can be calculated and in fact this calculation is the main tool to find appropriate model structures. For a prediction problem the predictive uncertainty can also be calculated with some effort via error propagation rules. In contrast, for projection problems, the predictive uncertainty in the results is often unknown due to the redefinition of the output data, or generation of input data.

From a mathematical point of view, the following problem appears frequently in the identification and prediction phases. The model structure does not match the system or the available set of observations is not sufficiently informative, so that the parameter estimation problem is ill-posed.

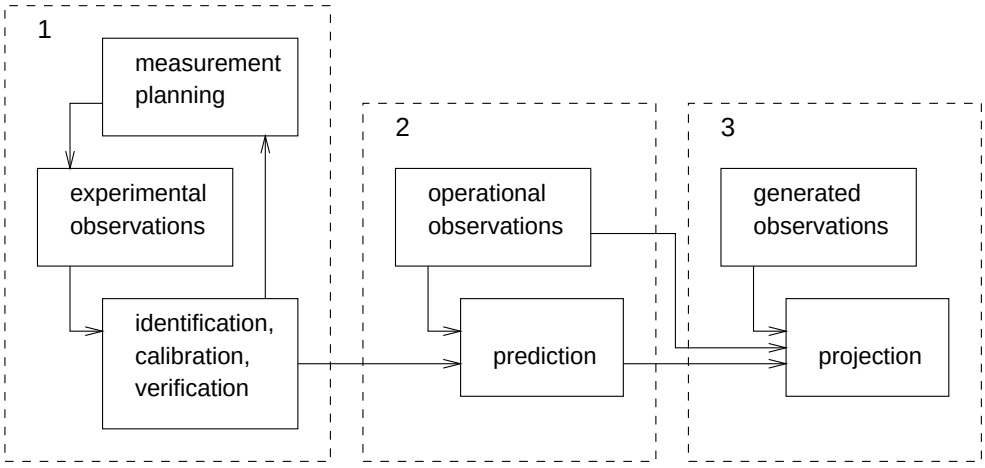

Figure 1.1: The common sequence in hydrologic prediction problems: 1) identification, 2) prediction and 3) projection.

For ill-posed problems the straightforward use of a prediction error criterion to find some optimal parameter set leads to models with poor extrapolation properties. This is clearly undesirable and the problem may be resolved by two general approaches:

1. the development of an alternative model structure, with fewer degrees of freedom and a more suitable parameterization that matches the system better; or
2. regularization of the identification algorithm by introducing constraints or penalties in order to reduce the excessive degrees of freedom towards reasonable values.

The first approach has been frequently applied to hydrological problems, examples are found in Jakeman et al. (1994); Ramos et al. (1995); Young and Beven (1994), and is also implicitly the philosophy behind the probability function approach for catchment modelling (Entekhabi and Eagleson, 1989; Moore and Clarke, 1981; Troch et al., 1994). The second approach has up to now not been applied to problems in surface hydrology but has a rich history in other geophysical disciplines (Menke, 1989; Tarantola, 1987). It should be noted that ill-posedness does not mean that a problem cannot be solved but rather that additional assumptions are required to constrain the solution space in order to achieve meaningful solutions. The key is then to have observations and models structured such that the change to different assumptions is easily made so that objectivity is enhanced. There exists a notable parallel to the solution of differential equations, which can only be solved meaningfully if boundary and initial conditions are specified.

Table 1.1: Characterization of three distinct phases in quantifying catchment scale overland flow.

	characteristics of		
phase	model structure	observations	predictive uncertainty
identification	unknown	heterogeneous	known
prediction	known - full	homogeneous	known
projection	known - simplified	partially generated	unknown

As mentioned previously the key activity in the identification phase is *parameterization.* For the prediction phase it is *calibration,* while for the projection phase it is *simplification.* In the identification phase functional relations are unknown and therefore restrictions on these have to be avoided, so in this phase there are limited possibilities for regularization. Therefore the model

structure is stepwise adjusted to yield a well defined problem. Especially changing the model resolution (which is of direct influence on the degree of ill-posedness) can be effective when an identification problem tends to become ill-posed (see Table 1.1). In the case of prediction and projection problems the adaption of model resolution is not possible since the model structure (which includes resolution) is by definition fixed, and in addition one already has gained insight in the system (many functional relationships are known). Therefore in these problems regularization techniques can be used. The key activities and the way in which ill-posedness is handled is summarized in Table 1.2.

In conclusion we can state that the process of catchment scale overland flow modelling comprises three distinct phases (identification, prediction, and projection), each of which has specific characteristics with regard to knowledge about model structure, availability of observations, and knowledge about predictive uncertainty. The key activities and the way in which ill-posedness can be dealt with in the three phases are distinct as well.

Table 1.2: Key activities and the way in which ill-posedness can be handled for different phases.

phase	key activity	handling of ill-posedness via
identification	parameterization	resolution
prediction	calibration	regularization
projection	simplification	regularization

1.6 Objective

In Sections 1.3 and 1.4 it has been explained that overland flow has been an object of study since the early thirties and has been quantitatively described as a component of distributed hydrologic models since the mid-sixties. While the class I models remained more or less unaltered a shift appeared in the formulation of class II models from the early eighties onwards, caused by the availability of digital terrain data. Notwithstanding its importance, topography is only one of the various important variables determining overland flow. The lack of other distributed data besides that derived from Digital Terrain Models (DTMs) makes it impossible to derive unique parameterisations of distributed hydrological processes; it leads to ill-posed problems. It was argued in Section 1.5 that this frequently stated feature of environmental systems deserves some nuancing, since it refers implicitly to three quite different phases in the modelling sequence. From a mathematical view point, there are two ways to obtain solutions in the case of ill-posedness: by model reduction or regularization. Taking this observation as a starting point, the objective of this dissertation is to develop and test techniques by partly furnishing the first two boxes of the scheme proposed in Figure 1.1, i.e. techniques to: 1) identify models for catchment scale overland flow prediction, and 2)apply models for prediction.

Throughout all modelling steps it will be attempted to use a set of model structures rather than single model structure and use both qualitative and quantitative observations. In addition, this study aims to collect overland flow observations in two experimental catchments in alternation with the development of modelling techniques.

This dissertation is subdivided in two main parts. The first part, covering Chapters 2 to 4, comprises an interpretation of the overland flow observations used in this dissertation, and the effectiveness of commonly used overland flow models. In this part the specific problems that have been briefly touched upon in the previous sections are articulated to set the stage for the remainder of the dissertation. The nature of overland flow in the two experimental catchments is described in Chapter 2, and a first interpretation of the data is provided via a regression model for overland flow

in Chapter 3. Then, in Chapter 4, the observations are analyzed with an archetypical parameter distributed overland flow model.

The second part, chapters 5 to 7, presents new approaches for scale dependent overland flow prediction. This part closely follows the structure of Figure 1.1. A framework that enables the identification of catchment scale overland flow models is described in Chapter 5. This approach is pursued in Chapter 6, using the observations presented in Chapter 2. Next, the problem of overland flow prediction when both a set of observations and a set of calibrated models are available is studied in Chapter 7. Finally in Chapter 8 the results of this study are placed in perspective and an outlook is given for further research.

2 Observations

2.1 Introduction

The basis for this dissertation is formed by observations over the period 1994 - 1998 in two experimental catchments. Throughout Chapters 3 to 8 these observations are used in different ways. In order to understand the many assumptions and implicit choices in the analyses of these Chapters, it is not only important to get a good insight in the physical nature of the catchments but also to be aware of the way in which the observations were obtained, interpreted and processed. This Chapter is meant to offer a concise description of the research catchments, a description of the available observations, an estimation of observation errors, and a first assessment of overland flow occurrence. It is organised as follows. In Section 2.2 and 2.3 the physical nature of the catchments is described, followed by an overview of the data that have been collected. In section 2.4 some important aspects of the observation techniques are discussed. This is followed by a discussion of observation uncertainty in section 2.5. In Section 2.6 the relation between overland flow height and extent is investigated. An assessment of overland flow correlations in space and time is made in Section 2.7. Finally results are discussed and some interesting aspects are highlighted in section 2.8.

2.2 Kaibo sud V5

Site description

The research area is a catchment located in Burkina Faso (West Africa) at $44^{\circ}11'$ N and $0^{\circ}56'$ E (310-325 m.a.s.l.) in the river valley of the Nakambé (White Volta, the biggest river of Burkina Faso), covering an area of 1.2 km^2. The catchment will be named *Kaibo* in what follows. It has a gently undulating topography and a main gully running from north to south (see Figure 2.1). From aerial photographs and field surveys it was observed that drainage density of ephemeral gullies varies from 0.5 $km\,km^{-2}$ north of the research area, to 1 $km\,km^{-2}$ south of the research area, as a result of increasing soil depths towards the south. The drainage pattern is dendritic, which is in correspondence with the shallow soils (0.4 *m* on average) and relative geological homogeneity (Skinner and Porter, 1992; Yameogo, 1988). Schist and granite are the major rock materials found in the catchment. The nature of soils in this landscape is largely determined by the parent material. The most important soil types in the area are Leptosols, Regosols and Cambisols (FAO, 1990). These soils are all formed in situ and not strongly developed, which is attributed to the relatively high rates of geological erosion (Sivakumar and Gnoumou, 1987). In general soils from granitic material contain kaolinitic clays and drain moderate to well (mainly Leptosols and Regosols in the area). Soils on schist contain montmoriollonitic clay which drain poorly (mainly Cambisols in the area). The sand content decreases on average from 40% in the upper 20 *cm* to 25% in the 20-40 *cm* soil layer and clay percentage increases from 30% in the top 20 *cm* to 40% in the underlying layer, which is caused by clay-illuviation (Dekker, 1996; Mulders, 1996). Periods of erosion and deposition have alternated during the most recent geologic history as a result of tectonic activity and sea-level changes. Presently an erosional development of streams is observed through the

stratified layers that are exposed in streambeds. Streams are generally found on bedrock, are irregular of shape and meander strongly, which is in correspondence with the very low slopes of around 2% in the area.

In addition to the information displayed in Figure 2.1, the topography of Kaibo is characterized here by the slope $tan(\beta)$, the upstream area A and the topographic index $ln(A/tan(\beta))$ (Beven and Kirkby, 1979) (see Figures 2.2 and 2.3). Upstream area is defined as the total catchment area above a point or short length of contour (Moore et al., 1991), and is commonly used for the automatic demarcation of channels, using a critical support area O'Callaghan and Mark (1984); Jenson and Domingue (1988); Tarboton et al. (1991); Martz and Garbrecht (1992). The specific catchment area is defined as the upstream area per unit width of contour. It has important hydrological significance as it has shown to be useful for determining relative saturation and therewith the propensity to generate saturation excess overland flow (Beven and Kirkby, 1979; Moore et al., 1991; Costa-Cabral and Burges, 1994). It has often been used in combination with other topographic parameters, most often with slope as used in this study. The topographic index has often been used for the prediction of hydrologic fluxes (e.g. Beven, 1997), in Chapter 6 its utility for overland flow prediction in the research areas of this study will be investigated. Figure 2.2 shows that the area is indeed flat and that there are only few locations with moderate slopes. Nonetheless the D8 algorithm appears to produce a reasonable flow direction map, which can be deduced from the correspondence between the stream channel as measured manually in the field and the locations where flow accumulates according to the D8 algorithm (see Figures 2.1 and 2.2).

The distributions of the main soil and land use types in the area are summarized in Figure 2.4. The soil map is the result of a classification of texture and depth maps, both of which have been derived through an interpolation of the available point observations in Dekker (1996); Mulders (1996); Mulders and Zerbo (1997); Verkleij (1998) by kriging. The vegetation map has been derived on the basis of a classification of the maps produced by Groot (1996); Rering (1997); Verkleij (1998).

The area has a semi-arid climate with an average precipitation of $880\,mm\,y^{-1}$, minimum and maximum temperatures of 19 and $32^{\circ}C$ respectively and a potential evapotranspiration of 2580 $2580\,mm\,y^{-1}$. The actual evapotranspiration in the area is approximately $620\,mm$ (about 70% of the rain), percolation to deeper layers is $80\,mm$ (about 10% of the rain) and discharge is $180\,mm$ (about 20% of the rain) (Autorité des Aménagement de vallees des Volta, 1979; Sivakumar and Gnoumou, 1987). The average rainy season last from May till October and displays a large inter- as well as intra-season heterogeneity with regard to total rain depth as well as the occurrence of dry spells (Some and Sivakumar, 1994). The natural vegetation of the area is savanna-woodland. It was in a natural state till the early-seventies. At that moment the successful control of Tsé-tsé initiated the process of bringing land into cultivation for arable farming and brought herding into the area. Presently the land is partly used for arable farming (with maize, shorgum, cotton and legumes as major crops), and partly as grassland for extensive grazing. On the arable land soil tillage takes place after $50-100\,mm$ of cumulative rain at the start of the wet season, followed by sowing and regular weeding. In general crops emerge approximately one month after the first rain, and roughness of the soil surface declines over the growing season due to slaking.

Observations

Observations were collected over the period April 1994 - August 1998. Over this period weather variables (temperature, radiation, relative air humidity, barometric pressure, wind speed and direction, and open pan evaporation) were measured with an automatic weather station at a single location. Rain was observed at various locations with tipping buckets from 1996 onwards and discharge was observed at the catchment outlet with a pressure transducer. Soil moisture was measured with a TDR device in plastic access-tubes at 10 locations once every 14 days, and the

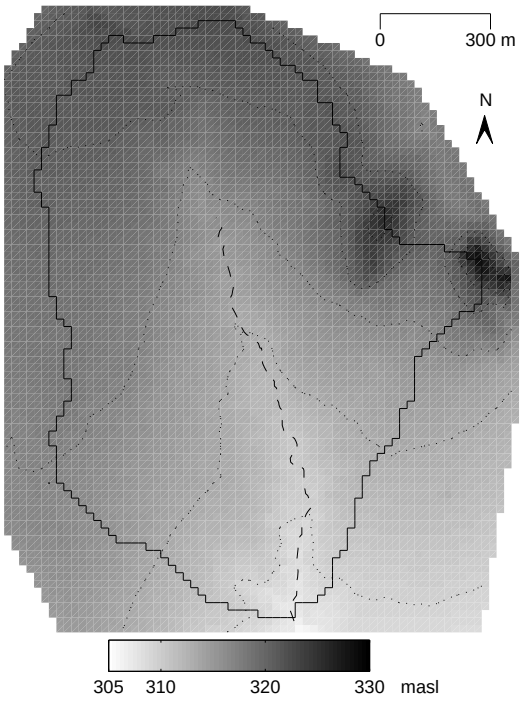

Figure 2.1: Topography of Kaibo, indicating elevation (grayscale), the catchment boundary (–), the main stream (− −) and the contours (···).

runoff from six runoff plots (three pairs of 5×10, 10×25 and $50 \times 100\,m$ in size) was measured using weirs. In addition, various observations have been collected in the period June-September 1998. In this period water table depth was measured manually along three transects with piezometers for 3 events. The structure of the subsurface was determined by geo-electric measurements (Hekman and Wierikx, 1998). In this period overland flow was observed during rain in two events. This was done by measuring water levels and flow velocities repeatedly at several points along a transect. In addition overland flow patterns were mapped just after rain for these two events along the transect. The location of the various observations is shown in Figure 2.6.

Several surveys were conducted to map the soil and geology in the area (Dekker, 1996; Mulders, 1996; Mulders and Zerbo, 1997; Verkleij, 1998). Agronomic surveys were conducted yearly to establish the land use of the entire catchment in each season (Groot, 1996; Rering, 1997; Verkleij, 1998; Wubda, 1998). In 1994 infiltration experiments were done on plots of $1\,m^2$ (Geelhoed, 1994; Hillenaar, 1995). In 1995 an accurate DTM of the terrain was constructed on the basis of observations with with a differential kinematic GPS system (Raaphorst, 1995), and visual assessment was made in 1997 (Wubda, 1998; Hekman and Wierikx, 1998).

Many of the observations mentioned above have been used to get an impression of the hydrology of the area and specify bounds and initial values for model parameters. Only a small subset of the values have been used directly for the calculation of overland flow depths. Those values that have been used directly are listed in Table 2.1. In total 124 rain events occurred during the research period, 28 of which produced discharge at the catchment outlet (see Figure 2.5). From these 124 events 60 were selected for a quantitative analysis. The set of 60 events included all the events that produced discharge at the catchment outlet, and 32 randomly selected events. Table 2.1 lists how much of each type of observation was used for calibration and validation purposes respectively.

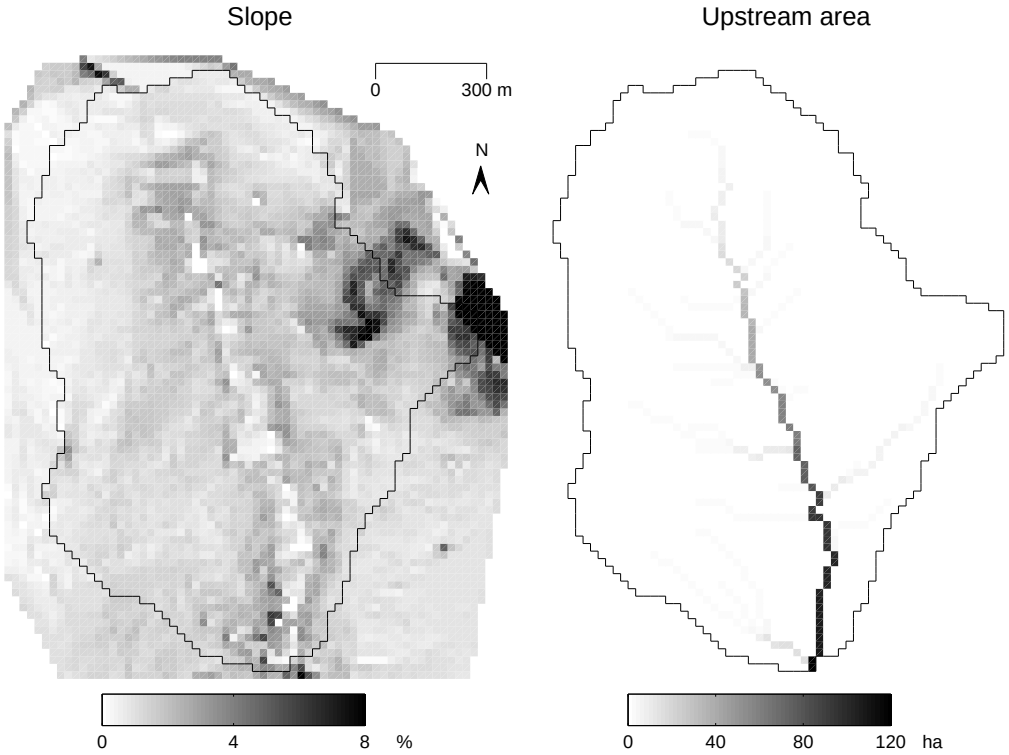

Figure 2.2: Distribution of slope and upstream area in Kaibo. The catchment area is calculated by the D8 flow-direction algorithm (O'Callaghan and Mark, 1984).

This table should be read as follows. In the calibration data set, rain has been observed at one location over 45 events, and at four locations over 27 out of these 45 events; catchment discharge has been observed at one location over 45 events, plot discharge has been observed at six locations (plots) over 14 of the 45 events, etc. It should be noted that the calibration and validation sets only overlap in space and not in time, i.e. the validation set contains different events than the calibration set. Some more details of the data set are provided in Appendix A.

Table 2.1: Number of locations and number of events where observations are used as calibration and validation data in Kaibo.

Type of observation		Calibration		Validation	
		locations	events	locations	events
p	rain	1 / 4	45 / 27	1 / 4	15 / 13
q_c	discharge - catchment	1	45	1	15
q_p	discharge - plot	6	14	6	4
o_h	overland flow - height	300	1	300	1
o_p	overland flow - paths	-	1	-	1
w	soil moisture	5	10	5	10

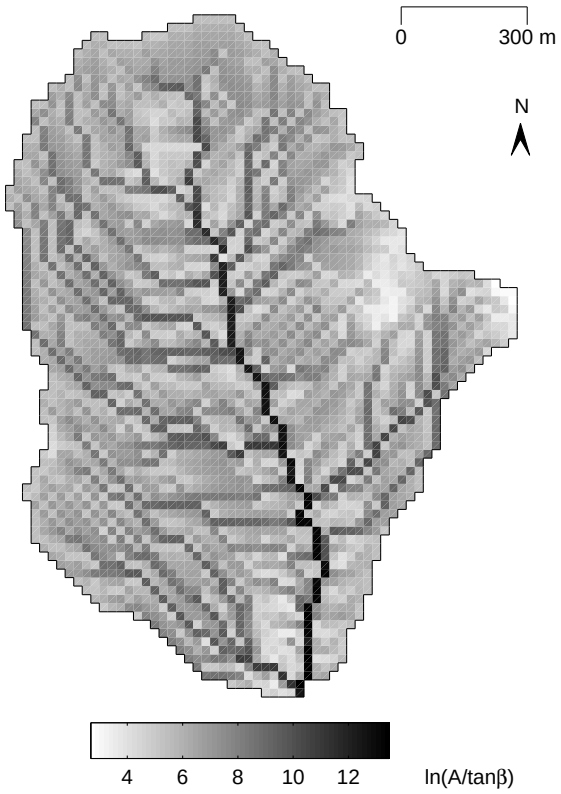

Figure 2.3: Distribution of the topographic index in Kaibo.

2.3 Estacion Experimental Forestal Horizontes

Site description

This research area is located in Costa Rica (Central America) at $10°43'$ N and $-85°36'$ E (160-190 m.a.s.l.), inside the park 'Estacion Experimental Forestal Horizontes' which is owned by the regional nature conservation agency (Area de Conservación de Guanacaste, ACG). It is a $2\,km^2$ catchment in the upper reach of the Tempisque basin, which will henceforth be called *Horizontes*. The area has a gently undulating topography and a main gully running from south-west to north-east (see Figure 2.7). Drainage density of ephemeral gullies varies between $1\,km\,km^{-2}$ to $2\,km\,km^{-2}$, with increasing densities towards the north. Drainage pattern is dendritic like in Kaibo. The nature of soils in this landscape is largely determined by the parent material, which is Ignimbrite. The major soils in Horizontes are Leptosols, Regosols and Vertisols, after FAO (1990). Leptosols and Regosols are formed in situ (Pierre, 1982; Vazquez Morear, 1991) and most soils are moderately well developed. There is a sharp distinction between soils with vertic and non-vertic properties, which largely coincides with topographic location. Soils at upslope locations have no vertic properties, drain moderately and contain mainly kaolinitic clay whereas soils in downslope areas have often vertic properties, contain montmoriollonitic clay and drain poorly when wet. The sand and clay contents are 35% and 20% respectively over the entire soil profile at upslope locations. And in downslope locations the sand and clay percentages are 20% and 40% respectively (Winters, 1995). In situations where soils with vertic properties are found at higher locations a local water table is found invariably. The recent geologic history is one of deposition

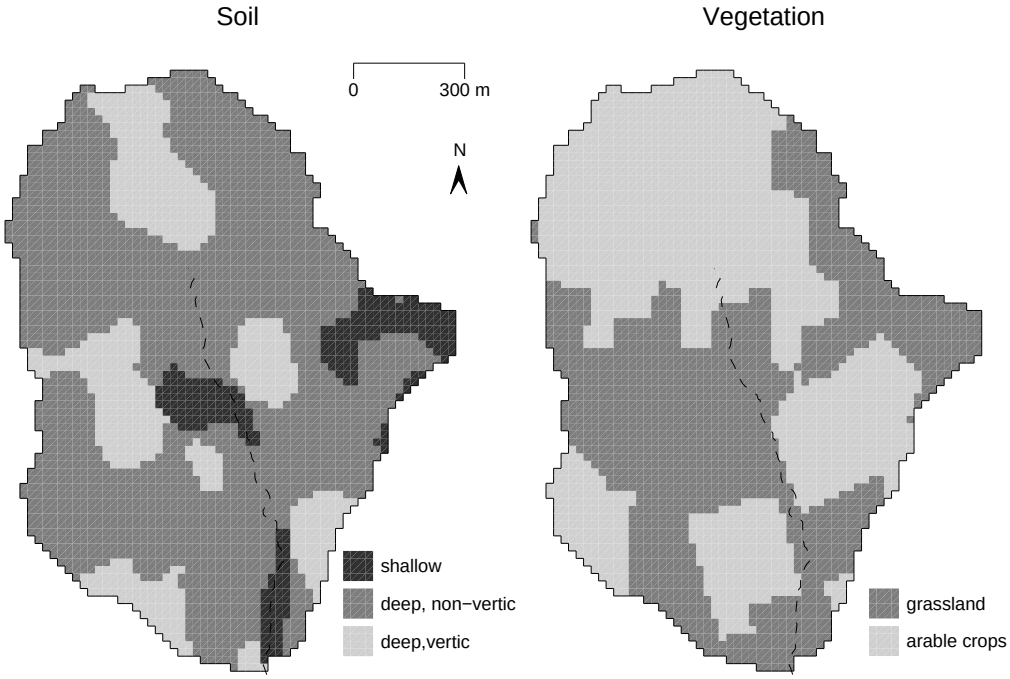

Figure 2.4: Soil and vegetation characteristics in Kaibo.

by the active volcanos east of the area (especially the Rincon de la Vieja, in the Center of Costa Rica), and a steady uplift of the area in the west. Erosion has been variable under influence of volcanic activity and sea-level changes (Castillo Muñoz, 1991). Presently no development of streams is observed. Streams are always found on bedrock, are heterogeneous with respect to size and shape and meander moderately. These characteristics correspond with the low slopes of around 5% in the area.

As for Kaibo the topography of Horizontes is further is characterized here by slope ($tan(\beta)$), upstream area (A) and topographic index ($ln(A/tan(\beta))$) (see Figures 2.8 and 2.9). Figure 2.8 shows that the area is generally undulating and that there are some steep ridges, which almost enclose some circular areas. As expected, on the basis of the moderate slopes, the D8 algorithm produces a reasonable flow direction map (viz. the correspondence between the stream channel as measured manually in the field and the locations where flow accumulates, see Figures 2.7 and 2.8).

The distributions of the main soil and land use types in the area are shown in Figure 2.10. The soil map is the result of a classification of texture and depth maps, both of which have been derived through an interpolation of the available point observations in Winters (1995) and own observations by kriging. The vegetation map has been derived on the basis of a classification of the available aerial photographs and field observations (van der Steeg, 1999; Winters, 1995).

The area has a semi-humid climate with an average precipitation of $1450\,mm\,y^{-1}$, minimum and maximum temperatures of 22 and $29^{\circ}C$ respectively and a potential evapotranspiration of $2230\,mm\,y^{-1}$. The actual evapotranspiration in the area is approximately $870\,mm$ (about 60% of the rain), percolation to deeper layers is $220\,mm$ (about 15 % of the rain) and discharge is $360\,mm$ (about 25% of the rain) (Proyecto Geotermico de Guanacaste, 1976; Oficina de hydrologia operativa, 1994). The average rainy season lasts from May till October and displays a large intra-season heterogeneity with regard to total rain depth (Proyecto Geotermico de Guanacaste, 1976).

The natural vegetation of the area is tropical dry forest, which is presently in an early stage of

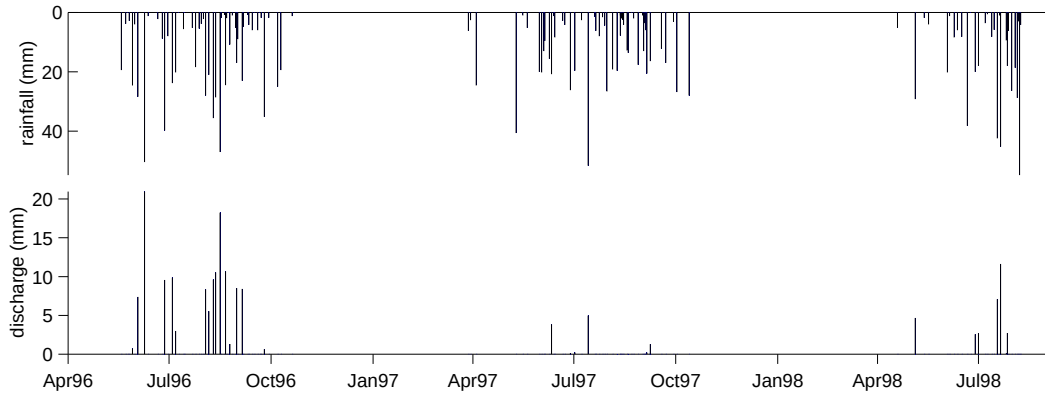

Figure 2.5: Rain (interpolated with an inverse distance technique and subsequently averaged over the catchment) and discharge at the outlet of Kaibo over the research period.

regeneration, starting from completely open grassland in 1989 (Janzen, 1991). Recent history of land use in the study area is a sequence of arable farming from the beginning of the 20th century (which probably goes back to the 18th century), with a sudden shift to extensive grazing in the early sixties (Edelman, 1992). Many of the shallow gullies in the area originate from this period of extensive grazing. In 1989 the land husbandry of the study area changed dramatically when it was acquired by ACG. From 1989 onwards ACG adopted a strategy of natural reforestation by reducing the cattle stock to low levels and re-planting some areas with young trees (Molina, 1994). Although the tree-density increased steadily during the research period, the influence of cattle on the terrain remained large. The animal tracks and resting places stayed largely free of vegetation.

Observations

Observations were collected over the period April 1996 - August 1998. Over this period weather variables (temperature, radiation, relative air humidity, barometric pressure, wind speed and direction) were measured with an automatic weather station at a single location, rain was observed at 6 locations with tipping buckets and discharge was observed at 6 locations with pressure transducers. In the period June 1997 - December 1997 post-event flow patterns were observed along two transects. Along these transects overland flow was observed with 24 collectors (crest stage tubes, see Figure 2.15). The location of these various observations are shown in Figure 2.12.

In 1997 experiments were conducted with a Guelph permeameter to establish the heterogeneity of infiltration capacity. In 1998 a DTM was constructed on the basis of observations with a differential kinematic GPS technique in combination with a conventional ground-based survey (Boerrigter, 1999). Several surveys were conducted to map the soil and geology in the area (van der Steeg, 1999; Winters, 1995).

A 44 ha sub-catchment of Horizontes, which is named Horicajo for the purpose of this research, has been studied in greater detail. The observations in Horicajo were made during the period period July 1997 till December 1997. At four locations rain has been measured using tipping buckets and at two locations discharge has been measured using v-crest weirs. For 7 events water table depth has been observed manually in 20 piezometers at hourly instants during and just after rain, and daily between rain events. Post-event overland flow patterns were observed for 5 events, and overland flow height as well as velocity were observed during 9 events along 4 transects. During the period 20 July - 4 October 1997, volumetric soil moisture has been measured at 40 locations once every 4 days, and during the period 4 October - 21 December 1997 at 60

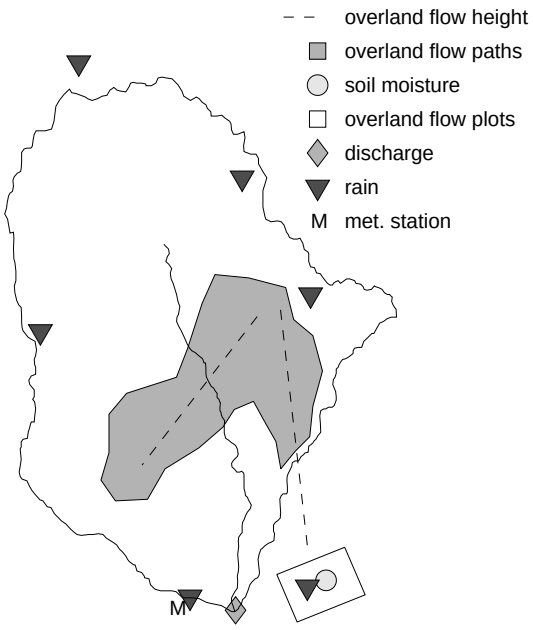

Figure 2.6: Location of observations in Kaibo.

locations once every 2 days (See Figure 2.14). For the soil moisture measurements a Trime TDR system (in plastic tubes) has been used, enabling the measurement of soil moisture over $20\,cm$ layers down to $80\,cm$. Terrain and soil have been mapped in detail in a similar way as done for the entire Horizontes catchment, however the conventional survey was done at a much denser net (approximately one observation at every $20 \times 20\,m$). In addition the geometry of small rills and drainage channels have been mapped. Soil colour, structure, depth, organic matter content, and texture have been determined at 90 locations, and the infiltration capacity has been determined at 30 of these locations, using a Guelph permeameter (both at 10 and $20\,cm$ depths). In addition soil colour, structure and texture (field-determined) have been observed at a regular spacing of $20 \times 20\,m$.

Similar to the data that were collected in Kaibo, many of the observations collected in Horizontes and Horicajo have been used to get an impression of the hydrology of the area and obtain parameter bounds. The observations that have been used directly for the calculation of overland flow depths in Horizontes are listed in Tables 2.2 and 2.3. In total 267 rain events occurred during the research period, 187 of which produced discharge at the catchment outlet (see Figure 2.11).

From these 267 events 60 were selected for a quantitative analysis. The set of 60 events included all the events for which observations were collected in Horicajo (31) and the remaining 29 events were selected randomly. Tables 2.2 and 2.3 lists how much of each type of observation was present in the data set used for calibration and validation purposes respectively. As with the Kaibo-data, the calibration and validation sets only overlap in space and not in time.

The location of the various observations are shown in Figures 2.12 and 2.14. In Figure 2.13 the sub-catchments that correspond with the main discharge measurement points in Figure 2.12 are delineated. Note that Horicajo coincides with sub-catchment 'f'. The meteorological station, as well as discharge and rain observations shown in Figure 2.12 are replicated in Figure 2.14, the remaining observations on the two maps do not overlap. Some more details of the data set are provided in Appendix A.

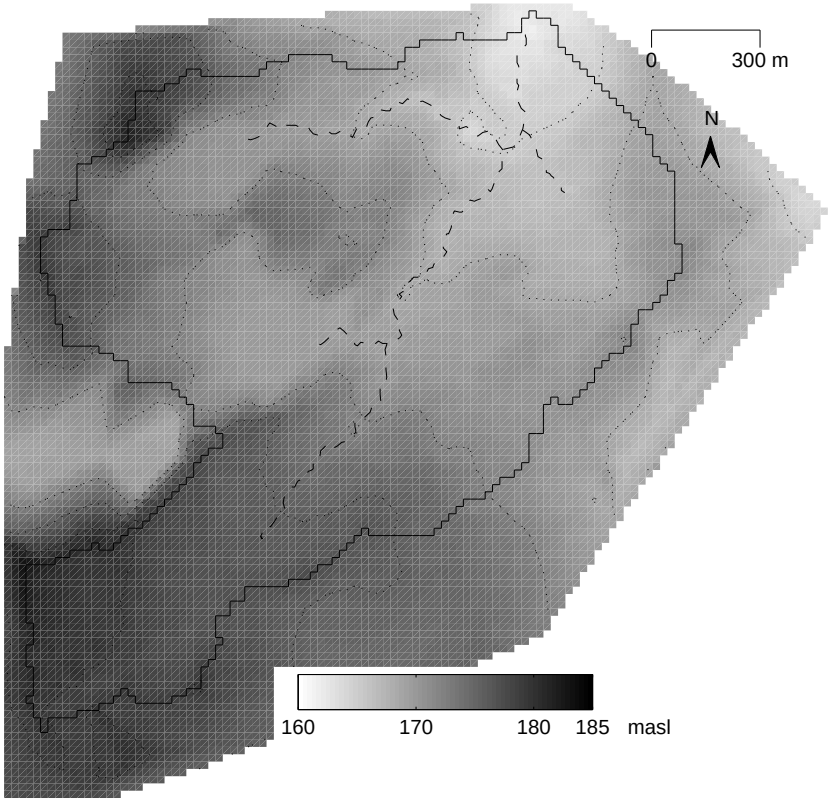

Figure 2.7: Topography of Horizontes, indicating elevation (grayscale), the catchment boundary (–), the main stream (− −) and the contours (· · ·).

2.4 Explanation of new observation techniques

The overland flow observations (o_c, o_h and o_p) were collected with non-standard techniques. In spite of the simple technology that these techniques use, they will be explained in some detail here for clarity.

The preparation for all these methods was to place markers in the field at regular distances in such a way that that a person's location (relative to earlier field visits) could be deduced to about 2 m accuracy. At each field visit the same route was followed via these markers. In Kaibo the markers were placed 50 m apart and in Horizontes at 25 m, in both cases along transects. The method to collect overland flow heights (coded as o_h) was as follows. Starting at the onset of the rain the route was followed from start to end and then back (in the case of Kaibo) or starting at the beginning again (Horizontes). Using a measuring stick with a scale, the overland flow depth was observed at each second step at the location of the heel. The flow velocity was observed at each 20th step by timing the duration of 1 m passage by 3 mm cork beads. In addition the flow velocity of currents deeper than 5 cm was observed with a current meter at a number of locations (5 in Kaibo and 10 in Horizontes). After passing 20 m, the extent of the surface covered by overland flow was estimated over that tract, covering an area of approximately $20 \times 2\,m$. Note that the flow velocity is required to estimate a discharge on the basis of an observed overland flow depth, so they are considered as part of the o_h observations.

Overland flow was observed with collectors (o_c) in the following way. The collectors of the type shown in Figure 2.15, made from PVC tubes, were placed at regular distances along a transect in the field. Insertion in the soil was such that openings in the horizontal tube were at the soil

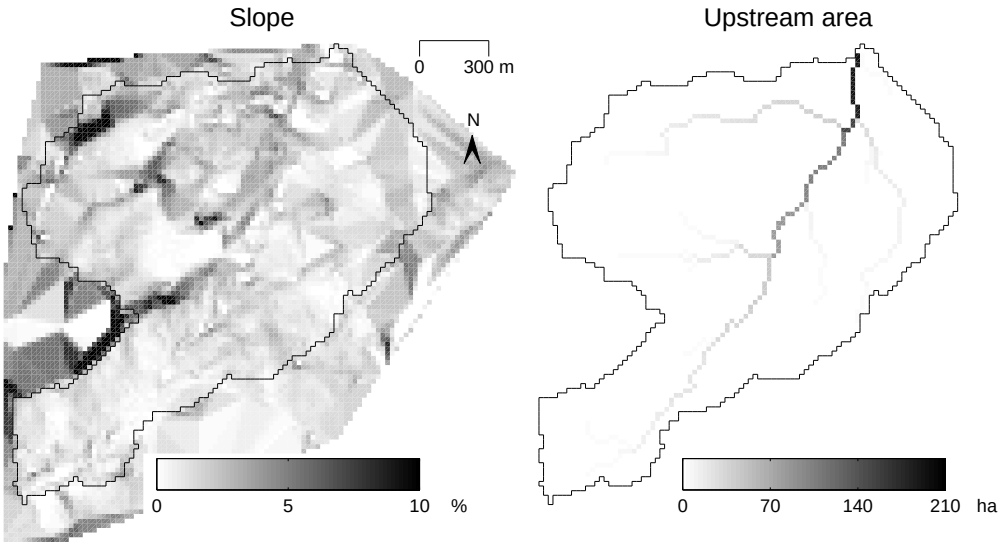

Figure 2.8: Distribution of slope and upstream area in Horizontes. The catchment area is calculated by the D8 flow-direction algorithm (O'Callaghan and Mark, 1984).

Table 2.2: Number of locations and number of events where observations are used as calibration and validation data in Horizontes.

Type of observation		Calibration		Validation	
		locations	events	locations	events
p	rain	2 / 6	14 / 31	2 / 6	2 / 13
q_c	discharge - catchment	2 / 6	14 / 31	2 / 6	2 / 13
o_c	overland flow - collectors	24	3	24	2
o_p	overland flow - paths	-	4	-	3

surface and facing the upslope direction. For each collector the upstream area was determined by manual measurements in the field. After a rain event the collectors were emptied and the volume in each was determined.

The observation of overland flow paths (o_p) was as follows. At each location along the transect, where overland flow height was observed during rain, the area where flow occurred was first traced downslope, until a junction with another flow path occurred. From this location the entire upslope area was traced and sketched on a map, subsequently the extent of the area was estimated. Traces of debris and ponded water were used to identify the area covered by overland flow.

2.5 Uncertainty of the observations

The observations summarized in this Chapter are not without uncertainty. Here three sources for this uncertainty are distinguished: 1) instrument errors; 2) conversion errors and 3) interpolation/averaging errors (which will henceforth be called interpolation errors). *Instrument errors* are random errors produced by the instrument in the observation process, i.e. independent of time, geographical location and assuming correct instrument operation and placement in the field. *Con-*

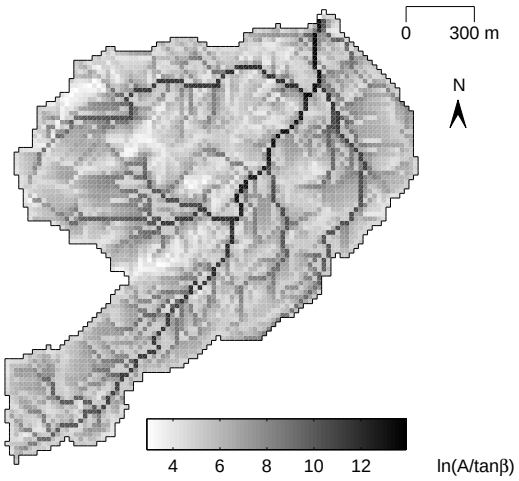

Figure 2.9: Distribution of the topographic index in Horizontes.

version errors are errors resulting from the conversion of observed quantities to desirable quantities using an empirical relationship. *Interpolation errors* are errors that result from the integration of observed quantities to the desired spatio-temporal units. In this section an attempt is made to estimate each of these errors for the various observations.

Strictly speaking conversion errors and interpolation errors are similar, in the sense that interpolation can also be regarded as a conversion via an empirical model. In practice however, the distinction is meaningful: conversion errors are assumed to be independent of timing and location whereas interpolation errors do have space and time ordinates. As a result conversion errors are functions of the *measurement technique* while interpolation errors are also a function of the *measurement layout* (e.g. observation density). A conversion error results from the calculation of a variable on the basis of observed quantities at similar spatial and temporal units (so called *support*). A good example is a stage-discharge relationship in a stream cross-section, which re-

Table 2.3: Number of locations and number of events where observations are used as calibration and validation data in Horicajo (only the rain and catchment discharge observations are subsets of the observations listed in Table 2.2).

	Type of observation	Calibration		Validation	
		locations	events	locations	events
p	rain	4	23	4	8
q_c	discharge - catchment	2	23	2	8
q_p	discharge - plot	4	11	4	4
o_c	overland flow - collectors	20	2	20	3
o_h	overland flow - height	300	2	300	3
o_p	overland flow - paths	-	4	-	3
s	water table depth	20	4	20	3
w	soil moisture	60	23	60	8

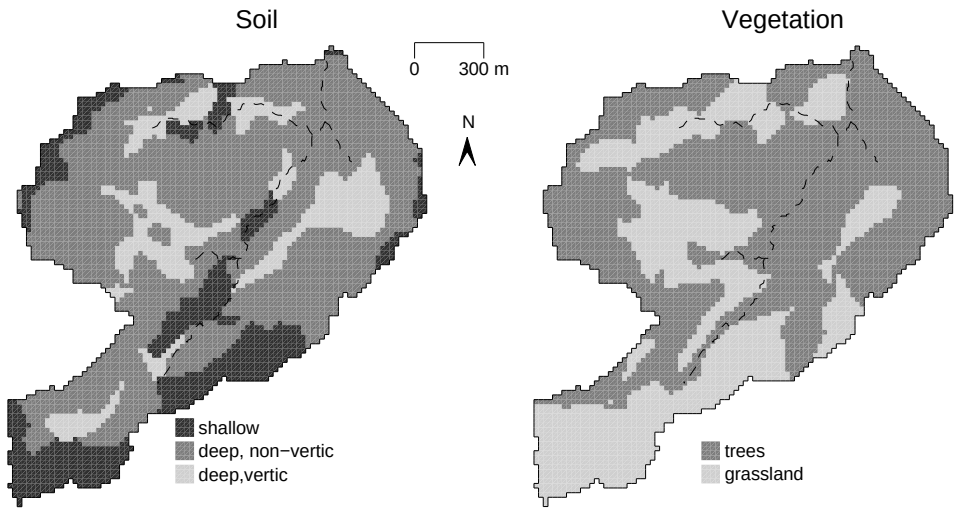

Figure 2.10: Soil and vegetation characteristics in Horizontes.

quires water height, average velocity and cross-section area to be observed. Such relations can be established repeatedly and the conversion error can be estimated by the deviation of the various observations from a fitted relationship. An interpolation error results from incomplete coverage of the study domain, differences between the support of observations and desired quantities, and uncertain system boundaries. Examples of the first factors are f.i. point observations of soil moisture or overland flow where average entities over 20×20 m model grid cells are required. An example of an uncertain system boundary in this context is f.i. an uncertain catchment boundary. Incomplete coverage of the domain and differences in support are particularly important if the process under study is heterogeneous and non-linear, implying that a value over a desirable spatio-temporal unit cannot be obtained by simple averaging.

In this study the three different errors have been quantified through *repetition* (in the case of instrument errors), *split-sample validation* (in the case of conversion errors) and *cross-validation* (in

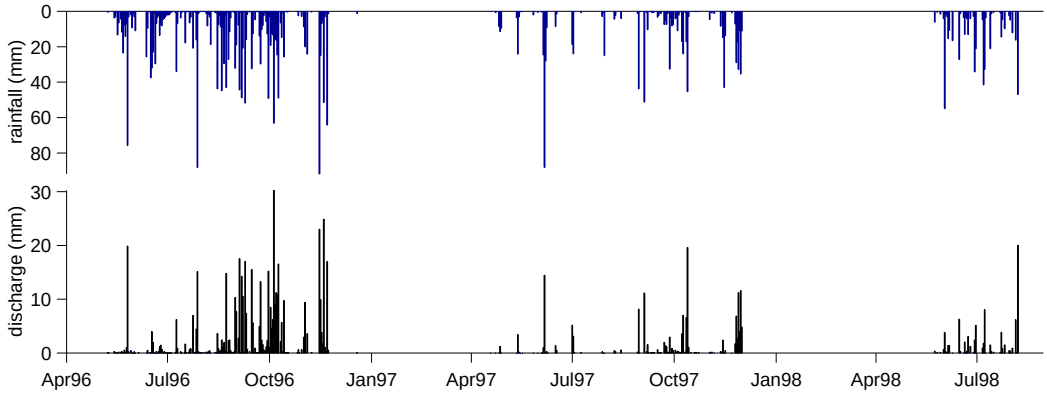

Figure 2.11: Rain and discharge at the outlet of Horizontes over the research period.

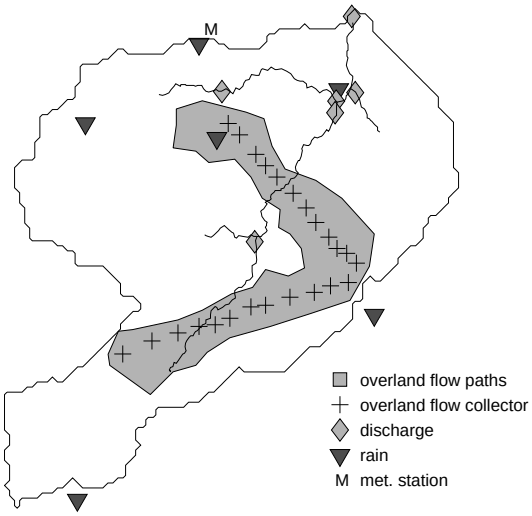

Figure 2.12: Location of observations in Horizontes.

the case of interpolation errors). *Repetition* is a procedure whereby the same instrument or measurement procedure measures a unit repeatedly. *Split-sample validation* is a procedure whereby the available observations are first split in two parts through a random selection procedure. One of the parts is used to calibrate a model. Subsequently the model is applied to the second part of the observations. Finally the prediction error is calculated. *Cross-validation* is defined as a procedure whereby a model (in this case an interpolation or averaging procedure) is repeatedly applied to all observations minus one randomly selected observation, whereafter the difference between the prediction and the left-out value is calculated.

All errors are expressed in *relative root mean squared error* (RRMSE), which is defined as

$$RRMSE := \sqrt{\frac{\sum_{i=1}^{I}\sum_{j=1}^{J}\left(\frac{obs_{i,j}-pred_{i,j}}{pred_{i,j}}\right)^2}{I \cdot J}}. \tag{2.1}$$

where the indices i and j refer to the ith time instant and jth location of the validation data, $obs_{i,j}$ are observations, $pred_{i,j}$ the model predictions and I and J the total number of time instants and locations for which validation data are available. In the case of the repetition procedure the average of the observations is taken as $pred_{i,j}$. The reason for the division of $(obs_{i,j} - pred_{i,j})$ by $pred_{i,j}$ is that for almost all relationships the observation error increases nearly proportional to the magnitude of the variable to be predicted.

The relationships required for measurement conversion were established for each of the catchments and instrument types, while limiting the possible forms to linear- or power-functions. The interpolation functions were established separately for the two catchments, limiting the possible interpolation models to be linear, distance weighted or semi-variogram based. The strategy to select the appropriate model for conversion or interpolation was as follows:

1. fit a linear relation through the observations (or, analogous, perform a linear interpolation) and calculate the RRMSE on the basis of the chosen validation strategy;

2. fit a power relationship (or distance weighted interpolation) and also calculate the RRMSE for this model;

3. use the power relationship (or distance weighted interpolation) if the strategy reduces the RRMSE by at least 0.05, otherwise use the linear relationship;

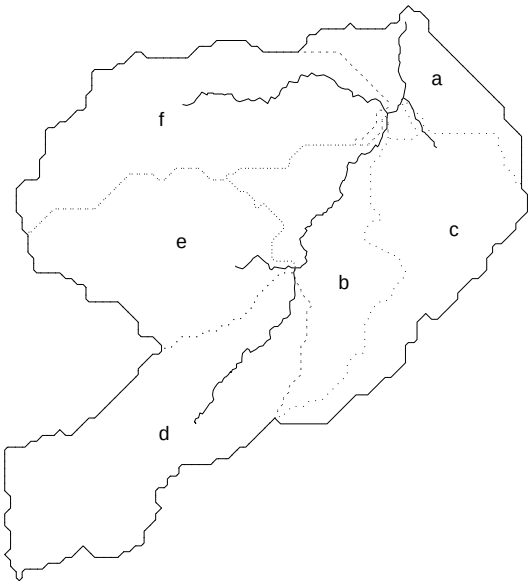

Figure 2.13: Sub-catchments of Horizontes.

4. in the case of interpolation, repeat steps 1 to 3 to compare optimal interpolation to both linear and distance weighted interpolation, whereby the semi-variogram for the optimal interpolation is derived interactively.

The interpolation error for discharge observations (q_c and q_p) refers to uncertainties in catchment and plot boundaries. Because in Kaibo as well as Horizontes there was a repetition of each plot, cross-validation could be applied to these data. But the uncertainty in catchment boundaries and, resulting from this, errors in the discharge observations (q_c) could not be established by cross-validation. This error has been determined in three different ways: 1) by comparing the catchment boundaries derived in various independent studies, 2) by applying different routing algorithms to the same DTMs and comparing the resulting catchment boundaries, and 3) by observations of flow-directions at the catchment boundaries during rain for different events and different seasons. The uncertainty with respect to the catchment size is determined by calculating the $\infty-$norm for all these different boundaries, resulting in a 'total uncertian catchment area' and using no prior assumption about catchment shape. The interpolation error for discharge observations is expressed as the total uncertain catchment area divided by the average catchment area. This can be defined as follows

$$RUBE := \frac{A_{max} - A_{min}}{\sum_{n=1}^{N}(A_n)/N} \tag{2.2}$$

where $RUBE$ stands for 'relative unknown-but-bounded error', A_{max} is the maximum catchment area observed over the N cases, A_{min} is the minimum catchment area, and A_n is the catchment area for case n. The above information is summarized in Table 2.4.

In Table 2.5 the instrument errors are listed. The instrument errors of the tipping buckets were determined by placing all tipping buckets under a laboratory rainfall simulator. The instrument errors of pressure transducers was determined by placing two identical instruments close together at the same location during an event, and repeating this at three different locations. The TDR-error was determined by comparing the readings from three pairs of tubes, placed close together. All other errors were determined by repeating a measurement over ten small areas five times in succession. Table 2.6 lists the conversion errors. This table clearly illustrates that the conversion errors are in general larger for overland flow then for streamflow, and that normally a linear re-

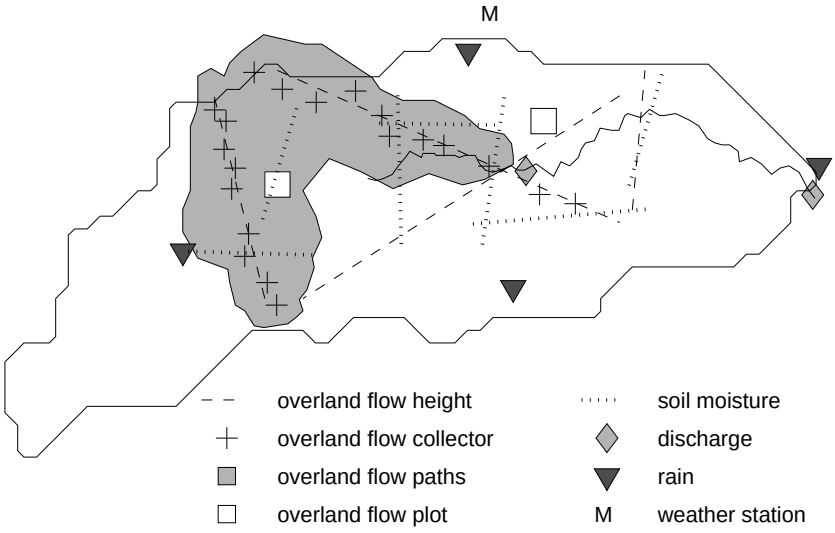

Figure 2.14: Locations of observations in Horicajo.

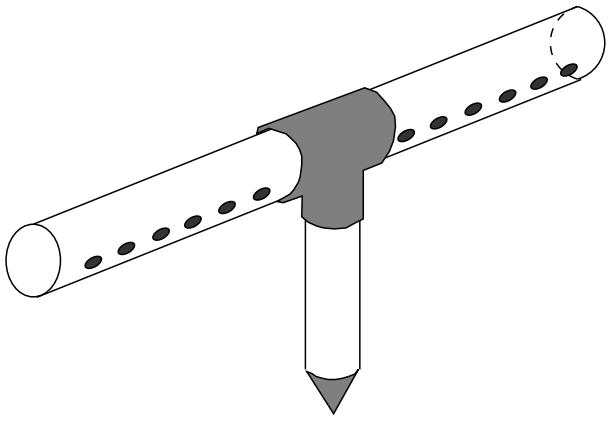

Figure 2.15: Overland flow collector used in the field research of Horizontes.

lation gives a satisfactory fit for overland flow whereas a power-relation is desirable for stream flow. Apart from observation density (listed in Tables 2.1, 2.2 and 2.3) the discepancy between the support of observations and the space-time units at which the values are desired (so-called model support) is a main determinant for the size of an interpolation error. Table 2.7 lists the observation support and model support for the various measurements. This table shows that there exists especially a discrepancy in space, whereas time support for observation and model is quite close. Therefore only errors due to spatial interpolation are considered in this study. Table 2.8 lists the interpolation errors, illustrating that the errors for overland flow larger for overland flow then for streamflow. The main causes for the various interpolation errors are listed in Table 2.9.

The fact that incomplete spatial or temporal coverage leads to averaging errors is a logical consequence of the non-linearity of the rainfall and flow processes involved. Also the uncertainty in the estimation of upslope areas (applicable to o_c, o_p and s) is obvious. But the explanation of the uncertainty in catchment and plot boundaries is less straightforward. Therefore these sources of uncertainty will be briefly discussed.

By comparing different interpolation techniques (applied to the original geodetic observa-

Table 2.4: Validation techniques and models or measures used to calculate the instrument errors, conversion errors and interpolation errors.

type of error:	validation technique:	model / measure:
instrument	repetition	average
conversion (only q and o)	split-sample	linear power
interpolation (all except q_c)	cross-validation	linear dist. weighted kriging
interpolation (only q_c)	repetition	$\infty-$norm

Table 2.5: Instrument errors, as determined by laboratory (l) / field (f) test. All tests were performed with four repetitions. All field tests were done in Horizontes.

observation	type of instrument	RRMSE in %
p	tipping bucket	2 (l)
q_c	pressure trans.	1 (l)
q_p	pressure trans.	3 (f)
o_h	manual (height)	5 (f)
o_c	manual (volume)	1 (f)
o_p	manual (coverage)	1 (f)
s	manual (depth)	1 (f)
w	TDR	3 (l/f)

tions), the uncertainty of catchment boundaries for flat areas becomes apparent. However, it turns out that the effects of using different interpolation techniques are still small (5 %) in comparison to the differences that arise due to the use of different routing algorithms (10 to 20 %), see Table 2.11. The different routing algorithms applied are the D8, MS and Dinf approaches. The D8 apporach, the simplest method which was originally proposed by (O'Callaghan and Mark, 1984), assigns flow from each grid cell to one of its eight neighbours in the direction with steepest downward slope. The MS (Multiple directions based on Slope) method, proposed by Freeman (1991), allocates flow fractions to each lower neighbour in proportion to the slope to an exponent towards that neighbour. The Dinf approach, introduced by Tarboton (1997), allocates flow fractions to either one or two neighbours in proportion to the aspect of a slope. For all interpolation procedures no constraints have been superimposed (such as the acceptance of a prior boundary or stream-bed) and for each of the routing algorithms the same 'lake-filling' procedure was used to remove pits. Since the course of stream-bed was relatively accurately established for both Kaibo and Horizontes all routing algorithms did acknowledge this quite well and all gave the outlet at the same location.

After the geodetic surveys for both Kaibo (Raaphorst, 1995) and Horizontes (Boerrigter, 1999) several attempts have been made to establish more accurate catchment boundaries in the field, it appeared that many of those catchment boundaries do in fact vary quite significant over time (Hekman and Wierikx, 1998; Wubda, 1998). Explanations for this were:

1. the direction of furrows in arable cotton fields determined flow direction (inter season as well as intra season, Kaibo);

Table 2.6: Conversion errors due to uncertainty of empirical relationships to derive observed flow volume from observations depths, all using either the power-relation volume = α depth $^{\beta}$ or the linear relation volume=a depth + b. The relations for the overland flow observations (o_h, o_c and o_p) have been established at 5 resp. 10 different locations for Kaibo and Horizontes, and were assumed to be valid for the entire catchment.

	RRMSE in %		relation		nr of obs. (repetitions)	
obs.	Kaibo	Horiz.	Kaibo	Horiz.	Kaibo	Horiz.
q_c	7	9	power	power	130 (-)	50 (-)[a]
q_p	3[b]	5	power	power	-[b]	50 (1)
o_h	17	8	linear	power	10 (5)	10 (10)
o_c	-	22	-	linear	-	10 (10)
o_p	23	16	linear	linear	10 (5)	10 (10)

[a] 50 observations have been made for each of the six locations
[b] the weirs used at these plots were calibrated in the laboratory

Table 2.7: Overview of the discrepancy between the support of the observations and the unit at which the value is desired (model support). Note that in this study the grid cells are 20×20 m.

	observation support		model support	
observation	space	time	space	time
p	$0.1\,m^2$	1 min.	grid cell	2 min.
q_c	catchment	1 min.	catchment	2 min.
q_p	grid cell	1 min.	grid cell	2 min.
o_h	$0.01\,m^2$	2 min.	grid cell	2 min.
o_c	$0.1\,m^2$	1 event	upslope area	1 event
o_p	$0.1\,m^2$	1 event	upslope area	1 event
s	$0.01\,m^2$	1 min.	upslope area	2 min.
w	$0.01\,m^2$	1 event	grid cell	1 event

2. the area is very flat so that the exact flow direction could only be determined on the basis of the overland flow observations during rain, but not on the basis of geodetic observations (Kaibo);

3. road deviations and animal tracks changed the flow direction (intra season both Kaibo and Horizontes);

4. an area was drained by several small ditches at two or more sides (i.e. in opposite directions), while sometimes one of these was blocked or backwater effects in the lowest ditch dammed the water up, leading to the drainage via both ditches (intra season as well as intra event, Horizontes).

The locations where these types of uncertainty existed are shown in Figures 2.16 and 2.17.

Attempts to refine the estimation of catchment boundaries on the basis of visual inspection (sometimes during rain) and using simple equipment failed for Kaibo, but gave a considerable improvement for Horizontes. When utilizing all resources, uncertainties of $1/4^{th}$ of the catchment area for Kaibo and $1/9^{th}$ for Horizontes remained. However, for Kaibo it was decided to omit the observations described in Wubda (1998) because of the relatively large deviations of these in

Table 2.8: Interpolation errors errors due to interpolation from the observation support to the model support.

	RRMSE/RUBE in %		relation		nr of locations	
obs.	Kaibo	Horiz.	Kaibo	Horiz.	Kaibo	Horiz.
p	12	7	dist. weight	kriging (spherical)	4	6
q_c	8^a	11^a	-	-	1	1
q_p	14	2	-	-	6	4
o_h	7	12	dist. weight	dist. weight	300	300
o_c	-	18	-	linear	-	44
o_p	18	21	linear	linear	10	10
s	-	14	-	kriging (exponential)	-	20
w	13	17	dist. weight	dist. weight	5	60

[a]Only q_c is expressed in RUBE, see Equation 2.2.

Table 2.9: Explanation of interpolation errors.

observation	Explanation
p	incomplete spatial coverage of catchment and non-linear process
q_c	uncertain and variable catchment boundaries (surface flow)
q_p	uncertain catchment boundaries (subsurface flow)
o_h	incomplete spatial and temporal coverage and non-linear process
o_c	incomplete spatial coverage and non-linear process / uncertain upstream area
o_p	incomplete spatial coverage and non-linear process / uncertain upstream area
s	incomplete spatial and temporal coverage and non-linear process / uncertain upstream area
w	incomplete spatial coverage and non-linear process

comparison to the other sources (Raaphorst, 1995; Hekman and Wierikx, 1998), which reduced the uncertainty to $1/12^{th}$ of the catchment area.

The large uncertainty of plot discharge in Kaibo was due to the presence of subsurface flow. After establishment of the plots and collection of observations over one season in Kaibo, it appeared that in a number of events saturation excess occurred, which had to be due to sub-surface flow where water from outside entered the plot. However the approximate volumes of this infiltration excess could be established by utilizing an additional model to pre-process the plot discharge observations (effectively as a measurement equation), significant prediction errors (14%) still remained.

There was no indication that the three error sources (instrument, conversion errors and interpolation/averaging errors) were related. Therefore, taking the maximum error (in Tables 2.5, 2.6 and 2.8) of each observation type is a conservative estimate, that will subsequently be used as the effective observation uncertainty in this study.

Table 2.10: The total observation error, obtained from the maxima in Tables 2.5 to 2.8.

observation	spatially defined on	temporally defined on	Total observation error RRMSE Kaibo	Horizontes
p	catchment	2 min.	12 %	7 %
q_c	catchment	2 min.	8 %	11 %
q_p	grid cell	2 min.	14 %	5 %
o_h	grid cell	2 min.	17 %	12 %
o_c	upslope area	1 event	-	18 %
o_p	upslope area	1 event	18 %	21 %
s	upslope area	2 min.	-	22 %
w	grid cell	1 event	23 %	17 %

Table 2.11: Catchment size (in ha) as calculated by different interpolation techniques, and routing algorithms (the D8, MS and Dinf algorithms as described by O'Callaghan and Mark (1984); Freeman (1991) and Tarboton (1997) respectively). For the MS method an exponent of 1.2 has been used.

	Kaibo			Horizontes		
	linear	cubic spline	kriging	linear	cubic spline	kriging
D8	123	118	132	201	216	212
MS	111	107	105	184	186	192
Dinf	159	141	146	215	214	231

2.6 Overland flow height and extent

On the basis of the observations described previously, two aspects of overland flow occurrence will be addressed here: height and extent. The frequency of the o_h observations (approximately one per 30 minutes for a given location) does not allow a differentiation in time but a spatial breakdown by the soil and vegetation classes (as displayed in Figures 2.4 and 2.10) is possible. The extent of overland flow has directly been observed through o_h and o_p. Naturally, extent is uniquely related to the height observations shown previously (in the same way as height and flow-volume are related), as long as the soil surface is not completely covered by water. In this study complete coverage over the observation areas of (approximately) $20 \times 2\,m$ was never encountered. In Figure 2.18 the relation between height and extent is plotted for the different soil and vegetation classes. The relations are all non-linear and sometimes contain thresholds (indicated by arrows in Figure 2.18). These tresholds were not identified on the basis of Figure 2.18 alone, but on the basis of qualitative observations on flow patterns. At the field locations indicated by the arrows in 2.18 it was observed that clear changes occured in rill patterns during the observation of overland flow heights and extent. At those locations average rill depth was measured at a later stage. In Figure 2.19 it is shown that the height at which these thresholds occur are very strongly related to the average rill depth. Each dot in this graph represents a threshold indicated in Figure 2.18. Note that the level of the threshold is approximately ten times as low as the average rill depth, assuming u-shaped rills this implies a rill density of 0.1. In fact figure 2.19 shows a slight decrease of effective rill density with increasing average rill depth. Notwithstanding the information about the height-extent relationship contained in the soil and vegetation classes, a lot of noise remains. This can be attributed to the effect of micro relief. It is obvious that not only due to the non-linearity of the relationship between overland flow height and extent, but also due to the distinct shapes of the overland flow height-extent relationships for different soil and vegetation classes, the space-time

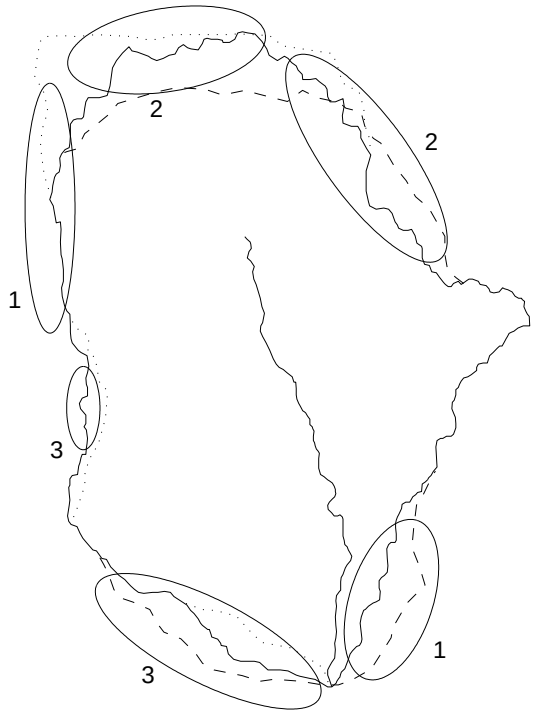

Figure 2.16: Uncertainty of catchment boundaries in Kaibo due to different sources. The dashed line is the catchment as described by (Wubda, 1998), the dotted line as desribed by (Hekman and Wierikx, 1998), and the solid line is the catchment boundary that was chosen in this study. The meaning of the numbers is explained on page 28.

distribution of overland flow extent will be quite different from that of overland flow height. In the remainder of this study only spatial distribution of overland flow height will be considered, converting the observations of overland flow extent at the individual locations to overland flow height.

2.7 Correlation in space and time

Like all hydrologic processes overland flow height exhibits autocorrelation in space as well as time. The question is however, how the autocorrelation functions look like, and what characteristic temporal and spatial scales can be revealed.

As expected, spatially there exists a large anisotropy of the overland flow distribution. In a slope direction the autocorrelations are much higher that in the contour direction (see the two plots at the left in the top row of Figure 2.20). In needs no explanation that flow concentrates in rills and small gullies that flow downslope, so that it is highly structured. Interestingly, the correlograms do reveal the effect of different soil units in Kaibo as well as Horizontes (see the points indicated by arrows in Figure 2.20). In Horizontes these jumps mark the transition from vertic to non-vertic soils, and in Kaibo probably the transition between deep and shallow soils (see Sections 2.2 and 2.3). When calculated per soil-vegetation unit (not shown in the figure) the correlograms do not show characteristic differences, probably because there are too few observations per unit. Below the correlograms for overland flow in Figure 2.20, the correlograms for clay content in the top 20 cm of the soil and rain depth are plotted. The graphs show that also for these processes there is an anisotropy for slope and contour directions as well as for low and high intensity rain. In Horizontes the points indicated by the arrows in the correlograms for overland flow can be found back in the

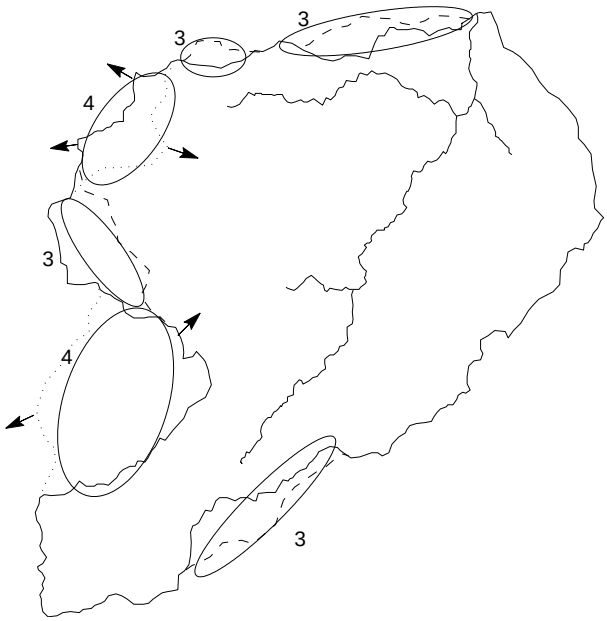

Figure 2.17: Uncertainty of catchment boundaries in Horizontes due to different sources. The dashed line is the catchment as obtained by conventional geodetic observations, the dotted line as desribed by processing the GPS observations Boerrigter (1999), and the solid line is the catchment boundary that results also including direct overland flow observations. The solid line was taken as catchment boundary in this study. The meaning of the numbers is explained on page 29.

correlograms for clay content, therewith underlining the aforementioned influence of verticity on overland flow patterns in Horizontes. The different spatial structures for low-intensity rain (here defined as an event with less than 2 $2 mm h^{-1}$) and high-intensity rain (an event with more than $10 mm h^{-1}$) is striking. In both catchments convective storms lead to high-intensity events which come with south-western high-velocity winds in Horizontes and southern winds in Kaibo, and have a relative short duration. Most stratiform storms, on the other hand lead to low-intensity events with a relatively long duration and come from a southern direction in Horizontes and a south-eastern direction in Kaibo. It is important to notice that already at distances of 300 to $500 m$ the autocorrelation of total event rain depth nearly halved in both high and low intensity rain events. The spatial correlation of rain has been determined by considering each event as independent, i.e. a long distance apart, and combining all observations from the different events. In time, the shape of the autocorrelation functions for overland flow (the two plots at the right in the top row of Figure 2.20) is more difficult to interpret, since it displays the combined heterogeneity of rainfall intensity and the upslope flow history. To separate these two effects, the overland flow during intense rainfall and during low-intensity rain is analysed separately. In the first case the heterogeneity of rainfall is dominating, whereas in the second, the effect of flow history (i.e. spatial heterogeneity of the upstream area) dominates. During high-intensity rain the autocorrelation of overland flow approaches zero already after 25 or 35 minutes in respectively Kaibo and Horizontes, whereas in low-rainfall conditions it does not even go to zero after 60 minutes. For rain the autocorrelation over space as well as time is greater than that of overland flow, as shown in the plots at the the bottom row of Figure 2.20.

These results show that it will be difficult to apply geostatistical tools to model overland flow. In the first place, the spatial process is anisotropic and structured (i.e. it organises into dendric shapes). It has been shown in geostatistical studies of soil moisture distributions, that even with

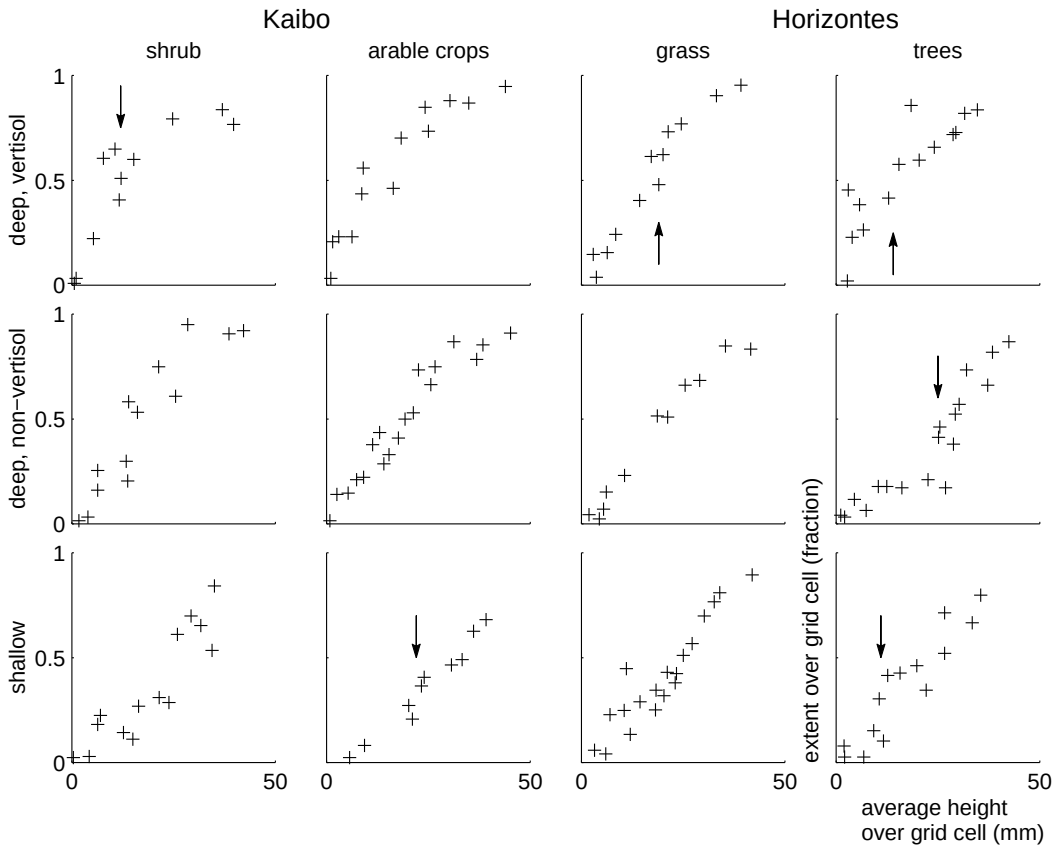

Figure 2.18: The relation between height and extent of overland flow within soil and vegetation classes, where the occurrence of thresholds is marked with arrows.

large observation densities it is hard to capture interconnectedness with geostatistical techniques (Western et al., 1998, 1999). The high non-linearity and temporal heterogeneity of the flow process as well as the strong directed spatial interaction (i.e. effects from upslope to downslope) add to these difficulties. Secondly, the dominant source of temporal heterogeneity, viz. rain or the flow history of upstream areas, determines the temporal correlation to a large extent.

2.8 Discussion

Comparing the catchments

In spite of the obvious differences between the two catchments (size, lithology, climate and land use), there are also quite some similarities. It are the resemblances between the two catchments which will be the main focus here, because these make it interesting to consider the catchments jointly in this study.

Both catchments are located in environments where runoff ratios of 0.2 - 0.25 are expected, which classifies them as dry catchments (Gan et al., 1997). In addition both data sets contain a relatively dry year and a relatively wet year (1997 and 1996 respectively for both catchments). Slopes and the distribution of topographical indices are quite similar (if areas of equal size are considered), however the drainage density is slightly higher in Horizontes. In both catchments a significant portion of the area has soils with vertic properties. These soils are expected to show a relatively sharp switch from a condition of no overland flow in a dry or semi-dry state to a

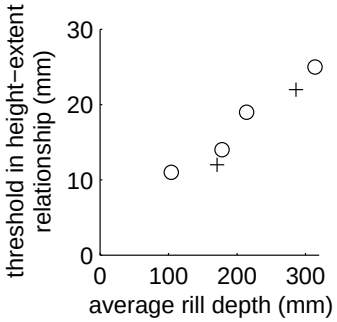

Figure 2.19: The relation between average rill depth and the location of thresholds in the height-extent relation of overland flow (see Figure 2.18) in Kaibo (+) and Horizontes (o).

condition with much overland flow when wet. The question remains however, at which state of wetness this occurs, and whether the hydrological relevance of this property at the catchment scale is not nullified by the spatial arrangement of the soil units or other factors such as e.g. vegetation. Finally there is the dichotomy between grass and no-grass (crops or trees) in the two catchments. No-grass implies in both cases that there is on average less soil coverage and a higher roughness. In Kaibo this is due to the arable cropping activities, and in Horizontes due to the effect of shading by trees and the hanging around of cattle. All these similarities suggest that a method for overland flow prediction should at least be applicable to both catchments to be of any use (Flanagan and Nearing, 1995; Gan and Burges, 1990). This correspondence does however not imply that overland flow patterns in the catchments are expected to be similar. The different location of the soil and vegetation units, relative to topography, rather suggest different overland flow patterns. On the basis of information from small experimental plots and in the literature about the Sahelian environment, one would in Kaibo expect no overland flow early in the season on agricultural land, and little overland flow on shrub-land, whereas later in the season the situation is the reverse (with much higher overland flow rates on the whole), mainly due to crust formation (Albergel et al., 1986; Albergel, 1987; Geelhoed, 1994). The effect of soil type and antecedent wetness is expected to be of little importance. In Horizontes, on the other hand, it are the vertic properties in combination with topography that are believed to be dominant over vegetation. This is due to the deeper soils, higher average catchment wetness, higher stability of the soil surface, and the close relation between vertic properties and topographic location. During early season especially the vertic soils are expected to produce low runoff rates, whereas in the late season these are expected to produce high runoff rates. These locations coincide generally with locations having a high upstream area.

The analysis in subsequent chapters (see especially Chapters 3 and 4) will nuance the above information, which is entirely based on existing literature. In the first place the marked effect of soil and vegetation differences on overland flow occurence needs to be proven, as well as the effects of season.

Uncertainty

The uncertainty of hydrological field data is rarely studied. The interest in this topic normally ends at the point where erroneous observations have been identified and removed and confidence in the integrity of the data has been established. During subsequent model identification or calibration sometimes a fixed observation error is assumed, but more commonly the observation error is neglected. It is clear from the estimated observation uncertainties, which may be as high as 20 %, that these are far from negligible here (see Table 2.10). The most eye-catching feature of the

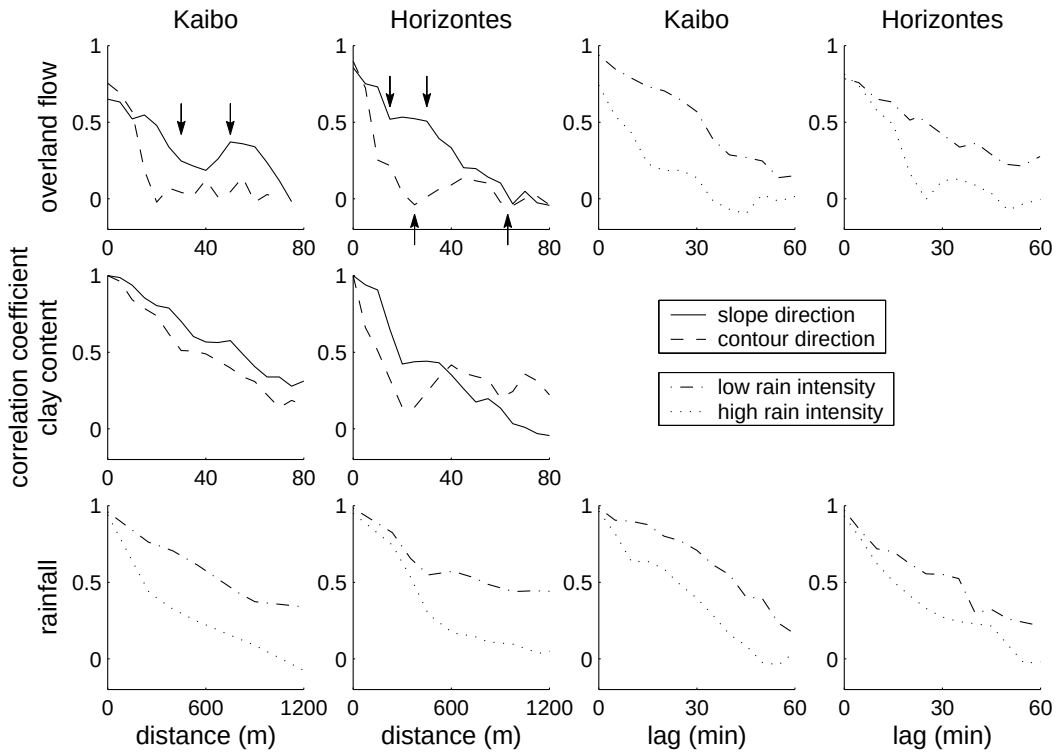

Figure 2.20: Autocorrelation of overland flow, clay content and rainfall in space (left two columns) and time (right two colums) for Kaibo and Horizontes. The arrows indicate the distances that are characteristic for the soil units in the area (see text).

observation errors in this study is perhaps the variability over different processes and observation techniques, and the relatively large contribution to the error through the process of interpolation or averaging. The question remains how stationary errors are and how they are actually distributed in space and time. These issues could not be investigated here due to data scarcity. To still get hold on the problem of understanding the contributions and structure of observation uncertainty, it has been broken down into three categories, viz. uncertainty caused by 1) measurement errors, 2) conversion errors, and 3) interpolation errors. It appeared that especially this last category contributed considerably to the observation uncertainty. Clearly, interpolation errors strongly depend on the mathematical techniques used for these purposes as well as the layout of the observations in space and time. For that reason these results are specific to these particular data sets and hard to generalize. Quite similar observations can however be found in the literature. where there is relatively much attention to the process of rainfall measurement. It has been illustrated by Ciach and Krajewski (1999) that, when disregarding malfunctioning of devices, especially the interpolation of rainfall observations leads to considerable errors. With regard to discharge observations, 4% change in peak discharge has been observed in controlled experiments on impervious surfaces that were repeated with nearly identical initial conditions (Wu et al., 1978, 1982). On pervious surfaces the situation is likely to become more uncertain. In a sprinkling plot experiment in Walnut Gulch it was found that, in spite of apparently equal initial conditions, observed peak discharges from runoff plots varied by nearly 35 % (Smith et al., 1994). These observations underline that the natural variability of hydrological processes is in general quite large. Since observation uncertainties provide the lower limit to the degree of accuracy that may be expected from models, the latter should not be expected to achieve a great degree of accuracy either.

Overland flow height and extent

The relationships derived in Section 2.6 highlight some aspects of overland flow that have not been encountered in the literature sofar. The relation between height and extent appears to be non-linear with several thresholds. The first derivative of the relation in Figure 2.18 (i.e. the change of the extent for a change in height) is very high. This implies that the observation of extent will be much more accurate than the observation of overland flow depth. This advantage of extent over height as an observable is enforced when considering the accuracy of the observation (especially when considering larger areas and low overland flow depths). The thresholds in the height-extent relationships appear to contain additional information about the geometry of the surface. This is illustrated in Figure 2.19, where the thresholds are related to the average rill-depth in the respective areas. This relation can be used to derive the effective rill density over an area (assuming constant rill form and depth), which is given by the slope of the relation. From the figure it can be concluded that this effective rill density remains constant for different levels of overland flow depth.

Correlation in space and time

The anisotropy of the overland flow distribution in space as well as time has been illustrated. Correlation lengths vary from 10 to 80 m for contour and slope directions respectively, and 25 to more than 60 minutes for intensive and non-intensive rain respectively. This property makes it difficult to model overland flow with geostatistical techniques, at least with the relatively small data set available in this study. Integration of secondary (indicator) data in prediction and simulation algorithms can alleviate some of the data problems. However, given that there are no clear-cut techniques available for this type of problem and that it is not even clear which secondary data will be suited for overland flow prediction, geostatistical techniques will not further be considered here.

3 Analyzing overland flow with a regression model

3.1 Introduction

In Chapter 2 it became clear that soil and vegetation units have marked effects on the occurrence of overland flow. The question arises whether these units can be used as building blocks for catchment scale overland flow prediction. This chapter tries to find an answer to this question by using the simplest possible class III model, in this way pursuing the ideas outlined in Section 1.3. The proposed model is static and only predicts total event overland flow, thus disregarding the heterogeneity whithin events. A second purpose of this chapter is to provide base-line predictions of overland flow, using a minimum of assumptions. These base-line predictions will later be used as a touch stone to which the results from more elaborate and demanding models are compared.

This chapter is organised as follows. In Section 3.2 the regression model is outlined. The model variables are derived from the original observations in Section 3.3. Section 3.4 shows the results of the model when used for spatial interpolation as well as extrapolation. The results are discussed and conclusions are drawn in Section 3.5.

3.2 Outline of a regression method for overland flow prediction

For the proposed regression approach a distinction is made between early season, late season, low rain intensity and high rain intensity conditions. In Table 3.1 the number of events for which the various overland flow and plot discharge as well as catchment discharge observations were made are listed. Note that for Kaibo the late season data for overland flow observations are lacking.

Table 3.1: Number of events for which overland flow data have been collected and a breakdown over season and rain intensity. o_h is overland flow height as observed during rain, o_p is the maximum overland flow coverage during an event, o_c is the number of full overland flow collectors at the end of an event, q_p is discharge from runoff plots, q_c is discharge as measured in the stream channel (see also Tables 2.1 to 2.3).

	Kaibo				Horizontes			Horicajo				
observation type	o_h	o_p	q_p	q_c	o_c	o_p	q_c	o_h	o_c	o_p	q_p	q_c
season average	2	2	14	60	5	7	60	5	5	7	15	31
early season	2	2	6	23	2	3	31	2	1	3	4	13
late season	-	-	8	37	3	4	29	3	4	4	11	18
low rain intensity	1	1	5	38	2	4	26	2	2	4	8	19
high rain intensity	1	1	9	22	3	3	34	3	3	3	7	12

In addition to this subdivision according to season and rain intensity, a spatial breakdown by the soil and vegetation classes is used as described in Section 2.6 (see Figures 2.4 and 2.10). Eventually the aim is to estimate overland flow height for each of these temporal and spatial

classes. To this end the various observations are converted to a similar unit, the *overland flow ratio* o^*, which is the total event overland flow height divided by the total event rainfall height. The uncertainty of the overland flow ratio is expressed by the relative root mean squared error (RRMSE, see Equation 2.1).

The o_h observations relate to this unit via summation over the relevant spatial and temporal domains. The conversion of o_p and o_c as well as the plot discharge q_p and catchment discharge q_c observations to o^* is described in detail in Section 3.3. The main steps for this conversion are as follows.

1. The maximum overland flow extent for an event (as determined by o_p) is related to the total event overland flow height, obtained by integrating the relevant o_h observations, on the basis of events and areas where both observations have been collected. A linear or power-relation is used for each vegetation class. The resulting quantity is named o_p^* (total overland flow height as estimated by o_p).

2. The number of full collectors (as determined by o_c) is related to the total event overland flow height (from o_h observations), on the basis of events and areas where both observations have been collected. A power-relation is used for each vegetation class, and the resulting quantity is named o_c^*.

3. The total-event plot discharge (during and till 10 minutes after rainfall, q_p^*) is related to total event overland flow height (from o_h observations), on the basis of events where both observations have been collected. A linear-relation is used for each plot.

4. The total-event catchment discharge (during and till 1 hour after rainfall, q_c^*) is related to total event overland flow height (from o_h observations), using a multi-variate linear model where each combined soil-vegetation class is one variable. For early and late season distinct relations are derived.

Subsequently the estimated total event overland flow depth for each period and soil-vegetation class is calculated by least squares estimation in the following way. First the estimated overland flow depth on basis of respectively o_h, o_p, o_c, q_p and q_c is written as a combination of five matrix equations. The separate matrix equations for a single event are

$$\begin{bmatrix} 1 & & \\ & \ddots & \\ & & 1 \end{bmatrix} \begin{bmatrix} o_1^* \\ \vdots \\ o_6^* \end{bmatrix} = \begin{bmatrix} o_{h,1}^* \\ \vdots \\ o_{h,6}^* \end{bmatrix} \Leftrightarrow \mathbf{I}\mathbf{o}^* = \mathbf{o}_h^* \tag{3.1}$$

$$\begin{bmatrix} 1 & & \\ & \ddots & \\ & & 1 \end{bmatrix} \begin{bmatrix} o_1^* \\ \vdots \\ o_6^* \end{bmatrix} = \begin{bmatrix} o_{p,1}^* \\ \vdots \\ o_{p,6}^* \end{bmatrix} \Leftrightarrow \mathbf{I}\mathbf{o}^* = \mathbf{o}_p^* \tag{3.2}$$

$$\begin{bmatrix} 1 & & \\ & \ddots & \\ & & 1 \end{bmatrix} \begin{bmatrix} o_1^* \\ \vdots \\ o_6^* \end{bmatrix} = \begin{bmatrix} o_{c,1}^* \\ \vdots \\ o_{c,6}^* \end{bmatrix} \Leftrightarrow \mathbf{I}\mathbf{o}^* = \mathbf{o}_c^* \tag{3.3}$$

$$\begin{bmatrix} g_1 & \cdots & & & 0 \\ & 0 & & & \\ \vdots & & g_3 & & \vdots \\ & & & 0 & \\ & & & & 0 \\ 0 & \cdots & & & 0 \end{bmatrix} \begin{bmatrix} o_1^* \\ 0 \\ o_3^* \\ 0 \\ 0 \\ 0 \end{bmatrix} = \begin{bmatrix} q_{p,1}^* \\ 0 \\ q_{p,4}^* \\ 0 \\ 0 \\ 0 \end{bmatrix} \Leftrightarrow \mathbf{J}\mathbf{o}^* = \mathbf{q}_p^* \tag{3.4}$$

$$\begin{bmatrix} \frac{A_{1,1}}{A_{tot,1}}g_1 & \cdots & \frac{A_{6,1}}{A_{tot,1}}g_6 \\ \vdots & & \vdots \\ \frac{A_{1,n}}{A_{tot,n}}g_1 & \cdots & \frac{A_{6,n}}{A_{tot,n}}g_6 \end{bmatrix} \begin{bmatrix} o_1^* \\ \vdots \\ o_6^* \end{bmatrix} = \begin{bmatrix} q_{c,1}^* \\ \vdots \\ q_{c,n}^* \end{bmatrix} \Leftrightarrow \mathbf{Ko}^* = \mathbf{q}_c^* \tag{3.5}$$

where the $*$-symbol indicates event-totals, the indices indicate crop-vegetation classes and the matrices are renamed at the righthand side for convenience. The first equation (3.1) seems redundant but is included for clarity (see Equation 3.6). Note that in equation 3.4, which gives the relation between observed discharge from runoff plots and the estimated overland flow depth, there are only observations for two soil-vegetation classes: grass on vertisol and grass on non-vertisol in both Kaibo and Horizontes. In Equation 3.5 $A_{i,j}$ stands for the area covered by soil vegetation class in catchment j and $A_{tot,j}$ is the total area of that catchment (so $\frac{A_{i,j}}{A_{tot,j}}$ is the relative area of the crop-vegetation class i in catchment j). There are 6 (sub-)catchments in Horizontes and only one in Kaibo. All values at the right-hand side are in *mm*. For each of the categories in Table 3.1 (i.e. season average, early season, etc.) all the relevant events are combined into a single matrix equation and total overland flow depth is divided by total event rainfall, thus yielding.

$$\begin{bmatrix} \mathbf{I} \\ \mathbf{I} \\ \mathbf{I} \\ \vdots \\ \\ \mathbf{J} \\ \vdots \\ \mathbf{K} \end{bmatrix} \mathbf{o}^* = \begin{bmatrix} \mathbf{o}_{h,1}^*/p_1 \\ \mathbf{o}_{h,2}^*/p_2 \\ \mathbf{o}_{p,1}^*/p_1 \\ \vdots \\ \\ \mathbf{q}_{p,1}^*/p_1 \\ \vdots \\ \mathbf{q}_{c,k}^*/p_k \end{bmatrix} \Leftrightarrow \mathbf{Lo}^* = \mathbf{y} \tag{3.6}$$

where $\mathbf{o}^* \equiv \frac{\mathbf{o}_i^*}{p_i} \forall\, i$, and the subscript numbers $i = 1 \ldots k$ denote the event numbers (the overland flow observations $\mathbf{o}_h^*$, $\mathbf{o}_p^*$ and $\mathbf{o}_c^*$ are available for only few events as shown in Table 3.1), and p_i is the rainfall in *mm* for event number i.

Since Equation 3.6 is over-determined a least-squares solution (i.e. estimates of $\mathbf{o}^*$) is easily found. However, to obtain realistic solutions to Equation 3.6, it is necessary to consider the observation errors which do not allow a statistical treatment (see Sections 2.4 and 2.8). Therefore here a deterministic solution is sought by assuming that the observation errors are unknown-but-bounded, which means that only the upper and lower bounds of the errors are known but any other information about its distribution is lacking. Hence the observation error (**e**) can be defined in terms of lower and upper bounds on **y**. The values listed in Table 2.10 are used as observation errors. Adding the observation errors to Equation 3.6 leads to a set of inequality equations

$$\begin{aligned} \mathbf{Lo}^* &\leq \mathbf{y} + \mathbf{e} \\ \mathbf{Lo}^* &\geq \mathbf{y} - \mathbf{e} \end{aligned} \tag{3.7}$$

A mini-max solution is determined for this set of equations using the simplex-based algorithm provided in Menke (1989). In some cases (Kaibo late season, and Horizontes early season) the minimization problem of Equation 3.7 is ill-posed. For that reason the following constraint is added to always obtain a unique solution.

$$\mathbf{Ko}^* = \overline{\mathbf{q}_c} \tag{3.8}$$

where $\overline{\mathbf{q}_c}$ is the total catchment discharge divided by total rainfall over the respective season. The mini-max solution minimizes the maximum deviation of observations from predictions. The

results of the above method appear to be equivalent to the weighted least-squares solution of equation 3.6, using variances proportional to the values in Table 2.10 and an $\infty-$norm.

The uncertainty of the derived $\mathbf{o}^*$-values is determined by cross-validation and expressed as RRMSE (see Equation 2.1). The cross-validation uses the following procedure.

1. a model is derived on the basis of all the observations at all locations except one observation type at one location; a location is defined at the model support (see Table 2.7).
2. the observations (for all available events) at the particular location are predicted by the derived model and the RRMSE values for these predictions are determined
3. step 1 and 2 are repeated for each location
4. the resulting RRMSE-values are averaged per soil and vegetation class

The reason for the spatial averaging in step 4 is that the observation density is too low and spread too uneven to allow a spatial interpolation on a statistical basis (e.g. through splines or kriging). The calculation of the RRMSE per soil and vegetation class still allows a spatial analysis of the error, albeit in a limited way.

3.3 Deriving model variables from original observations

Overland flow height and extent

As noted above, a relation between overland flow height and extent is required to relate o_h to o_p and o_c. The relations derived in Section 2.6 are defined for instantaneous values of extent. Since o_p and o_c give only event-maxima, the relations are not applicable to these data. Therefore new relations will be derived. For each event and spatial unit where a maximum extent is observed (o_p), the total event overland flow height is calculated by integrating the o_h observations for the respective area and event. It appears that different relationships can be distinguished in particular for different vegetation types, whereas soil plays no role. Figure 3.1 shows the results for Kaibo as well as Horizontes. The figure shows that a linear relationship is reasonable to relate the two quantities for shrub, arable crops and trees. For grass a power-relationship has to be used. Note that the equations are forced to pass zero.

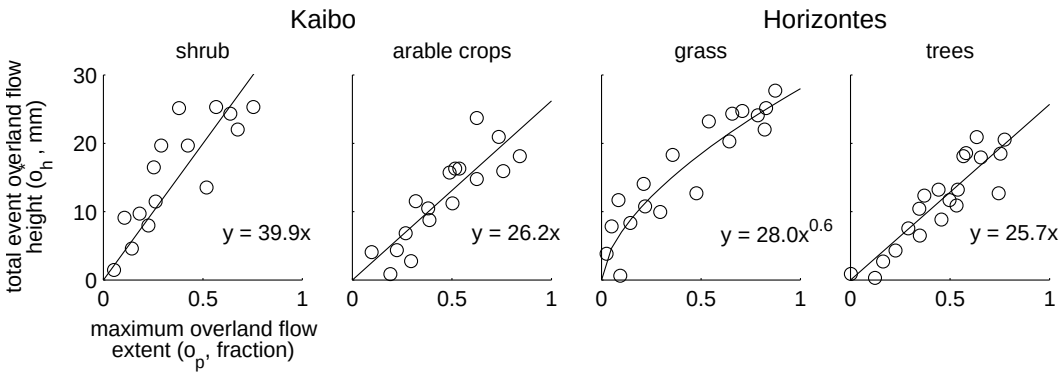

Figure 3.1: The relation between the maximum extent and total event overland flow height within vegetation classes.

Another estimator for the maximum overland flow extent over an event is the number of full collectors (as determined by o_c). In Horizontes 20 of such collectors have been used over 7 events,

and 24 over 5 events (see Tables 2.2 and 2.3). These observations are combined through normalization (division of the number of full collectors by the total number of collectors per vegetation class). Also in this case, vegetation is far more discriminating than soil and therefore only the relations between o_c and o^* are shown per vegetation class in Figure 3.2. A power function is used to describe the relation between the two quantities. Note that only a small part of the o_p, o_c and o_h observations are used to derive the relations in Figures 3.1 and 3.2.

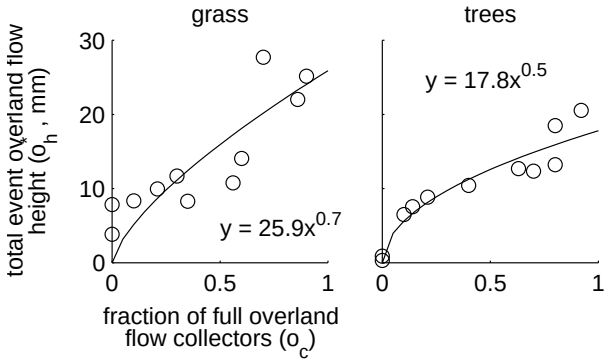

Figure 3.2: The relation between the number of full collectors and total event overland flow height within vegetation classes, for Horizontes.

Overland flow height and catchment discharge

The total-event plot discharge (q_p) and catchment discharge (q_c) is related to total event overland flow height (from o_h observations), using a multi-variate linear model where each combined soil-vegetation class is one variable. For early and late season distinct relationships are derived. In Table 3.2 the values of the six parameter estimates, as well as their standard deviation, are given for both early and late season. For Kaibo there are no data available to derive the late-season parameters. Since there are clear correspondences between the parameters for Horizontes and Kaibo in the early-season situation, the late-season parameters for Horizontes are used as late-season parameters for Kaibo as well in what follows. Note that in Table 3.2 only the value of g_i and its standard deviation is given (i.e. omitting the relative area $\frac{A_{i,j}}{A_{tot,j}}$, viz. Equation 3.5). Only part of the o_h, q_c and q_p data were used for this derivation. The parameter values provide two insights. In the first place the relative parameter differences between the classes indicate which of these are related to relatively high or low overland flow heights. Secondly, the average value of the parameters indicates whether there is, on the whole, re-infiltration of overland flow before it reaches the catchment outlet (in that case the average parameter value is smaller than one), or sub-surface flow (average parameter values bigger than one). The first interpretation learns that especially soil-vegetation classes g_4 to g_6 produce much overland flow in Kaibo and Horizontes in early season. The second interpretation shows that especially in Kaibo re-infiltration plays a large role in early season, especially on vertic soils. In Horizontes this is less the case. In late season it appears that some sub-surface flow takes place, especially on non-vertic soils and grass vegetation.

Table 3.2: The parameter values of a multivariate linear model, relating total overland flow of each soil-vegetation class to catchment discharge, for early and late season respectively (see Equation 3.5). For 'Kaibo - Late Season', only the q_p data were available for calibration, hence the values for g_2, g_4, g_5 and g_6 are missing. The value in brackets gives the standard deviation of the parameter estimate.

		Early Season		Late Season	
parameter	soil/vegetation	Kaibo	Horizontes	Kaibo	Horizontes
g_1	vertisol - grass	0.07 (0.02)	0.01 (0.02)	0.87 (0.49)	1.02 (0.31)
g_2	vertisol - no-grass	0.08 (0.04)	0.04 (0.02)	-	0.87 (0.23)
g_3	no-vertisol - grass	0.13 (0.09)	0.09 (0.06)	0.36 (0.23)	0.43 (0.13)
g_4	no-vertisol - no-grass	0.19 (0.10)	0.12 (0.09)	-	0.37 (0.16)
g_5	shallow - grass	0.18 (0.07)	0.22 (0.08)	-	0.41 (0.26)
g_6	shallow - no-grass	0.17 (0.06)	0.16 (0.10)	-	0.87 (0.29)

3.4 Results

Discharge at the catchment outlet

To get a first impression of the model performance the discharge predictions by the model are compared to the observed values. In Figure 3.3 the event totals of predicted versus observed discharge are plotted as a fraction of total event rain. For Kaibo the model slightly over-predicts discharge (especially low discharge ratios) and for Horizontes the model slightly under-predicts discharge (especially at high discharge ratios). There is no apparent difference between calibration and validation events. In Figure 3.4 the deviations of these predictions over the season are shown. The structured pattern for Kaibo is caused by the fact that 1997 was a dry year with very little discharge. For the decreasing trend in the prediction error for Horizontes no explanation was found.

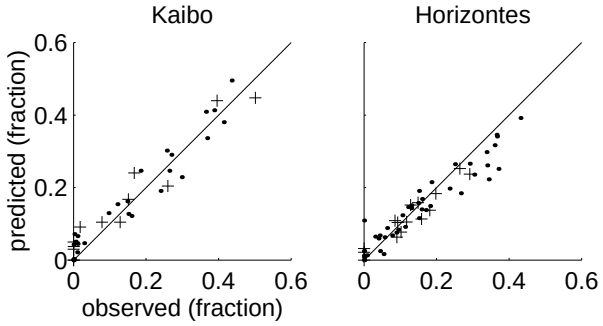

Figure 3.3: Observed versus predicted discharge ratios (event totals of discharge as fraction of total event rain) at the outlets of Kaibo and Horizontes for the calibration (•) and validation (+) data.

Spatial prediction

Spatial predictions of overland flow depth are made, using the model of Equations 3.7 and 3.8, the data described in Sections 2.2 and 2.3, and the relations shown in Figures 3.1 and 3.2. The observations used to establish the relations in Figures 3.1 and 3.2 and the parameters of Table 3.2 are not used in the predictions.

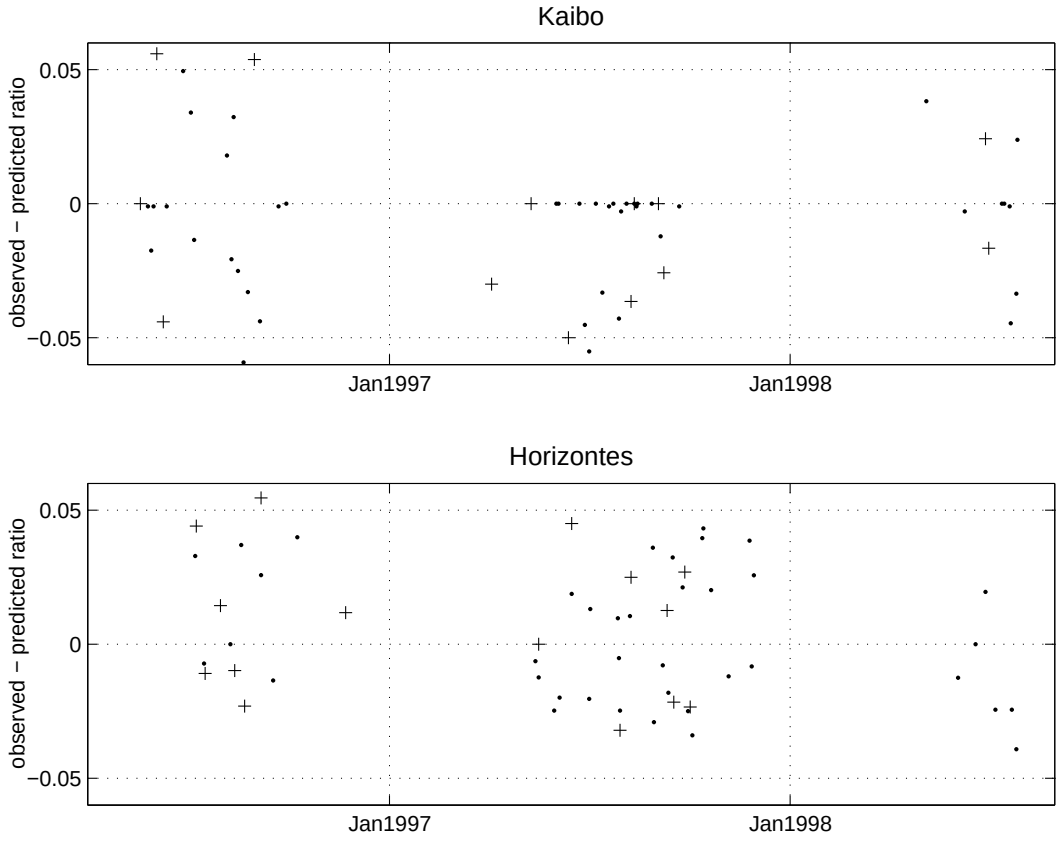

Figure 3.4: The difference between observed and predicted discharge ratios over time for Kaibo and Horizontes.

The results for the seasonal average overland flow ratio are shown in Figures 3.5 and 3.6, and the results for early and late season, as well as for low and high rain intensity are shown in Figures 3.7 and 3.8. In these figures the color scale is varied to focus on the spatial patterns (i.e. the effect of soil and vegetation), rather than on the differences between the figures. Seasonality appears to effect the impact of vegetation as well as soil. Especially the effect of vertisols in both Kaibo and Horizontes is striking: in early season overland flow is very low, whereas in late season the overland flow on these is high. In addition, the effect of crops/trees for Kaibo/Horizontes changes markedly over the season. In early season overland flow is lower than average, whereas in late season it is higher than average for these vegetation classes. It is noteworthy that the RRMSE of the prediction, which was obtained through cross validation is in many cases only slightly higher than the effective observation error (see Table 2.10), which implies that the model performs relatively well. In addition it turns out that the relative RRMSE is often high for small overland flow ratios (especially in early season and for low rain intensities). This implies that model error increases less with the predicted value as observation error does with observed values.

Extrapolating overland flow and discharge observations

The ultimate test of the suitability of the soil, vegetation and topographic classes is by testing the predictive capabilities of the observations at one of these classes not through interpolation, but through extrapolation. Here an attempt is made to perform such tests. Spatial extrapolation is applied by using the observations for the Horicajo sub-catchment to make predictions for the

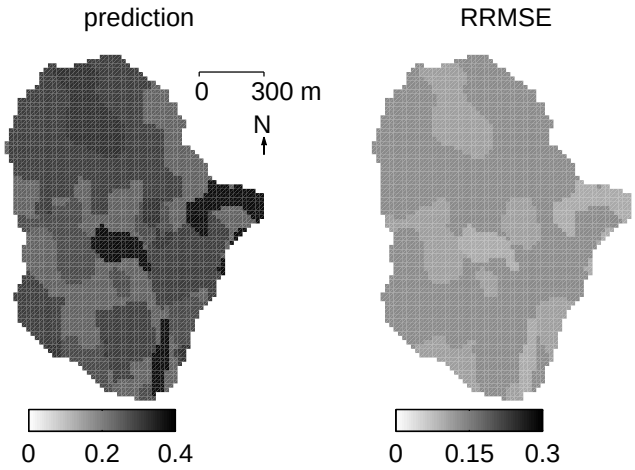

Figure 3.5: Predicted average overland flow ratio and RRMSE over the season for Kaibo.

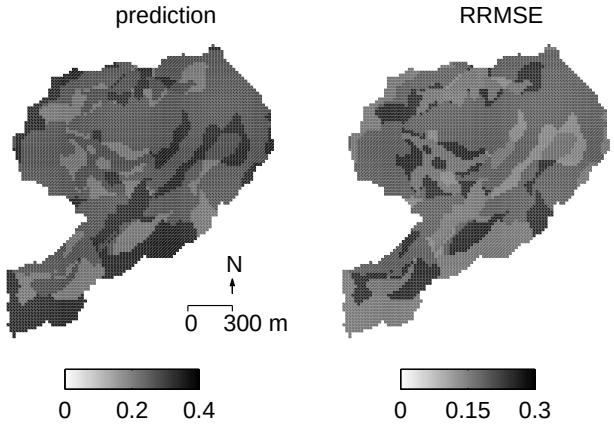

Figure 3.6: Predicted average overland flow ratio and RRMSE over the season for Horizontes.

same events over the entire Horizontes catchment. The procedure for this spatial extrapolation is as follows.

1. Overland flow depth and discharge are calculated on the basis of the observations in Horicajo for the various spatial units (formed by the soil-vegetation classes), whereby the observations used for parameterization (viz. Figures 3.1, 3.2 and Table 3.2) are omitted.

2. The values obtained for each spatial unit are assigned to the corresponding spatial units in the Horizontes catchment.

3. The average overland flow depth and discharge values are calculated for the three other sub-catchments of Horizontes (coded as resp. c, d and b & e together in Figure 2.13).

4. The estimated sub-catchment values are compared to the observed overland flow depths and discharge values per sub-catchment.

The predictive capabilities with regard to both discharge and overland flow are shown in Figure 3.9. The 124 data points in the left-hand graph result from 31 events over 4 sub-catchments, and the 42 points in the right-hand graph from 6 soil-vegetation units over 7 events. It turns out that

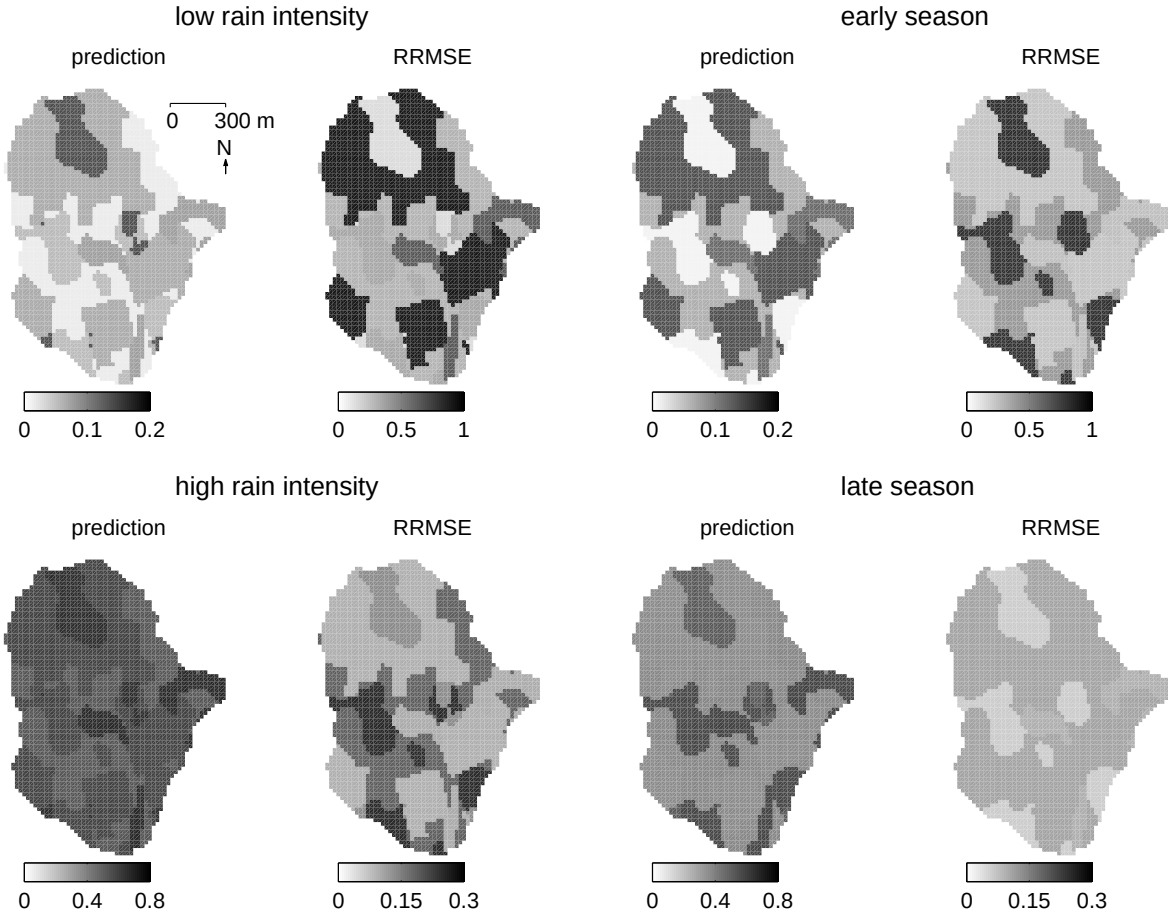

Figure 3.7: Predicted average overland flow ratio and RRMSE for low/high rain intensities and early/late season, Kaibo.

the prediction of discharge in the other sub-catchments of Horizontes by applying the model derived for Horicajo is quite well possible. Note that discharge prediction is possible by the last part (Equation 3.5) of the total overland flow regression model (Equation 3.6). In contrast, the extrapolation of overland flow gives worse results. A possible explanation for this phenomenon is that discharge is determined by two lateral flow components, viz. overland flow and sub-surface flow, whereby the total lateral flow is easier to predict than that of one of its components. Alternatively, this discrepancy can be attributed to the relative low overland flow observation density over Horizontes (i.e. a shortcoming in the measurement layout). Since there is no evidence for a different partitioning of the lateral flow components in Horicajo compared to Horizontes, the last explanation seems most likely.

3.5 Discussion and Conclusions

Combining different observations with a regression approach

The regression method presented in this chapter ties up different kinds of observations such as manually observed overland flow heights, overland flow in collectors and catchment discharge, via a two step approach: 1) by using linear and non-linear measurement equations to relate each observed quantity to the total-event overland flow height, and 2) by combining these overland flow

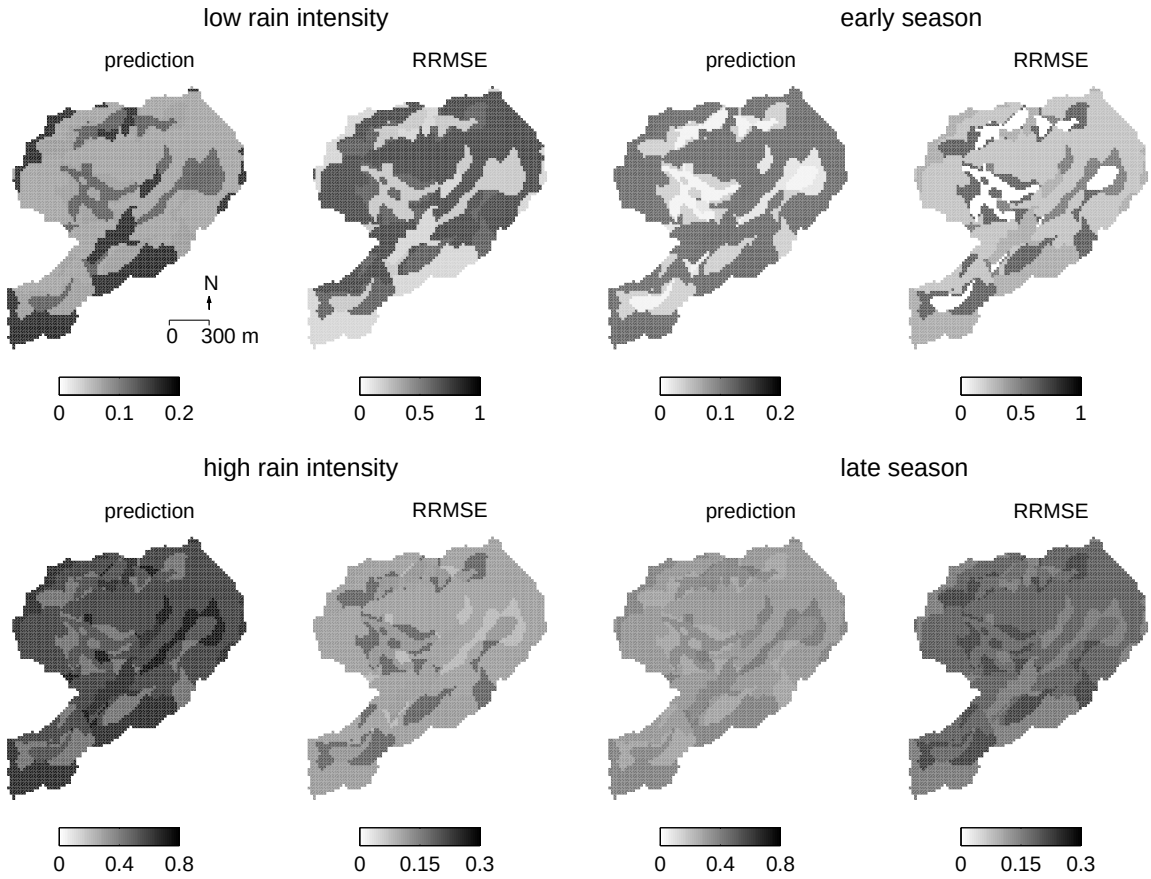

Figure 3.8: Predicted average overland flow ratio and RRMSE for low/high rain intensities and early/late season, Horizontes.

height observations from different sources in a linear problem with inequality constraints. In spite of the considerable observation errors (see Table 2.10), a unique solution can be found by using a mini-max criterion. The method is computationally very simple, which allows its application to large data sets and the calculation of the model performance via cross-validation as explained in Section 3.2.

Spatial predictions

It seems feasible to spatially predict overland flow occurrence with the proposed regression approach. Notwithstanding the substantial prediction errors (note that these are expressed as *relative* root mean squared error, see Equation 2.1), these do not overshadow the information contained in the overland flow predictions. Distinguishing between early and late season as well as between high and low intensity rain contributes substantially to this result. This is shown by the reduction of the prediction error when applying a seasonal breakdown or a breakdown according to rain intensity, relative to the prediction error when using a single model for the entire season. The subdivisions also provide some information about the processes that cause overland flow in the areas. In Kaibo overland flow depths are in particular high in late season on shallow soils with a shrub vegetation, and with high rain intensities on vertisols and shallow soils with a shrub vegetation. Low overland flow depths are encountered on vertisols in early season and on deep soils at low rain intensities. Apparently, saturation of the top-soil occurs on the shallow soils in late season and

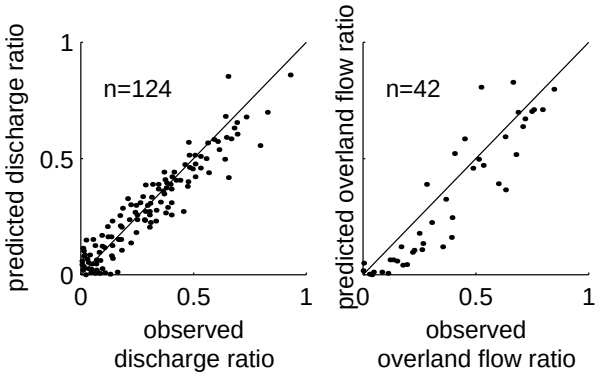

Figure 3.9: The relation between predicted and observed discharge and overland flow ratios. Predictions are based on extrapolation of observations in Horicajo.

intense-rainfall situations. The shrub vegetation occurs relatively often in combination with shallow soils and is associated with a relatively smooth and compact soil surface, which has a lower infiltration capacity than the equivalent soils under arable land. In Horizontes it are in particular the shallow soils that produce high overland flow depths, low overland flow depth is encountered on vertisols in early season and on deep soils with trees at low rain intensities.

The static model as a predictive tool

The possibility to use the model for predictive purposes was investigated in Section 3.4. The limited test (a split-catchment approach) for Horizontes showed that the prediction of discharge was possible but that overland flow prediction gave unsatisfactory results. The failure to predict overland flow sufficiently well was attributed to the low observation density of overland flow depth in Horizontes. Unfortunately such a test was not possible in Kaibo where there was only one discharge measurement location. In view of these results it is difficult to assess the predictive power of the static model presented here. At this point the question is relevant whether a different modelling approach would not be more appropriate for this predictive purposes. A dynamic (semi-) distributed model would be the natural candidate, given the widespread availability and use of these models. These models will however be equally difficult to evaluate for predictive purposes for the reasons given above. In the next chapter however, an attempt is made to investigate and predict overland flow with a distributed model.

4 Analyzing overland flow with a parameter distributed model

4.1 Introduction

It has been explained in Chapter 1 that overland flow is defined as that part of surface flow which has yet not entered channels of a given size. It may be caused by saturation of the soil from below (saturation excess) or above (infiltration excess). The conditions under which either infiltration excess or saturation excess may lead to overland flow have been studied in depth (Dunne et al., 1975), and in addition the quantitative description of overland flow hydraulics has received considerable attention in hydrology (e.g. Emmett, 1970; Moore and Foster, 1990; Parsons and Abrahams, 1992; Stone et al., 1996). It was also argued in Chapter 1 that infiltration and overland flow routing have been common components in distributed parameter models of catchment hydrology since the late sixties. The fact that functional relations as well as solution schemes used in these models remained largely unchanged since their conception in the early seventies could be interpreted as the relative mature understanding of this part of the hydrological system (e.g. Crawford and Linsley, 1966; Dooge, 1973). However, in spite of the understanding of these processes at the plot-scale, and the availability of distributed parameter models a quantitative prediction of overland flow or even a qualitative prediction of overland flow patterns *at the catchment scale* is not easily made. A main reason for this is the large heterogeneity of the factors controlling overland flow in combination with the limited ability to measure these factors (de Lima, 1989). This heterogeneity is believed to be especially apparent in dry catchments with a pronounced seasonal climate (Gan et al., 1997). In contrast with the distributed observation of atmospheric processes and some more static properties of the earth surface through remote sensing techniques, very little progress has been made in observing lateral water fluxes at the land surface. When considering overland flow, it appears that only saturation, discharge at the downslope end of slopes or the redistribution of a tracer have been measured in a few field experiments (e.g. Abrahams et al., 1986, 1989; Burt and Butcher, 1986; Scoging, 1992a). These variables are only indirectly linked to overland flow depth, duration or extent. So there is a kind of deadlock in both observation and modelling of overland flow: distributed models are believed to be finished (at least conceptually) but unfortunately of little purpose due to data scarcity. This implies there is, in general, no reason to collect field data from both a scientific (the system is understood) or an engineering (the model requires excessive amounts of field data for applications) viewpoint.

In this Chapter some of the underlying premises leading to this stalemate are critically investigated, concentrating on the two catchments that have been described in Chapter 2. A distributed parameter model for overland flow prediction in these catchments is proposed and with regard to this model three questions are investigated in particular:

1. Can the model be calibrated, in the sense that a set of nearly optimal parameters is derived which which can be used for predictive purposes?

2. How does the proposed model for overland flow compare with the alternative regression approach outlined in Chapter 3?

3. Does the model reproduce some of the spatial heterogeneity of overland flow?

This Chapter is organized as follows. In section 4.2 the overland flow model and its parameterization is outlined. This is followed by an explanation of the calibration procedure employed. Then, in section 4.4, the validity of the model is tested on the basis of discharge and overland flow observations. In Section 4.5 overland flow patterns in space and time are analyzed and compared to those of Chapter 2. The spatial heterogeneity of the predicted overland flow is compared to that of the observations in Section 4.6. Finally, results are discussed in Section 4.7.

4.2 Model description

The spatial distribution, coverage and depth of overland flow has been observed directly for only a limited number of events. Therefore an integrative framework is required to use the remaining data, mainly discharge but also information from infiltration experiments, to infer overland flow from the indirect observations. For this purpose a distributed overland-flow model is used, which will be described here.

The overland flow model describes infiltration by a simplified Green-Ampt infiltration model

$$r(x,t) = A(x,t) + \frac{b(x)}{t} \tag{4.1}$$

where $r(x,t)$ is the instantaneous infiltration rate in $mm\,min^{-1}$, $A(x)$ the final infiltration rate after a long period of rain in $mm\,min^{-1}$, $b(x)$ the soil moisture storage fill in *mm* and t is time after the start of a rainfall event in *min*. The soil moisture storage fill $b(x)$ is assumed to be a function of the following antecedent wetness index

$$b(x) = \frac{B(x)}{\overline{P}(x)} \sum_{k=1}^{10} \frac{P(x,k)}{k} \tag{4.2}$$

where k is an index indicating the day preceding the event, $P(x,k)$ is the rainfall at day k in *mm*, $\overline{P}(x)$ is the average rainfall over the decade preceding the event, and $B(x)$ is the soil moisture storage fill for average decade rain conditions in *mm*.

Rain excess, $e(x,t)$, is defined as

$$e(x,t) = p(x,t) - i(x,t) \tag{4.3}$$

where $p(x,t)$ is rain rate in $mm\,min^{-1}$.

The continuity and flow equation are given by

$$\frac{\partial q(x,t)}{\partial x} + \frac{\partial h(x,t)}{\partial t} = e(x,t) \tag{4.4}$$

$$q(x,t) = h(x,t)\sqrt{\frac{gh(x,t)sin(\beta(x))}{12f(x,t)}} \tag{4.5}$$

with

$$f(x,t) = fa(x) - \frac{h(x,t)}{fb(x)} \tag{4.6}$$

where $q(x,t)$ is unit width discharge in $mm^2\,min^{-1}$, $h(x,t)$ is flow height in *mm*, g the gravitational constant: 9810 $mm\,s^{-2}$, $\beta(x)$ is the slope gradient (-), $f(x,t)$ the Darcy-Weisbach friction factor, $fa(x)$ is the intial friction (-) and $fb(x)$ the rate of friction loss with increasing flow depth in

mm. Note that $\sqrt{\frac{gh(x,t)sin(\beta(x))}{12f(x,t)}}$ in equation 4.5 represents flow velocity, $V(x,t)$, in $mm\,min^{-1}$. For solving this system of equations a simple backwards difference finite difference solution is used:

$$\frac{q(x,t-\Delta t)-q(x-\Delta x,t-\Delta t)}{\Delta x}+\frac{h(x,t)-h(x,t-\Delta t)}{\Delta t}=e(x,t) \tag{4.7}$$

Which yields after rearrangement, and solving for $d(x,t)$:

$$h(x,t)=h(x,t-\Delta t)+e(x,t)\Delta t+\frac{\Delta t}{\Delta x}\left[q(x-\Delta x,t-\Delta t)-q(x,t-\Delta t)\right] \tag{4.8}$$

Initially, the flow depth at $t=t_0+\Delta t$ is determined entirely by $e(x,t)$, since inflow at the boundaries is zero. Routing over the surface is done by a drainage net which is calculated according the D8 algorithm by O'Callaghan and Mark (1984).

The above scheme appears to be stable for the spatio-temporal discretization of 20×20 m and 10 s, so that application of more complex difference schemes (e.g. a Lax-Wendroff scheme) is not required. The spatial resolution implies a problem with 6800 state variables for Kaibo and 8000 state variables for Horizontes. The model is a class II model (see section 1.3) in which infiltration is described empirically, lateral subsurface flow is absent and overland flow is represented by the kinematic wave approximation. The soil and vegetation classes (see Figures 2.10, 2.4) are used for parameter zonation (i.e. for each class a single parameter vector is allowed). The soil-vegetation classes are listed in Table 4.1 and a brief description of the four model parameters is given in Table 4.2.

Table 4.1: Coding of the different combinations of soil and vegetation (for Horizontes) and land use (for Kaibo) types.

code	soil	vegetation / land use
1	deep, vertic	non-trees / arable land
2	deep, vertic	trees / shrub land
3	deep, non-vertic	non-trees / arable land
4	deep, non-vertic	trees / shrub land
5	shallow	non-trees / arable land
6	shallow	trees / shrub land

Table 4.2: Parameter values assumed to be constant for the overland flow model.

code	unit	description
fa	–	initial Darcy-Weisbach friction
fb	*mm*	rate of loss of friction with increasing overland flow depth
A	$mm\,min^{-1}$	infiltration parameter: final infiltration rate
B	*mm*	infiltration parameter: soil moisture storage fill

4.3 Model calibration

It is well-known that a mini-max solution as in Section 3.2 cannot be easily found for non-linear models, as the model described by Equations 4.1 to 4.6. Therefore the model has been calibrated using an 2-norm, weighting all observations equally and using the (direct) controlled random

Table 4.3: An overview of the model entities to which the various observations are matched in the calibration.

		model unit		
	observations	time	space	matching with
q_c	discharge - catchment	1 min	grid cell[a]	catchment outlet
q_p	discharge - plot	1 min	grid cell	grid cells with upslope reaches of similar size with similar soil and vegetation
o_h	overland flow - height	2 min	grid cell	grid cells with upslope reaches of similar size with similar soil and vegetation
o_c	overland flow - collectors	event	vegetation unit	corresponding vegetation, using the number of full overland flow collectors and Figure 3.2
o_p	overland flow - paths, zero coverage	event	grid cell	grid cells with upslope reaches of similar size with similar soil and vegetation
o_p	overland flow - paths, maximum coverage	event	slope reach	upslope reaches of similar size with similar soil and vegetation, using maximum coverage and Figure 3.1
s	water table depth	event	slope reach	upslope reaches of similar size and with similar soil and vegetation
w	soil moisture	event	grid cell	grid cells with similar upslope reaches of similar size and with similar soil and vegetation

[a] only at the catchment outlet

search method introduced by Price (1979) with the software described in Stol et al. (1992). The reason for using a direct search method, as opposed to derivate-based optimization methods, is that the former is more robust (e.g. Johnston and Pilgrim, 1976; Hendrickson et al., 1988; Sorooshian et al., 1993). Table 4.3 lists to which model units the various observations are matched. More specifically, Table 4.3 gives the units over which the observations are averaged when used as calibration data. Clearly, very few model units will correspond exactly with the observation unit in terms of upstream area, soil, and vegetation type. On the other hand, it is undesirable to use an observation only for matching at a single grid cell, since this leaves the parameterization problem extremely ill-conditioned (e.g. Duan et al., 1992). To solve this problem a similarity index is used to determine the degree of correspondence between an observation unit with model units at other locations in the catchment. The upstream area and soil-vegetation classes are used for this purpose. The similarity index is calculated as follows.

$$S_{i,j} = \sqrt{\left(\frac{\sum_{c=1}^{6} \left(A_{obs,i,c} - A_{mod,j,c} \right)}{A_{mod,j}} \right)^2} \tag{4.9}$$

where $S_{i,j}$ is the similarity index for observation i and grid cell j. The index c ($= 1...6$) indicates one of the six soil-vegetation classes. $Amod_j$ (in m^2) is the upstream area for grid cell j. $A_{obs,i,c}$ (in m^2) is the area of soil-vegetation class c within the upstream area of observation i; and $A_{mod,j,c}$ (in m^2) is the area of soil vegetation class c within the upstream area of model grid cell j. Only those grid cells j are considered that have an upstream area close to A_i, i.e. $A_j = A_i \pm tolerance$. In this study the tolerance is set to $0.1A_i$. The weight attributed to an observation i in determining the value of a model unit j is inversely proportional to $S_{i,j}$. The uncertainties associated with each of the model variables are taken from Table 2.10. As noted previously, the algorithm chosen for

model calibration is a controlled random search procedure with constraints on the parameters. It gradually improves an initial set of parameters by replacing the worst parameter vector from the set by a better one. Optimization is done for six times four parameters (fa, fb, A and B, see Equations 4.1, 4.2 and 4.6), one for each soil-vegetation unit. After calculating for each observation i and all grid cells j the similarity indices $S_{i,j}$ (Equation 4.9), the parameter vector $\theta = [fa, fb, A, B]$ for each soil-vegetation unit is derived in the following way.

1. Generate around each initial parameter vector, 10^3 new vectors using a latin hypercube sampling scheme.

2. Determine the performance of each parameter vector by the following performance index

$$C := \left(\sum_{i}^{I} \sum_{j}^{J} \left| pred_{i,j} - \frac{obs_i}{S_{i,j}} \right|^2 \right)^{0.5}$$

   where I the total number of observations; J is the total number of grid cells; $pred_{i,j}$ is the model prediction related to observation i for grid cell j; obs_i is observation i; and $S_{i,j}$ is as defined in Equation 4.9. The best performing parameter vector is indicated by θ_b, with performance C_b, the worst performing parameter vector by θ_w with performance C_w, and the average parameter vector is indicated by $\overline{\theta}$ with performance $\overline{C}$.

3. A new parameter vector is generated based on the following procedure: a) one parameter vector θ is chosen randomly out of the existing vectors, b) an average parameter vector $\overline{\theta}$ is calculated on the basis of the existing parameter vectors minus the selected vector, c) the new parameter vector is calculated by $\theta_n = 2\overline{\theta} - \theta$.

4. If the generated new parameter value is outside the hypercube defined by the parameter set bounds, a new set of parameter values is generated (step 1), using the up-to-date hyperbox (see step 6).

5. Calculate C for θ_n (C_n), and replace the worst-performing parameter vector θ_w with θ_n if $C_n > C_w$.

6. Re-calculate the enclosing hyperbox for the new set of parameters.

7. Repeat the procedure from step 4, until $\left\| \frac{d\overline{C}}{d\theta} \right\|_2 < \frac{C_w - C_b}{C_b}$ (the 2-norm of the first derviate of $\overline{C}$ with respect to the calibrated parameters becomes smaller than a stop-criterium).

After deriving the parameter vector sets for the six soil-vegetation units (in a random order), the seven-step procedure is repeated several times, thereby again selecting the order of six soil-vegetation units randomly and each time randomly selecting values from the existing optimized parameter vector sets as initial values. The initial parameter values, which are listed in Table 4.4, are determined on the basis of observations on $1\,m^2$ runoff plots in Kaibo and with a Guelph permeameter in Horizontes (see Sections 2.2 and 2.3). More detailed information about the optimization procedure applied here, can be found in Hendrickson et al. (1988) and Price (1979).

The model is calibrated and validated for both Kaibo and Horizontes. As calibration data at first only the calibration events indicated in Table 2.1 have been used for Kaibo, and only the calibration events indicated in Tables 2.2 and 2.3 for Horizontes. Thereafter the calibration has been repeated, using both calibration and validation data in Tables 2.1, 2.3 and 2.2. For the case that only calibration data are used, the results are shown in Table 4.4. The results for using both calibration and validation data are shown in Table 4.5. The calibration is done on those two data

sets for two reasons: 1) to investigate the dependence of the optimal parameter values on the size of the calibration data set, 2) to enable the intercomparison with the results in Chapter 3, where the modelling approach required all data to be used for calibration. When comparing the results, in Tables 4.4 and 4.5, it is striking how little these differ. Apparently there is not much additional information contained in he validation data set. As shown in the tables the initial parameter values for the calibration procedure are equal for the two cases. The sensitivity to this initial value was also investigated. It appeared that, when selecting initial parameter values in the range 0.5 - 2 times the values listed in Table 4.4, different optimum parameter vectors were found. The range over which the optimum parameter vectors varied was not big. They were always located within the range of parameter values that yield $C - values$ within 10% of C_b (these ranges are given in Table 4.4 as well). The limits of those ranges were always quite constant and insensitive to the initial parameter vectors. Note that all parameters are assumed to be constant over time, which is probably a wrong assumption, considering some results that will be presented later. In Section 4.4 the validity of using the parameter ranges instead of single parameter values will be investigated.

4.4 Model validation

Preceding the interpretion of the model output, the model behaviour will be tested first. This testing, which will subsequently be called model validation, is in the first place done on basis of the discharge as well as overland flow data from both Kaibo and Horizontes. This is followed by an assessment of the antecedent wetness as a relevant factor for the model on the basis of Horicajo data. Finally the sensitivity of the predictions to changes in the parameter values is evaluated.

Discharge at the catchment outlet

In Figure 4.1 the event totals of predicted versus observed discharge (as a fraction of total event rain) are plotted and in Figure 4.2 the deviations of these predictions over the season are shown. From the plots can be inferred that discharge is not reproduced exceptionally well (viz. Figures 3.3 and 3.4). For both Kaibo and Horizontes the model slightly over-predicts for low ratio's and under-predicts at high discharge ratio's. An analysis of the prediction errors over time (see Figure 4.2) reveals that the prediction for both catchments has a negative bias, is skewed, and that there is no special trend over time or a demonstrable effect of seasonality for Horizontes, but that there is a strong negative bias for Kaibo in 1997. Especially for Horizontes the validation data seem to be reproduced worse than the calibration data.

To quantify the deviation of predictions from observations three statistical indices are used: relative root mean squared error (RRMSE), bias and the coefficient of efficiency (E_f) (Aitken, 1973; Green and Stephenson, 1986; Gupta et al., 1998; Nash and Sutcliffe, 1970). The three statistics are listed for the calibration and validation runs in Table 4.6. It appears that for the validation data considerably lower performance is obtained, which points at the likely over-parameterization of the model. Furthermore the table shows that the three statistics are stronlgy correlated. Therefore only the RRMSE will be used as a summary statistic in what follows.

Overland flow depth at various resolutions

The validation of the model with regard to its capability to predict the overland flow depth is done with the direct observations of overland flow (the observations o_h, o_c and o_p in the 'validation set' of Tables 2.1, 2.2 and 2.3). In Figure 4.3 the correspondence between these observed entities and the prediced values are shown for three levels of spatial averaging, i.e. averages for: 1) single grid cells (o_h) or for upslope reaches (o_c and o_p); 2) soil-vegetation units; and 3) an entire

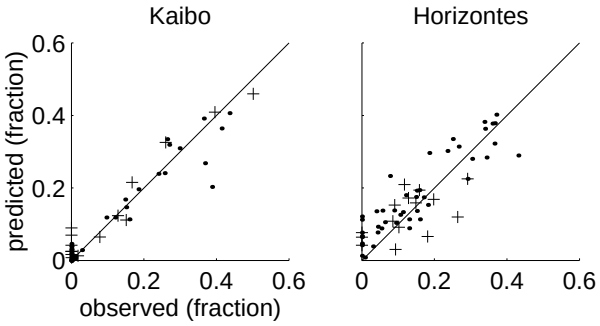

Figure 4.1: Observed versus predicted discharge ratios (event totals of discharge as fraction of total event rain) at the outlets of Kaibo and Horizontes for the calibration (•) and validation (+) data.

catchment. Not surprisingly, for increasing levels of spatial averaging the correspondence between observations and predictions increases (see Figure 4.3). The relatively large improvement when moving from the single grid cell or upslope reach to an average for the soil-vegetation unit, in comparison to that for moving from the soil-vegetation unit to the catchment is striking. It implies that the size of soil-vegetation units level out a large part the heterogeneity that is not captured by the distributed model.

In spite of the considerable scatter when considering the aggregation level of the grid cell or upslope reach, in all cases the correlation between observed and predicted overland flow ratios is quite large and gives no reason to reject the proposed model as improper for the system at hand.

The effect of pre-event wetness

Pre-event wetness (sometimes also called *antecedent wetness* in the hydrologic literature) is explicitly incorporated in the model via Equation 4.2. The fact that this term is commonly not encountered in similar parameter-distributed models (see Section 4.7) raises questions about its usefulness or validity. The effect of pre-event wetness on overland flow is studied here only for Horicajo, since this is the only site where the initial soil moisture content has been measured over a dense network. In Figure 4.4 the relation between pre-event soil moisture in the top 20 cm of a grid cell (an average of several TDR observations in that grid cell up to two days before an event, see Section 2.5) and predicted overland flow depth for that grid is shown for different soil and vegetation units in the two figures at the left. In the two figures at the right the same relation is shown but now with the average pre-event soil moisture content of the entire area upslope from the grid cell where overland flow is observed. The relation pictured in Figure 4.4 is in fact strongly supporting the assumption that pre-event wetness is positively related to overland flow (via Equation 4.2 it does so by reducing the infiltration) for all soil and vegetation types (at least for Horicajo). Furthermore it is shown that the pre-event soil moisture condition of the entire upslope area is much better related with the overland flow depth at a downslope grid cell than the soil moisture condition of the grid cell itself. Especially this last observation is a new insight. However a soil moisture - overland flow relationship helps to understand the occurence of overland flow, it does not provide a means to observe overland flow indirectly because soil moisture observations over large volumes are costly and perhaps even more difficult to acquire than direct overland flow observations (van Loon and Troch, 2002). This becomes even more apparent when the temporal change of soil moisture is considered for the different soil units. Figure 4.5 illustrates this by showing the ranges and averages of observed soil moisture content for the three different soil classes considered in this study. The soil moisture content of e.g. the shallow soils may be

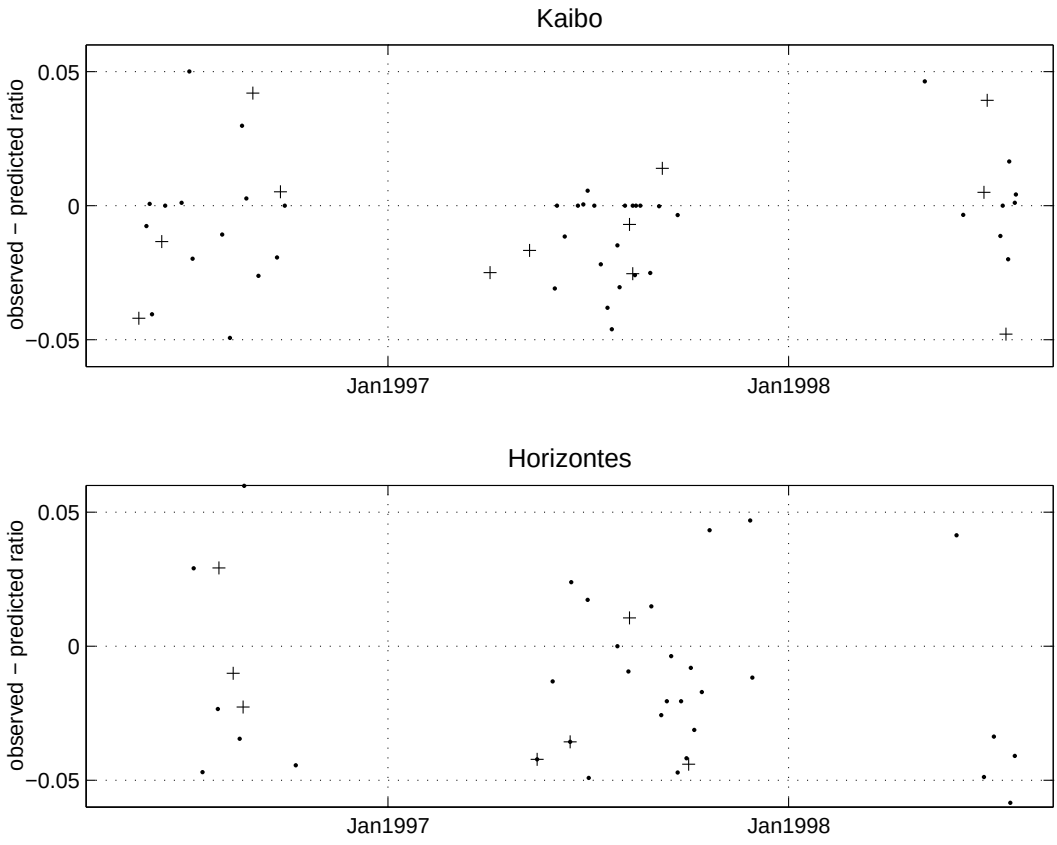

Figure 4.2: The difference between observed and predicted discharge ratios over time for Kaibo and Horizontes.

considerably higher than that in the other soils over the first part of the period, whereas it is lower in the second part of the period. A similar observation can be made with regard to the fluctuation in soil moisture content (for vertic soils it is less variable).

Other relationships between pre-event conditions (especially properties of the soil surface such as roughness, cracks and the presence of a crust) and overland flow may be established and show an even stronger relationship than that of pre-event wetness (especially so for Kaibo). However, there are not sufficient data available in this study to establish such relationships.

Sensitivity to variation in parameter values

It has been pointed out in Section 4.3 that the model is most likely over-parameterized in the sense that only a near-optimum parameter fit can be established more or less objectively through hyperboxes (i.e. parameter ranges for each of the parameters, see Tables 4.4 and 4.5). Here the effect of this over-parameterization is investigated in terms of prediction accuracy. This is done by selecting randomly 10.000 parameter vectors from the ranges listed in Table 4.4, subsequently predicting with each parameter vector and determining the RRMSE (on the basis of the validation data as described previously) for each prediction, and finally average the RRMSE. Another technique employed is to use the parameter vectors for prediction, then average the predictions at each time instant, and finally determine the RRMSE for the average result. In Table 4.7 the two methods (indicated as 'range' and 'ensemble') are compared with the result obtained when using the single 'optimum' parameter set for the prediction of discharge. The prediction with the param-

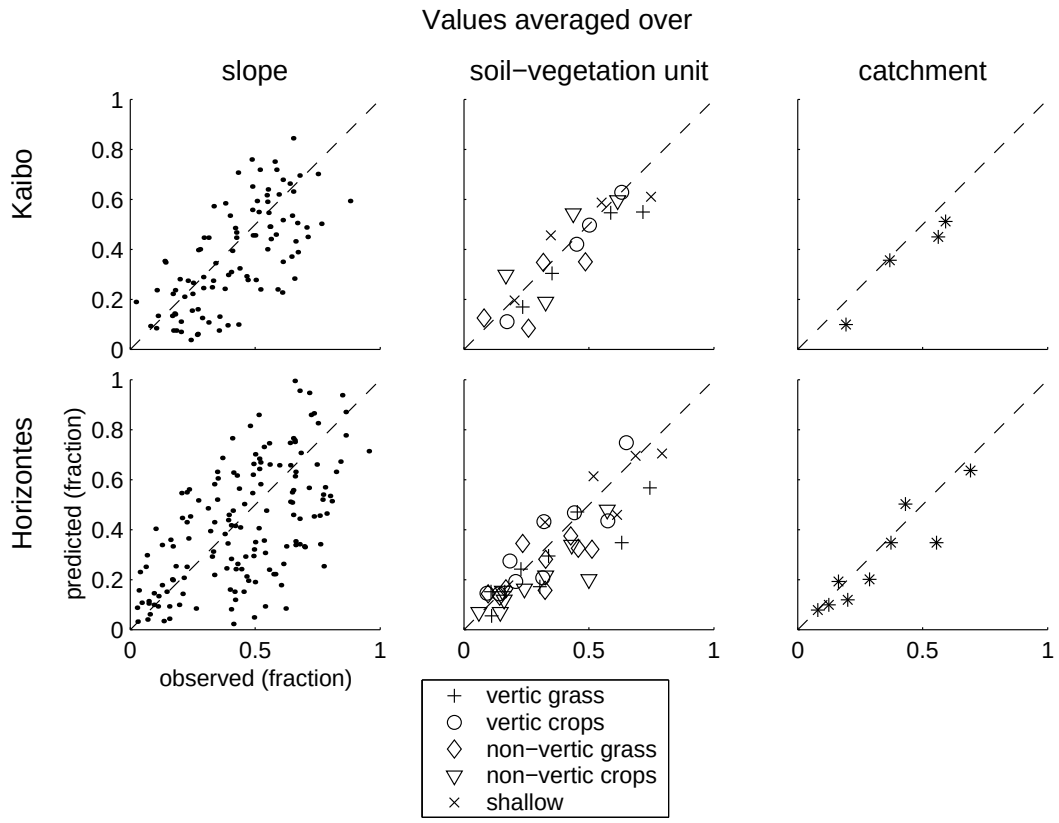

Figure 4.3: Correspondence between distributed overland flow observations and model predictions at three resolutions for Horizontes and Kaibo.

eters from the parameter range is only slightly worse than that with the 'optimum' value. Much more interesting is the fact that the ensemble prediction is smaller that the 'optimum' prediction. Apparently, the parameter range contains more useful information than the single 'optimum' parameter vector. This result implies that an ensemble method should be used for predicting with this model. Paradoxically, the implication is that although the model is over-parameterized, it does in this case not devaluate the model predictive capabilites. It is quite likely that there are strong correlations in the parameter space, leading to lower-dimensional sub-spaces. If such structures can be identified and sampling from these is facilitated, it is possible to considerably enhance the predictive capabilities of the model (e.g. Keesman and van Straten, 1990). With the limited set of observations available for this study such an identification is unfortunately not feasible.

Differences between split-sample and cross-validation

It has been outlined in Section 4.3 that the use of only a limited data set (labeled as 'calibration' data in Tables 2.1, 2.2 and 2.3) does not lead to inferior model results in comparison to using much more data (both 'calibration' and 'validation' data). For validation the use of one or the other data set may have quite significant results. In case the validation data is reserved for validation only, both split-sample adn cross-validation is possible. If this validation data is already used during calibration, only cross-validation can be applied to evaluate model performance. In Chapter 3 the entire data set was required for calibration, and as a result cross validation was applied. With the distributed model used here it was possible to calibrate the model on both the calibration data set or the entire data set. On the basis of these two calibrations, the differences between split-

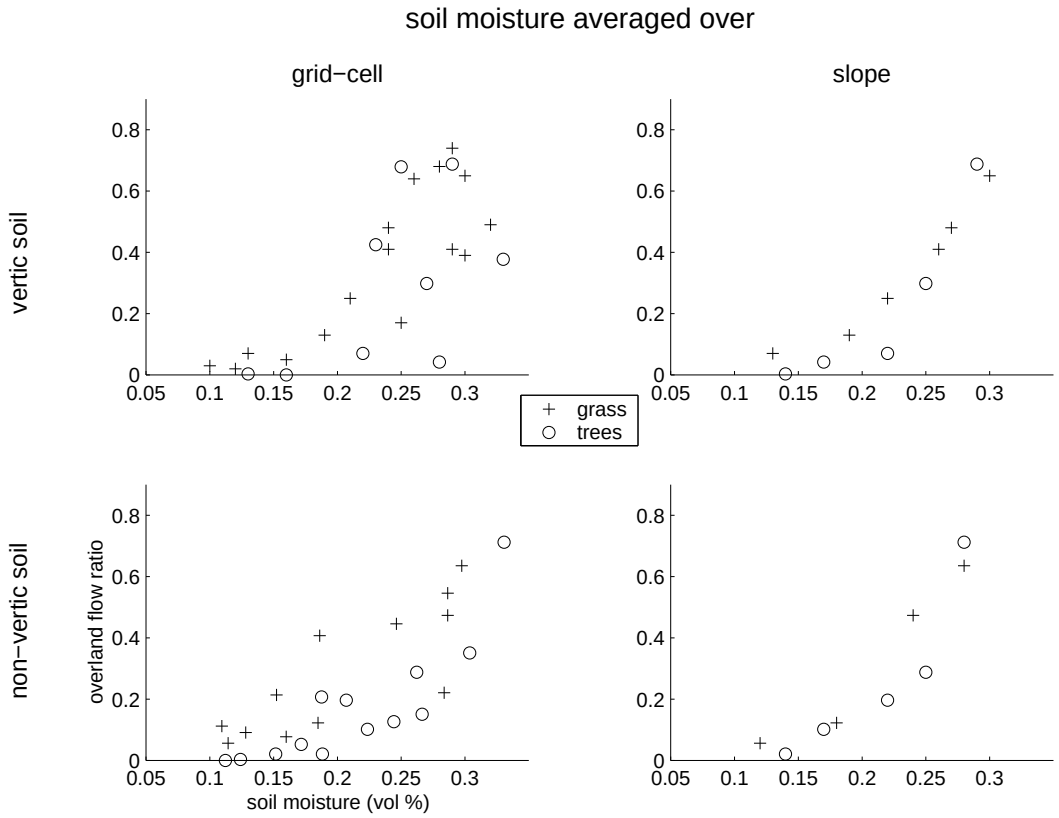

Figure 4.4: The relation between pre-event soil moisture content averaged over a model grid-cell (left) or area upslope from that grid-cell (right) and observed event average overland flow ratio for that grid-cell, considering different soil and vegetation units (the categories for 'shallow soil', are omitted because there are relatively few soil moisture observations on this unit). All observations are for Horicajo.

sample and cross-validation are investigated. In Table 4.8 the results are shown. It appears that the two validation techniques lead to results which are quite close. It is important to notice that (absolute) RMSE values for the split-sample and cross-validation techniques are divided by the same averaged observed values to obtain the RRMSE. Since split-sample validation provides a stronger test over time whereas cross-validation gives a stronger test over space, this result implies that variability in both space and time must be equally important (see the discussion on this in Section 3.5). A better validation data set (which should lead to higher RRMSE values) may be constructed by sampling from space as well as time. An important result is that both ways to validate lead to similar results since it implies that the results from the regression model in Chapter 3 can be compared with those here (see Section 4.5) and in subsequent chapters.

4.5 Overland flow patterns in space and time

Relation between overland flow and static catchment properties

Already prior to model calibration the spatial subdivision of the catchment has been imposed in order to yield a useful parameterization. This simple subdivision into six homogeneous zones of parameter values does however not imply that the spatial pattern of overland flow occurence is related in a simple way with these zones. This is partly due to rain heterogeneity, and even more

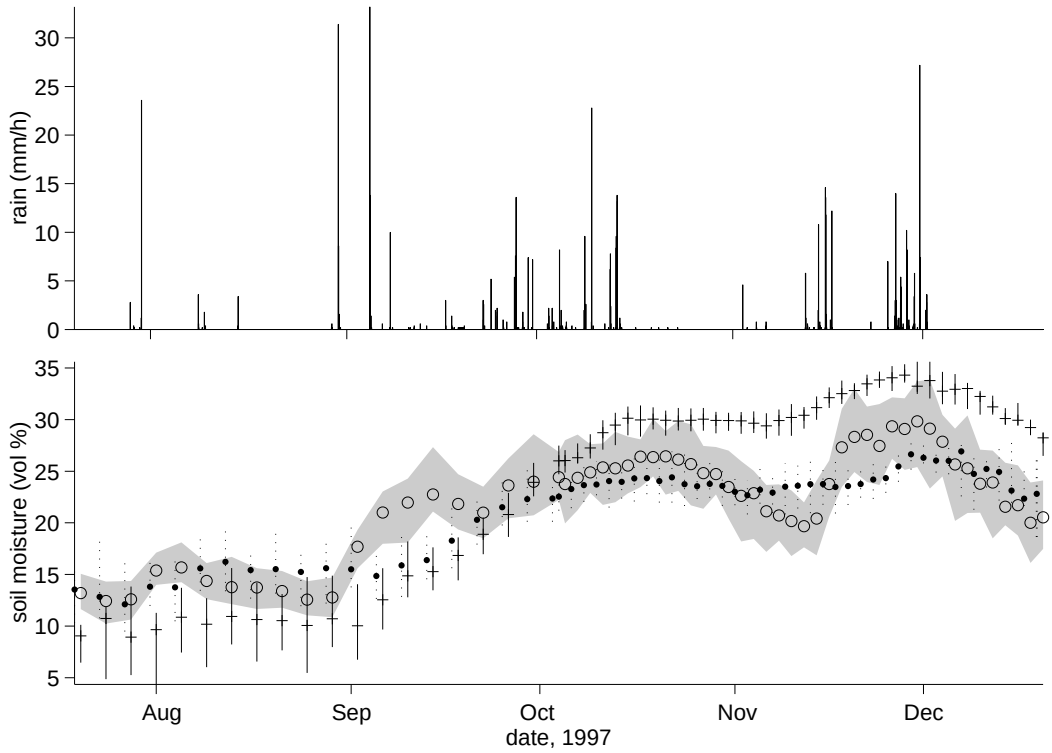

Figure 4.5: The change of soil moisture content for different soil types. The vertical solid lines indicate the range of soil moisture content for deep soils with vertic properties, the vertical dotted lines indicate the values for deep soils with non-vertic properties, and the the shaded area indicate the values for shallow soils. The symbols (+, • and o) indicate the average values for the respective soil types.

through topographic effects. This point is illustrated with Figures 4.6 and 4.7 that give the average overland flow maps over the entire wet season for Kaibo and Horizontes respectively.

When compared to Figures 2.3, 2.4, 2.9 and 2.10, Figures 4.6 and 4.7 suggest that in Kaibo especially vegetation and soil factors are correlated with overland flow occurence, whereas in Horizontes topography (in this case represented by the topographic index) is much more related. However these relationships cannot completely illuminate the driving forces of overland flow, since there are significant cross-correlations between the various topographic, soil and vegetation factors, it gives a qualitative idea about the differences between the different environments. Considering the relative similarity in soils between the two catchments, probably the dryer average conditions in combination with soil tillage activities on arable land in Kaibo cause these differences. This hypothesis implies that in wet late-season conditions, Kaibo should also display more influence from topography. When splitting the output data according to season or rain intensity, applying the same subdivision as in Chapter 3, it appears that indeed in dry conditions soil and vegetation units are the main determinants of overland flow, whereas in wetter situations topographic effects come into play. Overall, topographic influences remain stronger in Horizontes than in Kaibo (see Figures 4.8 and 4.9). The most striking characteristic of these maps are the very different patterns between early and late season as well as low and high rain intensity. This reinforces the suggestion that probably different parametrizations for each of these situations would lead to better model result. However, as was already noted in Section 4.2, the data set presently available contains not sufficient information to support such a parametrization.

The best (qualitative) explanation for the observed differences between the early and late sea-

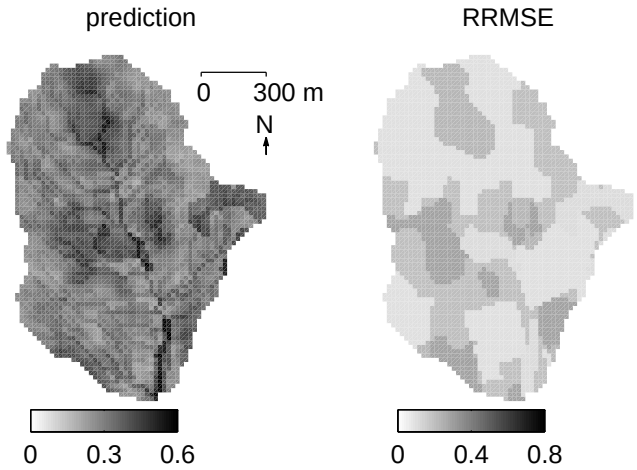

Figure 4.6: Predicted average overland flow ratio and RRMSE over the season for Kaibo.

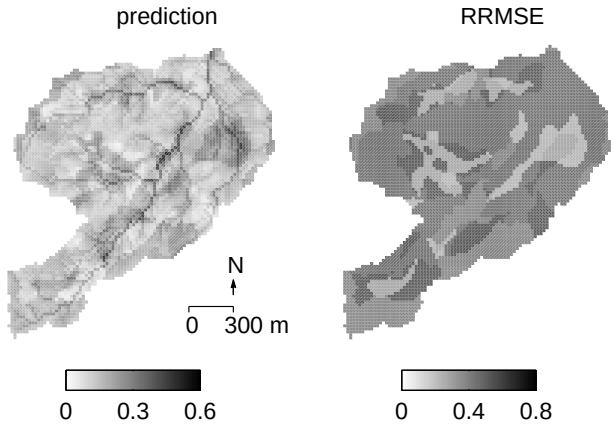

Figure 4.7: Predicted average overland flow ratio and RRMSE over the season for Horizontes.

sons is the pronounced dry season in combination with the vertic properties of some soil units. First of all there is the strong vegetative development over the season, in close interplay with the activity of soil macro fauna. And secondly there is the strong change of both storage capacity and permeability of vertic soils with increasing wetness. In early season, when the soil is dry, the cracks in the soils with vertic properties reduce the level of overland flow considerably. In late season when the soils are wetter and cracks have disappeared a reverse situation exists, then soils with vertic properties show a higher levels of overland flow because of very low infiltration capacities. Shallow soils tend to produce always more overland flow than the deeper soils.

When comparing the overland flow predictions as shown in Figures 4.8 and 4.9 to those displayed in 3.7 and 3.8 respectively, the relative differences (especially in RRMSE) are eyecatching. The RRMSE is for many soil-vegetation units almost twice as large for the model employed in this study in comparison to the regression model of Chapter 3.

4.6 Spatial heterogeneity, predicted and observed

In Figures 4.11 to 4.14 a more detailed analysis of the spatial patterns of observed and predicted relative overland flow depths is shown. In these figures the observed and predicted overland flow ratios are given for the four transects in Horicajo. In Figure 4.10 the location and the direction of

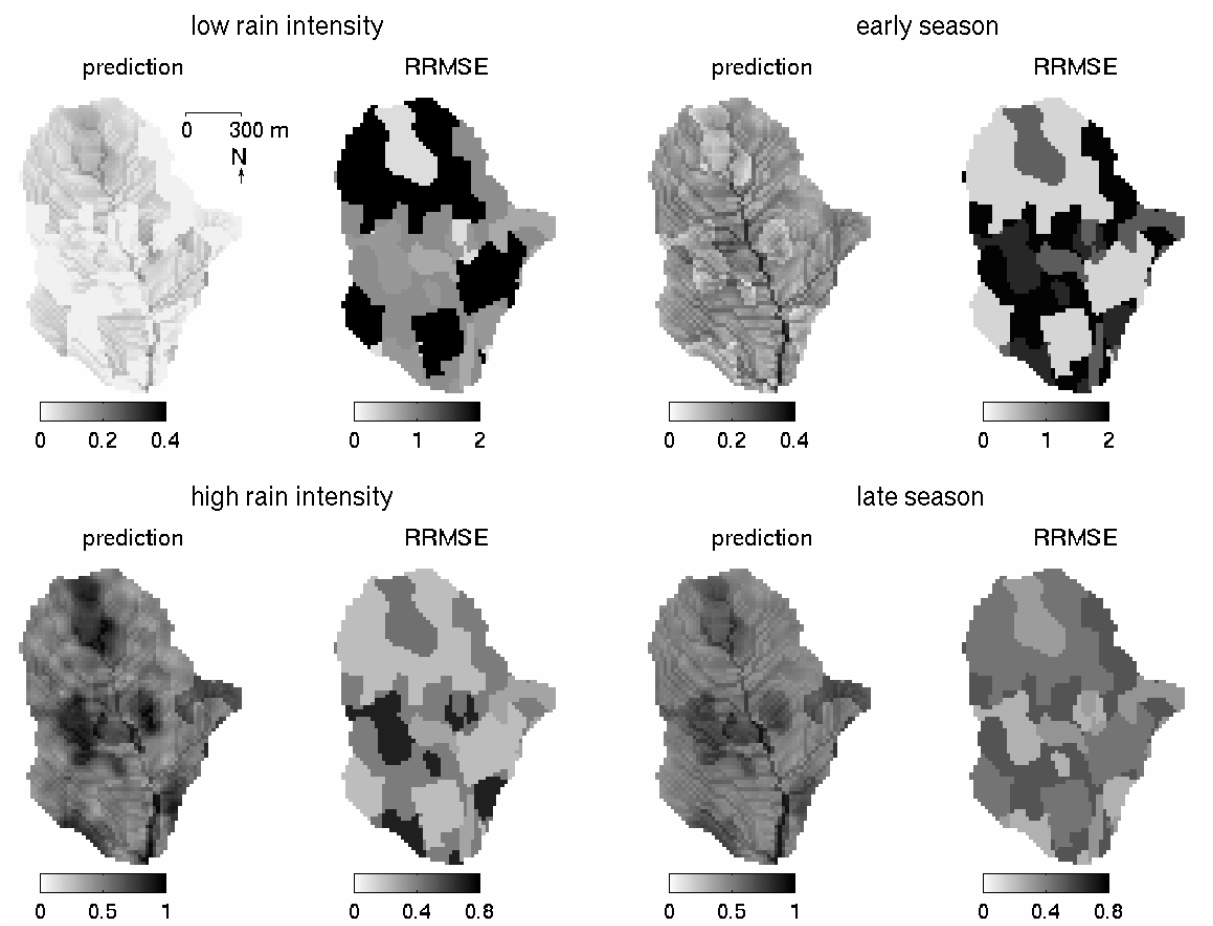

Figure 4.8: Predicted average overland flow ratio and RRMSE for low/high rain intensities and early/late season, Kaibo.

the four transects are shown. The three upper plots in Figures 4.11 to 4.14 displaying the observed and predicted relative overland flow depths for three events, and the lowest plot shows the elevation, upslope area and soil-vegetation types for the transect.. Figures 4.11 to 4.14 reveal that deviations between observed an predicted occur at all elevations, upstream areas and soil-vegetation types. The most extreme deviations are however seen at relatively high average overland flow depths. The figures illustrate that the spatial variability of the observed overland flow depth is higher than that of the model predictions. In spite of these shortcomings in the predictions the overland flow levels are reasonably reproduced at a coarse resolution, except for event three where the overland flow depth is consistently over-predicted. It is notable that for this third event the spatial variability for both model predictions and observations are higher than for the other events. It can be seen from the figures that the predicted overland flow patterns for the three events are more similar than the observed patterns. Overall it can be concluded that at the grid-scale overland flow is not predicted very well. In spite of this, there are still interesting correspondences between observed and predicted overland flow patterns as explained above.

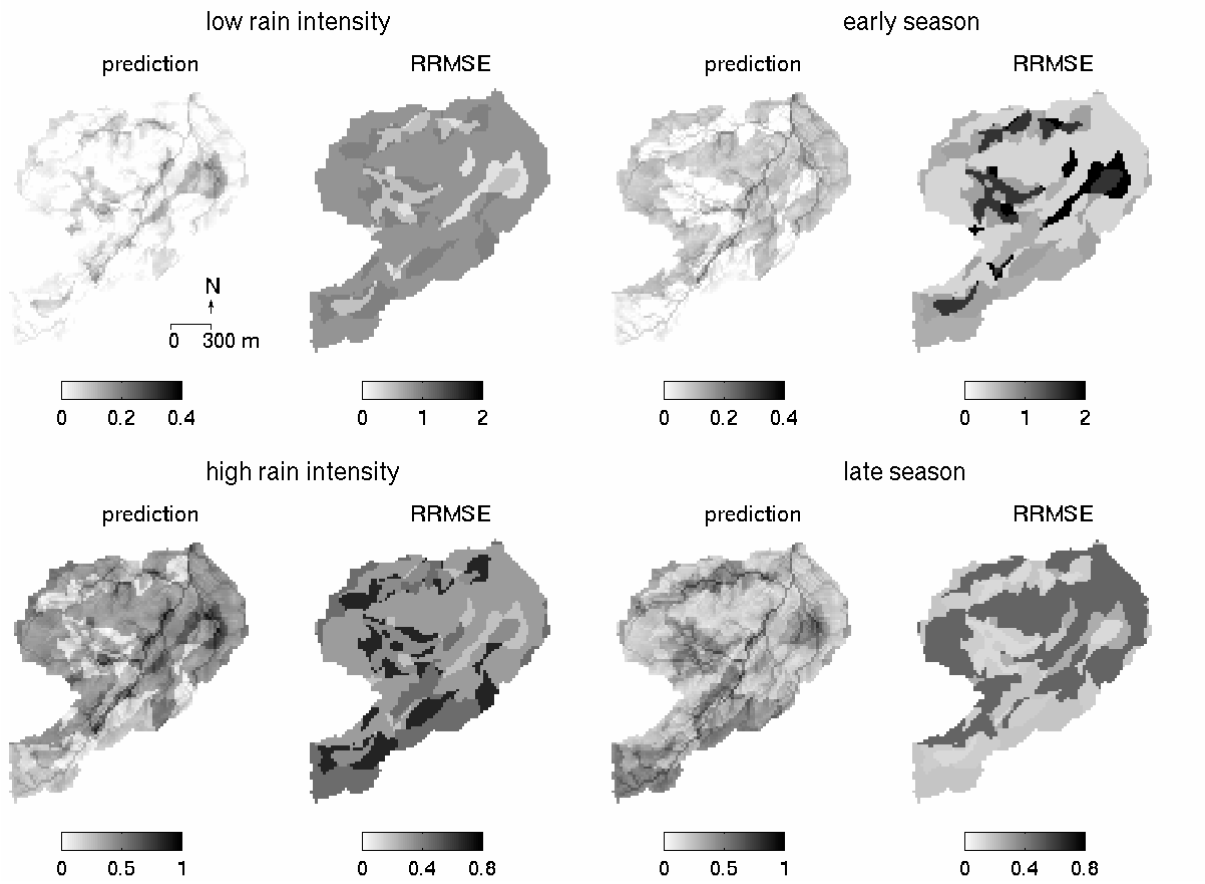

Figure 4.9: Predicted average overland flow ratio and RRMSE for low/high rain intensities and early/late season, Horizontes.

4.7 Discussion

Model form, its calibration and validation

The model chosen here has two main features which distinguishes it from most other overland flow models (e.g. de Lima, 1989; Scoging, 1992a; Flanagan and Nearing, 1995).

1. it has relatively few parameters, which is achieved by neclecting lateral sub-surface processes and using a limited number of soil-vegetation classes for parameter zonation;

2. it is event-based but explicitly and in a simple way incorporates the pre-event wetness in its parameterization of infiltration (viz. Equation 4.2).

For calibration use has been made of a similarity index, in order to match observations with model variables at distant locations but with supposedly similar features due to a correspondence in upstream area, soil and vegetation type. It is important to note that this procedure does not add assumptions to the model, since the parameter values were already linked to the same soil-vegetation units. It can be seen as a sophisticated way to use topographic (upstream area) as well as soil and vegetation information to regionalize local state-observations. It is notable that the pre-event wetness was not included in the initial versions of the model presented here. It has been implemented after earlier versions of model, with much more parameters, had been evaluated and did not perform well. The fact that the use of the zonation and the pre-event wetness, which both cause a

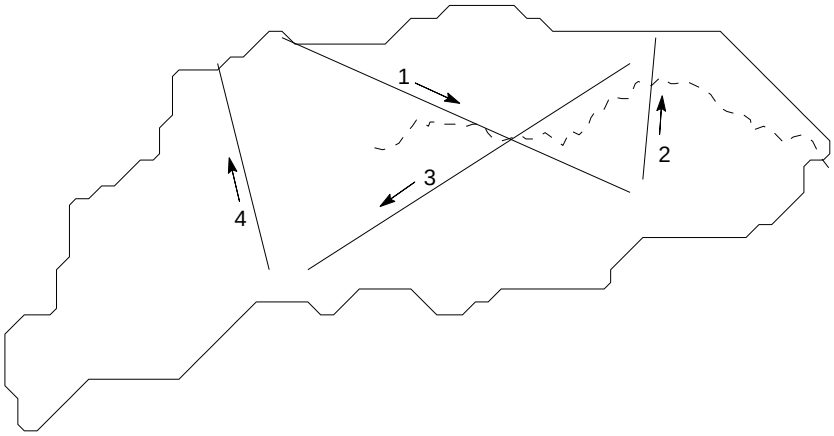

Figure 4.10: The location and direction of the four transects along which overland flow heights were observed in Horicajo (see also Figure 2.14).

coarsening of the effective model resolution did prove to be successfull, is an indication that the distributed model might be defined at a too fine resolution.

Model validation showed that discharge is not predicted very well by the distributed model (Figures 4.1 and 4.2 versus 3.3 and 3.4). At the size of the grid cells or single slopes overland flow depth is not reproduced very well, but at the level of soil vegetation units or the entire catchment the predictions are quite reasonable (Figure 4.3), implying that within soil-vegetation units a large part of the heterogeneity, that is not captured by the model at the resolution of a grid cell or upslope reach, is levelled out. The inclusion of pre-event wetness as a factor determining infiltration was tested.

Overland in Horizontes and Kaibo: correspondence and differences

The topographical information and the catchment-scale discharge observations are quite similar for Horizontes and Kaibo. This correspondence would suggest that overland flow patterns in the catchments are quite homogeneous and similar. In contrast, the geomorphological descriptions, in combination with the differences in land use dynamics, suggest big differences in mechanisms leading to overland flow. According to the model predictions the two catchments are quite dissimilar with respect to their overland flow mechanisms. In Kaibo soil and vegetation factors are more important in determining the occurence of overland flow, whereas in Horizontes it are mainly topographical factors. These effects can however not be separated completely since there is a strong spatial correlation between soil, vegetation and topography (see Figures 2.10 and 2.4). In Kaibo saturation excess runoff occurs only in 5 % of the events, whereas in Horizontes it is observed in almost 20 % of the events, but in all events the largest contribution to overland flow is infiltration excess.

Kaibo and Horizontes have catchment discharge/rain ratios of respectively ± 0.1 and ± 0.2. Both values appear to be close to what is expected in these environments (see Sections2.2 and 2.3). This index classifies both catchments as dry (Gan et al., 1997).

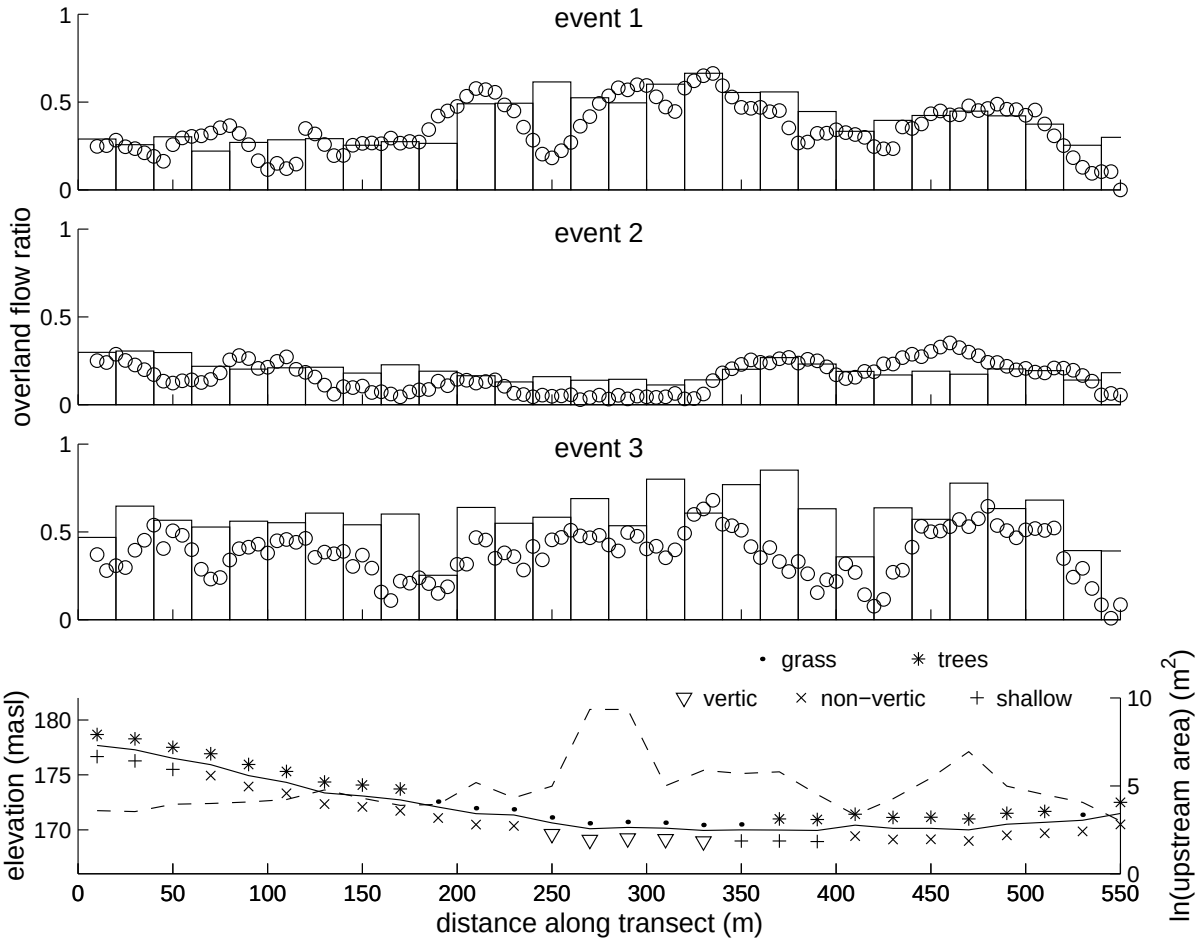

Figure 4.11: Observed (circles) and predicted (bars) overland flow ratios along transect 1 in Horicajo for three events (top 3 graphs). The bottom graph gives elevation (solid line), upslope area (log-scaled, dashed line) and soil-vegetation types, that correspond with the upper graphs.

Seasonality: single versus multiple model parameterizations

Also strong seasonal trends appear to exist. In this study it is shown that in both environments strong seasonal trends exist, with increasing levels of overland flow towards the end of the season. For Horizontes the trend can best be explained by the cracks in vertic soils under dry conditions (at the start of the wet season), and for Kaibo an additional explanation is the a decreasing soil roughness of the arable land over the season. In Kaibo the differences between early and late season are most pronounced. In spite of the qualitative nature of the observations and model predictions presented in Section 4.5, the seasonal trends are so obvious that these have to be taken into account in overland flow modelling. The observation that seasonal effects relate to the state of the soil surface, vegetative growth and biological activity is not new. The relation between a soil's infiltration capacity and crust formation as well as the activity of macro fauna have been reported before for the West African Sahel (Brouwer and Bouma, 1997; Hoogmoed and Stroosnijder, 1984; Stroosnijder and Hoogmoed, 1984; Hillenaar, 1995; Mando et al., 1996). However, the impact of these factors at the catchment scales have been largely neglected. The focus has instead been mainly on the heterogeneity of relief and rain (e.g. Albergel et al., 1986, 1987; Rodier, 1982; Rodier and Auvray, 1965; Sivakumar et al., 1991). For the dry forest area of

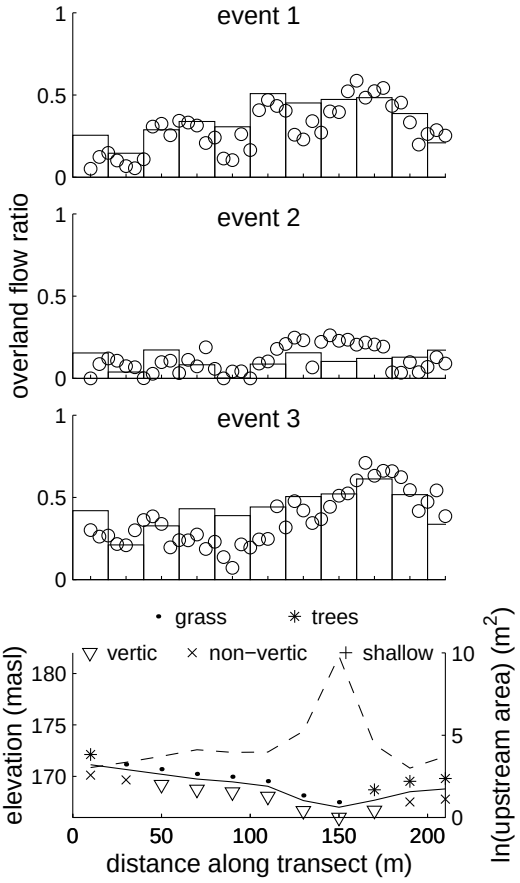

Figure 4.12: Observed (circles) and predicted (bars) relative overland flow depth along transect 2 in Horicajo for three events (top 3 graphs). The bottom graph gives elevation (solid line), upslope area (log-scaled, dashed line) and soil-vegetation types, that correspond with the upper graphs.

Horizontes several studies are know that pay attention to seasonal trends in relation to vegetation and soil fauna, but for these conditions the seasonal factors have never been related to hydrologic processes (Janzen, 1991). Strong seasonality implies that there are only two options for proper model parameterization:

1. use all seasonal factors for parameterization (consider them as as inputs, just as rain); or

2. parameterize a model for a period brief enough that all parameters can be considered constant.

Effectively both approaches have been followed in this study, albeit that the first was applied in a relatively simple way.

The distinction between soils with vertic and non-vertic properties deals with soil changes, and the distinctions between grass versus trees (Horizontes) or grass versus arable land (Kaibo) deal with differences in vegetative developement and land husbandry. In addition the pre-event wetness index partially reproduces a seasonal effect.

Recalibration on more restricted data sets (early season versus late season and low intensity versus high rain intensity) was also done. However, this was shown to be not effective: the approach requires a much larger data set to yield similar results (see Table 4.6). It it still possible

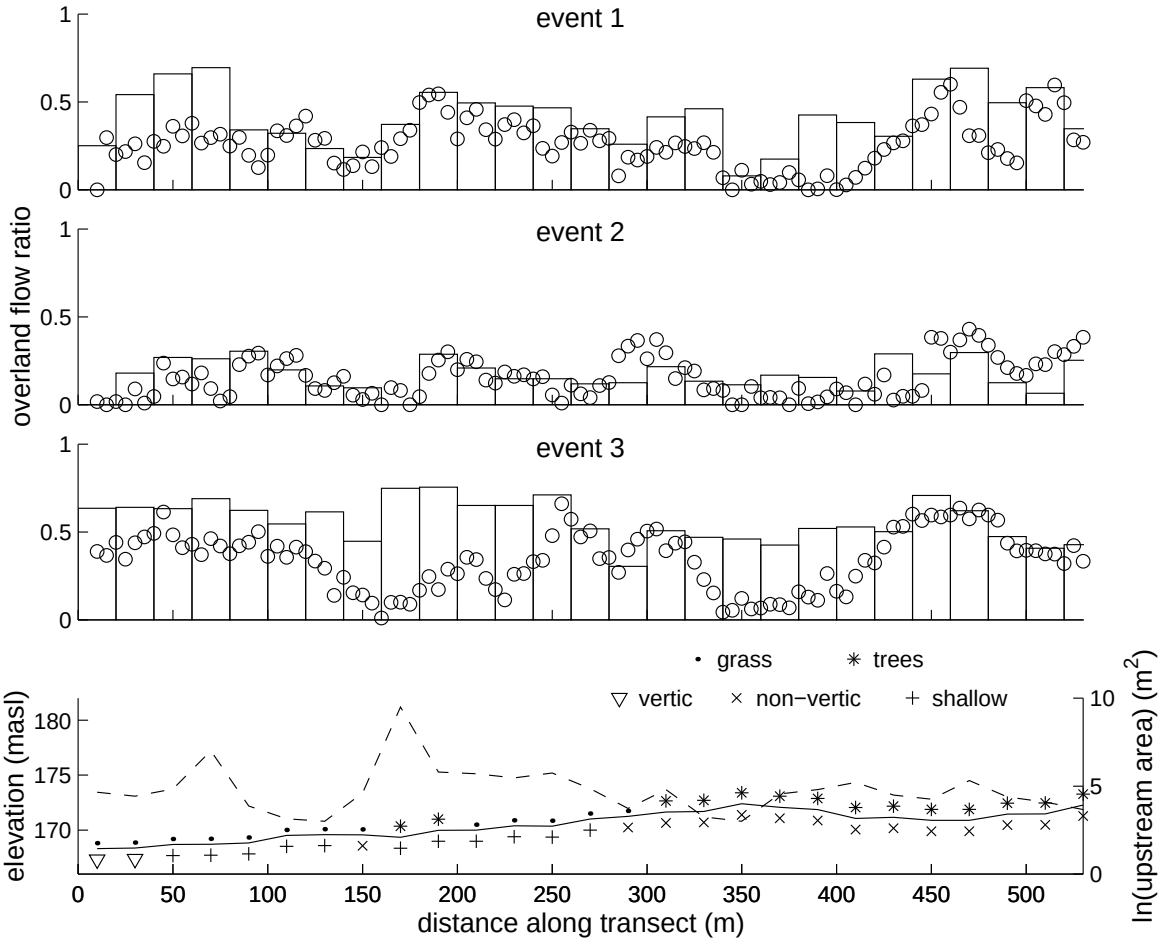

Figure 4.13: Observed (circles) and predicted (bars) overland flow ratios along transect 3 in Horicajo for three events (top 3 graphs). The bottom graph gives elevation (solid line), upslope area (log-scaled, dashed line) and soil-vegetation types, that correspond with the upper graphs.

that utilizing models for specific periods are more effective than a single model, but these would require more parismonious parameterizations which means effectively considering less zones (e.g. only distinguishing between vertic and non-vertic soils in early season, and between grass and no-grass in late season). It was beyond the scope of this chapter to test this idea, but it will be subject of investigation in Chapter 6.

Concluding remarks

To the questions that were posed at the start of in this Chapter some clear answers can be given.

A distributed model could be calibrated, after some zonation of the parameters was applied, and by using pre-event wetness as an additional forcing next to rain. Only ranges of near-optimal parameters could be defined, but simulation on the basis of these ranges did produce satisfactory results. In comparison to the regression approach outlined in Chapter 3, the model results are inferior at the resolution of both the soil-vegetation units and the catchment. Predictions at the grid-resolution seem to be untrustworthy. Overland flow is indeed heterogeneous in space and time in the two study catchments, also when averaged over an event. It is quite clear that a homogeneous layer of overland flow is a rarity, as much as the saturation of the surface soil layer over an entire

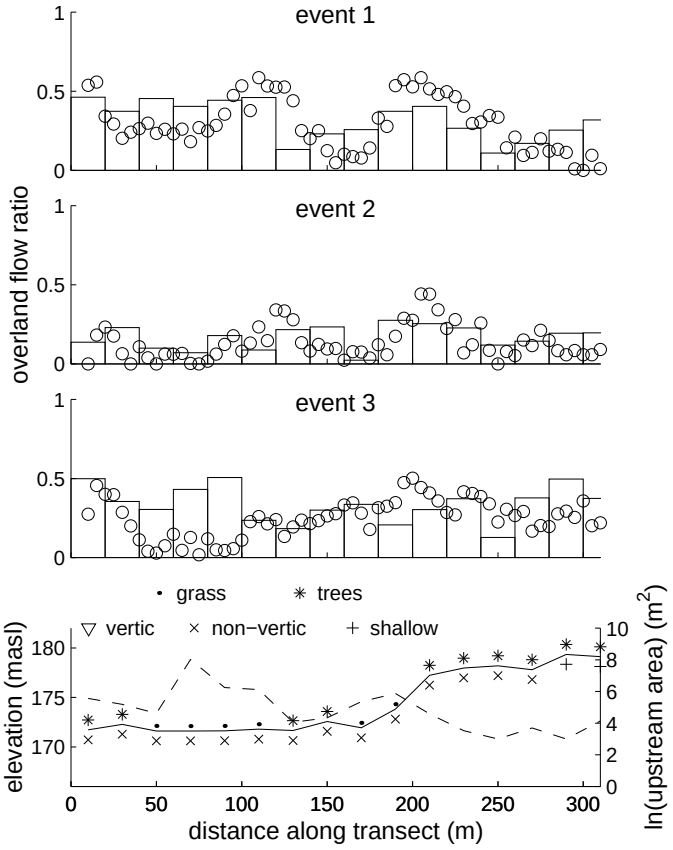

Figure 4.14: Observed (circles) and predicted (bars) overland flow ratios along transect 4 in Horicajo for three events (top 3 graphs). The bottom graph gives elevation (solid line), upslope area (log-scaled, dashed line) and soil-vegetation types, that correspond with the upper graphs.

slope reach. However, this heterogeneity is of a deterministic nature and can be understood and even be reproduced to some degree through a detailed observation of the terrain and a qualitative understanding of the system. In this study it has been shown that in both catchments the vertic nature of soils and the differences in vegetation cover do explain a lot of the heterogeneity of overland flow (see Figure 4.3). At the grid scale, the heterogeneity of overland flow observations are however not reproduced at all (see Figures 4.11 to 4.14).

Because the distributed model utilized in this study seems to be a reasonable overland flow predictor at coarse resolutions (i.e. predictions averaged over soil and vegetation units) while it appears to be a very poor predictor at the grid scale, the conclusion must be that the model does not fully exploit its distributed nature. This suggest that the model may require some conditioning, so-called regularization (Tarantola, 1987) with distributed information to perform better. At present there are however no techniques available that can apply regularization to dynamic models of this size (state vectors with more than 5000 variables). It is hard to interpret the results of this study to define further research questions. On the one hand the model is conceptually very simple and relatively parismonious when compared to other parameter distributed models. On the other hand the model is, due to its distributed nature, still very demanding to calibrate. For this reason system identification as well as regularization tools cannot easily be applied to this model to find a suitable parameterization and it is furthermore unsuitable for measurement optimization. The spatial lumping of this particular grid-based model is no solution to this problem. Such an

operation would change the connectivity of the drainage flow paths (Quinn et al., 1991) as well as the extent and meaning of the units for which the model is parameterized (Kim, 1995). The conclusion with regard to this point can be stated concisely as follows. Distributed models may be very good predictors for overland flow if properly reguralized and if the proper spatio-temporal resolution is chosen, but in general distributed models (just as the model used here, described by Equations 4.1 to 4.6) are too large for regularization and do not allow to easily vary resolution. Referring to Figure 1.1, Table 1.1 and Table 1.2, one could say that distributed models may in principle be suitable for prediction or projection (phase 2 and 3), but can never be appropriately be parameterized in an identification procedure (phase 1 of system modelling).

These answers are encouraging, at least to such an extent that in the following chapters a quest is made for better methods to exploit the data for overland flow prediction. Naturally, for these methods the foregoing results will be the touchstone.

Table 4.4: Initial parameter values for calibration and parameter values after calibration, using only calibration data. The initial parameter values are the same for Kaibo and Horizontes. The optimum parameter values are given in combination with the parameter-ranges that yield near-optimum predictions (i.e. RRMSE values up to 10% higher), in the colum '10% opt.'

		optimum parameter values			
	initial	Kaibo		Horizontes	
	par. value	10% opt.	optimum	10% opt.	optimum
Set 1:	*deep, vertic; non-trees / arable land*				
fa	20	17 - 21	18	14 -15	15
fb	15	9 - 14	13	12 - 15	13
A	0.4	0.22 -0.47	0.35	0.42 - 0.61	0.54
B	1.8	1.43 - 2.01	1.73	1.33 -1.96	1.72
Set 2:	*deep, vertic; trees / shrub land*				
fa	8	9 - 11	11	8 - 10	9
fb	6	6 - 8	7	3 - 6	5
A	0.2	0.21 - 0.35	0.34	0.23 - 0.36	0.36
B	2.3	2.08 - 2.45	2.11	1.93 - 2.24	1.95
Set 3:	*deep, non-vertic; non-trees / arable land*				
fa	20	10 - 20	11	8 - 20	14
fb	15	5 - 9	5	4 - 9	6
A	0.4	0.43 - 0.67	0.62	0.34 - 0.43	0.34
B	2.8	2.83 - 3.03	2.99	2.12 - 2.48	2.36
Set 4:	*deep, non-vertic; trees / shrub land*				
fa	8	4 - 5	5	3 - 4	3
fb	6	2.1 - 3.2	3	0.2 - 0.96	0.7
A	0.5	0.44 - 0.58	0.47	0.52-0.74	0.61
B	2.8	2.85 - 3.12	3.01	2.13-2.92	2.79
Set 5:	*shallow; non-trees / arable land*				
fa	4	1 - 3	1.6	2 - 3	2.1
fb	2	0.5 - 0.9	0.5	0.2 - 0.8	0.3
A	0.4	0.12 - 0. 41	0.39	0.4 - 0.74	0.61
B	1.5	1.51 - 1.86	1.76	1.52 - 1.98	1.92
Set 6:	*shallow; trees / shrub land*				
fa	4	1 - 4	1.9	2 - 4	1.7
fb	2	0.2 - 0.7	0.3	0.2 - 1.1	0.4
A	0.4	0.22 - 0. 47	0.28	0.54 - 0.83	0.76
B	1.5	2.01 - 2.54	2.10	1.32 - 2.41	2.16

Table 4.5: Initial parameter values for calibration and parameter values after calibration, using both calibration and validation data. The initial parameter values are the same as those in Table 4.4 and repeated here for clarity. The optimum parameter values are given in combination with the parameter-ranges that yield near-optimum predictions (i.e. RRMSE values up to 10% higher), in the colum '10% opt.'

		optimum parameter values			
	initial	Kaibo		Horizontes	
	par. value	10% opt.	optimum	10% opt.	optimum
Set 1:	*deep, vertic; non-trees / arable land*				
fa	20	17 - 20	18	13 -15	15
fb	15	7 - 13	12	13 - 15	14
A	0.4	0.18 -0.47	0.34	0.46 - 0.60	0.55
B	1.8	1.42 - 2.12	1.68	1.30 -2.03	1.69
Set 2:	*deep, vertic; trees / shrub land*				
fa	8	9 - 11	11	8 - 10	9
fb	6	6 - 8	7	3 - 6	5
A	0.2	0.31 - 0.39	0.35	0.23 - 0.36	0.36
B	2.3	2.00 - 2.51	2.05	1.93 - 2.24	1.95
Set 3:	*deep, non-vertic; non-trees / arable land*				
fa	20	10 - 20	11	8 - 20	14
fb	15	6 - 9	7	4 - 9	6
A	0.4	0.43 - 0.67	0.64	0.34 - 0.43	0.38
B	2.8	2.83 - 3.02	2.96	2.12 - 2.48	2.34
Set 4:	*deep, non-vertic; trees / shrub land*				
fa	8	4 - 5	5	3 - 4	3
fb	6	2.1 - 3.5	2.8	0.2 - 0.96	0.7
A	0.5	0.47 - 0.54	0.51	0.54-0.82	0.61
B	2.8	2.89 - 3.08	3.02	2.38-3.21	2.79
Set 5:	*shallow; non-trees / arable land*				
fa	4	1 - 3	1.6	2 - 3	2.1
fb	2	0.5 - 0.9	0.5	0.2 - 0.8	0.3
A	0.4	0.12 - 0. 41	0.39	0.4 - 0.74	0.61
B	1.5	1.51 - 1.86	1.64	1.52 - 1.98	1.81
Set 6:	*shallow; trees / shrub land*				
fa	4	1 - 4	1.9	2 - 4	1.8
fb	2	0.2 - 0.8	0.3	0.2 - 1.2	0.4
A	0.4	0.23 - 0. 53	0.31	0.63 - 0.95	0.82
B	1.5	2.01 - 2.86	2.61	1.31 - 2.57	2.38

Table 4.6: Efficiency (%), Bias (%) and RRMSE (fraction) of discharge prediction for calibration and validation sets, for Kaibo and Horizontes, using the optimum parameter values listed in Table 4.4.

		Kaibo		Horizontes	
event type	statistic	calibration	validation	calibration	validation
all events	E_f	83	76	87	72
	Bias	4	5	4	11
	RRMSE	0.08	0.11	0.09	0.13
low intensity	E_f	86	72	93	79
	Bias	4	5	7	13
	RRMSE	0.05	0.12	0.11	0.14
high intensity	E_f	83	69	91	72
	Bias	-2	-15	-3	15
	RRMSE	0.07	0.09	0.08	0.16
early season	E_f	72	67	81	73
	Bias	8	15	6	22
	RRMSE	0.11	0.13	0.1	0.11
late season	E_f	85	64	84	76
	Bias	12	24	-3	-14
	RRMSE	0.12	0.17	0.09	0.14

Table 4.7: RRMSE of discharge prediction for calibration and validation sets, for Kaibo and Horizontes. The results for using the single optium value listed in Table 4.4 are given in the column 'optimum', the results for predicting with a set of 10.000 individual parameter vectors for the 10%-range in Table 4.4 are given in the column 'range', and the results for predicting with the average of the same 10.000 parameter values are given in the column 'ensemble'.

	Kaibo			Horizontes		
event type	optimum	range	ensemble	optimum	range	ensemble
all events	0.11	0.13	0.08	0.13	0.14	0.07
low intensity	0.12	0.15	0.09	0.14	0.16	0.09
high intensity	0.09	0.12	0.07	0.16	0.17	0.11
early season	0.13	0.17	0.07	0.11	0.15	0.08
late season	0.12	0.13	0.06	0.14	0.15	0.07

Table 4.8: RRMSE of discharge prediction for validation with a split-sample and cross-validation, for Kaibo and Horizontes. The results are for using the ensemble prediction technique and using the parameter ranges listed in Table 4.4 (split- sample validation) and 4.5 (cross-validation).

	Kaibo		Horizontes	
event type	split-sample	cross-validation	split-sample	cross-validation
all events	0.08	0.09	0.07	0.10
low intensity	0.09	0.07	0.09	0.07
high intensity	0.07	0.08	0.11	0.09
early season	0.07	0.11	0.08	0.09
late season	0.06	0.07	0.07	0.06

5 Identification of scale dependent models: design of an algorithm[1]

5.1 Introduction

In the preceding chapters it has been argued on the basis the results of a regression model and a distributed overland flow model that these are not ideal for overland flow prediction. For the regression model the few possibilities to include system dynamics and the high data requirements when predicting at fine spatial resolutions are limitations. The distributed model, on the other hand, is not identifyable and lacks the flexibility to change the spatial and temporal model resolution easily. On the basis of this the question arises whether a model that is dynamic but contains fewer spatial elements than the distributed model of Chapter 5 would provide a good alternative. If so, the question is which (spatial and temporal) resolution to choose and also how to establish the structure of such a model. Beven (1995) and Klemeš (1983) argued that this goal might best be achieved by following a disaggregation approach. From their arguments also follows that at each resolution probably a specific model structure would be most appropriate, i.e. the model structures are supposedly *scale-dependent.* Finally, it seems likely that not a single model can stand out as being the optimal, even not at a single resolution, but possibly an entire set of models (e.g. Beven, 2001). These ideas are being tested here on the basis of a synthetic data set of water flow from a hillslope during and briefly after rainfall. A new identification method is developed for this purpose. The method derives an appropriate model structure at a given resolution, using a set of input-output data and some basic knowledge about the system. The method is based on Monte Carlo techniques and considers a *set of valid models*, rather than only one.

This chapter is structured as follows. In Section 5.2 an explanation of several concepts is given. This is followed by a detailed description of the way in which a set of models is formulated in Section5.3. Next, in Section 5.4, an algorithm to find appropriate models out of a model set is explained. The method is subsequently applied to a synthetic data set in Section 5.5. Following to that we discuss the strenghts and weaknesses of the method in Section 5.6. Conclusions are drawn in Section 5.7.

5.2 Explanation of concepts

In order to find a proper mathematical description of a hydrological system a set of models is used. The rules that define this set of models are called the *template*. The template comprises a list of state variables, possible inputs and auxiliary variables, an allowed number of parameters, maximum parameter ranges and allowed subdivisions of space and time. A specific combination of state variables, inputs, parameter ranges and subdivision of space and time is called a *model*. Each model satisfying the definition provided by the template can be written as a time-variable

[1] This chapter is an adapted version of: E. E. van Loon and K. J. Keesman. Identifying scale-dependent models: The case of overland flow at the hillslope scale. *Wat. Resour. Res.*, 36(1): 245-254, 2000.

physically based description of the hydrological system. The general form is as follows

$$\mathbf{x}_k = \mathbf{A}_k\mathbf{B}_k\mathbf{C}_k\mathbf{x}_{k-1} + \mathbf{A}_k\mathbf{u}_k \tag{5.1}$$

$$\mathbf{y}_k = \mathbf{H}_k\mathbf{x}_k + \mathbf{e}_k \tag{5.2}$$

where the vector $\mathbf{x}_k$ contains the state variables, and the vector $\mathbf{u}_k$ the inputs at time instant k. The matrices $\mathbf{A}_k$, $\mathbf{B}_k$ and $\mathbf{C}_k$ contain time-varying stochastic coefficients that are larger than zero and smaller than one, and are called *transition* matrices. The vector $\mathbf{y}_k$ contains the outputs, which should correpond with observations. The matrix $\mathbf{H}_k$ is the observation matrix, relating the model state variables to the observations. In this chapter $\mathbf{H}_k$ contains only ones and zeros and is constant over time. The vector $\mathbf{e}_k$ contains unknown-but-bounded (UBB) errors (see the discussion in Section 2.5), which means that only the upper and lower bounds of the errors are known but any other information about its distribution is lacking. Hence $\mathbf{e}_k$ is defined in terms of the lower and upper bounds, $\underline{\mathbf{e}}_k$ and $\overline{\mathbf{e}}_k$ respectively. In Appendix B a detailed derivation of this model is given.

The transition matrices contain the system-dynamics, and describe each a different aspect of a hydrologic system. $\mathbf{A}_k$ describes the partioning of water over the different state variables and is called the *partitioning* matrix, $\mathbf{B}_k$ determines the spatial redistribution of water and is called the *transport* matrix, $\mathbf{C}_k$ gives the partitioning between observable and unobservable state variables and is called the *internal-state* matrix. The partitioning matrix and internal-state matrix are not essentially different, but are distinguished to make a clear differentiation between the processes (state variables) that can be measured (e.g. surface runoff and infiltration) and those that can not be measured satisfactory (e.g. subsurface runoff and drainage). The column sums of the transition matrices are equal to one and each column may be thought of as a discrete probability distribution of the water transport process. The fact that the columns of the transition matrices sum to unity ensures that mass is conserved. The time-varying stochastic coefficients of the transition matrices are piecewise linear functions of state variables or input variables. These piecewise linear functions are called *kernel* functions. The coordinates of the breakpoints in the kernel functions are the model parameters.

On basis of the template various models, which may differ in detail and structure, are identified in two steps. First we perform an UBB calibration step. If a model with a specific parameter vector can reproduce the data within the error bounds specified during calibration, that model is called *behavioural* and stored in the *prior* model set. Secondly, the model is validated on independent data. If it can reproduce the data within the preset error bounds during this validation step, it is called *fit* and stored in the *posterior* model set. *Fitness* is thus our criterion for the appropriateness of a model. Subsequently the posterior model set is input to a *genetic* algorithm where elements of the fittest models in the posterior model set are combined into new models and where some elements are changed randomly. The resulting set of models, together with the models contained in the posterior model set, form the new prior model set. The loop of calibration, validation and generation of new models is repeated till the fitness of calibrated models does not increase anymore. The various terms are illustrated in the flowchart of Figure 5.1. A further explanation of the procedure is given in sections 5.3 and 5.4.

An example may further illustrate the meaning of the various terms and the functioning of the algorithm. It is shown how a suitable model may be found to describe a synthetic hydrological data set for 20 rain events at time instants of 5 minutes containing data over four equally sized spatial units along a slope. A model with the structure of Equation 5.1, with three state variables and three kernel functions is used to generate the synthetic data (see Appendix B for a detailed description of this model). Next, the algorithm as visualised in Figure 5.1 is used to find a model similar to the original on basis of the artificial data and an appropriate template. The template comprises infiltration, overland flow due to infiltration excess, overland flow due to saturation excess, and soil water ($s_{k,l}$, $r_{k,l}$, $t_{k,l}$ and $w_{k,l}$ respectively) as state variables, precipitation ($p_{k,l}$)

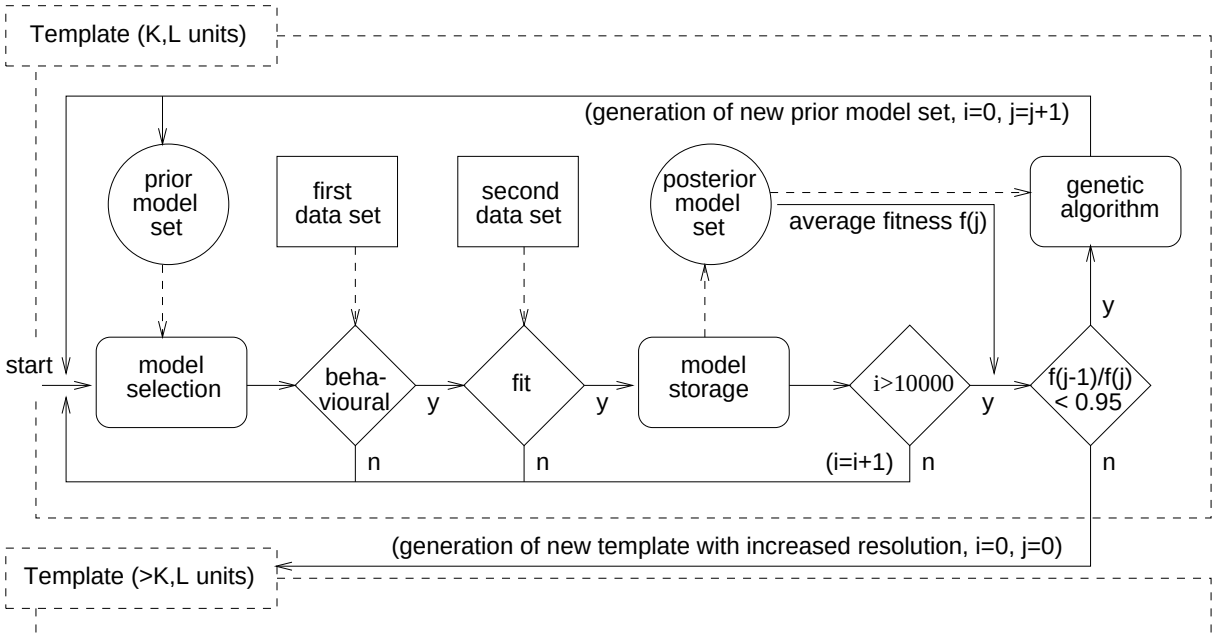

Figure 5.1: Flowchart, illustrating the data-flows in the model identification algorighm (see text).

as input, and the state variables and precipitation as possible independent variables in the kernel functions. Furthermore the template allows the spatial subdivision to vary between one and ten spatial units, the temporal subdivision to use time steps ranging from one to twenty minutes, and the kernel functions to use a maximum of 3 breakpoints.

During the first cycle of calibration and determination of fitness, 83 fit models are obtained, this set is used to generate a new set of 9917 models. By repeating the cycle of model calibration, determination of fitness and new model generation, the kernel functions as well as the spatial and temporal subdivision of the original model are approached already at the fourth iteration. This is illustrated in Figure 5.2, where only the average parameter values (not the parameter ranges) are displayed and for the transport matrix ($b_{k,l,m}$) only the kernel functions describing transport to one and three units downstream.

In the next section it is explained in detail how a set of models can be defined on basis of the above concepts.

5.3 Establishing a set of models

A template defines the allowed temporal and spatial subdivisions, inputs, state variables and auxiliary variables as well as the number of parameters for Equations 5.1 and 5.2. Here we will describe the template in some detail by first explaining the subdivision of the spatial and temporal domains, subsequently the choice and use of variables, and finally the definition of parameters.

Temporal and spatial subdivision

A rain event is subdivided into K temporal units and the catchment into L spatial units. Each input and state variable in a model is considered over a spatial unit l and at a time instant k. In this study the subdivision in time is regular and the size of the temporal units (T) ranges from 1 to 20 minutes, with steps of 1 minute (note that $K =$ duration of event$/T$).

To determine the range of possible spatial subdivisions the concept of upstream area is used.

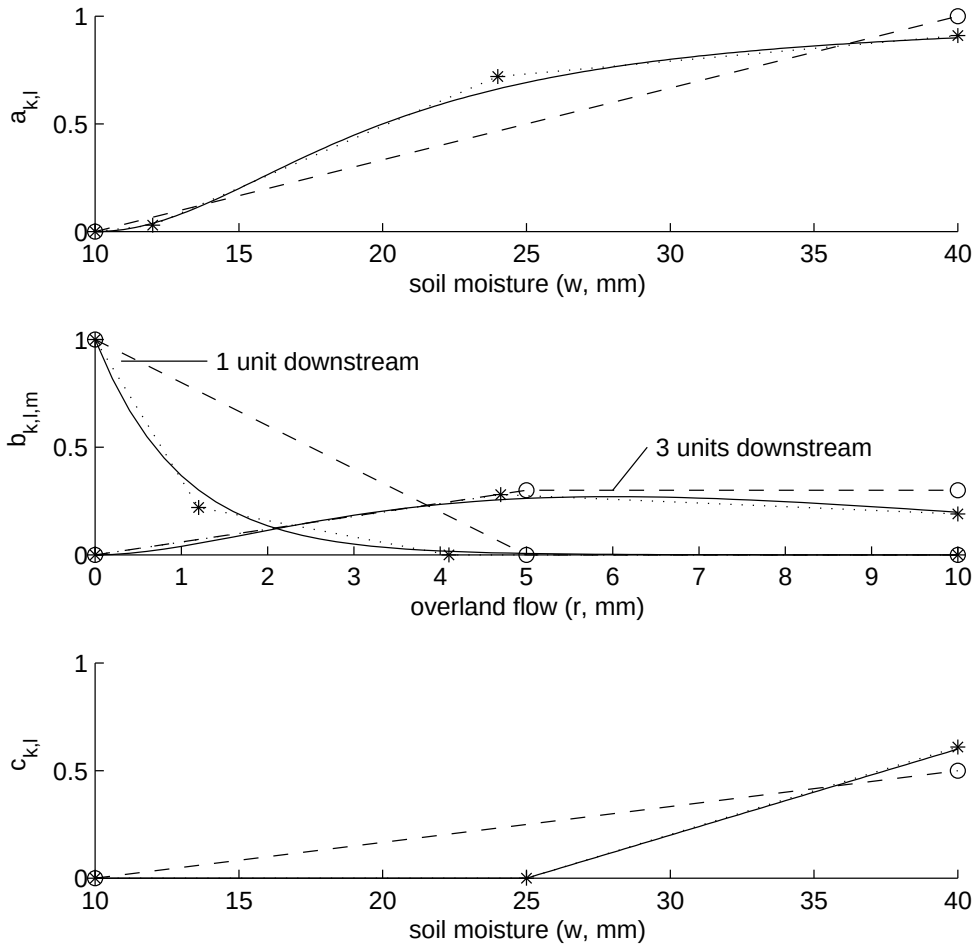

Figure 5.2: Kernel functions used in the original model (–) and the kernel functions derived by the identification method at the first iteration ($--$o) and fourth iteration ($\cdots*$) where the symbols denote the nodes at which the parameters are defined.

The upstream area of a spatial unit l is indicated as l^* and defined by the range of maximum and minimum upstream area within that unit. In this study the catchment is subdivided into 10 zones by 10 isolines of upstream area. The zones should be seen as smallest possible terrain units. In a specific model a minimum of 1 and a maximum of 10 units can be formed as connected combinations of these 10 smallest units. This yields a total of 512 possible spatial subdivisions.

Input and state variables

Recall that our focus is on overland flow during and just after rain in a catchment. Furthermore, in what follows we just consider one-dimensional overland flow and neglect evapotranspiration losses. Precipitation, over a spatial unit l and a time instant k, is the only input under consideration ($p_{k,l}$), see Appendix B. The state variables we consider are: infiltration into the soil ($s_{k,l}$), total soil moisture ($w_{k,l}$), overland flow due to infiltration excess ($r_{k,l}$) and overland flow due to saturation excess ($t_{k,l}$) - all expressed as depth in mm. By grouping for each variable the values for all L units at time instant k into column vectors, e.g. $\mathbf{r}_k = \begin{bmatrix} r_{k,1} & \cdots & r_{k,L} \end{bmatrix}^T$, the vectors $\mathbf{x}_k$ and $\mathbf{u}_k$ in the

physically based state space model with stochastic parameters (Equation 5.1) can be written as

$$\mathbf{x}_k = \begin{bmatrix} \mathbf{s}_k \\ \mathbf{r}_k \\ \mathbf{t}_k \\ \mathbf{w}_k \end{bmatrix}; \mathbf{u}_k = \begin{bmatrix} \mathbf{p}_k \\ 0 \end{bmatrix} \tag{5.3}$$

It will be assumed that the errors in rain and total soil moisture observations are 5% of the observed value, and in the other state variables 10%.

Model parameters and kernel functions

As noted previously, the coefficients in the transition matrices are results from kernel functions. We define the kernel functions as piecewise linear functions with one independent variable. In this study total soil moisture and rain, both for a unit l as well as averaged over an upstream area l^*, are considered as independent variables in the kernel functions ($w_{k-1,l}$, w_{k-1,l^*}, $p_{k,l}$ and p_{k,l^*}). For ease of notation we denote the independent variable of a kernel function as x (without an explicit reference to k and l), and the result of a kernel function is denoted as θ, where $\theta = f(x)$. A kernel function is defined on N points. N may vary between 1 (in case it is a constant, i.e. no dependence on x) and $N_{\max}$, which is 5 here. For each of the N points a triplet of one independent and two dependent variables is defined, the two dependent variables reflect the uncertainty in the coefficients: $\left[x_n, \underline{\theta}_n, \overline{\theta}_n)\right], n = 1, ..., N$. The highest and lowest values of x are the maximum and minimum values of the observed variable which is encountered in the data set to which x refers. Therefore the values x_1 and x_N are not specified as parameters, since these are provided by the data set. The value of the kernel function between the defined points ($x_n \leq x \leq x_{n+1}$) is found by linear interpolation. Figure 5.3 visualizes the form of the kernel functions; it shows that a range of possible parameter values is defined rather than a single parameter value as a function of an independent variable.

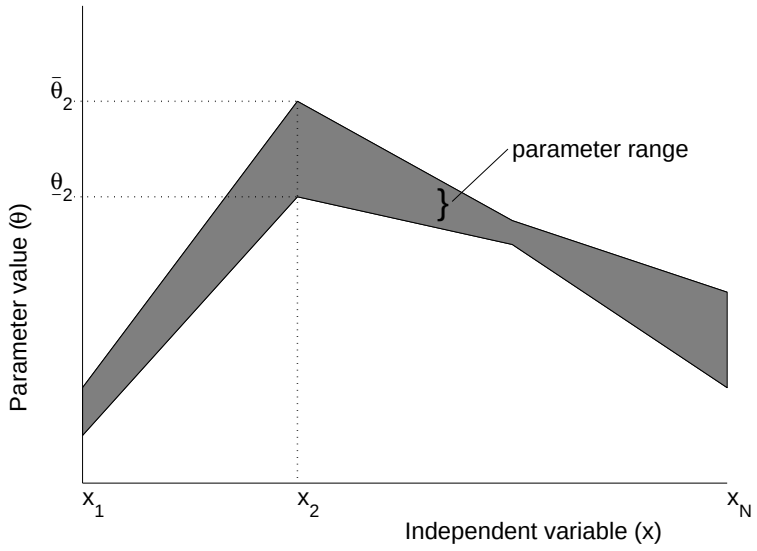

Figure 5.3: The form of kernel functions, showing the parameter values $\underline{\theta}_2 < \theta_2 < \overline{\theta}_2$ defined for a model state-variable or input x_2 and $N = 4$.

The form of the kernel functions is constrained by the definition of the transition matrices, which limits the possible range of θ to a minimum of zero and a maximum of one and the column sums of the transition matrices must sum to unity. Furthermore, each diagonal in the transition

matrices contains only one kernel function, and all kernel functions in a transition matrix use the same independent variable. However, each element in the transition matrices may have different values, since the values of the independent variables ($w_{k-1,l}, w_{k-1l^*}, p_{k,l}, p_{k,l^*}$) are different to each spatial element l.

Since there are two free to select diagonals in $\mathbf{A}_k$, L in $\mathbf{B}_k$ and one in $\mathbf{C}_k$, a model contains at maximum $(L+3)$ different kernel functions and $(3N_{\max}-2)(L+3)$ different parameters; in our example thus 169.

5.4 Finding appropriate models and parameters

Recall that our starting point is not a single model but a set of models, heterogeneous in terms of kernel functions, temporal and spatial resolutions. To identify the set of fit models a Monte Carlo procedure is used, where the following procedure is repeated till satisfactory results are obtained (see also the flow diagram in Figure 5.1). First a finite set of models, the prior set of models, is formed on basis of the template by random selection. After that each of the selected models is calibrated and tested and the fit models are retained in the posterior set of models. Finally elements of the most successful models with similar dimensions are interchanged or combined randomly by a genetic algorithm, to form, together with the posterior model set, the new prior model set. More specifically, and for completeness, we define the following steps:

1. Initialize: K=1, L=1, i=0, j=0

2. Select model structure randomly over the entire range of possible parameter combinations within the limits specified by the template or the prior model set and set counter $i = i+1$.

3. Calibrate selected model structure on a bounded-error data set to determine whether the model is behavioural, by evaluating 10^4 parameter vectors.

4. Back to step 2 if the model is non-behavioural.

5. Validate model on an independent data set to determine model fitness.

6. Back to step 2 if the model is unfit.

7. Store fit model in the posterior model set and determine average fitness of the models in the posterior set, f_j.

8. Back to step 2 until $i = 10^4$.

9. If $(f_{j-1}/f_j) > 0.95$ continue, else increase the allowed spatial or temporal resolution systematically with one step and go back to step 2.

10. Generate a new prior model set of $10^4 - m$ models with a genetic algorithm on basis of the m ($m \leq 10^3$) fit models in the posterior model sets with model dimensions of (K,L), (K-1,L-1), (K,L-1) and (K-1,L).

The steps of calibration (3), validation (5) and new model generation (10) are described in more detail below.

Model calibration

The algorithm as introduced by Keesman (1989) and Keesman and van Straten (1990) is used for calibration. It is a stochastic search procedure within a bounded-error context where for a given model structure the parameter vector (θ**),** containing the coefficients of the kernel functions that define the matrix elements of $\mathbf{A}_k$, $\mathbf{B}_k$ and $\mathbf{C}_k$, is repeatedly generated by a Latin hypercube sampling scheme from parameter ranges $\underline{\theta} < \theta < \overline{\theta}$ (prior parameter set), defining the kernel function. The prior parameter set is scaled to avoid dependence on prior information and to allow a direct interpretation in the original parameter set. Each parameter vector is evaluated by checking whether the calculated output ($\mathbf{x}_k$, for $k = 1, \ldots, K$) is located between the allowable deviations from the measured output ($\mathbf{y}_k + \overline{\mathbf{e}}_k$ and $\mathbf{y}_k + \underline{\mathbf{e}}_k$) (see Equations 5.1 and 5.2). If this is not the case, the parameter vector is rejected, and if it is the case it is retained in the posterior parameter set. This procedure is repeated till a sufficient number of parameter vectors in the posterior parameter set is obtained and new parameter ranges can be established.

Model validation

Behavioural models are tested by determining the quality with which a model can reproduce the behaviour observed in a data set which is not used for model calibration. The measure which indicates this quality is called fitness. Since each model is defined by a maximum and a minimum parameter vector, each particular model is run with a randomly selected parameter vector out of the specified range. For each rain event new parameter vectors are sampled. The criterion used for determining *fitness* is the number of times that the representation does not predict the results of the validation data set correctly out of the total number of temporal units and spatial units for all events ($k = K \times L \times number\,of\,events$). The ratio of number of incorrect predictions over total number of predictions is defined as the probability p. Then, fitness is defined as the chance that a model with a known fraction of p incorrect predictions (in the calibration phase), makes no more than 20% incorrect predictions in the validation phase, assuming a binomial distribution. Finally the 1000 fittest models are selected to form the posterior model set.

The fitness (F) as defined above is calculated by

$$F = \sum_{j=0}^{0.2k} \binom{k}{j} p^j q^{k-j} \tag{5.4}$$

where $q = 1 - p$. Evaluation of model performance in this way is consistent with the assumption of bounded errors, because no information other than correct or incorrect model predictions is used. In addition this criterion takes in a very elegant way the information about the *difference* between model performance during 'calibration' and 'validation' into account (via the probability p). No other criteria were found that also used this information. The criterion of allowing 20% incorrect predictions is of course arbitrary and can be set to any desirable value.

New prior model set generation

New models are generated with a genetic algorithm (Holland, 1975; Mitchell, 1996), which is implemented here as a selection and combination procedure where two models, randomly selected out of the set with fit models, interchange or replace some elements and undergo some random changes. The method assumes that models with a similar temporal and spatial subdivision are more likely to behave similar. This assumption allows the restriction that only models with similar temporal and spatial subdivision (differences up to five minutes or two spatial elements) are able to interact. The model elements to be interchanged or replaced are spatial subdivision and kernel functions, whereby the kernel functions with a large average parameter range have a high chance to

be replaced. Random changes are allowed in spatial subdivision, the independent variable used in the kernel functions (x), the number of parameters (N) and the parameter values themselves. After each calibration and validation step the genetic algorithm creates a single generation of offspring, which is used as a new prior model set.

Description of synthetic data set

A data set, to evaluate both the identification method and criteria for optimizing the measurements, is generated with a two-dimensional finite element representation of a hillslope. The hillslope considered is straight under 5° from the horizontal, has a length of 100 m, and a soil depth of 1 m. Along the slope it is subdivided into 104 elements and in the vertical direction into 8 elements (including the elements describing the soil surface). The input into the model is rain for each surface-element and further it contains the parameters describing overland flow, infiltration and saturated-unsaturated flow for the respective elements in the 2-dimensional domain. The model output comprises the water-fluxes through the 832 elements at each interval. The model parameters represent a loamy soil (overlaying an impermeable layer) without vegetation and little relief. Rain input is generated stochastically for 80 events, using different initial conditions for each event.

The finite element model uses the kinematic wave approximation to the St. Venant equations in order to describe overland flow (Henderson and Wooding, 1964) and the Richards' equation to describe infiltration and flow through the soil matrix (Freeze and Harlan, 1969). For the numerical solution of this problem we used a two-dimensional finite element scheme for flow through the soil matrix, coupled with a one-dimensional finite-element scheme for overland flow calculation, as described in Julien and Moglen (1990). The software codes of CASC2D and SWMS-2D (Šimůnek et al., 1994) have been coupled for this purpose. To generate rain inputs which vary in space and time, as well as spatially variable initial conditions at the onset of a storm a method presented by Freeze (1980) has been used. This method allows the generation of external storm properties from exponential distributions. The internal rain pattern is generated by the rain model of (Bras and Rodriguez-Iturbe, 1976). The parameters that were used for the stochastic generation of rain (80 events) as well as the soil and terrain properties were taken from Table 1 and Figure 7 in Freeze (1980).

The description of overland flow from a slope with unit width used here is given by

$$\frac{\partial h}{\partial t} + \alpha\gamma h^{\gamma-1}\frac{\partial h}{\partial x} + h^{\gamma}\frac{\partial \alpha}{\partial x} = p - \frac{h_{max}h}{h + n_{con}n}r \tag{5.5}$$

with $\alpha = \frac{\beta^{1/2}}{n}$ and $\gamma = \frac{5}{3}$, where h is the flow depth (in m), t is time (in s), p is rain rate (in $m\,s^{-1}$), r is infiltration rate as determined by soil moisture (in $m\,s^{-1}$), β is the average slope gradient, n is the Manning roughness coefficient (in $s\,m^{-1/3}$), h_{max} is a dimensionless coefficient determining the overland flow height where the entire soil surface is covered with water (here set to 0.03), and n_{con} (in $m^{4/3}\,s^{-1}$) is a coefficient to convert the manning roughness coefficient in a water height where half of the soil surface is covered with water (here set to 2), see Julien and Moglen (1990, Equation 6) and Woolhiser et al. (1996, Equations 4 and 5). The factor $\frac{h_{max}h}{h+20n}$ corrects the infiltration for incomplete coverage of the soil surface. The infiltration and movement of water through the soil is described by the Richards equation

$$\nabla(K_s K_r(x,t)\nabla(\psi(x,t)+z)) = C\frac{\partial \psi(x,t)}{\partial t} \tag{5.6}$$

where ∇ is the Laplace operator, K_s is saturated hydraulic conductivity, $K_r(x,t)$ is relative hydraulic conductivity, z is height above the water table or the height of the water layer h ($\psi(x,t)+z$ is the hydraulic head), C is specific moisture capacity and $\psi(x,t)$ is pressure head. The factor $\frac{mh}{h+20n}r$

(in Equation 5.5) is equal to the flux in the vertical direction as calculated by Equation 5.6. The $K(w)$ and $\psi(w)$ relationships are described by saturated hydraulic conductivity, porosity and a soil storage parameter as in Freeze (1980) (w is the soil water content).

5.5 Results

In this section we explore the relations between model performance (i.e. fitness), model structure and resolution. Hereto the data generated by the finite element model for 80 events is split in two groups of 40, the first of which is used for calibration and the second for the determination of fitness (i.e. validation). With the method presented in the first sections of this chapter a set of fit models is obtained for each space-time resolution on basis of these two groups of 40 events. This result is analyzed as follows. First the different aspects of the set of fit models are shown at different resolutions. Then the relation between the parameter uncertainty and model fitness is investigated. Following to that an analysis is made of the trade-off between resolution and the number of parameters per spatial unit in a model. Then the form of the kernel functions at different resolutions is investigated. And finally it is shown how the analysis of the kernel functions may lead to a revision of the template and a better insight in the (modelling of) water transport at the hillslope scale.

Fitness and resolution

The relation between model fitness over a range of temporal and spatial model resolutions is difficult to visualize since it constitutes four dimensions: temporal scale, spatial scale, the set with fit models and fitness itself. We tackle this problem by considering cross-sections of the set with fit models. At first the fitness of the fittest model at each resolution is shown, secondly the average fitness of the 10 fittest models, and at last the size of the set with fit models (see Figure 5.4). It turns out that the fittest models are found in a narrow region in the space-time domain, and that models with the highest fitness have both fine spatial and temporal resolutions. Fitness appears to be low especially when the spatial and temporal resolutions do not match (e.g. 1-minute time intervals in combination with 1 spatial element). The average fitness of the 10 fittest models at each resolution is more or less in line with this pattern. Interestingly, the average fitness at coarser resolutions deviates less than that at finer resolutions. However there appears to be a wide range of more or less fit models (with a fitness ranging from, 50-75), a narrow region with the fittest models clearly distinguishes itself in the time-space domain. In the bottom plot of Figure 5.4 the number of fit models is shown. This appears to be related to fitness of the fittest models in the sense that at the resolutiosn where the fittest models are encountered, also the largest sets found.

An aspect not displayed by these figures is the fact that a particular spatial resolution refers to a set of distinct spatial organizations. Upon analysis it appears that the fittest models constitute an organization that strives to equally sized elements, especially at finer resolutions. Therefore it can be said that the identified models approach the resolution and spatial structure of the original hydrologic model as much as possible.

Fitness and parameter range

The identification algorithm starts by assuming an initial parameter range for each parameter from 0 to 1, and gradually decreases this range by calibration until parameter ranges are obtained that cannot be improved further with the available calibration data. The average parameter range (see Figure 5.3) is a measure of the model quality (uncertainty), and should thus be related in some way to model fitness. However, this relation is not straightforward since the multi-dimensional

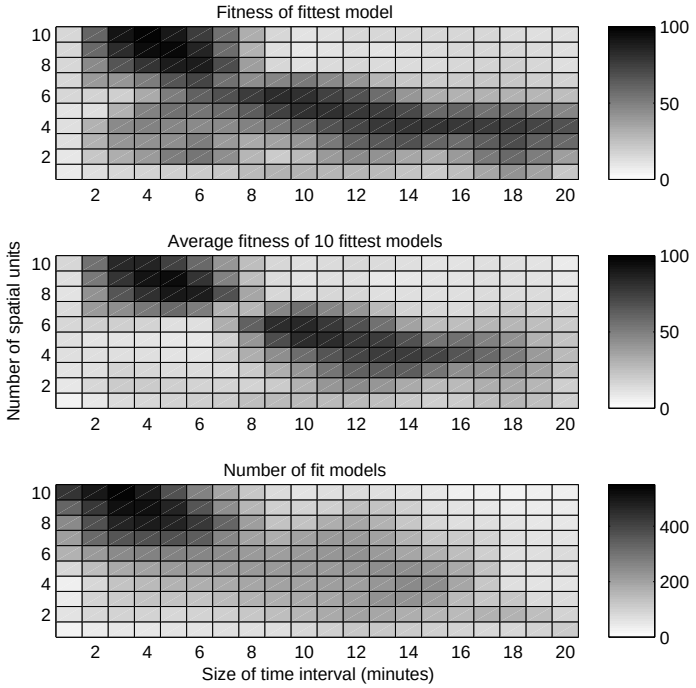

Figure 5.4: Properties of the set of fit models over the entire space-time domain.

parameter space may be complex. Notwithstanding this difficulty we try to explore the relations between the average parameter ranges of the three distinct transition matrices to fitness. First some sub-sets are selected out of the entire set with fit models, according to resolution: models with 1-4 spatial units and 10 min time intervals; models with 4-7 spatial units and 5 min time intervals; and models with 7-10 spatial units and 2 min time intervals. Then the models in each sub-set are grouped according to fitness, in bins of 10 units (e.g. those with a fitness between 15 and 25, those with a fitness between 25 and 35 etc.). For the models in the resulting groups, the average parameter ranges of all the parameters in each transition matrix are calculated. Figure 5.5 shows these relationships. It appears that the parameter ranges of the partitioning and internal state matrices are related to fitness especially at the coarsest resolutions, while the transport matrix shows hardly any relation and moreover constitutes the largest part of parameter uncertainty. An explanation for the differences between the behaviour in the transition matrices could be that the independent variables that were allowed in the kernel functions are simply better suited for the kernel functions in the partitioning matrix and internal state matrix than the transport matrices. The use of overland flow depth, duration and velocity as independent variables to decrease the parameter ranges of the transport matrix has been evaluated, but that did not result in any improvements.

Resolution and parameter-richness

The total number of parameters in a model is influenced by both the number of parameters in each distinct kernel function and the number of spatial elements. An interesting relation is found between the total number of parameters, the average number of parameters per kernel function, and the number of spatial elements of the fittest models. It appears that when moving from a coarse to a finer spatial resolution the total number of parameters in the fittest models stays almost constant (see Figure 5.6). From this it follows that for models with a finer resolution, the kernel functions contain on average less parameters. Figure 5.6 shows this trend for the kernel functions of the three separate transition matrices. There appear to be some subtle differences between the

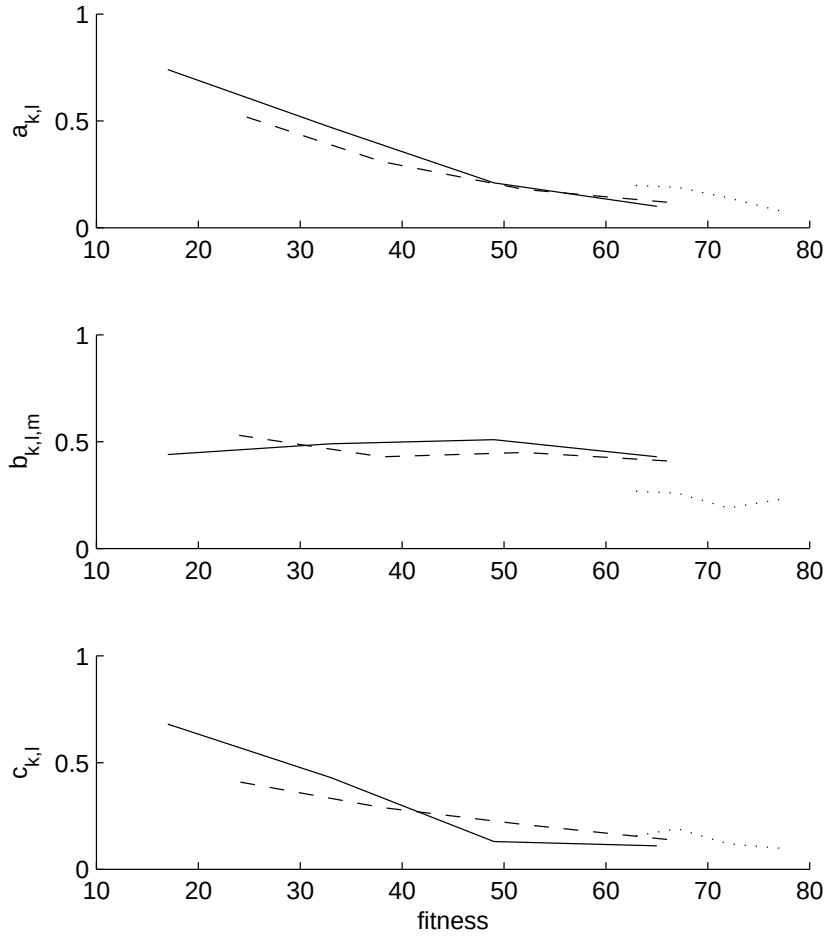

Figure 5.5: The relation between fitness and average parameter range of different kernel functions at three different resolutions. Values for fit models with 1-4 spatial units and temporal units of 10 minutes (–), models with 4-7 spatial units and temporal units of 5 minutes (−−), and models with 7-10 spatial units and temporal units of 2 minutes ($\cdots$).

kernel functions of the different transition matrices: the number of parameters in the transport matrix decreases faster and at a distinct rate as compared to the partitioning and internal state matrices. The similarity between the kernel functions of the latter two matrices is noteworthy, it indicates that the partitioning matrix and internal state matrix are not essentially different.

If a problem of similar dimensions as the template (10 units for soil surface and 10 for subsurface) would be represented by the combined kinematic wave and Richards equations as in Equations 5.5 and 5.6, in total 70 parameters would be used if the parameters are allowed to vary for each spatial unit. In this respect the number of parameters in the identified models (around 50) is low, especially when considering the fact that the identified models are stochastic (a stochastic model of the combined kinematic wave and Richards equations would require extra parameters to specify higher-order moments or bounds on each of the parameters). This means that the combined kinematic wave and Richards equations are not very efficient representations of a hydrologic system of the proposed dimensions (spatial units of 10 meters) from an identification viewpoint.

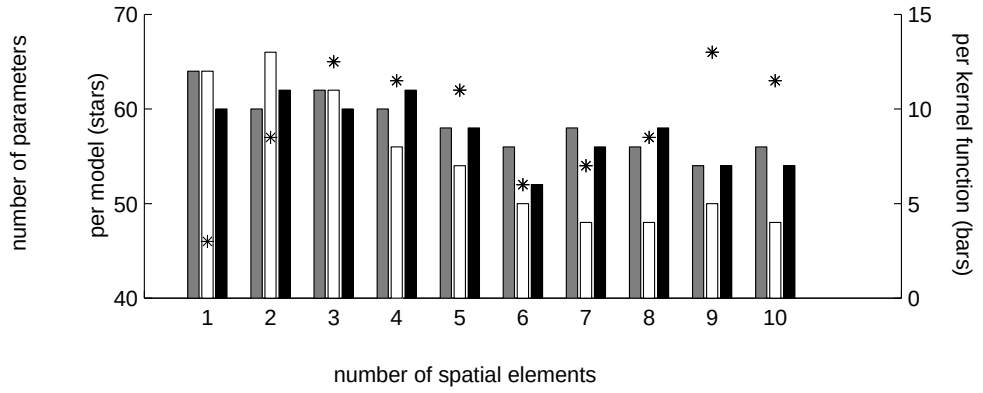

Figure 5.6: The number of parameters at different spatial resolutions; the grey bars give the number of parameters for the kernel functions in the partitioning matrix $(a_{k,l})$, the white bars for the kernel functions in the transport matrix $(b_{k,l,m})$ and the black bars for the kernel functions in the internal state matrix $(c_{k,l})$.

Resolution and kernel functions

The kernel functions relate a coefficient in one of the matrices $\mathbf{A}_k$, $\mathbf{B}_k$ or $\mathbf{C}_k$ to an independent variable. In this study total soil moisture and rain, both for a unit l as well as for an upstream area l^*, are considered as independent variables in the kernel functions (that is $w_{k-1,l}$, w_{k-1,l^*}, $p_{k,l}$ and p_{k,l^*}). Quite interestingly, all four independent variables are encountered in the set of fittest models, however at distinct temporal and spatial resolutions. It appears that among the fittest models, at coarse temporal and spatial resolutions precipitation on a unit ($p_{k,l}$) is generally the most suitable independent variable, and when moving to a finer spatial resolution precipitation of the whole upstream area for a unit (p_{k,l^*}) becomes more suitable. When considering fine temporal resolutions, total soil moisture is the best independent variable in the model, with at coarse spatial resolutions the unit itself ($w_{k-1,l}$) and at finer resolutions the upstream area as spatial component (w_{k-1,l^*}). These patterns are more or less equal in the three transition matrices, i.e. roughly the same independent variable is used in the fittest models at one resolution. In Figure 5.7 the dominant independent variable for the fittest models is shown over the space-time domain. Averaged kernel functions for the 10 fittest models at one specific resolution, describing the fraction partitioned to infiltration excess and saturation excess overland flow, are displayed (in this way leading to an average kernel function with much more nodes than each single kernel function would contain). The figure illustrates that at coarse spatial resolutions shifts from paritioning to infiltration excess towards partitioning to saturation excess overland flow (or vice versa), whereas at fine resolution shifts are abrupt. In other words: the meaning or definition of processes like 'infiltration' or 'saturation' is dependent on the spatial scale under consideration. The same pattern is observed in the internal-state matrix: the shift from non-mobile soil water to return flow is gradual at coarse resolutions and abrupt at fine resolutions. The kernel functions in the transport matrix undergo less significant changes as those in the partitioning and internal state matrices.

Kernel functions and understanding hillslope hydrology

A closer look at the kernel functions in the transport matrix reveals that those at coarse resolutions are double-peaked, whereas the kernel functions at fine resolutions are single-peaked. Characteristic forms for the different resolutions are shown in Figure 5.8. Double-peakedness points at the occurrence of parallel transport processes with different characteristic velocities. On basis of this observation the model template may be adapted by relaxing the assumption that lateral transport

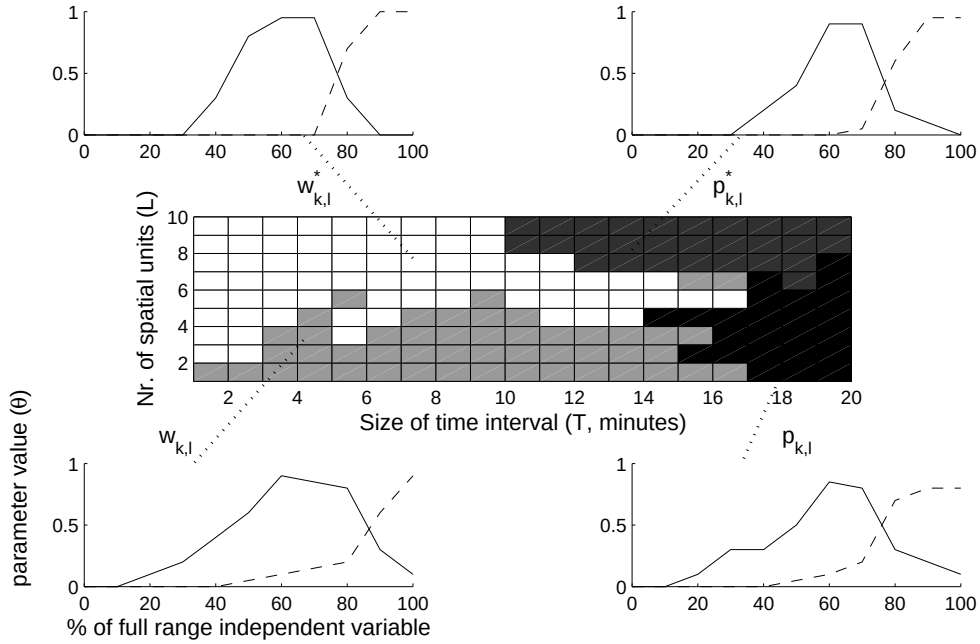

Figure 5.7: Typical forms of average kernel functions. The solid lines give the kernel functions that give the fractions partitioned to overland flow due to infiltration excess, the dashed lines the kernel functions of the fractions partitioned to overland flow by saturation excess (both in the partitioning matrix **A**).

of water takes place only over the soil surface, as shown in Appendix B. When identifying models with this new template which allows lateral transport through the subsurface, single peaked kernel functions are indeed obtained at all resolutions and a clear reduction of the parameter uncertainty in the transport matrix is achieved. However, only at the cost of parameter uncertainty in the other kernel functions (in the **A** and **C** matrices). The overall effect of this is a fitness increase at coarser spatial resolutions and a decrease at finer resolutions (see Figure 5.8). Since both surface and subsurface lateral flow do take place at any resolution (it does so in the finite element model used to generate our data) and models at a fine resolution correspond better to the finite element model, it is paradoxical that models at a coarser resolution do represent the processes of the finite element model better. It can be explained by considering the increased indeterminacy of the problem due to the increased number of parameters by the assumption of both surface and subsurface transport. Correct (i.e. assuming both surface and subsurface transport) and fit models at finer resolutions can only be obtained if extra observations of subsurface flow are used to condition the problem better.

5.6 Discussion

Accurate and at all resolutions correct experimental data of rain partitioning would have been ideal for the purpose of this study. Unfortunately a set with the desired properties was not available and does probably not exist. For this reason we had to reside to the generation of synthetic data to test our identification procedure. This has the advantage that the identification procedure could be evaluated efficiently (due to a 'truth' without error). A disadvantage of the use of synthetic data is the difficulty to transfer the results from this study to other hydrologic problems due to the fact that our 'truth' is generated by a numerical model, which may not be a good description itself for a real-life hydrologic situation. In addition we use an unrealistic high data resolution (all the

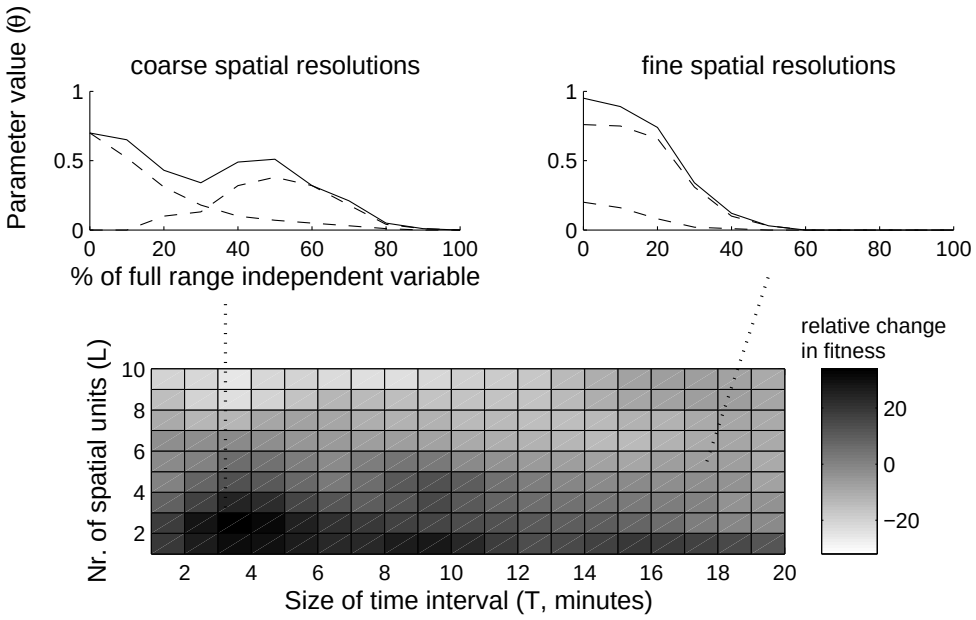

Figure 5.8: Typical kernel functions when one or two lateral flow paths (top axes, solid and dashed lines respectively) are allowed, and the change in fitness when two lateral flow paths are allowed in stead of only one (grayscale figure).

output from the finite element model, averaged over the appropriate units, is used) while real-life hydrologic problems are far more indeterminate. However this aspect was maintained on purpose, in order not to obscure the relationships we intended to highlight. The case where a sample is taken from the available data and where artificial measurement errors are introduced, so that a more realistic identification problem results, is a next step in this investigation.

The example to illustrate the identification method was in the first place meant to clarify the theoretical description of the algorithm. At the same time it showed that the method is able to find the 'true' temporal and spatial resolutions as well as kernel functions of a system with unknown structure and parameters. Due to the correspondence of the original model used for data generation and the template used in the identification method such a comparison was possible. The identification method was tested in this manner on numerous cases not reported here, and was generally able to identify the correct model. This allows the assumption that the identification method behaved as intended.

When identifying hydrologic systems normality and independence of various errors cannot be assumed, due to anisotropy in soil and terrain properties as well as the non-linearity of flow processes and the correlations between measurement error and system state. The consequences of these properties are that they preclude the use of the commonly used stochastic techniques and limit the possible solution technique to some iterative search through the set of models and parameters (Jakeman et al., 1994; Bras and Rodriguez-Iturbe, 1984). The algorithms used in this study acknowledge this limitation and work entirely with random searches and the assumption of unknown-but-bounded errors. The solution technique has many resemblances with some existing techniques (Beven and Binley, 1992), with as added value the integral search through both model and parameter sets in stead of only a parameter set. Also model resolution was not fixed a priori, but optimized by using a genetic algorithm. This approach has been proved successful in similar spatio-temporal problems (Meyer et al., 1989; Richards et al., 1990). In comparison with other generic modelling techniques such as e.g. neural nets, main advantages of the aproach in this study are that conservation of mass is imposed and that kernel functions can be interpreted in a physical

sense.

Although this study has shown some strengths of the technique, such as its general applicability as discussed above, the possibility to evaluate a large set of candidate models, and the possibility to interpret the identified models in a physical sense, we feel that there are certainly some weaknesses as well. In the first place, the resulting models may be relatively complex, which is a logical consequence of the way the template and kernel functions are formulated (and without it the whole method could not function), but which imposes problems when it comes to the analysis of the resulting models. Secondly the method is computationally intensive. And finally the resulting models have a relative poor fit as compared to methods with more strict assumptions on errors (like maximum-likelihood estimation, assuming Gaussian data). In tests with Gaussian data it was found that maximum-likelihood solutions using a $2-$ norm (least-squares solution) lead to fitnesses which were 20% higher than when using an $\infty-$ norm (corresponding to the unknown-but-bounded errors used in this study), for the models of this study. Again, this last aspect is a logical consequence of choices made earlier, which cannot be changed without loss of generality. As a consequence of these weaknesses the method is mainly suitable to identify a limited set of candidate models, that can be further optimized with more rigorous identification techniques (e.g. Norton, 1986; Ljung, 1987; Young and Beven, 1994). The trade-off between the use of a robust error criterion and overall model performance depends on resolution and model formulation and is therefore rather complex. It will be a rewarding topic of future research.

By applying the proposed identification techniques to a detailed data set of hillslope hydrology we obtain results that reconfirm the hypotheses of other studies: 1) various different rainfall-runoff models are identifiable at the hillslope scale, 2) qualitatively different models may show the same behaviour (Grayson et al., 1992b). In addition we hypothesize that: 3) the most successful (fittest) models are encountered at a narrow range in the space-time domain (Figure 5.4) the total parameter uncertainty is related to overall model success (Figure 5.5) the total number of model parameters of the most successful models does hardly change for different resolutions (Figure 5.6) the fittest models are qualitatively different, with respect to form as well as the independent variables in the kernel functions, at different resolutions (Figures 5.7 and 5.8). However most of the above hypotheses are probably not new, there is still disagreement among hydrologists about their validity (Blöschl and Sivapalan, 1995; Refsgaard et al., 1996). On basis of this single case, we cannot more than contribute marginally to this debate. We think therefore that not the results from the case study, but rather the framework explained in this study may contribute to a larger extent. It provides us with a tool for the systematic and repeated investigation of the same hypotheses under diverse circumstances (e.g. different model types, data sets, space and time scales). In particular the different dependencies between resolution and independent variables may be unraveled (see Figures 5.6 and 5.7), or desirable model structure and resolution may be determined for a specific problem (see Figures 5.7 and 5.8). In addition, as illustrated in Figure 5.8, the analysis of kernel functions over a range of resolutions may lead to insight in the hydrological processes and at the same time point at shortcomings in the observations.

5.7 Conclusions

In this study the main objective was to introduce a new method for identifying scale dependent models in a hydrological context. The method has been explained and applied to a hypothetical case at the hillslope scale. Some strengths and weaknesses have been highlighted. The main strengths being general applicability (regardless error structure or non-linearity), the possibility to evaluate a large set of candidate models, to interpret the identified models in a physical sense, and computational simplicity. Weaknesses are the relatively complex models that may result, the computation time required, and the relative poor fit of models as compared to methods with more

strict assumptions on errors. The method is therefore mainly suited to identify a limited set of candidate models, that can be further optimized with more rigorous identification techniques such as maximum likelihood estimation.

The additional objective to explore relations between model structure, resolution and uncertainty (i.e. the inverse of fitness) when predicting overland flow at the hillslope scale resulted in the finding that the three factors are clearly linked. In particular it was found that in the spectrum of temporal and spatial resolutions the fittest models are found in a narrow range, and have a small total parameter uncertainty, a constant number of parameters, and structural model differences at different resolutions.

6 Identification of scale dependent models: the case of catchment scale overland flow

6.1 Introduction

For the case of overland flow at the hillslope scale, it was found in Chapter 5 that uncertainty, resolution and scale dependent model structure are closely related. One of the questions arising from this theoretical study is whether these relations also exist at the catchment scale when using field observations (opposed to using synthetic hillslope-scale data as in Chapter 5). This issue is investigated here for the case of overland flow, using the data from Kaibo and Horizontes as described in Chapter 2. More precisely, the main objective of this chapter is to identify a set of overland flow models on the basis of the available field data for Kaibo and Horizontes and relate the structure of these overland flow models to predictive uncertainty and model resolution. When dealing with field observations, the collection of enough informative observations - to calibrate or identify any useful hydrological model at all - is not trivial (Gupta et al., 1998). This is partly due to the limited observability of hydrologic systems in general, but also to the limited tools available for measurement optimization. Measurement optimization does for that reason deserve some attention in relation to model identification. But since it is beyond the scope of this chapter to deal with this issue, the reader is referred to van Loon and Keesman (2001). As will be shown later, it is possible to identify a set of models that are suitable for overland flow prediction on the basis of the available observations, and this is taken as the starting point for the questions to be investigated here.

This chapter is structured as follows. A brief description of the model and method used for catchment-scale identification is given in Section 6.2. In Section 6.3 the optimal ensemble size for simulation with the model set is established. In Section 6.4 the identified models are validated by comparing discharge and overland flow predictions with observations. Overland flow patterns in space and time are analyzed in Section 6.5. Then, the sets with behavioural models are characterized in Section 6.6. This is followed by an analysis of the kernel functions in the various models in Section 6.7. Finally the results are discussed and conclusions drawn in Sections 6.8 and 6.9.

6.2 Description of the model template

The discrete state space model described by Equations 5.1 to 5.3 is applied to the Kaibo and Horizontes data. The structure of the model template is as follows. It describes overland flow during and just after rain in a catchment, where evapotranspiration losses are neglected. Precipitation ($p_{k,l}$) is the only input under consideration and the model state variables are infiltration into the soil ($s_{k,l}$), overland flow due to infiltration excess ($r_{k,l}$) and overland flow due to saturation excess ($t_{k,l}$) - all expressed as depth in mm (see Appendix B for a detailed explanation). Total soil moisture ($w_{k,l}$) is calculated on the basis of cumulative infiltration. All state variables are expressed as depth in mm. The subdivision in time is regular and models may operate at time steps of 5, 10, 15, 20, 25 and 30 minutes. In space a subdivision of 1 to 18 elements is allowed in Kaibo and a subdivision of 1 to 24 elements in Horizontes. The shape of the spatial units is limited to be a

(combination of a) soil unit, vegetation unit, zone of equal upslope area, and (in the case of Horizontes) the boundary of one of the six sub-catchments. The spatial distribution of upstream area was shown in Figures 2.1 and 2.7 and the boundaries of the six sub-catchments of Horizontes in Figure 2.13. Only one subdivision in upstream area is allowed in Horizontes, and two are allowed in Kaibo so that for Horizontes a maximum of 24 spatial units is obtained on the basis of these rules (6 soil-vegetation classes $\times$ 2 sub-catchments $\times$ 2 zones of upstream/downstream area), assuming that in each sub-catchment each soil-vegetation class occurs; and in Kaibo a maximum of 18 (6 soil-vegetation classes $\times$ 3 zones of upstream/downstream area). This subdivision was found to perform relatively well by trial and error. Also subdivisions on the basis of many (up to 20) iso-lines of upstream area and topographic index were evaluated, but these did not yield behavioural or fit models.

After identifying an initial set of models at the the coarsest spatial resolution (i.e. the entire catchment is one unit) using the method outlined in Section 5.4, the spatial units are established as follows.

1. The catchment is subdivided into several sub-units according to random combinations of the soil and vegetation classes. This starts at coarse resolutions whereafter the units are further subdivided until no model improvement is seen anymore.

2. The catchment is further subdivided according to an iso-line of upstream area. This starts at a one extreme, i.e. a zone with the smallest possible upstream area of $400\,m^2$ complemented by another zone of the remaining upstream area.

3. The iso-line of upstream area is shifted systematically with steps of $400\,m^2$ until the entire range of upstream area is covered.

4. For Kaibo a second iso-line of upstream area is evaluated as in steps 2 and 3. For Horizontes a catchment boundary is added by random selection.

5. Spatial sub-units are joined randomly and this is repeated 10^3 times.

In each of the above steps sets of fit models are established by retaining the fittest models obtained until then. The resulting units are irregular in shape and not ordered according to a toposequence. This implies that the *connectivity* (i.e. the estimated quantity of flow from one spatial unit to another on the basis of topography) cannot be calculated in a straightforward manner. A choice is made to determine the connectivity between two spatial units i and j on the basis of the D8-flow direction map which is defined on a 20×20 m grid (see Chapter 2), using the following expression

$$c_{i,j}(k) = \frac{flow\ from\ i\ reaching\ j\ after\ k\ time\ instants}{total\ flow\ from\ i\ not\ reaching\ j\ after\ k\ time\ instants} \quad for \quad k = 1, \ldots, 10$$

which is calculated as follows

$$c_{i,j}(k) = \frac{\mathbf{m}_j \mathbf{C}^k \mathbf{m}_i}{\mathbf{m}_i^T \mathbf{C}^k \mathbf{m}_i} \tag{6.1}$$

where $c_{i,j}(k)$ is the connectivity between spatial units i and j (i.e. estimated flow from i to j) for time instant k, $\mathbf{m}_j$ is a $(1,L)$ vector with ones and zeroes, indicating whether a grid cell is part of spatial unit j, $\mathbf{C}$ is the (L,L) connectivity matrix of the 20×20 m DEM (i.e. a different representation of the D8 flow direction map), $\mathbf{m}_i$ is a $(L,1)$ vector with ones and zeroes in the diagonal, indicating whether a grid cell is part of spatial unit i. Consider f.i. the simple case of flow along a straight slope of three segments for which the connectivity matrix is given by $\mathbf{C} = \begin{bmatrix} 0 & 0 & 0 \\ 1 & 0 & 0 \\ 0 & 1 & 0 \end{bmatrix}$, and the two upstream segments belong to a spatial unit i, while the downstream

segment belongs to spatial unit j. Now $\mathbf{m}_j = \begin{bmatrix} 0 & 0 & 1 \end{bmatrix}$ and $\mathbf{m}_i = \begin{bmatrix} 1 & 1 & 0 \end{bmatrix}^T$. For these values the result of Equation 6.1 is 2.

Evaluating Equation 6.1 for a range of values $k = 1, 2, \ldots, 10$ yields a distribution of $c_{i,j}$ over k. The mode of this distribution gives the most probable value of k, which can be interpreted as the characteristic duration of transport for flow from i to j. This value will be indicated as $\widetilde{k}_{i,j}$. The mean value of $c_{i,j}$ over the total range of time instants $k = 1, 2, \ldots, 10$ will be denoted by $\overline{c}_{i,j}$. These two entities can be defined more precisely by equations 6.2 and 6.3:

$$\widetilde{k}_{i,j} = max\left(c_{i,j}(k)\right) \tag{6.2}$$

$$\overline{c}_{i,j} = E\left[c_{i,j}(k)\right] \tag{6.3}$$

The independent variables allowed to determine the coefficients in the transition matrices are: $p_{k,l}$, p_{k,l^*}, $w_{k-1,l}$, w_{k-1,l^*}, where l^*refers to the area upstream of unit l. These variables are chosen on the basis of the results obtained in Chapter 5. The identification algorithm outlined in Chapter 5 (See also Figure 5.1) is applied to the calibration data of both the Kaibo and Horizontes catchments, (see Tables 2.1, 2.2 and 2.3). The scheme described in Section 5.4 is applied, using 75% of the calibration data in step 3 and 25% in step 5.

Model predictions and prediction errors are based on the averaged results from a number of randomly chosen models from the final set of fit models. The probability that a model is selected from the set is proportional to its fitness, which implies that a model may be selected more than once. The prediction error (expressed as RRMSE) is determined on basis of the validation data (see Tables 2.1, 2.2 and 2.3), and it is calculated according to Equation 2.1, i.e. in the same way as in Chapters 3 and 4. The reason for simulating with a model ensemble is based on the - initially unexpected - finding that the prediction error decreases with ensemble sizes down to a certain limit. The required ensemble sizes for this study are determined in Section 6.3.

6.3 Determination of the required ensemble size

The results of the identification algorithm is a set with 312 behavioural models for Kaibo and 503 models for Horizontes. The optimal ensemble size for predicting with these models is sought by determining the RRMSE of discharge and overland flow predictions on the basis of the validation data for a range of different ensemble sizes. In this case the RRMSE-values are averaged over the catchment and the entire simulation period. The results of this experiment are shown in Figure 6.1. The figure shows that for increasing ensemble sizes the prediction error decreases. This trend continues up to ensemble sizes of approximately 800 for Kaibo and almost 1000 for Horizontes. There are slight differences in these relationships for discharge and overland flow. Larger ensemble sizes appear to lead to the same minimum prediction errors. The explanation for this relation between ensemble size and prediction error is the relative heterogeneity of the model set. In a heterogeneous set of models, the effect of ensemble size is expected to be large whereas in a relatively homogeneous set it is expected to be small. This explanation suggests that the models derived for Kaibo are more heterogeneous than those for Horizontes. Figure 6.1 possibly contains other useful information to characterize the model sets, but since there is no theoretical framework available to do so we refrain from that. On the basis of the results shown in Figure 6.1 the ensemble size to be used in the remainder of this chapter is set to 1000 members for both Kaibo and Horizontes.

6.4 Model validation

The fact that large sets of behavioural models were found for both Horizontes and Kaibo is in itself already an indication that, given the model template, the identification method can work with field

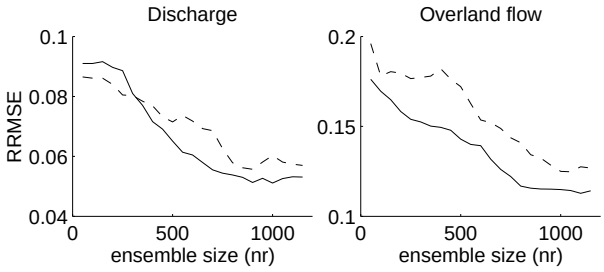

Figure 6.1: The effect of ensemble size on the total predictive uncertainty of discharge and overland flow for Kaibo (solid lines) and Horizontes (dotted lines).

observations at the catchment scale. The closeness of the observed and predicted discharges by the behavioural models during both the calibration and validation stage is shown in Figure 6.2. The figure shows that the deviation is more or less equaly for all discharges. There is a slight overprediction at low discharges, especially for Horizontes. The structure of the prediction error for the validation data is similar to that for the calibration data. This indicates that the calibration and validation set cover the same type of system-behaviour, and that the behavioural models are not over-parameterized. If these conditions were not met, the predictions for the validation data would be much worse. Figure 6.3 shows that the prediction errors seem to be stationary over time.

The ability of the behavioural models to predict overland flow ratios is analyzed by comparing observed and predicted overland flow ratios for different spatial units, in this case the soil-vegetation units and the entire catchment (similar to the analysis in Figure 4.3). Figure 6.4 shows the results. The observations in this graph are derived by averaging the different observations over the spatial units. Interestingly, the fit does not differ for the different resolutions as it did with the model in Chapter 4 where a better correspondence between observed and predicted was found at the catchment scale. A possible explanation for this phenomenon is that models at different spatial resolutions contain approximately an equal number of parameters, which leads eventually to an equal predictive uncertainty at the different resolutions (given that the system is represented correctly at the various resolutions). By a straightforward application of ensemble-prediction, coarse as well as fine-resolution models with a similar fitness have an equal chance of selection, leading to a predictability which is similar over all resolutions. This explanation implies that the use of finer-scale models for prediction at the finer resolutions (the figures at the left) and coarse scale models for prediction at coarser resolutions (figures at the right) should lead to better results. This is tested by using the fittest models at resolutions of 10 to 20 spatial units to predict the overland flow ratio for prediction at the resolution of soil-vegetation units, and using the fittest models at resolutions of 1 to 5 spatial units to predict overland flow depth at the catchment scale. In Figure 6.5 the results are shown. When comparing Figures 6.4 and 6.5 the expected pattern occurs, i.e. a better fit in the latter.

6.5 Overland flow patterns in space and time

The spatial prediction of the overland flow ratio by the behavioural models is shown in Figures 6.6 and 6.7, where the predictions are in fact averages of the ensemble predictions by 1000 randomly selected models. Similar to the results in Chapters 3 and 4, Figures 6.8 and 6.9 present predictions of seasonal average overland flow ratios as well as for subdivision according to season and rain intensity. When comparing these results with those in the previous chapters, several aspect stand out. The first is that the RRMSE of the prediction is higher than for predictions with the regression model, but on average lower than for predictions with the distributed model. Secondly,

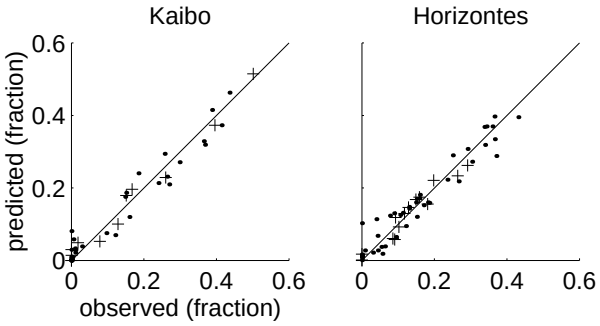

Figure 6.2: Observed versus predicted discharge ratios (event totals of discharge as fraction of total event rain) at the outlets of Kaibo and Horizontes for the calibration (•) and validation (+) data. The predictions are averages from an ensemble prediction (n=1000) with the set of fit models.

the RRMSE is distributed more evenly over space. Furthermore, it turns out that the patterns of overland flow occurrence are rather different, again, from those predicted by previous models.

6.6 Characterizing the sets with behavioural models

Models for the entire season

An overview over the sets with behavioural models is given in Table 6.1. The table lists model properties such as the number of spatial elements, the size of the temporal units and the number of parameters per spatial element. An intercomparison of the models derived for Kaibo with those for Horizontes learns that the most successful models feature a larger number of spatial elements and a finer temporal resolution for the Horizontes catchment. By also listing the 10% fittest models in the set, it is in addition shown that the spatial and temporal resolution as well as the fitness are coupled for both catchments. This pattern corresponds with the relations shown in Figures 5.4 and 5.6. The total number of parameters per spatial element is low for both catchments, compared to the results in Section 5.5 (Figure 5.6). This is notable since there is no super-imposed mechanism in the identification algorithm which leads to a minimization of the number of parameters. It is therefore a property of the system under study (constrained by the available observations and the minimum number of parameters required by the template). The number of spatial elements obtained in the fit models is half to one fourth of the possible number of spatial elements defined in the template. This means that some spatial units have been lumped and are considered as homogeneous with regard to their hydrological response. A way to quantify these effects is by relating the possible spatial subdivision (as specified in the model template) to the actual spatial subdivision (as laid down in a specific model in the set of fit models) via the following index.

$$d_h = \frac{lpost_h}{lpri_h}$$

where h is an index indicating which factor is considered (topographic, vegetation or soil), d_h is called *relative dissection*, $lpri_h$ (in m) is the total length of all vectors dissecting the units defined for factor h in the template, and is $lpost_h$ (in m) is the total length of all vectors dissecting the units defined for factor h in the set of fit models. The relative dissection for the factors topography, vegetation and soil of Kaibo and Horizontes is given in Table 6.2. The relative dissection is a measure for the relative homogeneity of a factor with regard to the occurrence of overland flow. A small relative dissection means in this context that the factor is relatively homogeneous and

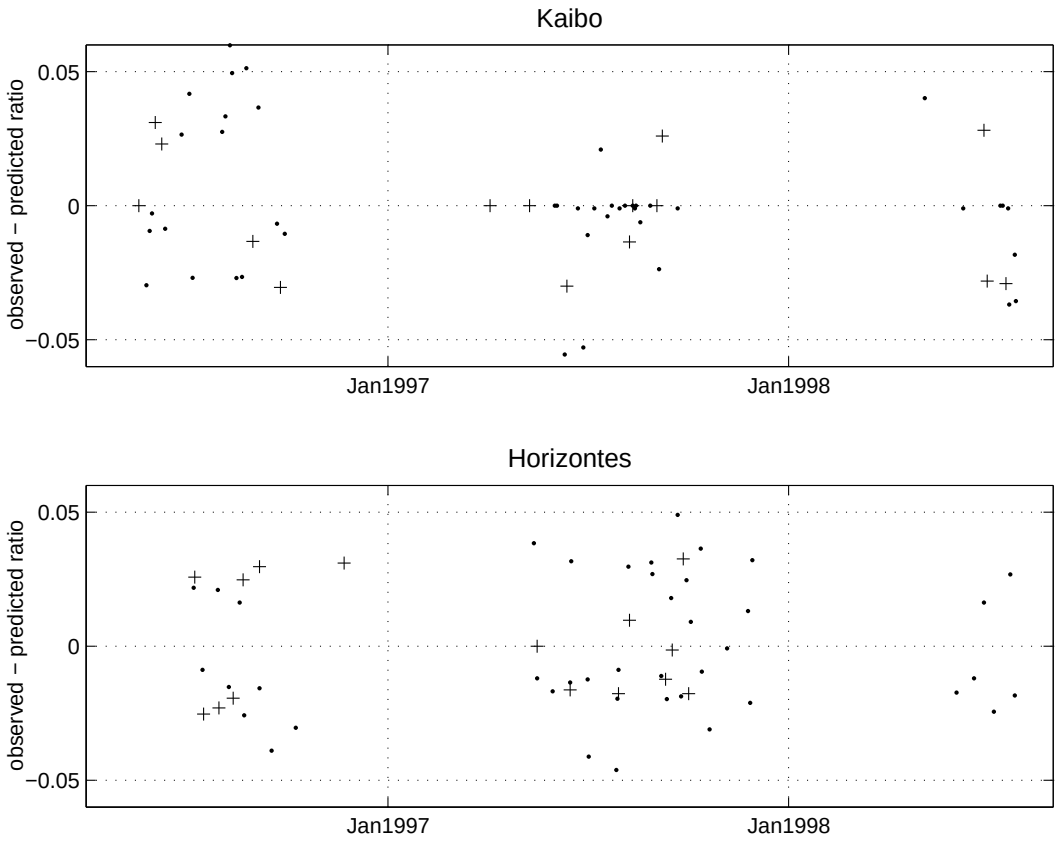

Figure 6.3: The difference of observed and predicted discharge ratios over time for Horizontes and Kaibo.

does as a consequence not need to be taken into account in the template. It turns out that for Kaibo especially land use and soil can be considered as homogeneous units while for Horizontes especially topography can be considered as homogeneous with regard to overland flow occurrence.

Another issue of interest is the actual value of the upstream area iso-lines in the fit models for Kaibo and Horizontes, which follow from the procedure outlined in Section 6.2. The distribution of these values are shown Figure 6.10 in the form of normalized frequency distributions. The Figure shows that two iso-lines occur frequently in Kaibo and one in Horizontes. The small peaks at the left-hand side in the graphs (upstream area = 0) exist because a few models do not use the upstream area for spatial sub-division. The probability distributions have averages of approximately 1.3 and 4.2 ha in Kaibo and 3.7 ha in Horizontes. Especially for Kaibo the distribution of iso-line values is quite peaked. Apparently, quite limited options for spatial subdivision are allowed by the system, leading to this particular pattern. The spatially averaged locations of the iso-lines in both Kaibo and Horizontes are shown in Figure 6.11.

Distinct models for early and late season, light and heavy rain

As has been shown in the preceding chapters and Section 6.5, there are marked seasonal differences in soil and vegetation development for both catchments and also marked differences for low and high rain intensities. Therefore the question arises whether a single set of fit models is really applicable over the entire season and for all types of events in both catchments. And if different

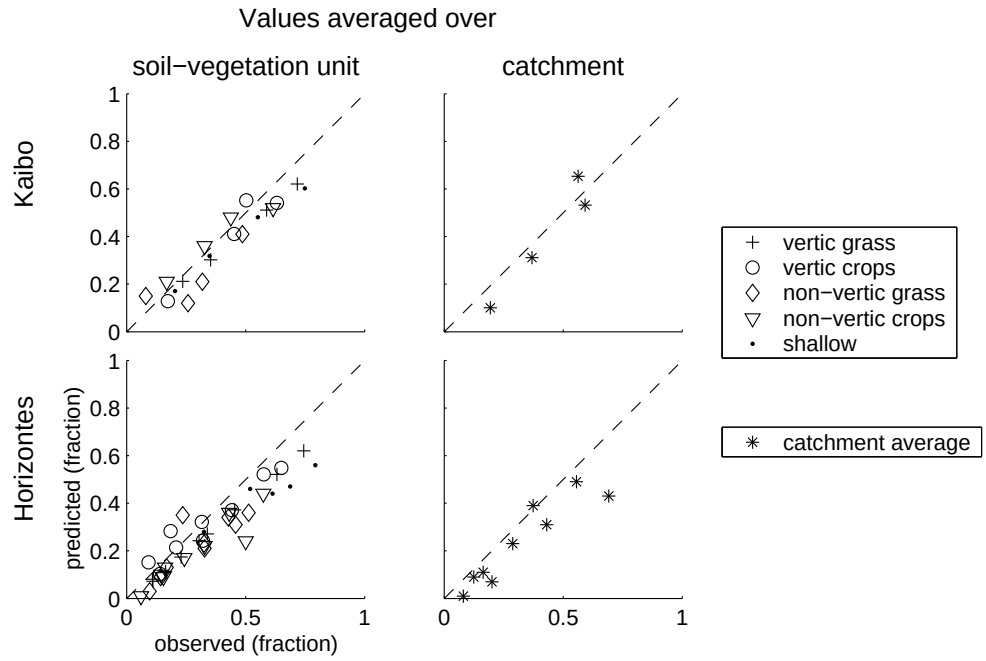

Figure 6.4: Observed versus predicted overland flow ratio per soil-vegetation unit and catchment, where the predictions are based on ensemble prediction (n=1000) with the set of fit models.

models are indeed identified for those different conditions, the question is what can be learned about the hydrologic system on the basis of these differences. As before, the effect of seasonality is investigated by applying the identification algorithm to 20 events that occurred in the first two months and last two months of the Kaibo and Horizontes catchments respectively. And the question whether the (rain) characteristics of an event are important is investigated by considering 20 events with a rain intensity lower than 5 $mm\,h^{-1}$ and 20 events with a rain intensity higher than 20 $mm\,h^{-1}$ for identification. Again, 75% of the data is used for calibration and 25% for validation.

The characteristics of the models, derived on the basis of the different sub-sets of the data, are listed in Tables 6.3 and 6.4. Since the data sets for low and high rain intensity as well as early and late season are less discriminating than the entire set of fit models, larger sets of fit models are expected for each of these cases. Interestingly, this is indeed the case when distinguishing between season (it results in larger sets of fit models for either season, with a higher average fitness), but not when distinguishing between low and high rain intensities (smaller sets with fit models are derived, with a fitness similar to that when considering the entire range of intensities). The spatial discretization of the catchments turns out to display an interesting shift in the case of seasonal differentiation. When taking the first two months of the season the marked effect of soil is observed in both catchments (it is hardly dissected), whereas at the end of the season it is land-use/vegetation which is the least dissected. The differentiation according to rain intensity seems to have no profound effects (see Table 6.5). On the basis of these results the conclusion is that for both catchments better models can be derived by distinguishing between early and late season, but not by distinguishing between light and intense rain. This is intuitively expected because vegetation and land surface changes are not taken into account into the model parameterization whereas rain (depth as well as intensity) is.

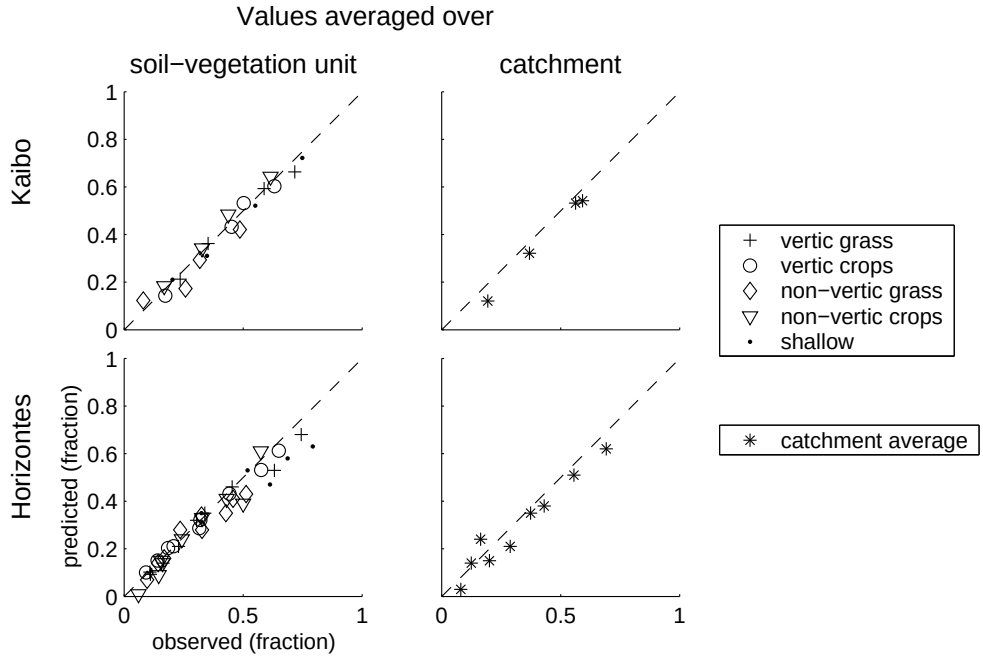

Figure 6.5: Observed versus predicted overland flow ratio per soil-vegetation unit and catchment, where the predictions are based on ensembles (n=1000) that are particularly suited for the resolution of the observations.

6.7 Characterizing the Kernel functions

The models identified in the previous sections are, because of the many parameters they contain, difficult to use for understanding the dynamics of the hydrological systems. Yet, the structure of the models is conceptually simple and not essentially different from those described in Chapters 3 and 4. The regression model of Chapter 3 as well as the distributed model formulated in Chapter 4 could e.g. also be formulated in the state-space form of Equations 5.1 and 5.2. A statistical analysis of the various model components may provide further insight, but presently there is no lead available as to which techniques could be used for that purpose. Another possibility to get hold of the information contained in the models is to replace the kernel functions by continuous functions with much less parameters so that these can more easily be interpreted or related to physical entities. The last technique has been applied here.

It was stated in Section 6.2 that the independent variables allowed in the kernel functions are $p_{k,l}$, p_{k,l^*}, $w_{k-1,l}$, w_{k-1,l^*}, (where l^*refers to the area upstream of unit l). Some of the resulting kernel functions for each of these independent variables are shown for the different transition matrices in Appendix E (Figures E.1 to E.3). The figures display a random selection of 5 out of the total number of kernel functions. As has been demonstrated before, kernel functions have a limited region of applicability in the entire space-time domain of the set with fit models. In Table 6.6 the main regions of occurrence of the various kernel functions in the space-time domain are listed. The table shows that not every independent variable is equally relevant for both catchments (i.e. is dominant in a large number of models), and that certain types of kernel functions are dominant at slightly different resolutions in the two catchments. Especially the variables $p_{k,l}$ and p_{k,l^*}, which are generally dominant at coarser scales (see also Section 5.6), occur at finer resolutions in the Horizontes catchment. This suggests that the flow process is generally faster in the case of Kaibo.

For each of the 'Kernel types' listed in Table 6.6 an analytic expression is sought. Relationships that apply reasonably well are the rectangular hyperbola for kernel functions in $\mathbf{A}_k$ and $\mathbf{C}_k$

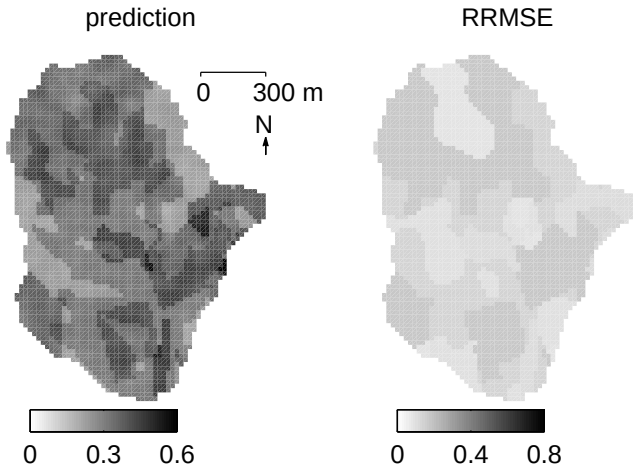

Figure 6.6: Predicted average overland flow ratio and RRMSE over the entire season for Kaibo.

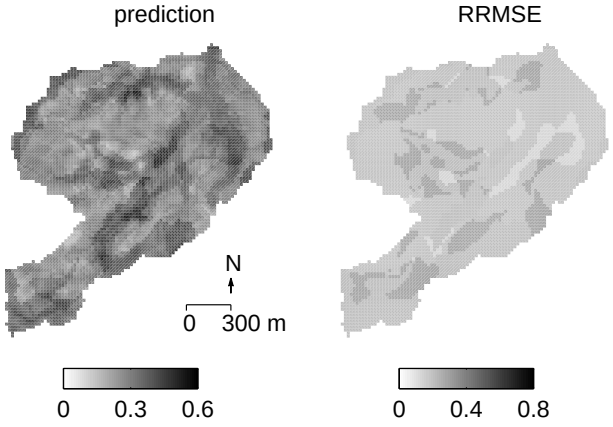

Figure 6.7: Predicted average overland flow ratio and RRMSE over the entire season for Horizontes.

and the gamma distribution (the derivate of the incomplete gamma function) for kernel functions in $\mathbf{B}_k$. The rectangular hyperbola is given by one of the following equations.

$$f(x) = \frac{x^n}{x^n + a^n} \tag{6.4}$$

$$f(x) = 1 - \frac{x^n}{x^n + a^n} = \frac{a^n}{a^n + x^n} \tag{6.5}$$

$$f(x) = \frac{(x_{max} - x)^n}{(x_{max} - x)^n + a^n} \tag{6.6}$$

$$f(x) = \frac{a^n}{a^n + (x_{max} - x)^n} \tag{6.7}$$

where a (> 0) is a factor determining the location of x where $f(x)$ reaches half of its maximum value, x_{max} is the maximum value that x may take, and n a coefficient determining the point of inflection of the curve. In practice equation 6.5 applies to the parameters determining infiltration (declining $f(x)$ for increasing values of $w_{k,l}$ and $p_{k,l}$), and equation 6.7 applies to the parameters

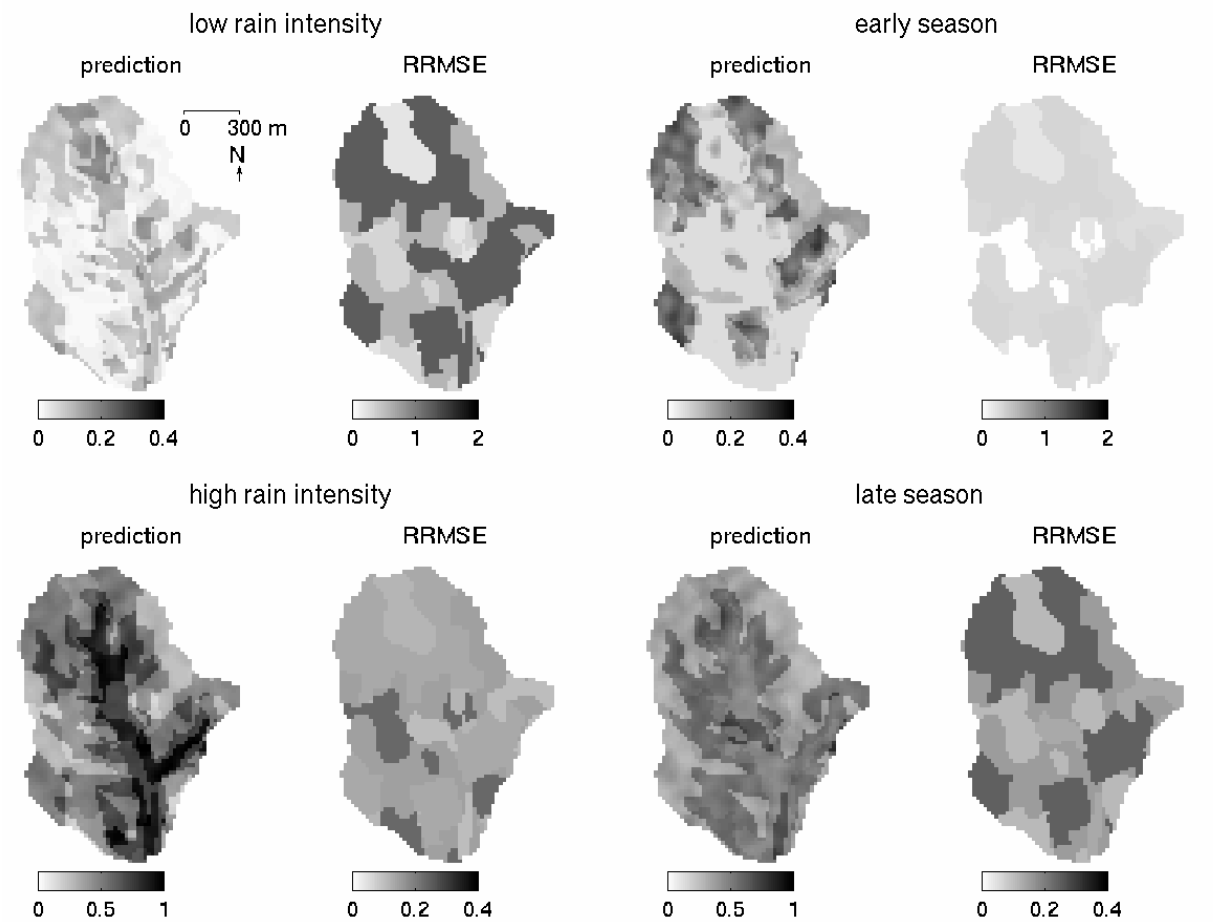

Figure 6.8: Predicted average overland flow ratio and RRMSE for low/high rain intensities and early/late season, Kaibo.

determining saturation excess runoff and return flow (increasing for increasing values of $w_{k,l}$ and $p_{k,l}$). The scaled version of the gamma distribution is given by

$$f(x) = \frac{\left(m\frac{x}{x_{max}}\right)^{(a-1)} e^{-\left(m\frac{x}{x_{max}}\right)}}{\Gamma(a)} \tag{6.8}$$

where a (≥ 1) is a shape factor, which may change the from of the distribution from exponential ($a = 1$) to Gaussian ($a = \infty$), m is a scale factor, and x_{max} is the maximum value that x may take. The parameter a in this equation is given by the product of an average a-value (a_{avg}) and characteristic time $\widetilde{k}_{ij}$ defined in Equation 6.2: $a = \widetilde{k}_{ij} a_{avg}$ and m is defened as an average m-value (m_{avg}) multiplied by the average connectivity defined in Equation 6.3: $m = \overline{c}_{ij} m_{avg}$. This reduces the number of parameters to be fitted to only two for this equation, i.e. a_{avg} and m_{avg}.

Through each of the groups with typical kernel functions an appropriate expression (either 6.4, 6.5, 6.6, 6.7 or 6.8) is fitted. The resulting parameter values are given in Tables 6.7 and 6.8. The functions are are plotted in Appendix E (Figures E.4 and E.5).

The kernel functions can be interpreted in a probablistic sense. The kernel function then provides an estimate of a transport or partitioning parameter ξ (i.e. $\xi := a_{k,l}; b_{k,l}\, or\, c_{k,l}$), conditional on the value that the indepentent variable in the kernel function takes (taking e.g. the kernel func-

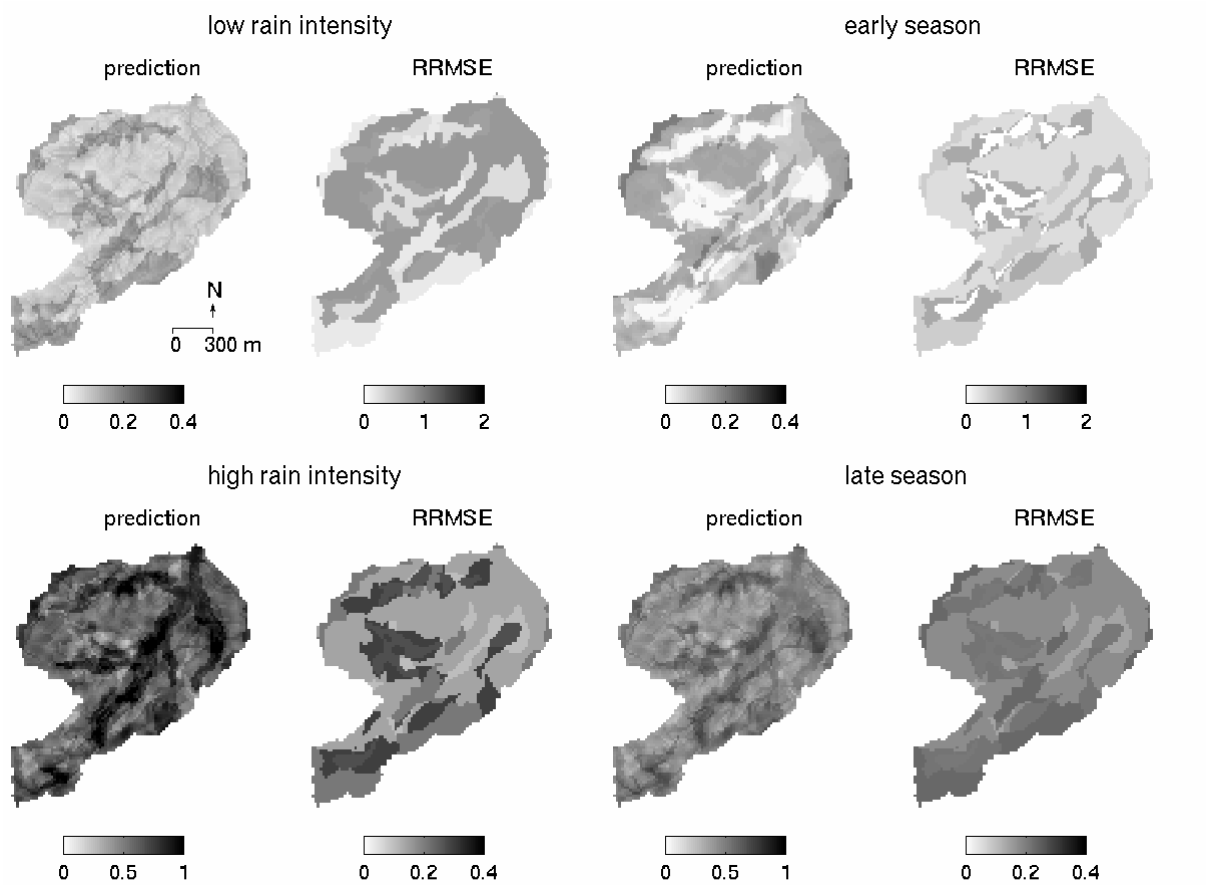

Figure 6.9: Predicted average overland flow ratio and RRMSE for low/high rain intensities and early/late season, Horizontes.

tion of Equation 6.4 with $p_{k,l}$ abbreviated as p):

$$E[\xi \mid x] = \frac{p^n}{p^n + a^n} \tag{6.9}$$

The formalism by Jaynes (Jaynes, 1963, 1982) then states that the best estimate of the conditional probability distibution $f(\xi \mid x)$ is given by

$$f(\xi \mid x) = \frac{e^{-\lambda\mu}}{C(\lambda)} \tag{6.10}$$

in which $C(\lambda)$ represents the kernel function, e.g. $\frac{x^n}{x^n+a^n}$, which should equal the integral of a negative exponential function:

$$C(\lambda) = \int_0^\infty e^{-\lambda\mu} d\mu = \frac{1}{\lambda} \tag{6.11}$$

Combining Equations 6.9, 6.10 and 6.11 leads to

$$f(\xi \mid x) = \frac{x^n + a^n}{x^n} e^{-(\frac{x^n}{x^n+a^n})\mu} \tag{6.12}$$

If for instance the probability distribution for x, $f(x)$, is known, the joint probability $f(\xi, x)$ can be calculated as the product of the two distributions, assuming they are independent. The conditional as well as joint probabilities can be used in probablistic models as those introduced and applied by e.g. Hoskings and Clarke (1990); Milly (1993) and Rodriguez-Iturbe et al. (1999).

Table 6.1: Characteristics of behavioural model sets for Kaibo and Horizontes. The numbers give the mean values while the ranges between brackets give the extreme values occuring in the set.

		Kaibo	Horizontes
all models	number of models in set	312	503
	average (min. - max.) of:		
	spatial elements (nr)	5 (1-7)	11 (4-14)
	temporal unit (min)	17 (5-30)	12 (5-20)
	pars. per spatial element (nr)	3.9 (2-4)	3.1 (2-5)
	fitness (-)	0.6 (0.3-0.9)	0.7 (0.4-0.9)
10% fittest models	number of models in set	31	50
	average (min. - max.) of:		
	spatial elements (nr)	6 (4-7)	13 (4-9)
	temporal unit (min)	14 (5-20)	7 (5-15)
	pars. per spatial element (nr)	2.2 (2-4)	2.3 (2-4)
	fitness (-)	0.8 (0.6-0.9)	0.8 (0.7-0.9)

Table 6.2: The relative dissection d_h of the topographic, vegetation and soil factors for Kaibo and Horizontes for the entire model set and the 10% fittest models.

	entire model set		10% fittest models	
factor (h)	Kaibo	Horizontes	Kaibo	Horizontes
Topography	0.32	0.21	0.42	0.14
vegetation	0.11	0.34	0.10	0.57
Soil	0.12	0.35	0.19	0.31

6.8 Discussion

This study shows that in spite of some marked differences between Kaibo and Horizontes, there are many similarities between the model sets describing these catchments. In the first place the same model template was used for both catchments. The relation between problem resolution, availability of observations and fitness seems to apply to both catchments. Also the shift in the independent variables from soil moisture at fine temporal resolutions to rain at coarse temporal resolutions is applicable to both Kaibo and Horizontes. The catchments differ with regard to the exact form of the kernel functions and the model resolutions to which different kernel functions apply. This can be explained by the difference in topography - Kaibo has longer slopes and less relief - and the limited spatial discretization of the models for the Kaibo catchment (Table 6.6).

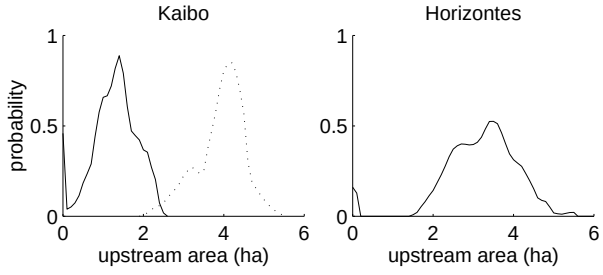

Figure 6.10: The normalized frequency distribution of the upstream area iso-lines in the fit models for Kaibo and Horizontes.

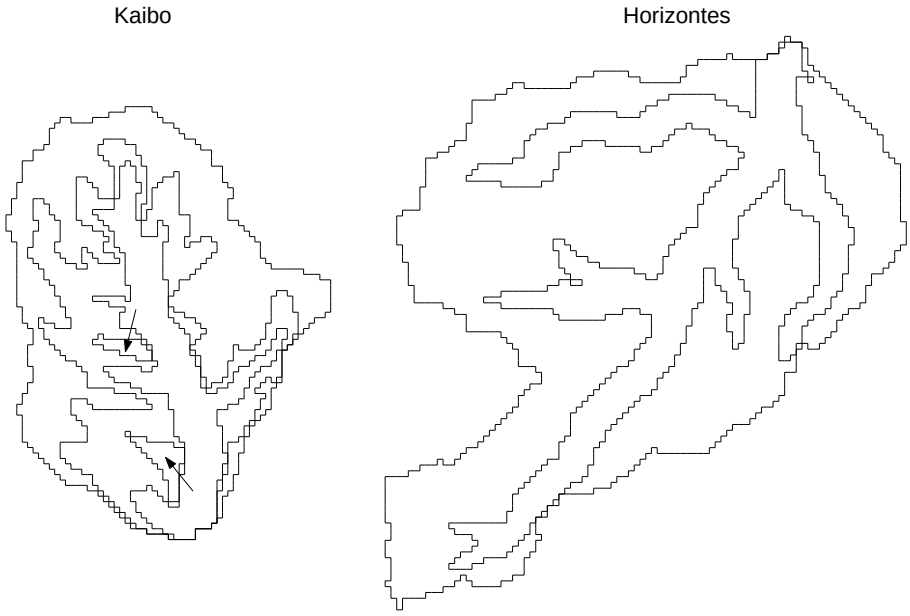

Figure 6.11: The spatially averaged location of the iso-lines for Kaibo and Horizontes. The two patches in Kaibo indicated by the arrows are outside both upstream area iso-lines.

This last factor may have been caused by the relatively few distributed observations in Kaibo. It is notable that the same shifts in the use of independent variables are found for the real data sets at the catchment scale as with the synthetic data set at the hillslope scale (see Chapter 5). It suggests that the source-driven system behaviour at coarse resolutions and sink-driven behaviour at fine resolutions is a property of the hydrologic systems at both scales. The size of spatio-temporal units to which 'coarse' or 'fine' refer depends on the heterogeneity of rain, soil and terrain characteristics (inputs and main model determinants), and differs for different areas. At the point where models are identified as 'fit' for a specific resolution it is perhaps irrelevant to bother about these heterogeneities. However, for the characterization and intercomparison of different catchments a quantification of this 'functional heterogeneity' might be of interest. As done in this chapter, model forms can be analyzed over a range of space-time resolutions, leading to the demarcation of kernel-shifts. Comparing the location of these kernel-shifts for Horizontes and Kaibo leads to the observation that the shift from source to sink-limited system behaviour occurs at a spatial resolution of approximately 7 units for the Horizontes catchment and 5 units for the Kaibo catchment. These resolutions correspond to physical dimensions of (on average) 300 m in Horizontes and 220 m in Kaibo.

Relating these dimensions with the spatial correlation structure of the rain, soil and vegetation characteristics indicates that especially the spatial structure of the rain (with auto-correlations dropping sharply at 350 and 200 m for Horizontes and Kaibo respectively) could give rise to this pattern. The spatial heterogeneities of soil and vegetation characteristics are approximately twice as large. This observation gives rise to the hypothesis that in the two study catchments the structure of a rain event is the most important determinant for overland flow patterns, instead of topography or the pre-event soil moisture distribution.

Applying the identification procedure to different sub-sets of the data, leads to very interesting results. In the first place, it shows that rain intensity does not influence the parameterization whereas seasonality (the time after start of the wet season) does. This means that the nature of the hydrologic system changes over the rainy season. It has been explained before (Section 4.7) that this change is caused by various strongly correlated processes: swelling and shrinking

Table 6.3: Characteristics of behavioural model sets for Kaibo and Horizontes, identified using 10 low-intensity and 10 high-intensity events

		Kaibo	Horizontes
low intenisty	number of models in set	214	351
	average (min. - max.) of:		
	spatial elements (nr)	5 (1-7)	11 (4-14)
	temporal unit (min)	17 (5-30)	12 (5-20)
	pars. per spatial element (nr)	3.9 (2-4)	3.1 (2-5)
	fitness (-)	0.6 (0.3-0.7)	0.7 (0.4 - 0.8)
high intensity	number of models in set	201	373
	average (min. - max.) of:		
	spatial elements (nr)	6 (4-7)	13 (4-9)
	temporal unit (min)	12 (5-15)	7 (5-15)
	parameters per spatial element (nr)	2.2 (2-4)	2.3 (2-4)
	fitness (-)	0.7 (0.4-0.8)	0.7 (0.3-0.8)

Table 6.4: Characteristics of behavioural model sets for Kaibo and Horizontes, identified using 10 events from the first two and 10 from the last two months of the rainy season.

		Kaibo	Horizontes
first two months	number of models in set	453	768
	average (min. - max.) of:		
	spatial elements (nr)	4 (1-6)	7 (4-9)
	temporal unit (min)	21(10-25)	14 (5-20)
	parameters per spatial element (nr)	2.8 (2-5)	3.0 (2-5)
	fitness (-)	0.8 (0.5-0.9)	0.8 (0.5 - 0.9)
last two months	number of models in set	519	873
	average (min. - max.) of:		
	spatial elements (nr)	5 (3-7)	8 (4-10)
	temporal unit (min)	14 (5-20)	11 (5-15)
	parameters per spatial element (nr)	2.3 (2-4)	2.2 (2-4)
	fitness (-)	0.8 (0.6-0.9)	0.9 (0.7-0.9)

of clays, vegetative developement, changing soil roughness due to the impact of rain, animals, tillage and soil macrofauna. A considerable heterogeneity within the model set derived on the basis of average-seasonal conditions, could be explained by shifts in these factors. However, the limited size of the data set, especially with regard to these seasonal factors, did not allow the parameterization of the various models with these newly identified factors.

For both catchments the kernel functions for partitioning could be estimated by a rectangular hyperbola, and the kernel functions for transport by gamma-distributions. As has been explained in Section 6.7, the functions can be interpreted in a probablistic sense. leading to *data-based* conditional and joint probability distributions of hydrological variables. The applicability of these distributions for practical purposes still needs to be tested.

6.9 Conclusions

The application of the identification procedure presented in Chapter 5 to the data of Chapter 2 led to results that corresponded closely with those obtained using the synthetic data set in Chapter

Table 6.5: The relative dissection d_h of the topographic, vegetation and soil factors for Kaibo and Horizontes, identified with 10 events in the first 2 months / last 2 months of the rainy season ('early/late season' in the table) and 10 low-intensity / high-intensity events.

	early / late season		low / high rain intensity	
factor (h)	Kaibo	Horizontes	Kaibo	Horizontes
Topography	0.42 / 0.54	0.31 / 0.34	0.28 / 0.24	0.23 / 0.26
Vegetation	0.24 / 0.05	0.34 / 0.17	0.09 / 0.11	0.28 / 0.25
Soil	0.12 / 0.39	0.15 / 0.41	0.10 / 0.11	0.35 / 0.32

Table 6.6: Overview of the (square) regions in the space-time domain where the different types of kernel functions are present in more than 50% / 90% of the fit models.

Transition	Kernel	Indep.	Kaibo		Horizontes	
matrix	type	var.	time (min)	space (nr)	time (min)	space (nr)
$\mathbf{A}_k$	1	$p_{k,l}$	20-30 / 20-25	1-4 / 1-3	15-30 / 15-25	3-8 / 2-4
	2	p_{k,l^*}	20-30 / 20-25	2-5 / 3-5	15-25 / 15-25	4-9 / 3-6
	3	$w_{k-1,l}$	15-25 / 15-20	4-7 / 5-7	10-20 / 15-20	4-14 / 9-14
$\mathbf{B}_k$	1	$p_{k,l}$	20-25 / 20-25	2-6 / 2-4	20-30 / 20-25	4-10 / 4-9
	2	p_{k,l^*}	15-30 / 20-25	1-4 / 2-4	15-30 / 20-30	4-9 / 4-8
	3	$w_{k-1,l}$	15-20 / 15-20	3-7 / 4-5	15-30 / 15-25	6-12 / 8-12
	4	w_{k-1,l^*}	15-25 / 15-20	5-7 / 6-7	10-20 / 10-15	5-16 / 9-15
$\mathbf{C}_k$	1	$p_{k,l}$	20-30 / 20-25	1-5 / 1-4	15-25 / 20-25	5-11 / 6-9
	2	p_{k,l^*}	15-30 / 15-20	3-5 / 4-5	10-25 / 15-25	4-9 / 4-8
	3	$w_{k-1,l}$	10-20 / 10-15	3-7 / 5-7	10-20 / 15-20	5-14 / 8-14

5. Therewith the conclusions of Chapter 5 are reinforced. Although the Kaibo and Horizontes catchments are different with respect to vegetation, soil, topography and the availability of distributed observations (see Chapter 2), quite similar model structures are identified as fit for both catchments. The fit models correspond with regard to the independent variables used at different resolutions and the size of the spatial and temporal units. Differences are formed by different discretizations and parameter values (the form of kernel functions).

From the results in this Chapter there are various options for further research, which will not further be explored in this dissertation. In relation to the shape of kernel functions a possibility is to re-calibrate the models with the continuous kernel functions and compare the re-calibrated models (again) with the data-based models. Another line of inquiry may be to search for other continuous kernel functions, having a better theoretical underpinning than those presented here. In relation to the spatial discretization it can be rewarding to apply the method demonstrated here to less complex catchments or even synthetic catchment-data to analyze in detail whether the method can recover important shifts in boundary conditions or media-properties of relevance in these cases as well.

Table 6.7: Parameter values for Equations 6.5 and 6.7 as fitted to each of the groups of typical kernel functions in Figures E.1 and E.3 for Kaibo / Horizontes.

Transition matrix	Kernel type	Parameters		
		a (unit)	x_{max} (unit)	n (-)
	for infiltration excess overland flow parameters $r_{k,l}$, Equation 6.4			
$\mathbf{A}_k$	1	14 / 23	-	1 / 1
	2	23 / 16	-	3 / 2
	3	19 / 21	-	4 / 3
	for saturation excess overland flow parameters $t_{k,l}$, Equation 6.7			
$\mathbf{A}_k$	1	18 / 21	42 / 45	4 / 2
	2	16 / 25	52 / 63	4 / 3
	3	9 / 5	35 / 32	2 / 2
	for return flow parameters $c_{k,l}$, Equation 6.4			
$\mathbf{C}_k$	1	28 / 21	62 / 54	4 / 2
	2	26 / 35	52 / 63	3 / 4
	3	31 / 38	49 / 63	4 / 3

Table 6.8: Parameter values for equation 6.8 as fitted to each of the typical kernel functions in Figure E.2 for Kaibo and Horizontes.

Kernel type (B)	Kaibo		Horizontes	
	m_{avg}	a_{avg}	m_{avg}	a_{avg}
1	20	0.8	14	0.9
2	24	0.9	18	0.9
3	40	0.9	17	0.7
4	34	0.8	19	0.6

7 Prediction through parameter and state regularization

7.1 Introduction

The problem of model structure identification as it has been dealt with in the previous chapters focuses on a single catchment and a limited observation period. For a hydrological model to be a useful tool in planning, it should be possible to apply that same model to other locations or time periods without redoing the structure identification or having to collect large amounts of observations. Another reason for not changing the model structure at different situations is to keep model results compatible with earlier results and therewith reasonably straightforward to interpret. On the other hand, it has become clear from numerous studies that a certain amount of re-calibration is always required in catchment modelling (Duan et al., 1992; Sorooshian, 1991; Sorooshian and Gupta, 1985). The question remains however, which parameters in the model are best suited for this purpose, how the parameter values can be determined and at which resolution the re-calibrated model should be defined. In view of previous work on model (re-)calibration, especially the last question is interesting since the choice for the resolution at which a hydrological problem is defined is often not discussed nor explained. Commonly, resolution is either set equal to that of the most detailed input data available, or the highest possible resolution is chosen within the operational limits. In surface hydrology this implies that spatial resolution is often chosen in relation to the terrain representation and temporal resolution in relation to the rain or discharge data. Data that are not available at the appropriate resolution are calculated at the corresponding elements and time instants by aggregation, disaggregation or interpolation. The direct consequences of a particular choice of the resolution for the predictive power and the uncertainty in parameter estimates are often overlooked. In the eighties and nineties 'scale problems' have received considerable attention in the hydrologic discipline (Blöschl and Sivapalan, 1995). The emphasis in these studies was on the translation of knowledge from one resolution to another by aggregation or disaggregation and on ways to deal with the discrepancy between integration volume or time of measurements and the size of model units. The effect of model resolution on prediction error and parametric uncertainty has, however, received scant attention. A notable exception is the relation between grid-DEM resolution and certain topographical indices which play an important role in many hydrological models (Walker and Willgoose, 1999). But also in this case the effect of resolution has not been investigated systematically in relation to general model performance. This is a remarkable situation, since a simple count of variables in any realistic hydrologic problem shows that the available observations alone cannot contain sufficient information to determine a distributed-parameter model to a reasonable degree, even not if the problem is limited to the re-calibration of a few parameters. The problem is said to be *ill-posed* (see Section 1.5). Even if enough data seem to be available to uniquely define a hydrologic problem (in 'less-distributed' models), it often appears that solutions are very sensitive to perturbations in the boundary conditions or input data. This is normally due to the stiffness (i.e. the presence of interacting slow and fast processes) of hydrologic models. This problem is also called *ill-posed.* When seeking a way to calibrate a model in face of ill-posedness, a common approach in many engineering disciplines is the de-

velopment of an alternative model structure, with fewer degrees of freedom and a more suitable parameterization. However, as pointed out above, in hydrological problems the change of model structure is often undesirable since it would render the model incompatible with other applications or make the model results difficult to interpret. Therefore the problem is usually handled by using additional information, in the form of assumptions about parameter values and relations between parameters. These assumptions, or the data on which assumptions are based, are unfortunately hardly ever made explicit, which impedes the possibility to compare and generalize models or model results (Grayson et al., 1992b). This limited ability to compare and generalize distributed parameter models has lead to the questioning and discussing the usefulness of such models, see the discussions in e.g. Beven (1995) and Loague (1990). To date, a follow-up from this point, e.g. through an investigation to the degree in which hydrologic models are ill-posed and how these can be conditioned with additional data, is lacking. Here the aim is now to provide such a follow-up by considering a *regularization* approach to combine a set of calibrated catchment scale models of overland flow with additional observations. First, a technique is presented to solve the calibration problem for a general class of ill-posed time-varying linear models of overland flow. Then in Section 7.3 the technique is applied to different sets of models and observations. This is followed by an inter-comparison of various ways to re-calibrate models in Section 7.4. The implications of the results are discussed and conclusions are drawn in Section 7.5.

7.2 Calibrating an ill-posed hydrological system through regularization

Conversion into standard linear time varying form

It has been shown in Chapters 5 and 6 that a large class of hydrological systems, which vary in time and space and are often non-linear, can be represented by linear time-varying state-space model according to Equations 5.1 and 5.2, which will be repeated here for convenience:

$$\mathbf{x}_k = \mathbf{A}_k\mathbf{B}_k\mathbf{C}_k\mathbf{x}_{k-1} + \mathbf{A}_k\mathbf{u}_k$$

$$\mathbf{y}_k = \mathbf{H}_k\mathbf{x}_k + \mathbf{e}_k$$

where $\mathbf{x}_k$ contains M state variables for each of the L spatial units and the input vector $\mathbf{u}_k$ contains at least L elements at time instant k (but $\mathbf{u}_k$ may be larger, depending on the structure of $\mathbf{A}_k$ and the amount of input variables). The structured matrices $\mathbf{A}_k$, $\mathbf{B}_k$ and $\mathbf{C}_k$ (transition matrices) contain time-varying coefficients θ_k which are stochastic functions of $\mathbf{x}_{k-1}$ or $\mathbf{u}_k$ and can only take values between zero and one ($0 \leq \theta_k = f(\mathbf{x}_{k-1}) \leq 1$). Examples of state variables are overland flow, infiltration and total soil moisture. Examples of inputs are rain, actual evapotranspiration and inflow from an upstream area. The vector $\mathbf{y}_k$ contains P observations and the matrix $\mathbf{H}_k$ is an observation matrix which relates the state variables to the observations, and the output error vector $\mathbf{e}_k$ contains modelling as well as observation errors. The specific model used here has been described in detail in Chapter 5.

In what follows, the focus is on either on-line estimating the unknown coefficients in the transition matrices or estimating the state variables at time instant k from observations available at time instant k (parameter and state estimation respectively). Hence both estimation techniques are recursive and rely on the assumption that the parameter vectors $\{\theta_k, \theta_{k+1}, \ldots\}$ are independent.

To apply the estimation techniques the above equations are converted to the following standard form

$$\mathbf{y}_k = \mathbf{D}_k\mathbf{m}_k + \mathbf{e}_k \tag{7.1}$$

where $\mathbf{y}_k$ is a vector with known values, $\mathbf{D}_k$ a matrix with known values, $\mathbf{m}_k$ a vector with values to be estimated, and $\mathbf{e}_k$ a vector with errors. The way in which Equations 5.1 and 5.2 have to be transformed to obtain equation 7.1 depends on whether we would like to consider *parameter estimation* or *state estimation.* In the case of *parameter estimation* the aim is to estimate the coefficients in the transition matrices. This requires the reordering of the parameters into a vector $\mathbf{m}_k$ and the ordering of the state variables into a matrix $\mathbf{D}_k$. In the case of *state estimation*, the parameters are unchanged but the state vector $\mathbf{x}_k$ is estimated, so the time-varying transition matrices are put in $\mathbf{D}_k$ and the state vector in $\mathbf{m}_k$. In spite of these differences it is *a priori* unclear to what extent both approaches will yield different results. Therefore both approaches are tested here, first the conversion into standard form for the case of parameter estimation will be worked out, and thereafter the conversion for the case of state estimation.

For *parameter estimation* we substitute equation 5.1 into 5.2. Hence,

$$\mathbf{y}_k = [\mathbf{H}_k\mathbf{A}_k\mathbf{B}_k\mathbf{C}_k]\,\mathbf{x}_{k-1} + [\mathbf{H}_k\mathbf{A}_k]\,\mathbf{u}_k + \mathbf{e}_k \tag{7.2}$$

where $\mathbf{x}_{k-1}$ can be substituted by its estimate $\widehat{\mathbf{x}}_{k-1}$. If $\mathbf{H}_k$ is invertible the estimate can be found from

$$\widehat{\mathbf{x}}_{k-1} = \mathbf{H}_k^{-1}\mathbf{y}_k$$

However, in what follows the general case is considered so that $\mathbf{x}_{k-1}$ is estimated from equation 5.1:

$$\widehat{\mathbf{x}}_{k-1} = \mathbf{A}_{k-1}\mathbf{B}_{k-1}\mathbf{C}_{k-1}\widehat{\mathbf{x}}_{k-2} + \mathbf{A}_{k-1}\mathbf{u}_{k-1} \tag{7.3}$$

The model parameters in the transition matrices can be estimated by $\widehat{\theta}_k = f(\widehat{\mathbf{x}}_{k-1})$. Clearly, for this method to work, $\mathbf{x}_0$ must be known or must be included in the estimation problem by augmenting θ_k. In this study $\mathbf{x}_0$ is assumed to be known and not included in θ_k.

Next, the known vectors $\mathbf{x}_{k-1}$ and $\mathbf{u}_k$ are put into the data matrix $\mathbf{D}_k$, and all the unknown parameters ($\mathbf{A}_k$, $\mathbf{B}_k$ and $\mathbf{C}_k$) are put in the parameter vector $\mathbf{m}_k$. A detailed derivation is given in Appendix C. Now equation 7.2 can be rewritten as equation 7.1. Recall that the elements of the vector $\mathbf{y}_k = \begin{bmatrix} y_k(1) & y_k(2) & \dots & y_k(P) \end{bmatrix}^T$ act as observations and the matrix $\mathbf{D}$ acts as 'design matrix' which embodies the geometry as well as inputs to the system, the elements in $\mathbf{m}_k = \begin{bmatrix} m_k(1) & m_k(2) & \dots & m_k(Q) \end{bmatrix}^T$ are the model parameters. In addition to the P observations there are some additional constraints. These arise from the fact that the columns of the transition matrices in the original model (equation 5.1) sum to unity. These constraints form an additional linear equation

$$\mathbf{y}_{cons,k} = \mathbf{D}_{cons,k}\mathbf{m}_{cons_k} \tag{7.4}$$

In order to relate $\mathbf{m}_{cons,k}$ to $\mathbf{m}_k$ it is multiplied with the matrix $\mathbf{H}_k$ (see Appendix C). Notice that the constraints in equation 7.4 are hard constraints which may not be violated. Even with these additional constraints there are, for any realistic distributed hydrological problem, relatively few observations available compared to the number of model parameters, so that information is lacking to determine uniquely all the model parameters. In addition it appears that solutions are generally sensitive to perturbations. The *parameter estimation* problem is thus ill-posed.

When considering *state estimation* we propose to rewrite Equations 5.1 and 5.2 is as follows.

$$\mathbf{y}_k - [\mathbf{H}_k\mathbf{A}_k]\,\mathbf{u}_k = [\mathbf{H}_k\mathbf{A}_k\mathbf{B}_k\mathbf{C}_k]\,\mathbf{x}_{k-1} + \mathbf{e}_k \tag{7.5}$$

which will be written for ease of notation into a regression form

$$\mathbf{y}_k^* = \mathbf{D}_k^*\mathbf{m}_k^* + \mathbf{e}_k \tag{7.6}$$

In this new formulation the elements of the vector $\mathbf{m}_k^* = [x_{k-1}(1)\dots x_{k-1}(4L)]$ are considered to be adjustable, i.e. they act as the model parameters that have to be estimated. To Equation 7.6

the same hard constraints (7.4) apply as to equation 7.1. But now these are imposed directly on the model states, expressed as a global mass balance (i.e. a mass balance at each time instant for the total catchment), i.e.

$$\sum_{l=1}^{L} (s_{k,l} + r_{k,l} + t_{k.l} - p_{k,l}) = 0 \; \forall \; k = 1, \ldots, K \tag{7.7}$$

which can be written in vector form as

$$\mathbf{v}\left[\mathbf{x}_{k-1} - \mathbf{x}_{k-2} + \mathbf{A}_{k-1}\mathbf{u}_{k-1}\right] = 0 \tag{7.8}$$

with

$$\mathbf{v} = \left[\begin{array}{cccccc} 1(1) & \ldots & 1(3L) & 0(1) & \ldots & 0(L) \end{array} \right]$$

Note that the vector **v**, comprising a $(1, 3L)$ sub-vector with ones and a $(1, L)$ sub-vector with zeros, simply sums the first three variables (each defined at L spatial units) of **x**, viz. **s**, **r**, and **t**. By defining $\mathbf{D}^*_{cons} = -\mathbf{a}$ and $\mathbf{y}^*_{cons} = \mathbf{a}\left[\mathbf{A}_{k-1}\mathbf{u}_{k-1} - \mathbf{x}_{\mathbf{k}-2}\right]$, Equation 7.8 can be written in the same way as equation 7.4.

Observer theory conventionally considers the following form of state estimation

$$\mathbf{x}_{k|k} = \mathbf{x}_{k|k-1} + \mathbf{K}_k \left(\mathbf{y}_k - \mathbf{H}_k \mathbf{x}_{k|k-1}\right) \tag{7.9}$$

where $\mathbf{x}_{k|k+1} = \mathbf{A}_k\mathbf{B}_k\mathbf{C}_k\mathbf{x}_{k-1} + \mathbf{A}_k\mathbf{u}_k$. In this framework the design and updating of the gain matrix $\mathbf{K}_k$ plays a central role. The reasons for not using this technique for state estimation here is to avoid the tuning of the gain matrix, which is a laborous task for the set of models under study. It is notable that in the estimation procedure proposed here $\mathbf{y}_k$ is used to estimate $\mathbf{x}_{k-1}$, whereas observer theory (Equation 7.9) conventionally uses $\mathbf{y}_k$ and $\mathbf{x}_{k-1}$ to estimate $\mathbf{x}_k$. At a later stage it may be interesting to compare the techique proposed here with the conventional observer theory (e.g. the Extended Kalman filter or Ensemble Kalman filter), especially because that has never been applied to the problem at hand and also allows the easy incorporation of global constraints (Equation 7.4).

Discrete inverse theory

The solution of equation 7.1 and 7.6 requires an inversion. Since both equations are mathematically equal, only equation 7.1 will be considered in what follows. The concept of the generalized inverse (**G**, also called pseudo-inverse) is used to find a solution to equation 7.1 (Rao and Mitra, 1971). The exact form of the generalized inverse depends on the problem at hand. Some frequently used generalized inverses are $\mathbf{G} = \left(\mathbf{D}^T\mathbf{D}\right)^{-1}\mathbf{D}^T$ (least squares solution) or $\mathbf{G} = \mathbf{D}^T\left(\mathbf{D}\mathbf{D}^T\right)^{-1}$ (minimum length solution). Notice that the generalized inverse is not a matrix inverse in the usual sense (like $\mathbf{D}^{-1}$); it is not square and neither **GD** nor **DG** needs to be equal to the identity matrix as will be shown later. For a given generalized inverse, the model parameters at each time instant k can be estimated from

$$\widehat{\mathbf{m}} = \mathbf{G}\mathbf{y} \tag{7.10}$$

where the subscript k is omitted for ease of notation.

The relation between the estimated and the true model parameters ($\mathbf{m}_{true}$) follows from inserting equation 7.1 in 7.10:

$$\widehat{\mathbf{m}} = \mathbf{G}\mathbf{D}\mathbf{m}_{true} + \mathbf{G}\mathbf{e} \tag{7.11}$$

where the $Q \times Q$ matrix **GD** ($\equiv \mathbf{R}$) is an orthogonal projection matrix, which is often referred to as *model resolution matrix*. In a statistical framework, the vector $\mathbf{R}\mathbf{m}_{true}$ is the expectation of $\widehat{\mathbf{m}}$, i.e. $E(\widehat{\mathbf{m}}) = \mathbf{R}\mathbf{m}_{true}$ if **G** is deterministic and $E(\mathbf{e}) = 0$. Since $E(\widehat{\mathbf{m}}) \neq \mathbf{m}_{true}$, except when $\widehat{\mathbf{m}}$ is the

least squares solution so that $\mathbf{GD} = \mathbf{I}$, it follows that it is likely to be biased. Equation 7.11 can be easily interpreted by rewriting it into

$$\widehat{\mathbf{m}} = \mathbf{m}_{true} + (\mathbf{GD} - \mathbf{I})\,\mathbf{m}_{true} + \mathbf{Ge} \tag{7.12}$$

which shows that the estimated parameter vector is a function of the true parameter vector, the deviation of the model resolution matrix from the identity matrix, and some mapping of the output error. In equation 7.12 the model resolution matrix shows how elements of the estimated parameter vector are linear combinations of the true parameters. In the ideal case, when each model parameter can be resolved, the resolution matrix equals an identity matrix.

Similarly, the estimated model parameters $\widehat{\mathbf{m}}$ may be used to evaluate how well predictions by the model correspond to the observed data through

$$\widehat{\mathbf{y}} = \mathbf{D}\widehat{\mathbf{m}} \tag{7.13}$$

where $\widehat{\mathbf{y}}$ is the predicted output $\mathbf{y}$. By substituting equation 7.10 into 7.13 and applying the same ordering as in equation 7.12 the following expression is obtained

$$\widehat{\mathbf{y}} = \mathbf{y} + (\mathbf{DG} - \mathbf{I})\,\mathbf{y} + \mathbf{e} \tag{7.14}$$

Here the $P \times P$ matrix $\mathbf{DG}\,(\equiv \mathbf{N})$ is called the *data information matrix*. This matrix describes how well the predictions match the original data, apart from the observation errors in $\mathbf{e}$. The diagonal elements in the information matrix indicate how much weight a datum has in its own prediction. It is interesting to notice that both the model resolution and data information matrices are not directly related to the observations ($\mathbf{y}$). This means that for certain cases where the pseudo-inverse $\mathbf{G}$ can be derived in advance, $\mathbf{R}$ and $\mathbf{N}$ can be established before collecting the experimental data.

Another measure for model quality is the covariance of the estimated model parameters. The (co)variances of the model parameters provide a measure for the model prediction uncertainty, and depends on the covariance structure of the data, the covariance of the prior model parameters and the way in which the error is mapped from data to model parameters. Here it is assumed that the covariance matrix of both the data $(\mathbf{C}_y)$ and the prior model parameters $(\mathbf{C}_m)$ are known. The covariance of the estimated model parameters is then given by

$$\mathbf{C}_{\widehat{m}} = \mathbf{G}\mathbf{C}_y\mathbf{G}^T + (\mathbf{R} - \mathbf{I})\,\mathbf{C}_m\,(\mathbf{R} - \mathbf{I})^T \tag{7.15}$$

The resolution matrix, information matrix and model covariance matrix are useful to define the criteria of a good inverse and thus implicitly good measures of the model quality (Backus and Gilbert, 1968; Jackson, 1972):

1. The estimated parameter vector is as close to the true parameter vector as possible. This implies that the resolution matrix should be close to the identity matrix, i.e. $\|\mathbf{R} - \mathbf{I}\|_F$ is as small as possible (where $\|\mathbf{X}\|_F = \left[\sum_i \sum_j [x_{i,j}]^2\right]^{0.5}$, the so-called Frobenius norm)

2. The estimated parameter vector should give a good fit to the data (i.e. model fit). This means that $\|\mathbf{N} - \mathbf{I}\|_F$ is as small as possible.

3. The uncertainties in the estimated parameters (e.g. expressed in terms of variances) should not be large. This means that $trace(\mathbf{C}_{\widehat{m}})$ is as small as possible.

The three criteria can not all be met in an ill-posed inverse problem, since there exists a trade-off between each pair of them, i.e. one can equally well optimize between model resolution and variance, data information and resolution, or data information and variance. Each of the

resulting trade-off curves have been applied in the past (Hansen, 1992; Menke, 1989). Other techniques to determine the so-called optimal rate of regularization in an inverse problem are based on entropy, or some sort of cross-validation (Press et al., 1992; Tarantola, 1987). A rather popular technique, due to its robustness and the avoidance of using the covariance matrix (equation 7.15), is generalized cross-validation (Golub et al., 1979; Hansen, 1998; Wahba, 1977). Generalized cross validation amounts to the minimization of the generalized cross validation function

$$f_{gcv} = \frac{\|\mathbf{y} - \mathbf{D}\widehat{\mathbf{m}}\|_2^2}{(trace(\mathbf{DG} - \mathbf{I}))^2} \tag{7.16}$$

where $\mathbf{G}$ is the parameter to be chosen. It is based on the philosophy that if an arbitrary element y_i is left out, the corresponding solution should predict this observation well; and that the choice of the solution should be independent of an orthogonal transformation of $\mathbf{y}$ (Hansen, 1998). This function f_{gcv} will be used in what follows to find a proper generalized inverse $\mathbf{G}$

Solution method

The generalized inverse $\mathbf{G}$ for our ill-posed problem can only be formed by including prior information to reconstruct lost information and/or regularization (dampening) factors to reduce instabilities. Therefore a set of parameter constraints is added to equation 7.1:

$$\begin{bmatrix} \mathbf{y} \\ \rho\mathbf{m}_{pri} \end{bmatrix} = \begin{bmatrix} \mathbf{D} \\ \rho\mathbf{I} \end{bmatrix} \mathbf{m} + \begin{bmatrix} \mathbf{e} \\ \mathbf{e}_{pri} \end{bmatrix} \tag{7.17}$$

where $\mathbf{I}$ is a $Q \times Q$ identity matrix and ρ is a so-called regularization parameter that will be explained later.

At this point differences arise between the approach of parameter versus state estimation solution (Equations 7.1 and 7.6 respectively). In the case of parameter estimation we use the averages of the stochastic parameters in the initially uncalibrated model (equation 5.1) as prior information ($\mathbf{m}_{pri}$), whereas in the case of state estimation we use prior estimates at a previous time instant ($\mathbf{m}^*_{k-1}$). It is noteworthy that in the case of state estimation it is possible to use additional observations, not included in $\mathbf{y}_k$, as extra constraints. This can be achieved by using the weighted average of prior estimates and additional observations (the weighted average is named $\mathbf{m}^*_{pri}$ here for convenience). More precisely, $\mathbf{m}^*_{pri,k}$ can be determined by the weighted sum of the estimates at a previous time instant ($\mathbf{m}^*_{k-1}$) and additional observations ($\mathbf{m}^o_k$) according to the following equation

$$\mathbf{m}^*_{pri,k} = (1 - o_k)\mathbf{K}\mathbf{m}^*_{k-1} + (o_k)\mathbf{L}\mathbf{m}^o_k \tag{7.18}$$

where $\mathbf{K}$ and $\mathbf{L}$ are cross-correlation matrices for $\mathbf{m}$ at a previous time instant and at distant locations respectively. o_k is zero for time instants where no observations are available, and has a fixed value when observations are available. In order to keep the comparison of parameter and state estimation on equal footing, this extended way of estimating $\mathbf{m}^*_{pri,k}$ is not applied here. Details about this approach can be found in van Loon and Troch (2002).

In both cases (parameter as well as state estimation) adding these additional constraints to Equation 7.1, gives a problem that can be solved in a least-squares sense. Depending on the regularization parameter ρ in Equation 7.17, the solution to Equation 7.17 will vary between the minimum length solution (i.e. the solution based on prior information in the case of parameter estimation, or additional observations in the case of state estimation) or the least squares solution in the observation space. As noted above, generalized cross-validation is used here to determine the desired value of ρ. The generalized inverse therefore gets of the following form

$$\mathbf{G} = \left(\mathbf{D}^T\mathbf{D} + \rho\mathbf{I}\right)^{-1}\mathbf{D}^T \tag{7.19}$$

The solution is found by applying the following steps. The mathematical operations involved in each step at each time instant k are given in Appendix D.

1. A singular value decomposition of $\mathbf{D}_{cons,k}$ is used to solve Equation 7.4, leading to a set of admissible values for $\mathbf{m}_k$.

2. A range of regularization values ρ_k is defined.

3. For each regularization value the solution of step 1 is substituted in Equation 7.17 and by using a singular value decomposition this equation is solved as well.

4. Each solution of step 3 is substituted in Equation 7.16 and the minimum f_{gcv} is selected. The ρ_k , $\mathbf{G}_k$ and $\widehat{\mathbf{m}}_k$ leading to this minimum form the desired solution.

Since Equation 7.2 varies over time, at each time instant (k) a different solution is obtained.

7.3 Description and use of models and data sets

The regularization algorithm described in Section 7.2 requires a prior model in combination with a data set. In this study the data for the Horizontes and Horicajo catchments are used. The models identified for Horizontes in Chapter 6 are used as prior models. Subsequently the set with prior models is used for predicting discharge in the entire Horizontes catchment for two different cases: 1) by using the discharge data for Horizontes for regularization, and 2) by using the discharge, overland flow and soil moisture data from the Horicajo sub-catchment for regularization. The prediction period for the Horizontes and Horicajo catchments covers 15 events. Both data sets contain observations on rain, overland flow, soil properties, vegetation properties and topography (not discharge). In addition, the Horicajo data set includes soil moisture observations (see Chapter 2). The overland flow and soil moisture observations are included in the output vector $\mathbf{y}$ (Equation 7.17). The soil-vegetation classes are used to extrapolate the observations from the observation units to the entire Horizontes catchment in the same way as described in Section 3.4 ('Extrapolating overland flow and discharge observations'). Prediction with the Horizontes data set represents a situation where relatively few observations are available over the appropriate area for which predictions are required, whereas prediction using the Horicajo data set represents the situation with relatively much observations over a sub-area from where predictions have to be extrapolated. Predictions for the the two cases are made in three different ways: 1) in open loop form (i.e. only using the required model inputs), 2) by applying parameter regularization, and 3) by applying state regularization. The regularization algorithm proceeds by first rewriting the prior models in the format of Equations 7.2 and 7.5 and subsequently applying the algorithms for parameter estimation and state estimation to each of the models and each event. In total five prediction runs result, the characteristics of which are summarized in Table 7.1. The prediction runs 2 to 5 do not make use of all the available data, but use subsets of various sizes. The largest subset only contains 75% of the data, while the remaining 25% is used for validation purposes. The nine subsets are established by a latin-hypercube sampling scheme, where 25, 50 and 75% of the observation time instants are combined with 25, 50 and 75% of the observation locations (thus yielding 9 combinations). In all cases 25% of the observation time instants and locations are used for validation. The naming of the subsets is shown in Table 7.2. The relative root mean squared error (RRMSE, see Equation 2.1) of the discharge prediction is considered for models at various resolutions and for the various sub-sets.

Table 7.1: An overview over the different prediction runs, note that the rainfall inputs for all prediction runs are for Horizontes and Horicajo.

prediction run	state observations from	regularization of
1	-	-
2	Horizontes	parameters
3	Horicajo	parameters
4	Horizontes	states
5	Horicajo	states

Table 7.2: Naming of nine sub-sets that result from combining 25, 50 and 75% of the observation times with 25, 50 and 75% of the observation locations in the complete data set; a fixed portion of 25% of the data is used for validation.

coverage	coverage in space		
in time	25%	50%	75%
25%	1.1	1.2	1.3
50%	2.1	2.2	2.3
75%	3.1	3.2	3.3

7.4 Results

Overall model performance

In Table 7.3 the characteristics of the set with prior models are listed. The models have been identified on the basis of the Horizontes data (see Chapter 6). This table shows that a wide range of different models does perform reasonably, since the 10% fittest models (bottom half of the table) display a wide variety of grid sizes, temporal units and parameters per spatial element. The variability of the fittest models approaches in fact the variability of the total model set (upper half of the table). A closer comparison of the upper and lower half of the table shows that those models performing best, have slightly finer spatial as well as temporal resolutions. The location of this optimum is the result of the complex interplay between the space-time distribution of rainfall, the spatial distribution of soil types, topography (average slope length, choice of spatial units relative to topographic features), and density of observations. However, here it is merely established on the basis of validation, and the available data set is not big enough to find a relationship between these factors and optimal resolution. The results for the open-loop application of the model to

Table 7.3: Characteristics of sets with prior models for the Horizontes catchment.

all models	number of models in set	503
	average (min. - max.) of:	
	spatial elements (nr)	7 (4-14)
	temporal unit (min)	12 (5-20)
	parameters per spatial element (nr)	3.1 (2-5)
	fitness (-)	0.7 (0.4-0.9)
10% fittest models	number of models in set	50
	average (min. - max.) of:	
	spatial elements (nr)	8 (4-9)
	temporal unit (min)	7 (5-15)
	parameters per spatial element (nr)	2.3 (2-4)
	fitness (-)	0.8 (0.7-0.9)

the Horizontes data are shown in Figure 7.1. The figure shows the time-averaged RRMSE of the discharge prediction for Horizontes as function of upstream area, for different model resolutions. In the same figure, also the RRMSE of the discharge prediction for the calibration period is shown. In both the calibration and the prediction periods the RRMSE appears to decline for increasing catchment size. In addition, the RRMSE for the calibration period is considerably smaller than that in the prediction period. The fact that a larger RRMSE is found when considering a smaller area, implies that the heterogeneity of the small area is not represented well by the model. This may have two causes: 1) the model units are too coarse to capture the system heterogeneity at this scale, or 2) the model is over-parameterized. Considering that the method used for system identification aims at avoiding over-parameterization (see Chapters 5 and 6), and that over all resolutions model performance is quite equal, the first is the most likely explanation for the bad predictions over small areas.

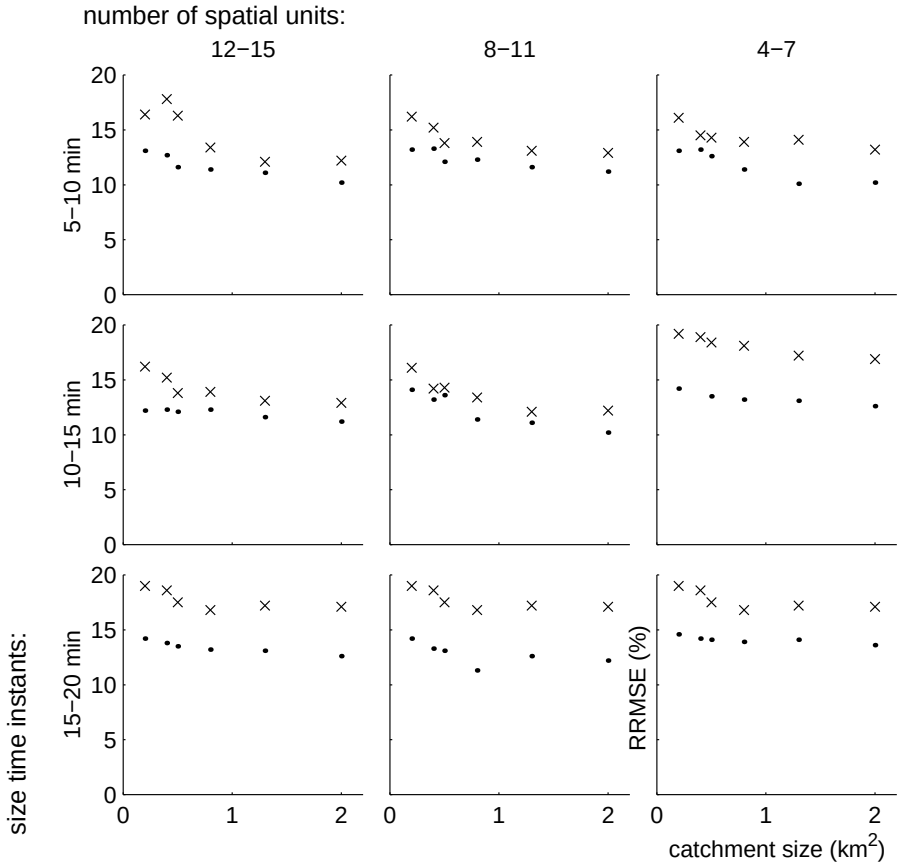

Figure 7.1: Time-averaged RRMSE of discharge prediction in Horizontes at six different measurement locations each with varying catchment size (see Figure 2.12), for open-loop models over the calibration (•) and the prediction (×) periods

Performance for varying data density

In Figure 7.2 the time-averaged RRMSE of the discharge prediction is shown for both parameter and state regularization, when using sub-set 1.1 of Horizontes (see Table 7.2). It shows that the RRMSE for these situations is considerably lower than that in the case of an open-loop prediction, at all resolutions but especially at the finer resolutions. State regularization leads most often to better predictions as parameter regularization. Figure 7.3 shows the same graphs then using sub-

set 1.1 of Horicajo. Here also the RRMSE of the discharge prediction is reduced, but on average less as when using the Horizontes data. As may be expected, the RRMSE for the measurement locations in the Horicajo catchment (the two catchment areas) are particularly low.

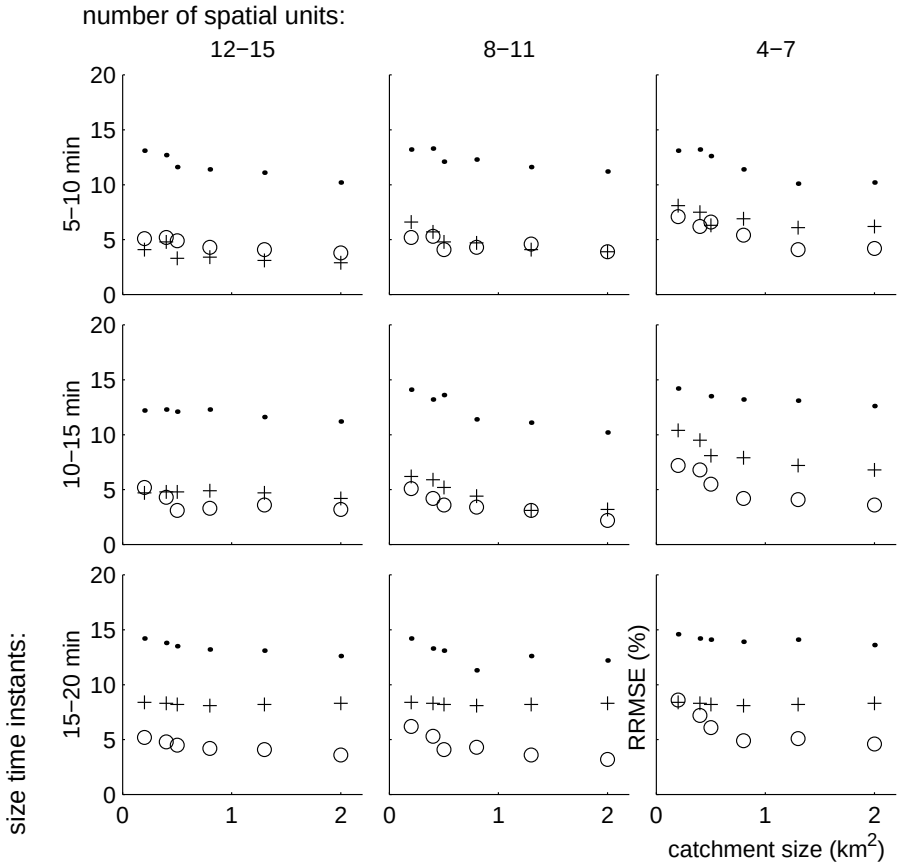

Figure 7.2: Time-averaged RRMSE of discharge prediction in Horizontes at different measurement locations (i.e. varying upstream area), for models with parameter (+) and state (o) regularization using data for Horizontes over the prediction period. As a reference, the RRMSE of the predictions over the calibration period are included (•, see Figure 7.1).

In what follows the RRMSE of the predictions will be averaged for the different measurement locations, i.e. the six values for parameter regularization in each of the nine graphs in e.g. Figure 7.2 will be averaged to one value. This allows to study the relation between the amount of data used for conditioning, the model resolution where the minimum RRMSE is found, and the value of the RRMSE itself. In Figure 7.4 the RRMSE is shown for different observation densities (using the Horizontes data and parameter regularization). The average RRMSE values of each plot in Figure 7.2 correspond to the values in the upper left corners of the nine plots in Figure 7.4 (+ in Figure 7.2) and Figure 7.5 (o in Figure 7.2). The axes (or cells) in each of the nine sub-plots of the figures are defined by Table 7.2, i.e. the lowest observation density is in the upper left corner and the highest observation density is in the lower right corner. It appears that for increasing observation densities in general the RRMSE decreases, and in addition the optimum RRMSE is found at the medium space-time resolutions. Figure 7.5 shows the same information when applying state estimation. Here the minimum RRMSE value is slightly smaller than that for parameter regularization, but only at high observation densities and at finer resolutions. The plots of RRMSE when using the Horicajo observations show a very similar pattern, but with RRMSE values that are slightly higher

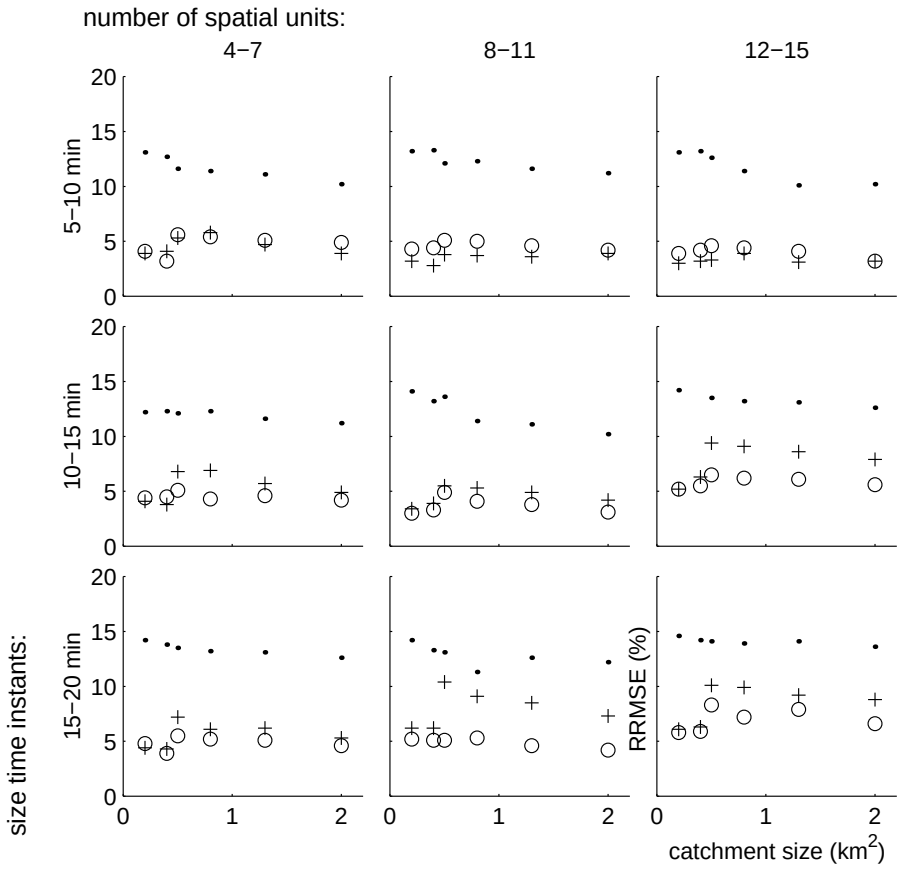

Figure 7.3: Time-averaged RRMSE of discharge prediction in Horizontes at different measurement locations (i.e. varying upstream area), for models with parameter (+) and state (o) regularization using data for Horicajo over the prediction period. As a reference, the RRMSE of the predictions over the calibration period are included (•, see Figure 7.1).

for parameter regularization and lower for state regularization (see Figures 7.6 and 7.7). In general, state regularization leads to better predictions at finer resolutions than parameter regularization, and parameter regularization to better performance at coarse resolutions.

7.5 Discussion and Conclusions

This study applies so-called Tikhonov regularization to the problem of combining model results with observations, in this way leading to predictions that are far better than the open-loop predictions with the same models. An objective and structured weighting of both components has been achieved through generalized cross-validation. Another way of seeing regularization is as a structured way of combining prior information (or assumptions) with an ill-posed hydrological problem to convert it into a well-posed problem. Two regularization strategies were compared: regularization of the model parameters, and regularization of the model state variables. It was shown that both techniques lead to similar results, which differ in some details. Parameter regularization leads to better results at low data availability, whereas state regularization leads to better results at high data availability. This result is consistent with the fact that there are fewer parameters than states to be estimated (see Chapter 6). State regularization realizes its best predictions at finer resolutions

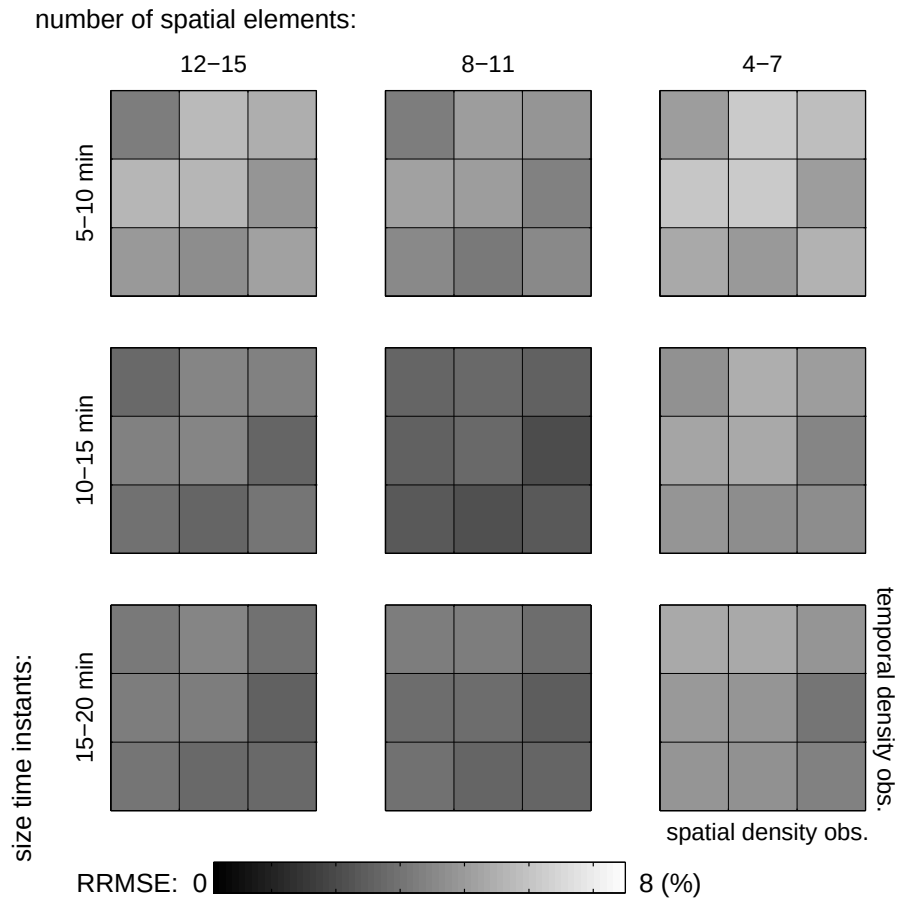

Figure 7.4: RRMSE of discharge predictions using Horizontes data and parameter regularization, for different resolutions and observation densities (see Table 7.2 for the meaning of the observation densities).

than parameter regularization. This can be explained from the fact that parameter regularization maintains the *relative* structure of the kernel functions over different spatial units, and is in that way less flexible than state regularization. The comparative advantage of this flexibility appears at higher data availability and finer resolutions.

This study does not compare the regularization approach, which updates states/parameters at each time instant, to that of (static) re-calibration. However, in a study where similar techniques have been applied it has been shown that re-calibration leads to considerably higher RRMSE and more structured prediction errors then regularization (van Loon and Troch, 2002). A comparison of the open-loop predictions over the calibration period itself with the reguralized predictions (Figures 7.2 and 7.3) also shows that even the best calibration feasible will not nearly approach the results of using a regularization approach. Against this background it is not worthwhile to consider this as an alternative to regularization. Moreover re-calibration is undesirable for practical reasons as explained in Section 7.1.

It is important to note that the methodology employed in this chapter can relatively easy be adapted to different models or observations. If a hydrologic model can be written in state space form (according to Equations 5.1 and 5.2), the solution algorithm (Section 7.2 and Appendix C) can be applied without any adjustments. This is an important asset since it means that different parameter distributed dynamic models can be evaluated with the same or different data for reg-

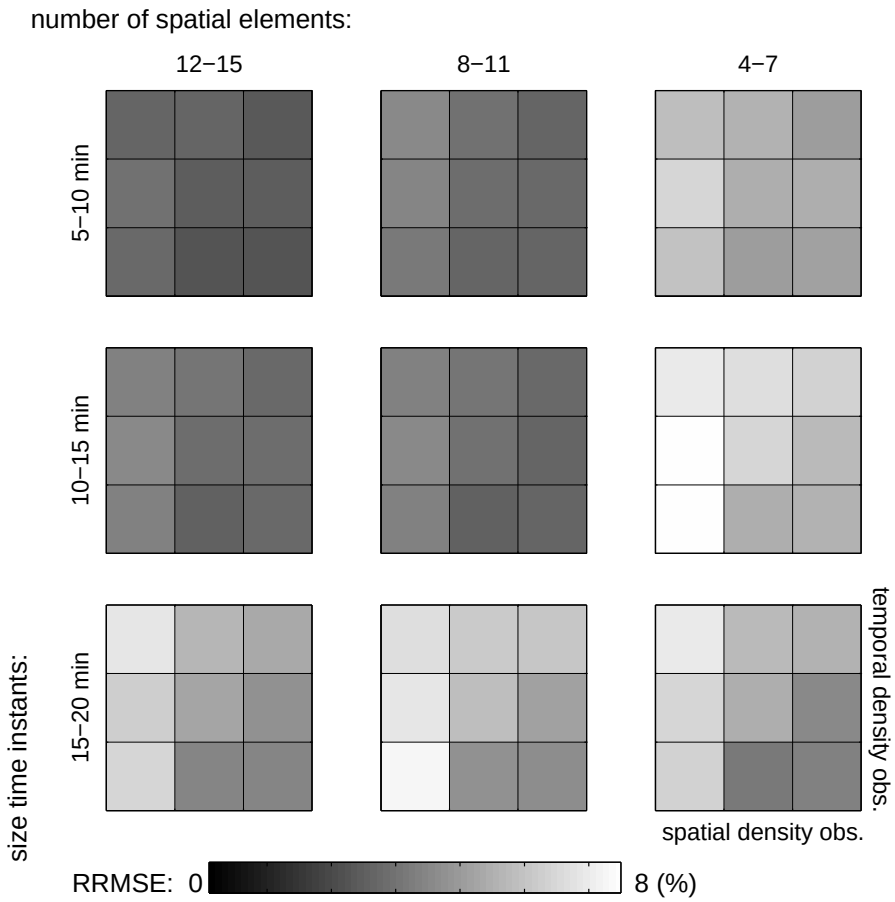

Figure 7.5: RRMSE of discharge predictions using Horizontes data and state regularization, for different resolutions and observation densities (see Table 7.2 for the meaning of the observation densities).

ularization relatively easy, without the requirement to include exactly the same state variables in the model dynamics. This point has been demonstrated in this study by using a set of models instead of a single model in order to generate a prediction. Characteristic for the technique used in this study is that it only requires the solution of (many) constrained linear regression problems of moderate size, for which there are numerous efficient solution algorithms available.

A line of investigation which may be pursued is the integration of the techniques presented in this study with the data assimilation approaches developed in the atmospheric and oceanographic disciplines (see Bennett, 1992; Daley, 1991; McLaughlin, 1995, e.g.). Until now the regularization approach has not been used for data assimilation, and here its utility for hydrological problems has been demonstrated. Considering the ease with which regularization can also be integrated in the Kalman filter and Kalman smoother (Boutayeb et al., 1997; Reif et al., 1998), and the relative success of the Ensemble Kalman filter to problems of a realistic size (Evensen, 1992; Evensen and van Leeuwen, 1996; Houtekamer and Mitchell, 1997), a very fruitful enterprise might be the combination of the two techniques.

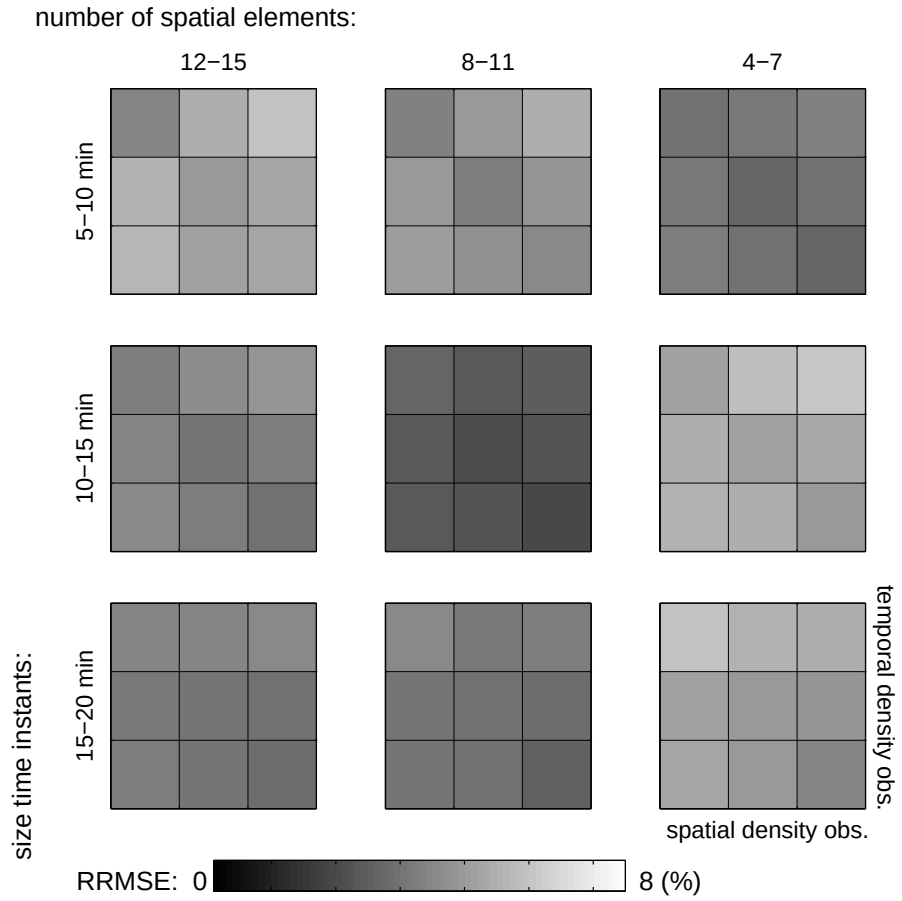

Figure 7.6: RRMSE of discharge predictions using Horicajo data and parameter regularization, for different resolutions and observation densities (see Table 7.2 for the meaning of the observation densities).

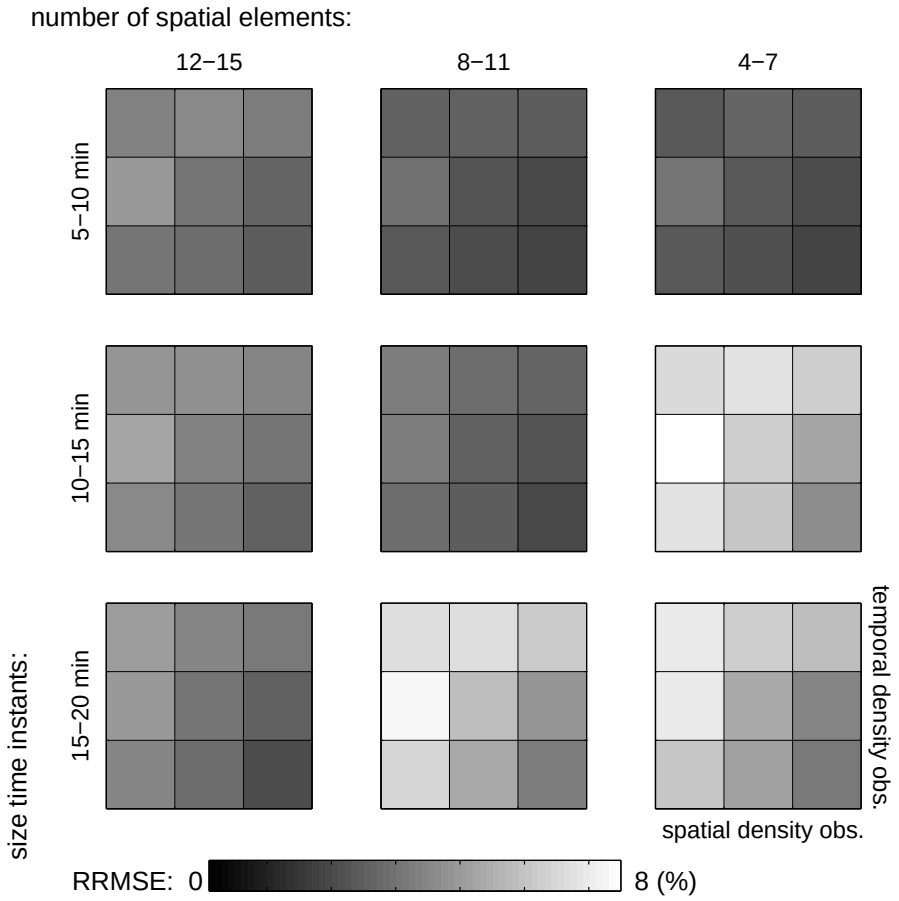

Figure 7.7: RRMSE of discharge predictions using Horicajo data and state regularization, for different resolutions and observation densities (see Table 7.2 for the meaning of the observation densities).

8 Epilogue

8.1 Putting the parts together

Three main ideas have led to this research. The first was the experience from earlier field work in the tropics that depth, extent and duration of overland flow are among the easiest observations to collect over large areas - if there is the opportunity (and willingness) to work in the rain. Overland flow is namely one of the few hydrologic phenomena that is visible, leaves traces (even when no tracers are applied) and occurs only over a limited period of time. The second idea was to pursue the techniques to establish parameter sets of equal likelihood by Fedra (1983); Keesman (1989) and Beven and Binley (1992) a bit further towards establishing model sets of equal likelihood. The third idea was to establish techniques to evaluate the consequences of the resolution of parameter distributed models for predictive and parametric uncertainty in those models. The latter was motivated by the observation that the choice to define a hydrological problem at a certain resolution is often not discussed nor explained. On the contrary, model resolution is commonly chosen rather ad-hoc by either making it equal to that of the most detailed input data available, or the highest possible resolution is chosen within the operational limits. In surface hydrology this implies that spatial resolution is often chosen to equal the terrain representation and temporal resolution to equal the rain or discharge data. Data which are not available at the appropriate resolution are estimated at the corresponding elements and time instants by aggregation, disaggregation or interpolation, in this way introducing a considerable observation uncertainty. The direct consequences of choosing a particular resolution for the predictive power and the uncertainty in parameter estimates are often ignored or overlooked.

All three ideas have been worked out in some detail and have been applied in this dissertation. But not until now, after analyzing the observations and testing the classical modeling approaches for overland flow prediction as well as the newly developed scale-dependent models, it is appropriate to evaluate those initial ideas. Here we seek to answer the question how useful overland flow observations and scale dependent models appear to be in relation to the available alternatives. Implicitly, the question whether the appropriate resolution can be established for the scale dependent model is enclosed therein. The questions of data and model utility are very much intertwined and will be answered here by first analyzing the strengths and weaknesses of the different models for identification purposes, then by comparing the different models with regard to their predictive uncertainties and subsequently by quantifying the effects of omitting observations during model identification and calibration respectively.

Identification

There exist no rigid quantitative measures to determine the utility of a certain model structure for system identification. Identification namely implies that part of the system is unknown and that via a series of automated or manual analyses the required mathematical relationships to determine the system completely are established. For each model structure the analyses differ as well as the complexity of the unknown structures to be established, which makes it difficult to compare models in this respect. Still an attempt is made here to do so. The three modelling approaches are

evaluated with respect to two criteria: 1) the ease with which their structure can be determined in the two study catchments, and 2) the flexibility to change the model structure in response to new insights from the identification procedure or the availability of new observations.

From an identification viewpoint the regression approach to describe catchment scale overland flow, as applied in Chapter 3, is the most simple and straightforward approach that can be applied. The only prior decisions required to determine the model structure are: 1) the spatial discretization of the catchment and the temporal sub-division of the study period; and 2) the form of the measurement equations, relating the various observations to the single observable to be estimated (average overland flow height in this case). Since we deal with a static system both steps are very easily made and re-made if necessary. The other side of the coin is that there is not much to be learned from this identification exercise. In the first place it is not possible to include process dynamics in the model structure, and secondly the spatial and temporal subdivision is determined *a priori* and cannot be established by the model itself or derived in some iterative way from model identification results.

The distributed model outlined in Chapter 4 is with regard to the first criterion the opposite. It is extremely complex to even identify small parts of the dynamic model because of its size and its non-linear dynamics. Therefore parameterizations such as the infiltration equation and the parameter zonation have essentially to be assumed *a priori*. These parameterizations are not changed easily because there is a considerable effort required in calibrating the distributed model and there are not much alternatives available from the literature. If different parameterizations and parameter zonations are compared this can lead to a lot of insight. It is however important to notice that these insights are often related to very specific conditions and can therefore not easily be generalized. An example of the type of knowledge that may be obtained from identification with the distributed model is the pre-event wetness index that was found to determine an infiltration parameter. There are no examples available in the literature where a number of possible parameterizations or zonations are evaluated in a structured way to identify a distributed hydrological model. In combination with the notion that many studies take place with the help of similar types of distributed models as used here, it indicates that there is not much potential for these models in an identification context.

The scale-dependent models as applied in Chapters 5 and 6 are, in contrast, specifically designed to enable system identification for this class of problems. Although the complexity of the several calculation steps to identify these models is much larger than with the regression model, not to mention the computational effort, it is clearly feasible. In terms of what can be learned from the identification procedure all the results from Section 5.6 can be taken as an example. Statistical analyses indicated the interrelationships between model resolution, the number of model parameters and the dominance of several independent variables. In general, the number of model parameters is constant over the different resolutions, implying that the required number of model parameters is mainly a function of the information content of the observations, and not so much of the process resolution, which is logical because the identification method is to a large extent data-based. Considering the use of 'standard data', i.e. rainfall and catchment discharge at a single point, various statements have been made about the permissible model complexity. Beven (1989) commented that three to five parameters should be sufficient to reproduce most of the information, and Jakeman and Hornberger (1993) found that around 6 parameters is the maximum number permitted. In addition, several studies came to the conclusion that more complex models (10 to 20 parameters) did worse than simple models (5 to 15 parameters) (Gan et al., 1997; Hornberger et al., 1985; Loague and Freeze, 1985). In this study internal state data, such as discharge of subcatchments, overland flow and soil moisture, have been used in addition to the standard rain and catchment discharge data. As a result models with more parameters have been identified here, viz. 30 - 40 parameters in Chapter 5 and 40 - 60 in Chapter 6. It is not easy to generalize these results

because the number of parameters can be reduced by a factor two to three once the models have been identified without losing much information, as illustrated in Section 6.7. With regard to the independent variables in the overland flow models the result found for the synthetic data as well as the Kaibo and Horizontes catchments is that in models defined at fine resolutions soil moisture is most suitable as a driving state variable, whereas in models defined at coarse resolutions rain is the key variable. It suggests that the source-driven system behaviour at coarse resolutions and sink-driven behaviour at fine resolutions is a property of the hydrologic systems at both the hillslope and catchment scales. The size of spatio-temporal units to which 'coarse' or 'fine' refer depends on the heterogeneity of rain, soil and terrain characteristics (inputs and main model determinants), and differs for different areas. Most of the results from the identification procedure applied in Chapters 5 and 6 are of a global nature, i.e. the details of single models are not highlighted. It remains to be investigated whether considering the single models in more detail provides information that can be used for further model structure. It also remains to be seen if and how lessons learned via this class of scale dependent models can be used effectively in distributed models.

Prediction

There are many quantitative criteria available to evaluate the ability of models to make predictions (see e.g. Table 4.6). In this overview we limit ourselves, again, to the RRMSE by combining results presented in the preceding chapters. The question is to what degree a model's prediction can be trusted and how the three models differ in this respect. For each of the soil-vegetation classes the RRMSE for prediction over the average season is given in Table 8.1. In this table the vegetation classes for 'shallow' are combined since shallow with trees (in Horizontes) and arable land (Kaibo) cover a very small portion the area. The table highlights two interesting features of the overland flow predictions. In the first place it illustrates that for all three model the prediction errors for Kaibo are smaller than for Horizontes. This was unexpected since less observations were collected in Kaibo. From this it follows that the models used are less suitable for Horizontes, possibly because the area is more heterogeneous. Secondly, the prediction errors of the regresion and scale dependent models show a large correspondence, with regard to both the relative differences between the soil-vegetation classes and the differences between Kaibo and Horizontes. The distributed model appears to have large prediction errors especially for Horizontes.

It should be noted that the regression model requires the direct observation of the states over the prediction period, which implies that much more information is used than in the open-loop predictions as applied in Chapters 4 and 6. In this respect the regression model is comparable to the method applied in Chapter 7.

Observation

The differences between the various models can only be seen in perspective when related to the effect of the observations. The utility of different types of overland flow observations will here be determined by assessing the relative effect that the omission of a single observation type has on model performance, the so-called *drop-efficiency*. Drop-efficiency is determined for omitting each distinct type of observation from the calibration as well as validation set. Obviously, this will only give indicative results, since for each catchment different observation densities are available and some observations (o_c and s) are absent in Kaibo. The drop efficiency is only analyzed in terms of RRMSE, and with respect to calibration over the entire season (see also Table 4.6). It is notable that the RRMSE values represent a minimal output, since the determination of each drop-efficiency value leads to a model with different parameter values that can in principle reproduce the type of output presented Chapters 3, 4 and 6. The results are displayed in Table 8.2. The remarkable pattern displayed in Table 8.2 is that for all three models the different data have a similar

Table 8.1: A comparison of the prediction errors for overland flow by the three models, as measured by the RRMSE.

	model type					
	regression		distributed		scale dependent	
soil-vegetation type	Kaibo	Horiz.	Kaibo	Horiz.	Kaibo	Horiz.
deep, vertic	0.11	0.15	0.24	0.23	0.10	0.13
non-trees / arable deep, vertic	0.12	0.18	0.29	0.29	0.10	0.20
trees / shrub deep, non vertic	0.14	0.20	0.11	0.52	0.18	0.20
non-trees / arable deep, non vertic	0.14	0.27	0.20	0.45	0.14	0.28
trees / shrub shallow	0.10	0.17	0.12	0.38	0.12	0.20
catchment avg.	0.13	0.20	0.16	0.42	0.15	0.21

effect, leading to the important conclusion that in the end it is not the model that needs to be evaluated critically but the (sub)optimality of the available data. Especially the negative values of the discharge from runoff plots in Kaibo (q_p) seem strange in this table, the negativity implies that the results from these plots are in conflict with the other information from the catchment. Apparently this conflict could not be resolved by differently parameterizing or calibrating the models, and therefore inclusion of these observations led to worse results. Note that these observations were also used for (cross-)validation. The table makes also clear that the direct observation of overland flow (especially o_h, o_c and o_p jointly) is of great importance for the model results, especially when considering the fact that these observations cover only a few events, whereas the discharge and soil moisture observations cover many. In the bottom two rows of Table 8.2 also the effect of omitting one or two locations for rainfall observations from the calibration and validation sets is presented. In these cases the observations of the remaining points were used to estimate areal rainfall by linear interpolation. It was already clear from the analyses in Chapter 2 that rain has very short correlation lengths in the two research areas. In combination with the conclusion in Chapter 6 that the space-time structure of rain is a dominant factor determining overland flow patterns, the large effect of omitting the rain observations is not surprising.

Another pattern that may be read from the table is that the utility of output observations with a large spatial support (i.e. covering a large area of 500 m^2 or more) outweigh that of point-scale observations such as discharge from small plots, overland flow collected in small collectors, ground water as measured by piezometers and soil moisture observations. In addition to this the observation of catchment discharge in combination with a dense spatial rain observation is indispensable under all circumstances.

General conclusions

The combination of the three analyses on identification, prediction and observations provides the necessary information to get back to the objective of this dissertation which is to develop new techniques to identify models for catchment scale overland flow prediction, and apply these for prediction. Other important aims were to collect both qualitative and quantitative overland flow observations in different catchments and to use a set of model structures rather than a single model structure with both qualitative and quantitative observations. Whereas we can briefly state that all of these goals have been met with some success, the conclusions deserve some nuancing on the basis of what is presented in the previous sections. First of all, the scale-dependent model appears

Table 8.2: The drop efficiency (relative increase in RRMSE for overland flow prediction) when omitting different data types in different models during calibration, for Horizontes and Kaibo.

model:	regression		distributed		scale-dep.	
omitted data	Kaibo	Horiz.	Kaibo	Horiz.	Kaibo	Horiz
q_c (outlet)	0.43	0.51	0.66	0.47	0.32	0.58
q_c (sub-catchments)	-	0.12	-	0.23	-	0.24
q_p	-0.11	0.04	-0.34	0.12	-0.12	0.13
o_h, o_c and o_p	1.17	1.31	0.92	1.03	0.73	0.94
o_h	0.21	0.32	0.24	0.33	0.36	0.47
o_c	-	0.22	-	0.15	-	0.25
o_p	0.14	0.24	0.19	0.23	0.13	0.31
s	-	0.07	-	0.09	-	0.13
w	0.02	0.41	0.12	0.21	0.05	0.18
p (one location)	0.54	0.31	0.42	0.27	0.56	0.23
p (two locations)	-	0.56	-	0.34	-	0.47

to offer especially new opportunities for model identification. For prediction not so much progress is expected by the proposed technique, because of the large dependence of its performance on the available data (viz. Table 8.2). In the second place, the collected overland flow data, in combination with all the other hydrologic and geophysical data, did turn out to be very valuable throughout the entire study. And the fact that similar observations were collected in two different catchments did considerably add to their utility. Finally, the use of model sets was an integral and indispensable part of the identification procedure. For prediction it did, somewhat surprisingly, also play a significant role as the use of model ensembles lowered prediction errors.

8.2 Is the problem solved?

To the end of identifying and calibrating models, and use these for prediction this research has solved some modestly demarcated problems. But matching these solutions with the requirements from engineering and scientific problems in this area, i.e. the large scale collection, interpretation and processing of overland flow data, changes perspective dramatically. In this light the various techniques that were presented and evaluated are rather makeshift measures to combat symptoms of the real problem: absolute data scarcity. This study has only indirectly and marginally contributed to a solution for this problem: by demonstrating the utility of directly observing overland flow coverage. The key-role that this observation can play was underlined by the results in Table 8.2. This finding may help to stimulate the development of Remote Sensing technology to specifically monitor surface water. To date surface water can already be observed from various satellite-based or Airborne sensors (e.g. Koblinsky et al., 1993; Massonnet and Rabaute, 1993; Smith et al., 1993; Smith, 1997). The spatial resolution as well as the temporal frequency of these observations are however still too low to be of any value for overland flow monitoring, and there are no new techniques foreseen that may fill this gap. The overland flow predictions by the distribued model used in this study appears to be relatively uncertain (see Chapter 4). Considering the relative similarity between the model used here and the many others found in the literature, predicting overland flow with distributed models seems to be of little use in general. Note that this is not to answer the question whether distributed models can be *useful* for hydrologic *research* (gaining understanding, generating synthetic data sets for benchmarking, evaluating laboratory experiments etc.) - they can! It also says not much about the potential of those models when

used in combination with state observations (like discharge) in stead of the open-loop form as in Chapter 4. It was shown in Chapter 7, in this case with scale-dependent models, that there are appropriate techniques for on-line state or parameter estimation that considerably enhance model performance.

A lesser-problem will be addressed in this context as well. It is the continuing debate about the question whether model parameters can be determined more objectively, i.e. with less calibration, if defined at finer spatial resolutions. In preamble to studies that identify or evaluate a certain hydrological model it is common to put the presented model in perspective by placing it somewhere on a scale between distributed-parameter models on one end and lumped models on the other Blöschl and Sivapalan (1995); O'Connell (1991). This habit is part of a good scientific practice to specify the purpose of a model and the conditions (including scale) where it may be applied. Interestingly, the spectrum of models (from distributed-parameter to lumped) itself has become subject of discussion in the argument as to what extent the resolution is a reflection of different modeling philosophies Beven (1996); Refsgaard et al. (1996). One view is that there is no essential difference which can merely be attributed to the number of parameters in a model (and in proportion to that the resolution at which a model applies) whereas the other view is that the nature of the parameters is different at different resolutions such that in distributed models less calibration-per-parameter has to take place. In other words: one view does not attribute any but a documentary value to the fact that a model is more or less distributed-in-the parameters, whereas the other uses it as a criterium to calibrate and validate the models differently. The discussion is of interest when the prediction of rain partitioning in a catchment is required at more than one resolution. The first view would suggest that different models should be used at different resolutions, whereas the second view could support the idea to identify a model at the most detailed resolution required and derive models at coarser resolutions by aggregation. In this dissertation the problem was approached with the first view as a null hypothesis, and on basis of the findings that at different resolutions qualitatively different models appear to be the fittest (see Chapters 5 and 6), there is no reason to take a different point of view. This result can hopefully help to end the debate and focus the scientific attention to a more rewarding topic, related to the observation problem described above. Each model resolution (rather than each model parameterization) has specific requirements with regard to both quantity (number) and quality (type) of observations. The question is how to systematize these relations. This is an issue that has hardly been investigated but seems to be most rewarding and moreover achievable in the light of recent research results (van Loon and Keesman, 2001).

8.3 Left-overs

The investigations in this study have answered a few questions but by doing so raised many new ones, which in some way seems perhaps disappointing but is from a scientific viewpoint in fact encouraging. Being able to formulate relevant research questions namely implies that there are handles to investigate and thus further understand a system or problem. In this final section, some of those new questions arising from this research are formulated.

Two related questions with regard to the use of model ensembles appear as a result of the findings in Section 4.4 (Table 4.8) and Section 6.3 (Figure 6.1): 1) why exactly does the prediction with parameter ensembles (Section 4.4) or model ensembles (Section 6.3) lead to better prediction statistics, and 2) what can be learned about the model or parameter set by analyzing relations like those shown in Figure 6.1. The facts that very few studies have investigated these issues in the earth-science disciplines and that the results are so far not conclusive (Krishnamurti et al., 1999; Doblas-Reyes et al., 2000) add to the relevance of these questions. In weather forecasts the use of model ensembles is quite common (e.g. Houtekamer and Derome, 1994; Houtekamer and

Lefaivre, 1997), the way in which ensembles are used there by applying variation to the model states or sometimes parameters to track state divergence, often in a recursive state estimation framework, is however different from the way it has been applied here.

More fundamental questions relate specifically to the scale-dependent models: 1) whether the transition matrices can be used to formulate data-based probability density functions of the transport and partitioning process (as suggested in Section 6.7); and 2) whether these can be used in probabilistic hydrological models or be compared with the commonly assumed distributions in hydrologic modelling like gamma, Weibull or Poisson. If certain (sets of) distribution functions are found to be valid for certain storms or storm characteristics, these can perhaps throw new light on the structure of successful models. Furthermore such distribution functions would form excellent summary models for practical use, provided that they give acceptable results. In this respect it is interesting to notice that the use of distribution functions is common in the hydrologic disciplines but the functions used are normally specified *a priory* to enable an analytical treatise of a particular hydrological problem as in Moore and Clarke (e.g. 1981) and Entekhabi and Eagleson (1989).

This study has shown that it is possible to derive representative relationships that describe overland flow at the scale of a catchment on the basis of point scale observations. A vital step in establishing the variation at a coarse scale is to link the point observations with easily observable indicator data, which can be observed at a high density or coarser resolutions. In this way one can merge 'soft' information with conditional prior multivariate probability density functions of coarse resolution overland flow functions derived from a limited amount of 'hard' measurements. In this study soil, vegetation and topography have been used as such soft data in a very simple way. A more elaborate and perhaps more effective method might be to use remotely sensed observations (as indicative for vegetation and soil moisture) as soft-data. These observations have the distinct advantage that the need to first interpolate the scattered information to a grid is removed. The MSG and ENVISAT satellites, which are to be launched in 2002 may offer new opportunities to perform such a study.

With regard to overland flow this study has emphasized the importance of appropriate observations as well as the possibility to use coverage data for this purpose. These notions may help in the design of new observation technology but before such an enterprise can take place it is necessary to first explore the possibilities in detail in an experimental field or laboratory setup. In small-scale experiments it is possible to utilize visible light or infra-read images for observing overland flow. This type of imagery data will at the same time confront the modelling techniques used in this study with more realistic data sets. A laboratory study will have an additional advantage of bringing the study domain closer to the scale at which the more established hydrologic models are defined. This considerably eases the comparison of the scale-dependent models used in this study and the physically based models commonly encountered in this discipline.

In the face of all these new questions and leads for further research it is clearly time to stop writing and start doing.

Appendix A: Summary of the data used

This appendix gives a brief summary of the event totals of rain, discharge and overland flow observations collected in Kaibo, Horizontes and Horicajo. The total event rainfall is based on a spatial interpolation of the observed rainfall at each observation time. The discharge values are for the catchment outlet only. The values for the different runoff plots (six in Kaibo and four in Horicajo) are averaged. Only the events are listed where overland flow observations have been collected as well. All values are given as event totals in *mm*. The overland flow observations with collectors and paths are converted to depth in *mm* by the relations listed in Tables (see also Figures 3.1 and 3.2).

Table A.1: Relations used to convert the observations on maximum overland flow extent during an event to total event overland flow height in *mm*, per catchment and vegetation class.

Catchment	Vegetation type	$overland\ flow height =$
Kaibo	arable	$26.2\,(max extent)$
	shrub	$39.9\,(max extent)$
Horizontes	grass	$28.0\,(max extent)^{0.6}$
	trees	$25.7\,(max extent)$

Table A.2: Relations used to convert the observations on fraction of full collectors during an event to total event overland flow height in *mm*, per vegetation class (note that collectors were only used in Horizontes and Horicajo).

Vegetation type	$overland\ flow height =$
grass	$25.9\,(fract.\ full)^{0.7}$
trees	$17.8\,(fract.\ full)^{0.5}$

Table A.3: Average rain, discharge and overland flow data for the events in Kaibo, Horizontes and Horicajo where overland flow observations were available. All values are event totals in *mm*.

		discharge		overland flow		
date	rain	catchment	plot	height	collector	path
Kaibo						
13/7/98	8.2	0	1.7	2.3	-	2.9
15/7/98	5.8	0	1.3	1.3	-	1.6
Horizontes						
14/5/97	3.2	0.2	-	-	1.1	0.3
5/6/97	24.6	1.0	-	-	1.7	2.3
16/6/97	8.6	1.4	-	-	3.1	2.2
13/10/97	45.4	19.6	-	-	31.2	28.4
14/10/97	3.0	1.1	-	-	2.3	1.1
27/11/97	17.2	2.8	-	-	-	2.7
29/11/97	11.0	4.0	-	-	-	5.1
Horicajo						
16/6/97	8.6	1.3	1.4	-	-	2.3
30/7/97	25.0	0	2.6	2.4	1.9	3.1
9/8/97	2.4	0.3	0.9	0.3	0.8	0.6
29/8/97	1.2	1.8	-	-	-	0.5
30/8/97	43.8	8.1	24.2	25.1	27.3	19.6
16/9/97	3.4	0.6	1.3	1.2	0.7	0.8
2/10/97	4.2	0.5	-	1.6	2.2	2.3

Appendix B: Derivation of state-space model

Derivation

In our class of models we consider at time instant k and spatial unit l only one input, the precipitation $p_{k,l}$; and three state variables: the amount of water stored in the soil $s_{k,l}$, and the amount of overland flow due to infiltration excess, $r_{k,l}$ or due to saturation excess, $t_{k,l}$. Initially lateral water movement is only allowed over the soil surface for clarity, this restriction is relaxed later. With these conventions a representation of the hydrological system, describing the partitioning of precipitation into water at the surface and water in the soil for each (k,l), can be formulated in a balance equation as

$$r_{k,l} + s_{k,l} + t_{k,l} = \varphi_1 p_{k-m;l-n} + ... + \varphi_{m*n} p_{k,l} \tag{B.1}$$

Equation B.1 states that a component of the water balance, measured for a time instant k and a location l, may originate from precipitation up to m intervals back and from n distinct locations (some of the φs may be zero). The cumulative amount of storage in unit l, $w_{k,l}$, is defined as

$$w_{k,l} = (1 - c_k) w_{k-1,l} + s_{k-1,l} \ , \text{ with } w_{0,l} = w0_l \tag{B.2}$$

where c_k is the fraction of storage which returns to the soil surface (exfiltrates), and $w0_l$ is the initial amount of soil water.

The right-hand side of an error free balance equation (equation B.1) can also be expressed in terms of the sum of actual precipitation and surface runoff with subsurface flow (replacing the effect of precipitation on previous time instants and distinct locations). First the sum of subsurface and surface runoff, denoted by $\mathbf{i}_k$, is defined as

$$\mathbf{i}_k \equiv \mathbf{C}1_k \mathbf{w}_{k-1} + \mathbf{r}_{k-1} + \mathbf{t}_{k-1} \tag{B.3}$$

where $\mathbf{w}_{k-1}$, $\mathbf{r}_{k-1}$and $\mathbf{t}_{k-1}$are vectors with the elements $w_{k-1,l}$, $r_{k-1,l}$ and $t_{k-1,l}$ respectively, and $\mathbf{C}1_k$ is a diagonal matrix with elements that give the chance of $w_{k-1,l}$ subject to exfiltration. All vectors have dimension L. Secondly, to account for transportation vector $\mathbf{i}_k$ is multiplied with a transport matrix and added to the precipitation at instant k:

$$\mathbf{j}_k \equiv \mathbf{B}1_k \mathbf{i}_k + \mathbf{p}_k \tag{B.4}$$

where $\mathbf{p}_k$ is a vector with the elements $p_{k,l}$ and $\mathbf{B}1_k$ is an (L,L) matrix with the elements b_{ij}, which denote the chance that water is transported over the soil surface from the spatial unit j to unit i.

The partitioning of rain between storage (s), surface runoff (r) and subsurface runoff (t) is given by:

$$\mathbf{s}_k = \mathbf{A}1_k \mathbf{j}_k \tag{B.5}$$

$$\mathbf{r}_k = \mathbf{A}2_k \mathbf{j}_k \tag{B.6}$$

$$\mathbf{t}_k = \mathbf{j}_k - \mathbf{s}_k - \mathbf{r}_k = (\mathbf{I} - \mathbf{A}1 - \mathbf{A}2)\mathbf{j}_k \tag{B.7}$$

where $\mathbf{s}_k$, $\mathbf{r}_k$ and $\mathbf{t}_k$ are vectors, each with L elements ($s_{k,l}$, $r_{k,l}$ and $t_{k,l}$ respectively); $\mathbf{A}1_k$ is an (L,L) diagonal matrix with elements denoting the chance that water enters the soil over a unit (k,l); and

$\mathbf{A}2_k$ is an (L,L) diagonal matrix with elements denoting the chance that rain rate is higher than infiltration capacity. Equation B.2 can be put in vector form as:

$$\mathbf{w}_k = (\mathbf{I} - \mathbf{C}1_k)\mathbf{w}_{k-1} + \mathbf{s}_{k-1} \tag{B.8}$$

where $\mathbf{I}$ is an (L,L) identity matrix.

By combining Equations B.3 and B.4 we obtain

$$\mathbf{j}_k \equiv \mathbf{B}1_k(\mathbf{C}1_k\mathbf{w}_{k-1} + \mathbf{r}_{k-1} + \mathbf{t}_{k-1}) + \mathbf{p}_k \tag{B.9}$$

And Equations B.5 to B.8 can be combined to

$$\begin{bmatrix} \mathbf{s} \\ \mathbf{r} \\ \mathbf{t} \\ \mathbf{w} \end{bmatrix} = \begin{bmatrix} \mathbf{A}1 & 0 \\ \mathbf{A}2 & 0 \\ \mathbf{I} - \mathbf{A}1 - \mathbf{A}2 & 0 \\ 0 & \mathbf{I} \end{bmatrix} \begin{bmatrix} \mathbf{j}_k \\ (\mathbf{I} - \mathbf{C}1_k)\mathbf{w}_{k-1} + \mathbf{s}_{k-1} \end{bmatrix} \tag{B.10}$$

Now B.9 and B.10 can be combined and rearranged into a matrix equation that describes the state of the system (storage and runoff) as a linear combination of input and its state one time instant before:

$$\begin{bmatrix} \mathbf{s} \\ \mathbf{r} \\ \mathbf{t} \\ \mathbf{w} \end{bmatrix} = \begin{bmatrix} \mathbf{A}1 & 0 \\ \mathbf{A}2 & 0 \\ \mathbf{I} - \mathbf{A}1 - \mathbf{A}2 & 0 \\ 0 & \mathbf{I} \end{bmatrix} \left(\begin{bmatrix} \mathbf{B}1 & 0 \\ 0 & \mathbf{I} \end{bmatrix} \begin{bmatrix} 0 & \mathbf{I} \\ \mathbf{I} & 0 \\ \mathbf{I} & 0 \\ \mathbf{C}1 & \mathbf{I} - \mathbf{C}1 \end{bmatrix}^T \begin{bmatrix} \mathbf{s} \\ \mathbf{r} \\ \mathbf{t} \\ \mathbf{w} \end{bmatrix}_{k-1} + \begin{bmatrix} \mathbf{p} \\ 0 \end{bmatrix} \right) \tag{B.11}$$

where all vectors and matrices are specified for time interval k, unless labelled otherwise, and the vectors and matrices are named as follows:

$$\mathbf{x}_k = \begin{bmatrix} \mathbf{s} \\ \mathbf{r} \\ \mathbf{t} \\ \mathbf{w} \end{bmatrix}_k ; \ \mathbf{u}_k = \begin{bmatrix} \mathbf{p} \\ 0 \end{bmatrix}_k ; \ \mathbf{A}_k = \begin{bmatrix} \mathbf{A}1 & 0 \\ \mathbf{A}2 & 0 \\ \mathbf{I} - \mathbf{A}1 - \mathbf{A}2 & 0 \\ 0 & \mathbf{I} \end{bmatrix};$$

$$\mathbf{B}_k = \begin{bmatrix} \mathbf{B}1 & 0 \\ 0 & \mathbf{I} \end{bmatrix}_k ; \mathbf{C}_k = \begin{bmatrix} 0 & \mathbf{I} & \mathbf{I} & \mathbf{C}1 \\ \mathbf{I} & 0 & 0 & \mathbf{I} - \mathbf{C}1 \end{bmatrix}_k$$

It is now easily seen that Equation B.11 equals equation 5.1. With respect to $\mathbf{C}_k$ it is important to notice that in this particular situation the columns sum to unity, which means that no drainage out of the upper soil layer takes place (the hillslope considered, has an impermeable underground).

Now we can relax the restriction that lateral water transport takes only place over the soil surface by replacing the identity matrix in the transport matrix, $\mathbf{B}_k$, which then reads as follows

$$\mathbf{B}_k = \begin{bmatrix} \mathbf{B}1 & 0 \\ 0 & \mathbf{B}2 \end{bmatrix}_k$$

where $\mathbf{B}2$ is a is an (L,L) matrix with elements b_{ij} that denote the chance that water is transported though the soil from a unit j to unit i.

Example models

For the example in Section 5.2 (Figure 5.2) a model with the following elements was used.

The vector with state variables, $x = \begin{bmatrix} \mathbf{s}_k & \mathbf{r}_k & \mathbf{w}_k \end{bmatrix}^T$ so that $M = 3$; the vector with inputs $u = \begin{bmatrix} \mathbf{p}_k & 0 \end{bmatrix}^T$; the spatial subdivision of $L = 4$; the temporal subdivision of $T = 5$ minutes; and three kernel functions for the partitioning matrix $a_{k,l}$; the transport matrix $b_{k,l,m}$; and the internal state matrix $c_{k,l}$ are given by:

$$a_{k,l} = \frac{(w_{k-1,l} - 10)^2}{(w_{k-1,l} - 10)^2 + 100} \tag{B.12}$$

$$b_{k,l,m} = \left(\frac{r_{k-1,l}}{m}\right)^{m-1} \frac{e^{-\left(r_{k-1,l}/m\right)}}{\Gamma(m)} \tag{B.13}$$

$$\begin{array}{rl} c_{k,l} = 0 & for \quad w_{k-1,l} \leq 25 \\ c_{k,l} = 0.4 w_{k-1,l} & for \quad w_{k-1,l} > 25 \end{array} \tag{B.14}$$

as previous $k = 1, \ldots, K$ denotes a time instant, and $l = 1, \ldots, L$ a spatial element.

These model elements can be written in the form of a state space model as give by equation 5.1.

$$\begin{bmatrix} \mathbf{s}_k \\ \mathbf{r}_k \\ \mathbf{w}_k \end{bmatrix} = \begin{bmatrix} \mathbf{A}1_k & 0 \\ \mathbf{I} - \mathbf{A}1_k & 0 \\ 0 & \mathbf{I} \end{bmatrix} \left(\begin{bmatrix} \mathbf{B}1_k & 0 \\ 0 & \mathbf{I} \end{bmatrix} \begin{bmatrix} 0 & \mathbf{I} & \mathbf{C}1_k \\ \mathbf{I} & 0 & \mathbf{I} - \mathbf{C}1_k \end{bmatrix} \begin{bmatrix} \mathbf{s}_{k-1} \\ \mathbf{r}_{k-1} \\ \mathbf{w}_{k-1} \end{bmatrix} + \begin{bmatrix} \mathbf{p}_k \\ 0 \end{bmatrix} \right) \tag{B.15}$$

$$\mathbf{s}_k = \begin{bmatrix} s_{k,1} & s_{k,2} & s_{k,3} & s_{k,4} \end{bmatrix}^T$$

$$\mathbf{r}_k = \begin{bmatrix} r_{k,1} & \cdots & r_{k,4} \end{bmatrix}^T$$

$$\mathbf{w}_k = \begin{bmatrix} w_{k,1} & \cdots & w_{k,4} \end{bmatrix}^T$$

$$\mathbf{p}_k = p_k \begin{bmatrix} 1 & 1 & 1 & 1 \end{bmatrix}^T$$

$$\mathbf{A}1_k = \begin{bmatrix} a_{k-1,1} & & & \\ & a_{k-1,2} & & \\ & & a_{k-1,3} & \\ & & & a_{k-1,4} \end{bmatrix}$$

$$\mathbf{B}1_k = \begin{bmatrix} b_{k-1,1,1} & & & \\ b_{k-1,2,2} & b_{k-1,2,1} & & \\ b_{k-1,3,3} & b_{k-1,3,2} & b_{k-1,3,1} & \\ b_{k-1,4,4} & b_{k-1,4,3} & b_{k-1,4,2} & b_{k-1,4,1} \end{bmatrix}$$

$$\mathbf{C}1_k = \begin{bmatrix} c_{k-1,1} & & & \\ & c_{k-1,2} & & \\ & & c_{k-1,3} & \\ & & & c_{k-1,4} \end{bmatrix}$$

Appendix C: Reformulation of discrete time state-space models

In this appendix the matrix formulations of equation 7.1 as derived from equation 7.2 and 7.3 is given. Equation 7.1 is

$$\mathbf{y}_k = \mathbf{D}_k\mathbf{m}_k + \mathbf{e}_k \tag{C.1}$$

where the elements of the $(P,1)$ vector $\mathbf{y}_k$ are considered observations and the matrix $\mathbf{D}_k$ is called a design matrix. The elements in the $(Q,1)$ vector $\mathbf{m}_k$ are the model parameters. The vectors $\mathbf{x}_{k-1}$ and $\mathbf{u}_k$ are put into the matrix $\mathbf{D}_k$, and the unknown elements in the matrices $\mathbf{H}_k\mathbf{A}_k\mathbf{B}_k\mathbf{C}_k$ and $\mathbf{H}_k\mathbf{A}_k$ are put into the vector $\mathbf{m}_k$ in the following way:

$$\mathbf{D}_k = \begin{bmatrix} \widehat{\mathbf{x}}_{k-1}^T & & & \mathbf{u}_k^T & & \\ & \ddots & & & \ddots & \\ & & \widehat{\mathbf{x}}_{k-1}^T & & & \mathbf{u}_k^T \end{bmatrix} \tag{C.2}$$

$$\mathbf{m}_k = \begin{bmatrix} (\mathbf{H}_k\mathbf{A}_k\mathbf{B}_k\mathbf{C}_k)_{1,:}^T \\ \vdots \\ (\mathbf{H}_k\mathbf{A}_k\mathbf{B}_k\mathbf{C}_k)_{P,:}^T \\ (\mathbf{H}_k\mathbf{A}_k)_{1,:}^T \\ \vdots \\ (\mathbf{H}_k\mathbf{A}_k)_{P,:}^T \end{bmatrix} \tag{C.3}$$

where $(\mathbf{H}_k\mathbf{A}_k\mathbf{B}_k\mathbf{C}_k)_{p,:}^T$ denotes the transpose of the pth row of the matrix. Note that $\mathbf{H}_k$ is a $P \times ML$ matrix and that $\mathbf{D}_k$ has P rows and $Q(= MPL + PL)$ columns.

The additional constraints, arising from the fact that the columns of the transition matrices in the original model (equation 5.1) sum to unity, are given by

$$\mathbf{y}_{cons,k} = \mathbf{D}_{cons,k}\mathbf{m}_{cons,k} \tag{C.4}$$

In vector-matix form:

$$\mathbf{y}_{cons} = \begin{bmatrix} \mathbf{z}_1 & \mathbf{z}_2 \end{bmatrix}^T$$

$$\mathbf{D}_{cons} = \begin{bmatrix} \mathbf{z}_1(1) & & & & & & \\ & \ddots & & & & & \\ & & \mathbf{z}_1(LM) & & & & \\ & & & \mathbf{z}_2(1) & & & \\ & & & & \ddots & & \\ & & & & & \mathbf{z}_2(L) \end{bmatrix}$$

$$\mathbf{m}_{cons,k} = \begin{bmatrix} (\mathbf{A}_k\mathbf{B}_k\mathbf{C}_k)_{:,1} \\ \vdots \\ (\mathbf{A}_k\mathbf{B}_k\mathbf{C}_k)_{:,LM} \\ (\mathbf{A}_k)_{:,1} \\ \vdots \\ (\mathbf{A}_k)_{:,L} \end{bmatrix}$$

where the vectors $\mathbf{z}_1$ and $\mathbf{z}_2$ are given by

$$\mathbf{z}_1 = \begin{bmatrix} 1(1) & 1(2) & \dots & 1(LM) \end{bmatrix}$$

$$\mathbf{z}_2 = \begin{bmatrix} 1(1) & 1(2) & \dots & 1(L) \end{bmatrix}$$

and where $\mathbf{D}_{cons}$ is an $S \times S^2$ matrix ($S = ML + L$) and $(\mathbf{A}_k\mathbf{B}_k\mathbf{C}_k)_{:,j}$ denotes the jth column of the matrix $(\mathbf{A}_k\mathbf{B}_k\mathbf{C}_k)$. $\mathbf{m}_k$ can be obtained by first multiplying $\mathbf{m}_{cons,k}$ with an output matrix $\mathbf{H}_{cons}$ which is given by

$$\mathbf{H}_{cons} = \begin{bmatrix} \mathbf{H}_k(1) & & \\ & \ddots & \\ & & \mathbf{H}_k(S) \end{bmatrix}$$

The result is a vector

$$\widetilde{\mathbf{m}}_k = \begin{bmatrix} (\mathbf{H}_k\mathbf{A}_k\mathbf{B}_k\mathbf{C}_k)_{:,1} \\ \vdots \\ (\mathbf{H}_k\mathbf{A}_k\mathbf{B}_k\mathbf{C}_k)_{:,LM} \\ (\mathbf{H}_k\mathbf{A}_k)_{:,1} \\ \vdots \\ (\mathbf{H}_k\mathbf{A}_k)_{:,L} \end{bmatrix}$$

To obtain vector $\mathbf{m}_k$, vector $\widetilde{\mathbf{m}}_k$ is reformatted by placing each ith element of the jth column in the matrix $\mathbf{H}_k\mathbf{A}_k\mathbf{B}_k\mathbf{C}_k$ from element $i + P(j-1)$ in vector $\widetilde{\mathbf{m}}_k$ into element $j + LM(i-1)$ in vector $\mathbf{m}_k$; and each ith element of the jth column in the matrix $\mathbf{H}_k\mathbf{A}_k$ from element $PLM + i + P(j-1)$ in vector $\widetilde{\mathbf{m}}_k$ into element $PLM + j + L(i-1)$ in vector $\mathbf{m}_k$.

Appendix D: Algorithm to calculate regularization via Singular Value Decomposition

In this appendix the mathematical operations are given for the steps briefly listed in section 8.2.

1. Solve equation 7.4 by a singular value decomposition of $\mathbf{D}_{cons}$

$$\mathbf{D}_{cons} = \mathbf{U}\Lambda\mathbf{V}^T = \begin{bmatrix} \mathbf{U}_p & \mathbf{U}_0 \end{bmatrix} \begin{bmatrix} \Lambda_p & 0 \\ 0 & 0 \end{bmatrix} \begin{bmatrix} \mathbf{V}_p & \mathbf{V}_0 \end{bmatrix}^T = \mathbf{U}_p\Lambda_p\mathbf{V}_p^T \tag{D.1}$$

   where $\mathbf{U}$ is an $S \times S$ matrix that spans the data space, and $\mathbf{V}$ is an $S^2 \times S^2$ matrix that spans the model parameter space. The matrix Λ is an $S \times S^2$ matrix, comprising a submatrix Λ_p with p non-zero singular values $(\lambda_1 \ldots \lambda_p)$ in the diagonal and zero matrices at the right and bottom. $\mathbf{U}_p$ and $\mathbf{V}_p$ consist of the first p columns of $\mathbf{U}$ and $\mathbf{V}$ respectively. The general solution of equation 7.4 (with $\mathbf{m} = \mathbf{H}_{cons}\mathbf{m}_{cons}$) is then

$$\mathbf{m} = \mathbf{H}_{cons}\mathbf{V}_p\Lambda_p^{-1}\mathbf{U}_p^T\mathbf{y}_{cons} + \mathbf{H}_{cons}\mathbf{V}_0\mathbf{q} \tag{D.2}$$

   where $\mathbf{H}_{cons}\mathbf{V}_p\Lambda_p^{-1}\mathbf{U}_p^T\mathbf{y}_{cons}$ is a particular solution, and $\mathbf{H}_{cons}\mathbf{V}_0\mathbf{q}$ (a sum over the null eigenvectors) as its null solution, see Wunsch and Minster (1982); Menke (1989).

2. Generate 200 logarithmically distributed values of ρ between two properly chosen parameters $\underline{\rho}$ and $\overline{\rho}$ ($\underline{\rho}$ and $\overline{\rho}$ have to be located such that the minimum of the generalized cross-validation function f_{gcv} is within this range). In this study the values are $\underline{\rho} = 3.6 \cdot 10^{-15}$ and $\overline{\rho} = \max\left(\lambda_p; \underline{\rho}\lambda_1\right)$, where λ_p and λ_1 are respectively the smallest and largest singular values in Λ_p.

3. Equation D.2 is substituted into 7.17, which after rearranging, gives

$$\begin{bmatrix} \mathbf{y} \\ \rho\mathbf{m}_{pri} \end{bmatrix} - \begin{bmatrix} \mathbf{D} \\ \rho\mathbf{I} \end{bmatrix} \mathbf{H}_{cons}\mathbf{V}_p\Lambda_p^{-1}\mathbf{U}_p^T\mathbf{y}_{cons} = \begin{bmatrix} \mathbf{D} \\ \rho\mathbf{I} \end{bmatrix} \mathbf{H}_{cons}\mathbf{V}_0\mathbf{q} + \begin{bmatrix} \mathbf{e} \\ \mathbf{e}_{pri} \end{bmatrix} \tag{D.3}$$

   which in short-hand notation can be rewritten as

$$\mathbf{y}_q = \mathbf{D}_q\mathbf{q} + \mathbf{e} \tag{D.4}$$

   with unknown vector $\mathbf{q}$, which is estimated by

$$\widehat{\mathbf{q}} = \left(\mathbf{D}_q^T\mathbf{D}_q\right)^{-1}\mathbf{D}_q^T\mathbf{y}_q \tag{D.5}$$

   Equation D.5 is solved numerically through the singular value decomposition of the matrix $\mathbf{D}_q = \mathbf{U}_q\Lambda_q\mathbf{V}_q^T$ and subsequent substitution into equation D.5, to yield

$$\widehat{\mathbf{q}} = \mathbf{V}_q\Lambda_q^{-1}\mathbf{U}_q^T\mathbf{y}_q \tag{D.6}$$

   The vector $\widehat{\mathbf{q}}$ can then be inserted in equation D.2 to give $\widehat{\mathbf{m}}$. Step three is repeated for each value of r, generated in step 2.

4. This last step comprises the calculation of $\mathbf{N} = \mathbf{DG} = \left(\mathbf{U}_q \Lambda_q \mathbf{V}_q^T\right)\left(\mathbf{V}_q \Lambda_q^{-1} \mathbf{U}_q^T\right) = \mathbf{U}_q \mathbf{U}_q^T$ and the substitution of $\mathbf{N}$ and $\widehat{\mathbf{m}}$ in equation 7.16 for each ρ, and subsequently the selection of the solution that gives the smallest f_{gcv}.

Appendix E: Shape of kernel functions

In this Appendix continuous functions are fitted through the piecewise linear kernel functions. For each of the 'Kernel types' listed in Table 6.6 an analytic expression is fitted. An impression of the shape of the different kernel functions is given by Figures E.1, E.2 and E.3. In these figures the average kernel parameter values (i.e. the middle from the parameter range, see Figure 5.3) are displayed. The five kernel functions displayed in each graph are obtained by five times randomly drawing the respective kernel function from the model set.

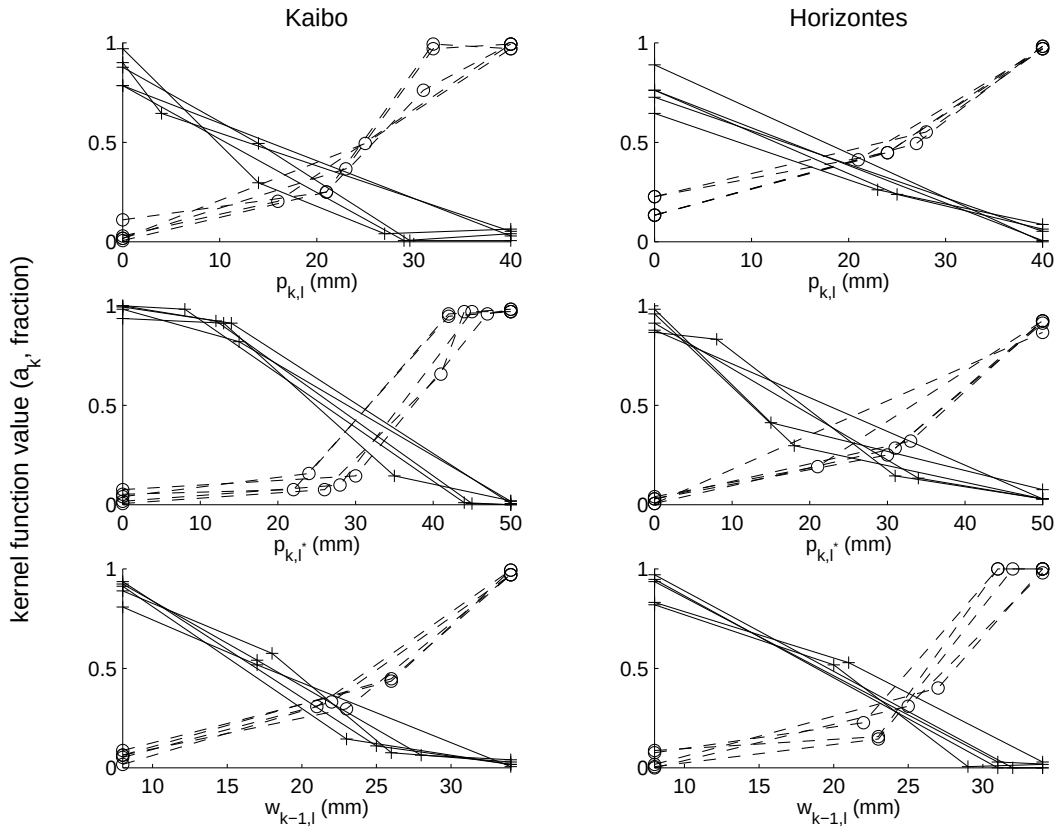

Figure E.1: Form of kernel-functions of the partitioning matrix (A) for different independent variables for Kaibo and Horizontes. The solid lines represent the parameter $s_{k,l}$, and the dashed lines the parameter $t_{k.l}$.

As explained in Section 6.7 functions that apply reasonably well are the rectangular hyperbola for kernel functions in A and C and the gamma distribution (the derivate of the incomplete gamma function) for kernel functions in B. For clarity these are listed here again. The rectangular hyperbola is given by one of the following equations.

$$f(x) = \frac{x^n}{x^n + a^n} \tag{E.1}$$

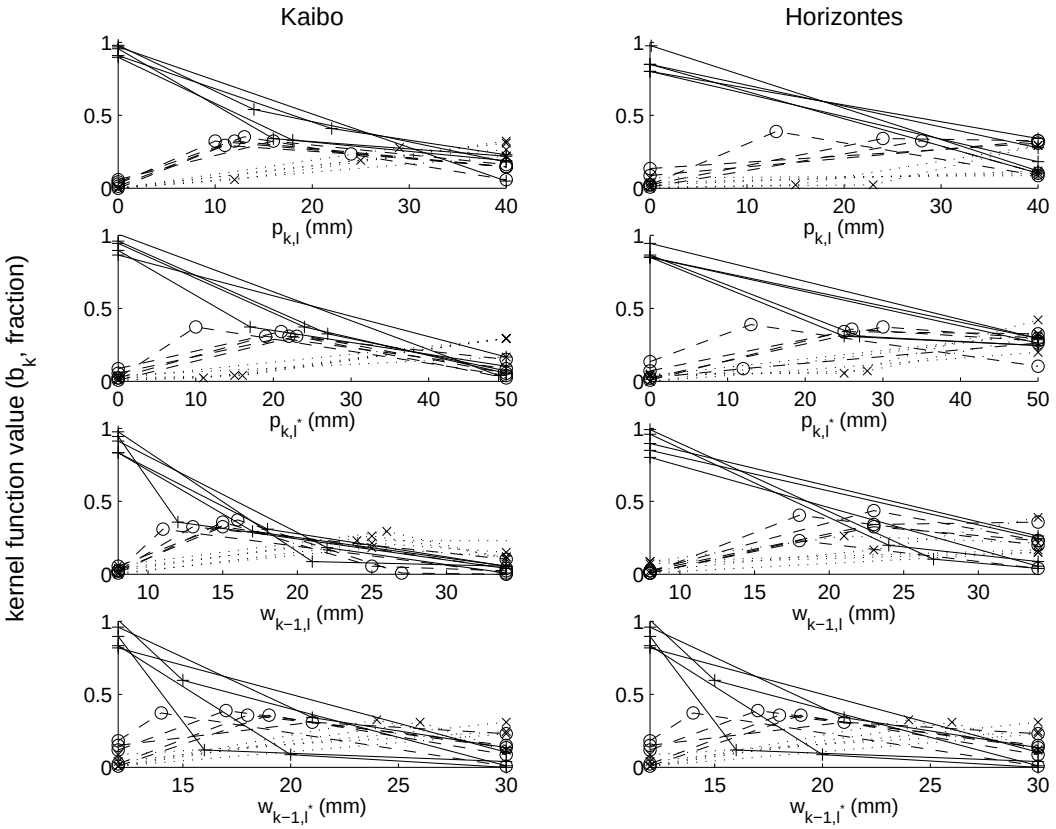

Figure E.2: Form of kernel-functions of the transport matrix (B) for different independent variables for Kaibo and Horizontes.

$$f(x) = 1 - \frac{x^n}{x^n + a^n} = \frac{a^n}{a^n + x^n} \tag{E.2}$$

$$f(x) = \frac{(x_{max} - x)^n}{(x_{max} - x)^n + a^n} \tag{E.3}$$

$$f(x) = \frac{a^n}{a^n + (x_{max} - x)^n} \tag{E.4}$$

where a (> 0) is a factor determining the location of x where $f(x)$ reaches half of its maximum value, x_{max} is the maximum value that x may take, and n a coefficient determining the point of inflection of the curve. In practice equation 6.5 applies to infiltration (declining for increasing values of $w_{k,l}$ and $p_{k,l}$), and equation 6.7 applies to saturation (excess) and return flow (increasing for increasing values of $w_{k,l}$ and $p_{k,l}$). The scaled version of the gamma distribution is given by

$$f(x) = \frac{\left(m\frac{x}{x_{max}}\right)^{a-1} e^{-\left(m\frac{x}{x_{max}}\right)}}{\Gamma(a)} \tag{E.5}$$

where a (> 1) is a shape factor, which may change the from of the distribution from exponential ($a = 1$) to Gaussian ($a = \infty$), m is a scale factor, and x_{max} is the maximum value that x may take. Through each of the groups with typical kernel functions an appropriate equation (either 6.4, 6.5, 6.6, 6.7 or 6.8) is fitted. The resulting equations are plotted in Figures E.4 and E.5. The parameters of each function are specified in Chapter 6, Tables 6.7 and 6.8.

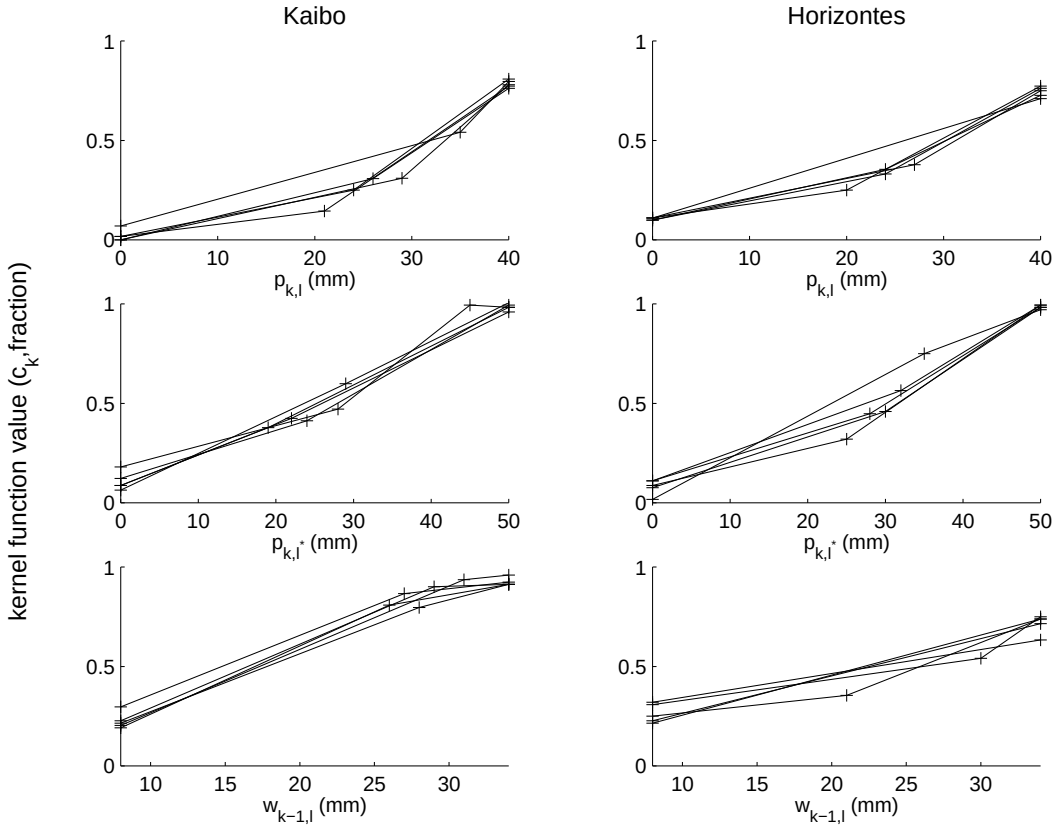

Figure E.3: Form of kernel-functions of the internal state matrix (C) for different independent variables for Kaibo and Horizontes.

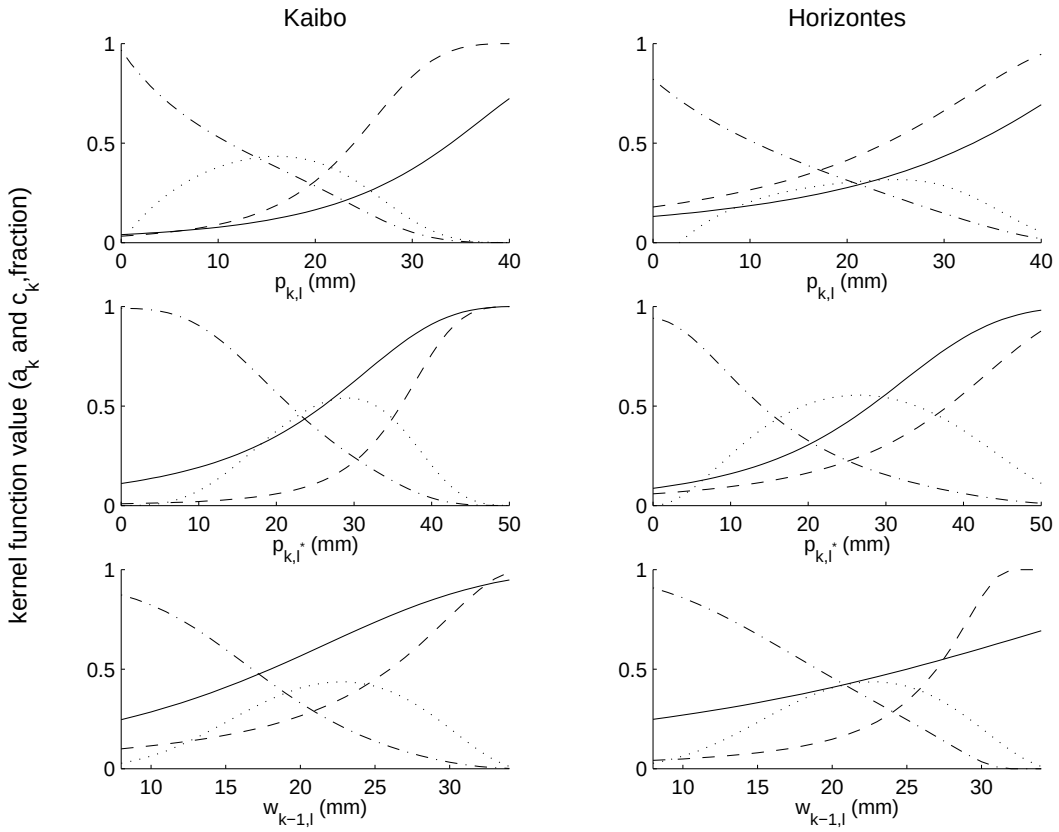

Figure E.4: Fitted curves for the kernel-functions of the partitioning and internal state matrices (A and C resp.) for different independent variables for Kaibo and Horizontes The dash-dotted lines represent the parameter $s_{k,l}$, the dashed lines the parameter $t_{k,l}$, the dotted lines the parameter $r_{k,l}$, and the solid line $c_{k,l}$

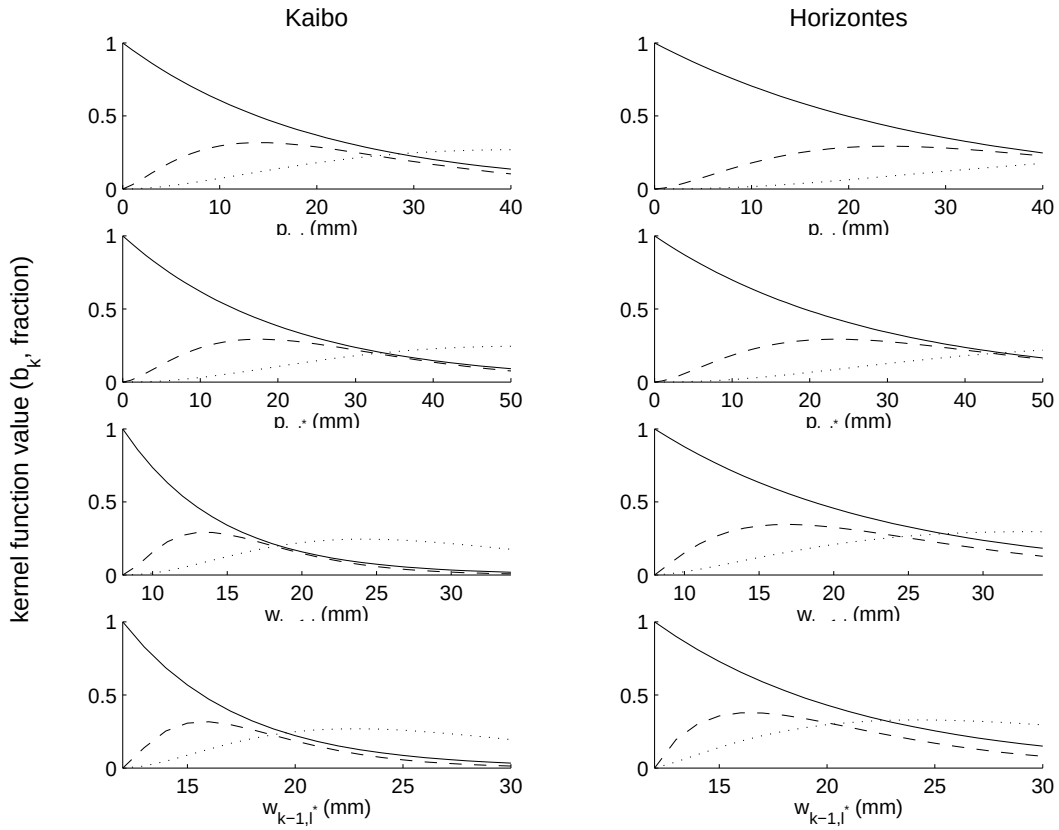

Figure E.5: Fitted curves for the kernel-functions of the transport matrix (B) for different independent variables for Kaibo and Horizontes

Summary

The goal of this study is to collect and analyze overland flow data at the catchment scale and to improve the techniques to identify catchment scale overland flow models for predictive purposes. The legitimacy of this goal is outlined in Chapter 1 where the history and the state of the art of overland flow modeling is described. The remainder of the dissertation is subdivided in two main parts. The first part, covering Chapters 2 to 4, comprises an interpretation of the overland flow observations in two experimental catchments and the effectiveness of commonly used overland flow models. In this part the specific problems when using the existing techniques for overland flow prediction are outlined. The second part, Chapters 5 to 7, presents new approaches for *scale-dependent* overland flow prediction. In Chapter 8 the results of this study are placed in perspective and an outlook is given for further research.

Overland flow is that part of the surface water that moves over the soil surface, while not being concentrated in rills or channels of a given size (then it is called channel flow). The point where overland flow ends and channel flow starts, spatially as well as temporally, can only be defined subjectively and approximately. Overland flow may originate from saturation of the soil either from above or below. When saturated from above, the quantity of rain and water from upstream areas exceeds the soil's infiltration capacity and when saturated from below the matrix pressure of the soil is positive due to pressure from soil water *in situ* or from upstream soil volumes. On natural surfaces overland flow is very heterogeneous and unsteady, with flow depths ranging from 1 to 100 *mm* and flow velocities between 0.01 and 1 $m\,s^{-1}$ within a small area. The knowledge of overland flow is important because it is the main determinant for sediment transport by water, the transport and fate of nutrients and (agro)chemicals which reside on the soil surface, and the size and the shape of flood peaks. Nearly all surface flow starts as overland flow in the upper reaches of a catchment and travels some distance before reaching a rill or channel. In spite of this important role that overland flow plays in various instances, it has hardly ever been observed over areas larger than a few hectares through direct quantitative or qualitative measurements.
The nature of overland flow in two experimental catchments is described in Chapter 2. The first catchment, *Kaibo*, is located in Burkina Faso (West Africa) at $44^{\circ}11'$ N and $0^{\circ}56'$ E (310-325 m.a.s.l.) in the river valley of the Nakambé (the White Volta) and covers an area of 1.2 km^2. The catchment has a semi-arid tropical climate with an average precipitation of 880 $mm\,y^{-1}$, minimum and maximum temperatures of 19 and $32^{\circ}C$ respectively and a potential evapotranspiration of 2580 $mm\,y^{-1}$. The actual evapotranspiration in the area is approximately 620 *mm* (70% of the rain), percolation to deeper layers is approximately 80 mm (10% of the rain) and discharge is approximately 180 mm (20% of the rain). The average rainy season last from May till October and displays a large inter- as well as intra-season heterogeneity with regard to total rain depth as well as the occurrence of dry spells. The natural vegetation is savanna-woodland and the area is now partly used for arable crops and extensive grazing. The second catchment, *Horizontes*, is located in Costa Rica (Central America) at $10^{\circ}43'$ N and $-85^{\circ}36'$ E (160-190 m.a.s.l.), inside the park 'Estacion Experimental Forestal Horizontes' (part of the regional nature conservation agency, ACG). It is 2 km^2 in size and has a sub-humid tropical climate. The average rainfall is 1450 $mm\,y^{-1}$, minimum and maximum temperatures are 22 and $29^{\circ}C$ respectively and the potential evapotranspiration is 2230 $mm\,y^{-1}$. The actual evapotranspiration in the area is approximately 870 *mm* (60% of the

rain), percolation to deeper layers is approximately 220 *mm* (15% of the rain) and discharge is approximately 360 *mm* (25% of the rain). The average rainy season lasts from May till October and displays especially a large intra-season heterogeneity with regard to total rain depth. The natural vegetation of Horizontes is tropical dry forest, which is presently in an early stage of regeneration, starting from completely open grassland in 1989.
In Kaibo observations were collected over the period April 1994 - August 1998. Over this period weather variables were measured with an automatic weather station at a single location. Rain was observed at various locations with tipping buckets from 1996 onwards and discharge was observed at the catchment outlet with a pressure transducer. Soil moisture was measured with a TDR device in plastic access-tubes at 10 locations once every 14 days, and the runoff from six runoff plots (three pairs of 5×10, 10×25 and 50×100 *m* in size) was measured using flumes. In addition, various observations have been collected in the period June-September 1998. In this period water table depth was measured manually along three transects with piezometers for 3 events. The structure of the subsurface was determined by geo-electric measurements. In this period overland flow was observed during rain in two events. This was done by measuring water levels and flow velocities repeatedly at several points along a transect. In addition overland flow patterns were mapped just after rain for these two events along the transect. An accurate DTM of the terrain was constructed on the basis of observations with a differential kinematic GPS system, and visual assessments were made in subsequent surveys. Several other surveys were conducted to map the soil, geology and land use in the area.
In Horizontes observations were collected over the period April 1996 - August 1998. Over this period weather variables were measured with an automatic weather station at a single location, rain was observed at 6 locations with tipping buckets and discharge was observed at 6 locations in the main gully with pressure transducers. In the period June 1997 - December 1997 post-event flow patterns were observed along two transects. Along these transects overland flow was observed with 24 collectors. A DTM was constructed on the basis of observations with a differential kinematic GPS technique in combination with a conventional ground-based survey. Several other surveys were conducted to map the soil, geology and vegetation in the area. A 44 ha sub-catchment of Horizontes, which is named Horicajo, has been studied in greater detail. The observations in Horicajo were made during the period period July 1997 till December 1997. At four locations rain has been measured using tipping buckets and at two locations discharge has been measured using v-crest weirs. For 7 events water table depth has been observed manually in 20 piezometers at hourly instants during and just after rain, and daily between rain events. Post-event overland flow patterns were observed for 5 events, and overland flow height as well as velocity were observed during 9 events along 4 transects. During the period 20 July - 4 October 1997, volumetric soil moisture has been measured at 40 locations once every 4 days, and during the period 4 October - 21 December 1997 at 60 locations once every 2 days. For the soil moisture measurements a TDR system with plastic access tubes has been used, enabling the measurement of soil moisture over 20 *cm* layers down to 80 *cm*. Terrain and soil have been mapped in detail and in addition the geometry of small rills and drainage channels have been mapped. Soil colour, structure, depth, organic matter content, and texture have been determined at 90 locations, and the infiltration capacity has been determined at 30 of these locations, using a Guelph permeameter. In addition soil colour, structure and texture (field-determined) have been observed at a regular spacing of 20×20 *m*.
For Kaibo as well as Horizontes the data from 60 rainfall events are used for calibration and validation in this study. The set of 60 events for Horizontes includes the 31 events for which observations in Horicajo are available.
Three aspects of the observations are investigated in some detail: the measurement uncertainty, the relation between overland flow extent and height, and autocorrelation of overland flow in space and time. The measurement uncertainty is estimated on the basis of repetition, split-sample valida-

tion and cross-validation for the various observations. The total measurement uncertainty results from three sources: random errors produced by the instrument during the observation process, conversion errors resulting from the conversion of observed quantities to desirable quantities using an empirical relationship, and interpolation errors that result from the integration of observed quantities to the desired spatio-temporal units. It appears that especially interpolation errors contribute to the total measurement uncertainty and that, when considering the combined effect of the error sources, overland flow observations on the basis of visual inspection, ground water observations (Horizontes) and soil moisture observations (Kaibo) are relatively uncertain with an unknown stochastic error structure. Therefore an unknown-but-bounded (UBB) error structure is used to for their characterization. The overland flow extent appears to be related to overland flow height in a non-linear way. There exist significant differences for these relationships between Kaibo and Horizontes as well as the different soil and vegetation types. Tresholds that occur in the extent-depth relations can be related to average rill depth. The anisotropy of the overland flow distribution in space as well as time is illustrated with correlograms in which correlation lengths vary from 10 to 80 *m* for contour and slope directions respectively, and 25 to more than 60 minutes for intensive and non-intensive rain respectively.

A first analysis of the data is provided via a regression model for overland flow in Chapter 3. The regression method ties up different kinds of observations such as overland flow heights, overland flow in collectors and catchment discharge, via a two step approach: 1) by using linear and non-linear measurement equations to relate each observed quantity to the total-event overland flow height, and 2) by using this overland flow height in that linear regression equation. Given the data with UBB observation errors, a unique solution to this problem has been found by using a mini-max criterion. The method appears to be computationally very simple, which allows its application to large data sets and the calculation of the model performance via cross-validation. After calibration the overland flow predictions for soil-vegetation units with the regression model appear to be rather good, especially when distinguishing between early and late season or high and low intensity rain. With a split-catchment approach, using the Horizontes data, the possibility to use the model for predictive purposes in an un-calibrated catchment is investigated. It shows that the prediction of discharge was possible but that overland flow can not be predicted with a satisfactory accuracy.

In Chapter 4, the observations are analyzed with an archetypical parameter distributed overland flow model. The threefold aim of this analysis is to investigate: 1) whether the model can be calibrated, in the sense that a set of nearly optimal parameters is derived which can be used for predictive purposes; 2) how the proposed model compares to the alternative regression approach outlined in Chapter 3; and 3) whether the model does reproduce some of the spatial heterogeneity of overland flow. In two aspects the model differs from most other overland flow models: 1) it has relatively few parameters; and 2) it is event-based but explicitly and in a simple way incorporates the pre-event wetness in its parameterization of infiltration. To calibrate the model a similarity index has been used to match observations with model variables at distant locations but with supposedly similar features due to a correspondence in upstream area, soil type and vegetation type. This calibration procedure has proven to perform quite well. After model calibration the model is tested on the basis of discharge and overland flow observations. From these tests it appears that the model can indeed be calibrated. The distributed model appears to be a worse predictor of both discharge and overland flow in comparison to the regression model. The observed heterogeneity of overland flow is not reproduced by the model at the grid resolution but is reasonably well predicted at the resolution of soil-vegetation units. According to the model predictions Kaibo and Horizontes are quite dissimilar with respect to their overland flow patterns. In Kaibo soil and vegetation factors are more important in determining the occurrence of overland flow, whereas in Horizontes it are mainly topographical factors. These effects can however not be separated com-

pletely since there is a strong spatial correlation between soil, vegetation and topography. Kaibo and Horizontes have catchment discharge/rain ratios of respectively ± 0.1 and ± 0.2. Both values appear to be close to what is expected in these environments. Also strong seasonal trends appear to exist, with increasing levels of overland flow towards the end of the season. For Horizontes the trend can best be explained by the cracks in vertic soils under dry conditions, and for Kaibo an additional explanation is the a decreasing soil roughness of the arable land over the season. In Kaibo the differences between early and late season are most pronounced. In spite of the qualitative nature of the observations and model predictions presented, the seasonal trends are so obvious that these have to be taken into account in overland flow modelling. There are two options to do this: 1) by using all seasonal factors for parameterization (i.e. use seasonal factors as model inputs); or 2) parameterize a model for a period brief enough so that all parameters can be considered constant. Both approaches have been tested in this study. The distinction between soils with vertic and non-vertic properties deals with soil changes, and distinctions between grass versus trees (Horizontes) or grass versus arable land (Kaibo) deal with differences in vegetative development and land husbandry. In addition the pre-event wetness index partially reproduces a seasonal effect. Re-calibration on more restricted data sets (early season versus late season and low intensity versus high rain intensity) was also done but did not lead to improved model predictions, possibly because the data sets were too small for that purpose.

A framework for identifying *scale-dependent* hydrological models is described in Chapter 5. The method works with a so-called model template in which the state variables, independent variables, the range of allowed space and time resolutions and the allowed minimum and maximum number of parameters are specified. On the basis of the template a genetic algorithm searches for optimal model structures, which are calibrated with a Monte Carlo procedure using the UBB error data. Special features of the method are the facts that the spatial elements in the resulting models may vary in size and the models are of a stochastic nature because parameter ranges rather than parameter values are defined. In addition, the resulting models, which comprise a partitioning matrix, a transport matrix and an internal state matrix, can be interpreted in a physical sense since these matrices denote different flow process. The method has been applied to a synthetic data set, generated with a coupled overland flow and 2D Richards model at the hillslope scale (100 *m* in length and a 1 *m* soil depth) and a rainfall generator. The identification method generates a large set of fit (well-behaving) models that differ in parameterization and resolution. An analysis of the fittest models leads to a number of interesting insights. The fittest models are found at a narrow range of space-time resolutions, ranging from 4 *min* with 10 units to 18 *min* with 4 units. The fittest models constitute an organization that strives to equally sized elements, especially at finer resolutions. The parameter ranges of the partitioning and internal state matrices in the models are related to fitness especially at the coarsest resolutions (smaller parameter ranges lead to higher fitness), while the transport matrix shows hardly any relation and moreover constitutes the largest part of parameter uncertainty. When moving from a coarse to a finer spatial resolution the total number of parameters in the fittest models remains almost constant. The fittest models are qualitatively different at different resolutions, with respect to form as well as to the independent variables in the kernel functions. Soil moisture is the state variable that influences model dynamics mostly in models with a fine temporal resolution whereas rainfall is the most important driving force in models at coarse temporal resolutions. The main strengths of the method are its general applicability (regardless error structure or non-linearity), the possibility to evaluate a large set of candidate models, to interpret the identified models in a physical sense, and computational simplicity. Weaknesses are the relatively complex models that may result from the identification procedure, the computation time required, and, in this particular case with UBB error data, the relative poor fit of models as compared to methods with more detailed assumptions on errors. The method is therefore mainly suitable to identify a limited set of candidate models, that can be

further optimized with more rigorous identification techniques.

In Chapter 6 the framework presented in Chapter 5 is applied to the Kaibo and Horizontes data with the objective to identify a set of overland flow models and relate the structure of these to predictive uncertainty and model resolution. It was not clear *a priori* whether the identification procedure does work for the catchments, given that it has only been tested with synthetic hillslope-scale data, but it turns out that the method generates large sets of fit models for both Kaibo and Horizontes. It is investigated how the model sets can effectively be used for prediction. A choice is made to use ensemble simulation where a number of models are drawn randomly from the set and the final prediction is the average over the different models. It appears that for increasing ensemble sizes the prediction error decreases. This trend continues up to ensemble sizes of approximately 800 for Kaibo and almost 1000 for Horizontes. There are slight differences in these relationships for discharge and overland flow. The explanation for this relation between ensemble size and prediction error is the relative heterogeneity of the model set. A choice is made to simulate with ensembles of 1000 members in the remainder of this study. The ensemble predictions show good performance on the validation data with a slight over-prediction of low catchment discharges, especially for Horizontes. The structure of the prediction error for the validation data is similar to that for the calibration data. The ability of the identified models to predict overland flow ratios is analyzed by comparing observed and predicted overland flow ratios for different spatial units, in this case the soil-vegetation unit and the entire catchment. Interestingly, the fit does not differ for the different resolutions as it does with the distributed model, where a better correspondence between observed and predicted was found at the catchment scale. A possible explanation for this phenomenon is that models at different resolutions contain approximately an equal number of parameters, which leads eventually to an equal predictive uncertainty at the different resolutions. By a straightforward application of ensemble-prediction, coarse as well as fine-resolution models with a similar fitness have an equal chance of selection, leading to a predictability which is similar over all resolutions. This explanation implies that the use of finer-scale models for prediction at the finer resolutions and coarse scale models for prediction at coarser resolutions should lead to better results. A test confirms this hypothesis. In spite of the marked differences between Kaibo and Horizontes, there are many similarities between the model sets describing these catchments: 1) the same model template was used for both catchments, 2) the relation between problem resolution, availability of observations and fitness seems to apply to both catchments, and 3) the shift in the independent variables from soil moisture at fine temporal resolutions to rain at coarse temporal resolutions is applicable to both Kaibo and Horizontes. The catchments differ with regard to the exact form of the kernel functions and the model resolutions to which different kernel functions apply. This can be explained by the difference in topography - Kaibo has longer slopes and less relief - and the limited spatial discretization of the models for Kaibo. This last factor may have been caused by the relatively few distributed observations in Kaibo. It is notable that the same shifts in the use of independent variables are found for the real data sets at the catchment scale as with the synthetic data set at the hillslope scale (in Chapter 5). It suggests that the source-driven system behaviour at coarse resolutions and sink-driven behaviour at fine resolutions is a property of the hydrologic systems at both scales. The model forms are analyzed over a range of space-time resolutions, leading to the demarcation of kernel-shifts. Comparing the location of these kernel-shifts for Horizontes and Kaibo leads to the observation that the shift from source to sink-limited system behaviour occurs at a spatial resolution of approximately 7 units for Horizontes and 5 units for the Kaibo. These resolutions correspond to physical dimensions of (on average) 300 m in Horizontes and 220 m in Kaibo. Relating these dimensions with the spatial correlation structure of the rain, soil and vegetation characteristics indicates that especially the spatial structure of the rain (with auto-correlations dropping sharply at 300 and 200 m for Horizontes and Kaibo respectively) could give rise to this pattern. The spatial heterogeneities of soil and vegetation characteristics are

approximately twice as large. This observation gives rise to the hypothesis that in the two study catchments the structure of a rain event is the most important determinant for overland flow patterns, instead of topography or the pre-event soil moisture distribution. Applying the identification method to different sub-sets of the data, leads to very interesting results. In the first place, it shows that rain intensity does not influence the parameterization whereas seasonality (the time after start of the wet season) does. This means that the nature of the hydrologic system changes over the rainy season. It has been explained before that this change is caused by various strongly correlated processes: swelling and shrinking of clays, vegetative developement, soil roughness changes (due to the impact of rain, animals and soil tillage) and biologic activity. A considerable heterogeneity within the model set derived on the basis of average-seasonal conditions, can be explained by shifts in these factors. However, the limited size of the data set, especially with regard to these seasonal factors, does not allow the parameterization of the various models with these newly identified factors. For both catchments the kernel functions for partitioning can be estimated by a rectangular hyperbola, and the kernel functions for transport by gamma-distributions. The functions can be interpreted in a probabilistic sense, leading to data-based conditional and joint probability distributions of hydrological variables. The applicability of these distributions for practical purposes still needs to be tested.

In Chapter 7 the problem of overland flow prediction is studied for cases where observations are available in combination with a set of calibrated models. The technique used to combine prior models results with observations is known as Tikhonov regularization. Within this regularization framework generalized cross-validation is used to obtain desirable weights between prior model predictions and observations. Two regularization strategies are compared: regularization of the model parameters, and regularization of the model state variables. It is shown that both techniques lead to similar results, which differ in some details. Parameter regularization leads to better results at low data availability, whereas state regularization leads to better results at high data availability, which is consistent with the fact that there are fewer parameters than states to be estimated. The fact that state regularization realizes its best predictions at finer resolutions than parameter regularization can be explained by considering that parameter regularization maintains the *relative* structure of the kernel functions over different spatial units, and can in this way less efficiently exploit the additional degrees of freedom offered by a finer resolution. The comparative advantage of this flexibility appears at higher data availability and finer resolutions. A comparison of the open-loop predictions over the calibration period itself with the reguralized predictions shows that even the best calibration feasible will not nearly approach the results by using a regularization approach. Against this background it is not worthwhile to consider model re-calibration as an alternative to regularization. The regularization methodology employed here can relatively easily be adapted to different models or observations. This point has been demonstrated in this study by using a set of models instead of a single model in order to generate a prediction. Considering the ease with which regularization can also be integrated in the Kalman filter and Kalman smoother and the relative success of the Ensemble Kalman filter to problems of a realistic size, a very fruitful enterprise might be the integration of regularization in the Ensemble Kalman filter as well.

Chapter 8 concludes the dissertation by combining some of the information presented earlier with new information about the relative value of observations. The effectiveness of each of the three modelling approaches, the regression model, the distributed model and the scale-dependent models for identification and prediction is reviewed first. It is concluded that while clearly the scale-dependent models have distinct advantages for model identification, for prediction the model differences are less clear. By comparing the effect of omitting each of the observation types (e.g. discharge observations or overland flow observations) during model calibration, the relative value of the observations is determined. It turns out that the effect of omitting nearly each of the observation types leads to changes in prediction errors that are larger than the intra-model differences

with regard to those prediction error. The conclusion is that model differences are relatively unimportant, and that the emphasis for this type of research should in any case be on data collection and analysis. Unfortunately the conclusions do not solve the problem of improving overland flow prediction because the desired observation techniques are not available now or in the near future for large scale applications. An outlook on further research into this area therefore mainly focuses on theoretical issues such as the possibility to investigate the scale-dependent models in more depth, establish probabilistic models on the basis of the scale-dependent models and compare the scale-dependent models once again with both a distributed model and laboratory-scale experiments.

Samenvatting

Het doel van deze studie is gegevens over oppervlakte-stroming (*overland flow*) te verzamelen en te analyseren en om methoden te ontwikkelen voor de identificatie van voorspellende modellen voor oppervlakte-stroming op stroomgebied-schaal. De verantwoording voor dit onderzoeksdoel wordt in Hoodstuk 1 gegeven, waar tevens de historie en de huidige modellering van oppervlakte-stroming is beschreven. De rest van de dissertatie is onderverdeeld in twee delen. Het eerste deel, dat hoofdstukken 2 tot en met 4 beslaat, bestaat uit een interpretatie van de verzamelde gegevens over oppervlakte-stroming in twee experimentele stroomgebieden en de effectiviteit van veelgebruikte modellen in het beschrijven van de oppervlakte-stroming. In dit deel worden de specifieke problemen beschreven die optreden bij de bestaande modelleertechnieken. In het tweede deel, bestaand uit hoofdstukken 5 tot en met 7, worden nieuwe technieken gepresenteerd voor het schaal-afhankelijk modelleren van oppervlakte-stroming. In Hoofdstuk 8 worden de resultaten van deze studie in perspectief geplaatst en wordt een aanzet gegeven voor verder onderzoek.

Oppervlakte-stroming is het deel van het oppervlaktewater dat over de grond stroomt en zich nog niet heeft geconcentreerd in rillen of beken van een gegeven grootte - dan wordt het *"channel flow"* genoemd. Het punt waar oppervlakte-stroming stopt en *"channel flow"* begint, in ruimte zowel als tijd, kan enkel subjectief en bij benadering aangegeven worden. Oppervlakte-stroming kan ontstaan door verzadiging van de bodem zowel van beneden uit als van bovenaf. Bij verzadiging van bovenaf overschreidt de hoeveelheid regen en water van het bovenstroomse gebied de infiltratiecapaciteit, bij verzadiging van onderuit is de matrixpotentiaal van de bodem positief door druk van bodemvocht ter plekke of in het bovenstroomse bodemvolume. In natuurlijk terrein is oppervlakte-stroming zeer heterogeen en niet-stationair, met waterdieptes van 1 tot 100 *mm* en stroomsnelheden van 0.01 tot 1 $m\,s^{-1}$ binnen een klein gebied. De kennis van oppervlakte-stroming is belangrijk omdat het de belangrijkste factor is voor sedimenttransport door water, het transport en het lot van (landbouw)chemicaliën op de grond, en de vorm alsmede grootte van afvoerpieken. Bijna al het oppervlaktewater begint als oppervakte-stroming in het bovenstrooms gebied van een stroomgebied en verplaatst zich enige afstand voordat het een ril of beek te bereikt. Ondanks het belang van oppervlakte-stroming, is het nauwelijks bestudeerd over gebieden van meer dan enkele hectaren door direkte kwantitatieve of kwalitatieve metingen.

De oppervlakte-stroming zoals die voorkomt in twee experimentele stroomgebieden wordt in Hoofdstuk 2 beschreven. Het eerste stroomgebied, Kaibo, ligt in Burkina Faso (West Afrika) op $44^{\circ}11'$ N en $0^{\circ}56'$ O (310-325 m.a.s.l.) in het stroomgebied van de Nakambé (de Witte Volta), en beslaat een gebied van 1.2 km^2. Het stroomgebied heeft een semi-aride tropisch klimaat met een gemiddelde jaarlijkse neerslag van 880 $mm\,y^{-1}$, minimum and maximum temperaturen van respectievelijk 19 and $32^{\circ}C$ en een potentiële evapotranspiratie van 2580 $mm\,y^{-1}$. De actuele evapotranspiratie is ongeveer 620 *mm* (70% van de regen), percolatie naar diepere bodemlagen is ongeveer 80 *mm* (10% van de regen) en afvoer is ongeveer 180 *mm* (20% van de regen). Het gemiddelde regenseizoen duurt van mei tot oktober en is zeer heterogeen zowel binnen als buiten het seizoen met betrekking tot regenhoeveelheid en de duur van droge perioden. De natuurlijk vegetatie is savanne. Het gebied wordt nu voor het grootste gedeelte gebruikt voor akkerbouw en extensieve beweiding. Het tweede stroomgebied, *Horizontes*, bevindt zich in Costa Rica (Centraal Amerika) op $10^{\circ}43'$ N en $-85^{\circ}36'$ O (160-190 m.a.s.l.), binnen het natuurpark 'Estacion Exper-

imental Forestal Horizontes' (onderdeel van de regionale organisatie ACG). Het is 2 km^2 groot en heeft een sub-humide tropisch klimaat. De gemiddelde regenval is 1450 $mm\,y^{-1}$, minimum and maximum temperaturen zijn respectievelijk 22 and 29°C en de potentiële evapotranspiratie is 2230 $mm\,y^{-1}$. De actuele evapotranspiratie is ongeveer 870 *mm* (60% van de regen), percolatie naar diepere bodemlagen is ongeveer 220 *mm* (15% van de regen) en afvoer is 360 *mm* (25% van de regen). Het gemiddelde regenseizoen duurt van mei tot oktober en laat een grote variatie in regenhoeveelheid zien tussen de seizoenen. De natuurlijke vegetatie in Horizontes is een gedeeltelijk bladverliezend tropisch bos. Vanuit een situatie met open grasland in 1989 verkeert het gebied medio '90 in een vroeg stadium van regeneratie.
In Kaibo zijn gegevens verzameld gedurende de periode april 1994 - augustus 1998. Weersgegevens zijn verzameld met een automatisch weerstation op één locatie, regen is gemeten op verschillende locaties met automatische regenmeters (z.g. "tipping buckets") vanaf 1996 en afvoer is gemeten met een druksensor in de rivierbedding. Bodemvocht is bepaald met een TDR-instrument in plastic buizen op 10 plaatsen elke 14 dagen, en afvoer van zes afstromings-percelen (drie paren met afmetingen van 5×10, 10×25 en 50×100 m) is gemeten met meetgoten (waarin ook druksensoren). Daarnaast zijn er ook verschillende andere waarnemingen gedaan in de periode juni 1998 - september 1998. De schijn-grondwaterspiegel is in deze periode gemeten langs drie raaien met peilbuizen voor drie buien en de structuur van de ondergrond is bepaald met geoelectrische metingen, oppervlakte-stroming is waargenomen gedurende twee buien. Dit is gedaan door waterhoogte en snelheid herhaaldelijk op verschillende punten langs twee raaien te bepalen, en daarnaast stromingspatronen van oppervlaktewater in kaart te brengen direct na deze buien voor diezelfde raaien. Een nauwkeurig digitaal terrein model (DTM) is gemaakt op basis van metingen met een differentiële kinematische GPS-techniek. Later zijn visuele controles van stroomgebiedsgrenzen en lokale hoogten en laagten in het veld gemaakt. Diverse andere campagnes zijn uitgevoerd om bodem, geologie en landgebruik in het gebied in kaart te brengen.
In Horizontes zijn gegevens verzameld gedurende de periode april 1996 - augustus 1998. Weersgegevens zijn gemeten met een automatisch weerstation op één locatie, regen is gemeten op zes plaatsen met automatische regenmeters en afvoer is gemeten op zes plaatsen in de rivierbedding met druksensoren. In de periode juni 1997 - december 1997 zijn de stromingspatronen na drie buien bepaald langs twee raaien. Langs dezelfde raaien is ook oppervlakte-stroming gemeten in 24 kleine collectoren. Een DTM is gemaakt met een differentiële kinematische GPS-tecniek in combinatie met conventionele geodetische metingen. Diverse andere meetcampagnes zijn uitgevoerd om bodem, geologie en vegetatie in kaart te brengen. Een 44 *ha* deel-stroomgebied van Horizontes, Horicajo genaamd, is in meer detail bestudeerd. De waarnemingen in Horicajo zijn verzameld gedurende de periode juli 1997 - december 1997. Op vier plaatsen is regen gemeten met automatische regenmeters en op twee plaatsen is afvoer gemeten met v-vormige overlaten en druksensoren. Voor zeven buien is de hoogte van de grondwaterspiegel ieder uur waargenomen met de hand in 20 stijgbuizen tijdens en direkt na de buien, en dagelijks tussen de buien. De stromingspatronen na een bui zijn bepaald voor vijf buien, en de waterhoogte en snelheid zijn gemeten voor negen buien langs vier raaien. Gedurende de periode 20 juli 1997 - 4 oktober 1997 is het volumetrisch vochtgehalte bepaald op 40 locaties eens in de vier dagen, en gedurende de periode 4 oktober - 21 december op 60 lokaties eens in de twee dagen. Voor deze vochtmeting is een TDR-systeem in plastic buizen gebruikt, waarmee per laag van 20 *cm* gemeten is tot een diepte van 80 *cm*. Terrein en bodem zijn gedetailleerd in kaart gebracht samen met de geometrie van rillen en geulen. De kleur, structuur, diepte, textuur en het organische stof gehalte van de bodem zijn bepaald op 90 plaatsen, en de infiltratiecapaciteit is bepaald op 30 van deze paatsen met een Guelph permeameter. Daarnaast zijn kleur, structuur en textuur van de bodem in het veld gemeten op een regelmatig grid van 20×20 *m*.
Voor zowel Kaibo als Horizontes zijn de gegevens van 60 buien gebruikt voor calibratie en val-

idatie doeleinden in latere hoofdstukken. Tot de 60 buien behoren ook 31 buien waarvoor ook gegevens van Horicajo beschikbaar zijn.
Drie aspecten van de waarnemingen zijn in detail onderzocht: de meetonzekerheid, de relatie tussen de bedekkingsgraad en waterhoogte bij oppervlakte-stroming, en de autocorrelatie van oppervlaktestroming in ruimte en tijd. De meetonzekerheid wordt geschat op basis van herhaling, opsplitsing van de dataset en kruis-validatie. De totale meetonzekerheid is de resultante van drie bronnen: willekeurige fouten die door het meetinstrument of de meettechniek worden geproduceerd, conversiefouten die ontstaan door de omrekening van geobserveerde eenheden naar wenselijke eenheden, en interpolatiefouten die ontstaan door eenheden om te zetten naar wenselijke tijds- en ruimte-eenheden. Het blijkt dat vooral interpolatiefouten aanzienlijk bijdragen aan de totale meetonzekerheid en dat, als het gecombineerde effect van de foutbronnen in beschouwing wordt genomen, met name oppervlakte-stroming op basis van visuele waarnemingen, grondwater waarnemingen (Horizontes) en bodemvocht waarnemingen (Kaibo) relatief onzeker zijn en een onbekende foutstructuur hebben. Daarom wordt een *"unknown-but-bounded"* (UBB) foutstructuur gebruikt als karakterisering van de meetonzekerheid. De bedekkingsgraad van oppervlakte-stroming blijkt niet-lineaire te zijn gerelateerd aan de gemiddelde diepte ervan. Er zijn aanzienlijke verschillen tussen deze relaties voor Kaibo en Horizontes en verschillende bodem- en vegetatietypen. De knikpunten in de relaties geven drempelwaarden aan en kunnen worden gerelateerd aan gemiddelde rildiepte. De anisotropie van de oppervlakte-stroming in zowel ruimte als tijd wordt geïllustreerd met correlogrammen, waarin de correlatielengtes variëren van 10 tot 80 m voor respectievelijk contour- en hellingrichting, en 25 tot meer dan 60 minuten voor respectievelijk intensieve en niet-intensieve neerslag.

Een eerste analyse van de waarnemingen wordt gemaakt met een regressiemodel in Hoofdstuk 3. De regressiemethode combineert de verschillende soorten waarneminen zoals waterhoogte van oppervlakte-stroming, opgevangen oppervlakte-stroming in collectoren en stroomgebiedsafvoer via een twee-staps benadering: 1) door lineaire en niet-lineaire meetvergelijkingen te gebruiken om iedere waargenomen eenheid naar totale-bui oppervlakte-stromingshoogte om te zetten, en 2) door deze totale-bui oppervlakte-stromingshoogte in een lineaire regressievergelijking te gebruiken. Op basis van de waarnemingen met UBB foutstructuur, is er een unieke oplossing van dit probleem gevonden met het mini-max criterium. De methode blijkt rekentechnisch erg simpel, wat het toelaat grote hoeveelheden gegevens te analyseren en de kwaliteit van het model met kruis-validatie te evalueren. Na calibratie blijken de door het regressiemodel voorspelde oppervlakte-stromingshoogten goed overeen te komen met de waarnemingen, vooral wanneer onderscheid gemaakt wordt tussen het voor- en naseizoen of lage en hoge regenintensiteit. Door een model op het Horicajo deel-stroomgebied te calibreren en op Horizontes toe te passen, wordt de mogelijkheid onderzocht om het model te gebruiken voor voorspellingen op een ander soortgelijk stroomgebied zonder hercalibratie. Het laat zien dat op die manier goede afvoervoorspellingen van het totale stroomgebied mogelijk zijn, maar dat oppervlakte-stroming zich op deze manier niet erg nauwkeurig laat voorspellen.

In hoofdstuk 4 worden de observaties geanalyseerd met een karakteristiek ruimtelijk verdeeld oppervlakte-stromingsmodel. Het drievoudige doel van deze analyse is om te onderzoeken: 1) of het model gecalibreerd kan worden, in de zin dat een set bijna-optimale parameters kan worden bepaald die te gebruiken zijn voor modelvoorspellingen, 2) hoe de modelvoorspellingen zich verhouden tot de resultaten van de alternatieve regressiemethode uit Hoofdstuk 3; en 3) of het model de ruimtelijke heterogeniteit van oppervlakte-stroming enigzins reproduceert. Het gebruikte model verschilt in twee opzichten van de meeste andere ruimtelijk verdeelde oppervlakte-stromingsmodellen: 1) het bevat relatief weinig parameters, en 2) het betrekt ook op eenvoudige wijze de natheid van de bodem voorafgaand aan een bui in de berekening van infiltratie (via een z.g. vochtigheids index). Om het model te calibreren is een zogenaamde *"similarity in-*

dex" gedefinieerd om waarnemingen aan modelvariabelen te koppelen die wel overeenkomen qua bovenstroomsgebied, bodem- en vegetatietype maar naar een andere plaats in het stroomgebied verwijzen. Deze calibratieprocedure blijkt tamelijk goed te werken. Na modelcalibratie wordt het model gevalideerd met afvoer en oppervlakte-stromings waarnemingen. Uit deze tests blijkt dat het model inderdaad redelijk gecalibreerd is, hoewel het ruimtelijk verdeelde model zowel afvoer als oppervlakte-stroming duidelijk minder goed voorspelt dan het regressiemodel. De geobserveerde heterogeniteit van oppervlakte stroming wordt niet gereproduceerd door het model op de grid-resolutie maar wordt redelijk voorspeld op de resolutie van bodem-vegetatie eenheden. Uit de voorspellingen voor Kaibo en Horizontes kan afgeleid worden dat de stroomgebieden nogal verschillen met betrekking tot de patronen van oppervlakte-stroming. In Kaibo blijken bodem- en vegetatiefactoren tamelijk belangrijk in het bepalen van oppervlakte-stroming, terwijl het in Horizontes meer de topografische factoren zijn. Deze effecten kunnen echter niet geheel gescheiden worden omdat er een sterke correlatie bestaat tussen bodem, vegetatie en topografie. Kaibo en Horizontes hebben stroomgebiedsafvoer/regenval fracties van respectievelijk ± 0.1 en ± 0.2. Beide waarden komen overeen met de verwachtte waarden voor deze typen van terrein en klimaat. Er blijken ook sterke seizoentrends te zijn, waarin oppervlakte-stroming toeneemt naarmate het seizoen vordert. Voor Horizontes kan de trend het best verklaard worden door de scheuren in de vertische grond onder droge condities, en voor Kaibo kan een aanvullende verklaring gevonden worden in de afnemende ruwheid van het akkerland over het seizoen. In Kaibo zijn de verschillen tussen voor- en naseizoen het meest uitgesproken. Ondanks de kwalitatieve aard van de waarnemingen en modeluitkomsten zijn de seizoentrends zo duidelijk dat deze in acht moeten worden genomen bij de modellering van oppervlakte-stroming. Er zijn twee mogelijkheden om dit te bewerkstelligen: 1) door het meenemen van de relevante factoren in de parameterisatie, of 2) het parameteriseren van een model voor een kortere periode zodat de parameters wel als constant beschouwd kunnen worden. Beide mogelijkheden zijn gedeeltelijk getest in deze studie. Het onderscheid tussen bodems met vertische en niet-vertische eigenschappen parameteriseert eventuele bodem-veranderingen, en het onderscheid tussen gras versus bomen (Horizontes) of gras versus akkers (Kaibo) parameteriseert de verschillen tussen vegetatieve ontwikkeling en landgebruik. Daarnaast reproduceert de vochtigheids-index het seizoenseffect ten dele. Hercalibratie met meer specifieke datasets (voorseizoen versus naseizoen en lage regenintensiteit versus hoge intensiteit) is ook toegepast, maar leidt niet tot betere modelvoorspellingen omdat de datasets door de opsplitsing waarschijnlijk te klein zijn geworden.

In Hoofdstuk 5 wordt een raamwerk om *schaal-afhankelijke* hydrologische modellen te identificeren gepresenteerd. De methode werkt met een zogenaamd *modelsjabloon* waarmee de toestandsvariabelen, inputvariabelen, het bereik van toegestane ruimte- en tijdsresoluties, alsmede de toegestane minimale en maximale aantallen parameters worden vastgelegd. Op basis van het sjabloon zoekt een genetisch algorithme naar optimale modelstructuren die worden gecalibreerd met een Monte Carlo procedure, gebruikmakend van de waarnemingen met UBB-foutstructuren. Bijzondere eigenschappen van deze techniek zijn dat de ruimtelijke elementen van de resulterende modellen kunnen variëren in grootte en dat de modellen in wezen stochastisch van aard zijn omdat parameterverzamelingen in plaats van éénduidige parameterwaarden zijn vastgelegd. Daarnaast zijn de modellen opgebouwd uit fysisch interpreteerbare eenheden - een partitioneringsmatrix, een transportmatrix en een interne-toestandsmatrix - die gekoppeld kunnen worden aan specifieke stromingsprocessen. De identificatiemethode is toegepast op een kunstmatige dataset, die is gegenereerd met een 1D oppervlakte-stromingsmodel gekoppeld aan een 2D Richardsmodel op hellingschaal ($100m$ lengte en $1m$ diepte) en een neerslagmodel. De identificatiemethode genereert een grote set met *geschikte* modellen (*fit models*) die verschillen in parameterisatie en resolutie, waarbij geschiktheid slaat op de mate waarin de modelvoorspellingen binnen het vooraf gedefinieerde gebied van waarnemingen + UBB fouten blijft. Een analyse van de geschikste mod-

ellen leidt tot een aantal interessante inzichten. De meest geschikte modellen komen voor langs een nauwe band van ruimte-tijdsresoluties, variërend van 4 *min* met 10 eenheden tot 18 *min* met 4 eenheden. De meest geschikte modellen streven naar een structuur met ruimtelijke eenheden van gelijke grootte, vooral bij fijne resoluties. Het parameterbereik van de partitionerings- en interne-toestandsmatrices in de modellen is, vooral bij de grofste resoluties, gerelateerd aan de modelgeschiktheid (een kleiner parameter-bereik is gerelateerd aan hogere modelgeschiktheid), terwijl de transportmatrix nauwelijks een relatie te zien geeft en bovendien het leeuwendeel van de parameteronzekerheid herbergt. Voor verschillende resoluties is de hoeveelheid parameters in de meest geschikte modellen constant. De geschiktste modellen zijn kwalitatief verschillend bij verschillende resoluties met betrekking tot zowel de vorm als de onafhankelijke parameters in de kern-functies. Bodemvocht is de toestandsvariabele die de modeldynamiek het meest beinvloedt in modellen met een fijne tijdsresolutie terwijl regenval de belangrijkste drijvende kracht is in modellen die gedefinieerd zijn op grove tijdsresoluties. De sterkste punten van de methode zijn de algemene toepasbaarheid (ongeacht fout-structuur of niet-lineariteit), de mogelijkheid een grote verzameling kandidaatmodellen te evalueren, de geidentificeerde modellen fysisch te interpreteren en de rekentechische eenvoud. Zwakke punten zijn de relatief ingewikkelde modellen die kunnen ontstaan na de identificatie, de benodigde rekentijd, en - in dit specifieke geval met gegevens met UBB-fouten - de relatieve slechte fit van de modellen in vergelijking tot methoden met meer gedetailleerde aannamen over fouten. De methode is daarom vooral geschikt om een beperkte verzameling kandidaatmodellen te identificeren welke vervolgens verder geoptimaliseerd kunnen worden met meer rigide identificatietechnieken.

In Hoofdstuk 6 wordt het raamwerk van Hoofdstuk 5 toegepast op de Kaibo en Horizontes gegevens met het doel om een verzameling oppervlakte-stromingsmodellen te identificeren en de stuctuur ervan te relateren aan voorspellingsonzekerheid en modelresolutie. Het is *a priori* niet duidelijk of de identificatieprocedure wel werkt voor de beide stroomgebieden, aangezien het alleen met kunstmatige gegevens op hellingsschaal is getest. Het blijkt dat ook voor de stroomgebiedsgegevens de methode leidt tot een grote verzameling van geschikte modellen voor zowel Kaibo als Horizontes. Eerst wordt onderzocht hoe de modelverzameling effectief gebruikt kan worden voor voorspelling. Er is een keus gemaakt voor groeps-voorspellingen (*ensemble predictions*) waarbij een aantal modellen willekeurig getrokken worden uit de geïdentificeerde verzameling en de uiteindelijke voorspelling het gemiddelde is van de verschillende modelvoorspellingen. Het blijkt dat voor toenemende groeps-grootte de voorspelfout afneemt. Deze trend zet door tot een groeps-grootte van ongeveer 800 voor Kaibo en 1000 voor Horizontes. Er zijn kleine verschillen in deze relatie voor afvoer en oppervlakte-stroming. De verklaring voor deze relatie tussen groeps-grootte en voorspelfout is de relatieve heterogeniteit van de modelverzameling. Een keuze is gemaakt om met groepen van 1000 modellen te werken in de rest van de studie. De groeps-voorspellingen reproduceren de validatiegegevens van afvoer goed, met een lichte overschatting van de lage afvoeren, vooral voor Horizontes. De structuur van de voorspelfout over tijd is vergelijkbaar met die bij de calibratiegegevens. De geschiktheid van de geïdentificeerde modellen om oppervlakte-stroming te voorspellen is getoetst met validatiegegevens voor bodemvegetatie eenheden en het gehele stroomgebied. Interessant is dat de afwijking van voorspellingen en observaties niet afneemt bij een grovere resolutie zoals bij het gedistribueerde model. Een mogelijke verklaring hiervoor is dat modellen bij verschillende resoluties wel een gelijk aantal parameters hebben, wat uiteindelijk leidt tot een gelijke voorspelfout. Door het rechttoe-rechtaan toepassen van ensemble voorspelling hebben modellen met zowel grove als fijne resoluties met een zelfde geschikheid dezelfde kans geselecteerd te worden. Deze verklaring impliceert dat het gebruik van fijne-resolutie modellen voor voorspellingen op fijne schaal en grove resoluties voor voorspellingen bij grove schaal tot betere resultaten leidt. Een test bevestigt dit. Ondanks de duidelijke verschillen tussen Kaibo en Horizontes, zijn er veel overeenkomsten tussen de mod-

elverzamelingen die de stroomgebieden beschrijven: 1) het zelfde modelsjabloon kan worden gebruikt voor beide stoomgebieden, 2) de relatie tussen resolutie, de beschikbaarheid van gegevens en de model geschiktheid is toepasbaar op beide stroomgebieden, en 3) de verschuiving in onafhankelijke variabelen van bodemvocht bij fijne resoluties naar regen bij grove resoluties treedt op in zowel Kaibo als Horizontes. De stroomgebieden verschillen met betrekking tot de exacte vorm van de kern-functies en de resoluties waarop de kern-functies van toepassing zijn. Dit kan worden verklaard door de topografie - Kaibo heeft langere hellingen en minder relief - en de beperkte ruimtelijke discretisatie van de modellen voor Kaibo. Dit laatste kan zijn veroorzaakt door de weinige ruimtelijk verdeelde waarnemingen in Kaibo. Het is opmerkelijk dat dezelfde veranderingen in onafhankelijke variabelen van de kern-functies optreden bij de echte dataset op stroomgebiedschaal als bij de kunstmatige dataset op hellingschaal (in Hoofdstuk 5). Het suggereert dat het bron-gedreven systeemgedrag bij grove resoluties en het bestemming-gedreven bij fijne resoluties een eigenschap van het hydrologische systeem op beide schalen is. Modelvormen kunnen worden geanalyseerd over een bereik van ruimte-tijdsresoluties om veranderingen in kern-functies aan te gegeven. Bij vergelijking van de locatie van deze verandering in kern-functies voor Horizontes en Kaibo blijkt dat de verschuiving van bron-gedreven naar bestemming-gedreven systeemgedrag optreedt bij resoluties van 7 eenheden bij Horizontes en 5 eenheden bij Kaibo. Deze resoluties komen overeen met gemiddelde fysische dimensies van $300\,m$ in Horizontes en $220\,m$ in Kaibo. Als deze dimensies gerelateerd worden aan de ruimtelijke correlatiestructuur van regen-, bodem- en vegetatiekarakteristieken blijkt dat vooral regen (met autocorrelaties die scherp afnemen bij 300 en $200\,m$) tot dit patroon kan leiden. De ruimtelijke heterogeniteit van zowel bodem als vegetatiekarakteristieken is bijna twee maal zo hoog. Deze vaststelling leidt tot de hypothese dat in de twee studiegebieden de structuur van regenbuien de belangrijkste bepalende factor is voor oppervlakte-stromingspatronen op stroomgebiedschaal, in plaats van topografie of de natheid van de bodem voorafgaand aan een bui. Toepassing van de identificatiemethode op verschillende deel-verzamelingen van de waarnemingen, leidt tot interessante resultaten. Allereerst toont het aan dat regenintensiteit de parameterisatie niet beinvloedt, terwijl seizoensinvloeden (de tijd verstreken na het begin van het natte seizoen) dat wel doen. Dit betekent dat de aard van het hydrologische ssyteem verandert over het regenseizoen. Zoals eerder verklaard, wordt deze verandering veroorzaakt door verschillende sterk gecorreleerde processen: het zwellen en krimpen van kleigrond, vegetatieve ontwikkeling, bodemruwheidsveranderingen (onder invloed van regen, dieren en grondbewerking) en biologische activiteit in de bodem. Een aanzienlijke heterogeniteit binnen de modelverzameling op basis van de gemiddelde seizoencondities kan worden verklaard door verschuivingen in deze factoren. Desondanks kan door de beperkte grootte van de set waarnemingen de modelverzameling niet opnieuw geparameteriseerd worden met de seizoensfactoren. Voor beide stroomgebieden kunnen de kern-functies voor partitionering beschreven worden door een rechthoekige-hyperbool en de kern-functies voor transport met gamma-verdelingen. De functies kunnen probablistisch worden geinterpreteerd, wat leidt tot waarneming-gebaseerde voorwaardelijke en gecombineerde kansdichtheden van hydrologische variabelen. De toepasbaarheid van deze verdelingen voor praktische doeleinden moet nog getoetst worden.

In Hoofdstuk 7 wordt het probleem bestudeerd van de voorspelling van oppervlakte-stroming wanneer zowel modelinvoer als waarnemingen van toestandsvariabelen beschikbaar zijn in combinatie met een gecalibreerde modelverzameling. De techniek die hier wordt gebruikt om *a priori* modeluitkomsten met waarnemingen zo te combineren, dat verbeterde posteriori modelresultaten worden verkregen, staat bekend als Tikhonov regularisatie. Binnen dit regularisatie-raamwerk wordt algemene-kruisvalidatie *(generalized cross-validation*) gebruikt om de gewenste weging tussen modelvoorpsellingen en waarnemingen te vinden. Twee regularisatiestrategiën worden vergeleken: regularisatie van de modelparameters en regularisatie van de modeltoestandsvariabelen. Er wordt aangetoond dat beide technieken tot gelijkaardige resultaten leiden die in enkele

details verschillen. Parameter-regularisatie leidt tot betere resultaten bij de beschikbaarheid van weinig gegevens, terwijl toestand-regularisatie tot betere resultaten leidt bij de beschikbaarheid van veel gegevens. Dit is in overeenstemming met het feit dat er minder toestanden zijn dan parameters om te schatten. Het feit dat de beste voorspellingen door toestand-regularisatie bij fijnere resoluties optreden dan door parameter-regularisatie kan worden verklaard door te beschouwen dat parameter-regularisatie de relatieve structuur van de kern-functies handhaaft tussen de verschillende ruimtelijke eenheden, waardoor het de extra vrijheidsgraden bij een fijnere resolutie niet kan benutten. Het relatieve voordeel van deze flexibiliteiet wordt duidelijk bij grote beschikbaarheid van waarnemingen en fijnere resoluties. Een vergelijking van de *"open-loop"* voorspellingen over de calibratieperiode zelf met de geregulariseerde voorspellingen laat zien dat zelfs de best mogelijke calibratie de resultaten van de geregulariseerde voorspelling niet benadert. Door dit resultaat is het overbodig hercalibratie als een alternatief voor regularisatie te bestuderen. De hier toegepaste regularisatietechniek kan relatief eenvoudig worden aangepast aan verschillende modellen of waarnemingen. Dit punt is gedemonstreerd in deze studie door gebruik te maken van een verzameling modellen in plaats van een enkel model. Het gemak waarmee regularisatie in het Kalman filter en de Kalman smoother kan worden toegepast in combinatie met het succes van de Ensemble Kalman filter voor problemen van realistische grootte, suggereert dat de toepassing van regularisatie in het Ensemble Kalman filter ook nuttig kan zijn.

Hoofdstuk 8 besluit de dissertatie door het combineren van enkele gegevens die eerder zijn gepresenteerd met aanvullende informatie over de relatieve waarde van observaties. Voor het regressie model, het gedistribueerde model en de schaal-afhankelijke modellen wordt eerst bekeken wat de effectiviteit voor identificatie en voorspelling is. De conclusie luidt dat de schaal-afhankelijke modellen duidelijke voordelen hebben in de modelidentificatie stap, terwijl voor voorspelling de verschillen tussen de modellen minder duidelijk zijn. Door voorspellingen te vergelijken bij weglating van een observatietype (bijvoorbeeld de waarnemingen van stroomgebiedsafvoer of oppervlakte-stroming) tijdens model-calibratie, wordt de relatieve waarde van de waarnemingen vastgesteld. Het blijkt dat het effect van het weglaten van bijna ieder type waarneming tot veranderingen in de voorspellingsfouten leidt die groter zijn dan de verschillen in voorspellingsfout tussen de modellen onderling. De conlusie op basis hiervan is dat modelverschillen relatief onbelangrijk zijn, en dat de nadruk voor dit type onderzoek in elk geval op gegevensverzameling en analyse moet liggen. Helaas leiden deze conclusies niet tot een verbetering in het voorspellen van oppervlakte-stroming omdat de vereiste waarnemingstechnieken nu en in de nabije toekomst niet beschikbaar zijn voor grootschalige toepassing. Daarom concentreert de beschouwing voor verder onderzoek zich vooral op theoretische vragen zoals de mogelijkheid om de schaal-afhankelijke modellen in meer detail te onderzoeken, om probablistische modellen te ontwikkelen op basis van de schaal-afhankelijke modellen, en de schaal-afhankelijke modellen opnieuw te vergelijken met zowel een ruimtelijk verdeeld model als experimenten op laboratorium-schaal.

Bibliography

Abbott, M. B., Bathurst, J. C., Cunge, J. A., O'Connell, P. E. and Rasmussen, J. (1986) An introduction to the European Hydrological System — Système Hydrologique Européen, "SHE", 1: History and philosophy of a physically-based, distributed modelling system. *J. Hydrol.*, **87**, 45–59.

Abrahams, A., Parsons, A. and Luk, S. H. (1986) Field measurement of the velocity of overland flow using dye tracing. *Earth Surface Processes and Landforms*, **11**, 653–657.

Abrahams, A. D., Parsons, A. J. and Luk, S. H. (1989) Distribution of depth of overland flow on desert hillslopes and its implications for modelling soil erosion. *J. Hydrol.*, **106**, 177–184.

Aitken, A. (1973) Assessing systematic errors in rainfall-runoff models. *J. Hydrol.*, **20**, 121–136.

Albergel, J. (1987) *Genèse et prédétermination des crues au Burkina Faso. Du m^2 au km^2, étude des paramètres hydrologiques et de leur évolution.* Ph.D. thesis, Université Paris VI.

Albergel, J., Chevallier, P. and Lortic, B. (1987) D'Oursi à gagara: Tranposition d'un modèle de ruissellement dans le Sahel (Burkina Faso). *Hydrol. continentale*, **2**, 77–86.

Albergel, J., Ribstein, P. and Valentin, C. (1986) L'infiltration, quels facteurs explicatifs? Analyses sur 48 parcelles du Burkina Faso. In *Journées hydrologiques de l'ORSTOM á Montpellier 17-18 Septembre 1985*, 26–48. ORSTOM.

Arnold, J. G. and Allen, P. M. (1992) A comprehensive surface-groundwater flow model. *J. Hydrol.*, **142**, 47–69.

Autorité des Aménagement de vallees des Volta (1979) Etude hydrogeologique du secteur Manga Kaibo. *Tech. rep.*, Laboratoire Central de Hydraulique de France, Ouagadougou, Burkina Faso.

Backus, G. and Gilbert, F. (1968) The resolving power of gross earth data. *Geophys. J. R. Astr. Soc.*, **16**, 169–205.

Beck, M. (1987) Water quality modeling: A review of the analysis of uncertainty. *Wat. Resour. Res.*, 1393–1442.

Beck, M., Jakeman, A. and McAleer, M. (1995) Construction and evaluation of models of environmental systems. In *Modelling Change in Environmental Systems* (eds. A. Jakeman, M. Beck and M. McAleer), chap. 1. John Wiley & Sons.

Bellman, R. and Åström, K. J. (1970) On structural identifiability. *Mathematical Biosciences*, **7**, 329–339.

Bennett, A. F. (1992) *Inverse Methods in Physical Oceanography*. Cambridge University Press.

Beven, K. (1984) Infiltration into a class of vertically non-uniform soils. *Hydrological Sciences Journal*, **29**, 425–434.

— (1985) Distributed models. In *Hydrological Forecasting* (eds. M. G. Anderson and T. P. Burt), 405–435. John Wiley & Sons.

— (1989) Changing ideas in hydrology — the case of physically-based modelling. *J. Hydrol.*, **105**, 157–172.

— (1991) Infiltration, soil moisture, and unsaturated flow. In *Recent Advances in the Modeling of Hydrologic Systems* (eds. D. S. Bowles and P. E. O'Connell), chap. 7. the Netherlands: Kluwer Academic Publishers.

— (1995) Linking parameters across scales: Subgrid parameterizations and scale dependent hydrological models. *Hydrol. Proc.*, **9**, 507–525.

— (1996) A discussion of distributed hydrological modelling. In *Distributed Hydrological Modelling* (eds. M. B. Abbott and J. C. Refsgaard), chap. 13A, 255–278. Kluwer Academic Publishers.

— (2001) On modelling as collective intelligence. *Hydrol. Proc.*, **15**, 2205–2207.

Beven, K. and Binley, A. (1992) The future of distributed models: Model calibration and uncertainty prediction. *Hydrol. Proc.*, **6**, 279–298.

Beven, K. and Wood, E. F. (1993) Flow routing and the hydrological response of channel networks. In *Channel Network Hydrology* (eds. K. Beven and M. J. Kirkby), 99–128. John Wiley & Sons.

Beven, K. J. (1993) Estimating transport parameters at the grid scale: on the value of a single measurement. *J. Hydrol.*, **143**, 109–123.

Beven, K. J. (ed.) (1997) *Distributed Hydrological Modelling: Applications of the TOPMODEL Concept.* Advances in Hyrological Processes. Chichester: John Wiley & Sons.

Beven, K. J. and Kirkby, M. J. (1979) A physically based variable contributing area model of basin hydrology. *Hydrol. Sci. Bull.*, **24**, 43–69.

Beven, K. J., Wood, E. F. and Sivapalan, M. (1988) On hydrologic heterogeneity - catchment morphology and catchment response. *J. Hydrol.*, **100**, 353–375.

Binley, A. and Beven, K. (1992) Three-dimensional modelling of hillslope hydrology. *Hydrol. Proc.*, **6**, 347–359.

Blöschl, G. and Sivapalan, M. (1995) Scale issues in hydrological modelling: a review. *Hydrol. Proc.*, **9**, 251–290.

Boerrigter, E. (1999) *Relating gully properties to a digital elevation model generated with GPS-measurements.* Master's thesis, Wageningen Agricultural University.

Boutayeb, M., Rafaralahy, H. and Darouach, M. (1997) Convergence analysis of the extended Kalman filter used as an observer for nonlinear deterministic discrete-time systems. *IEEE Transactions on Automatic Control*, **42**, 581–586.

Bras, R. and Rodriguez-Iturbe, I. (1976) Rainfall generation: A non-stationary time-varying multidimensional model. *Wat. Resour. Res.*, **12**, 450–456.

Bras, R. L. and Rodriguez-Iturbe, I. (1984) *Random Functions and Hydrology*. Addison-Wesley Publishing Company.

Bronstert, A. and Palte, E. J. (1997) Modeling of runoff generation and soil moisture dynamics for hillslopes and micro-catchments. *J. Hydrol.*, **198**, 177–195.

Brooks, R. and Corey, A. (1966) Properties of porous media affecting fluid flow. *J. Irrig. Drain. Div Am. Soc. Civil Eng.*, **92**, 61–88.

Brouwer, J. and Bouma, J. (1997) *Soil and crop growth variability in the Sahel: highlights of research (1990-95) at ICRISAT Sahelian Center*. Information bulletin no. 49. Andhra Pradesh, India: ICRISAT.

Burt, T. P. and Butcher, D. P. (1986) Development of topographic indices for use in semi-distributed hillslope runoff models. *Z. Geomorph. N.F. Suppl.-Bd.*, **58**, 1–19.

Castillo Muñoz, R. (1991) Geología de Costa Rica. In *Historia natural de Costa Rica* (ed. D. H. Janzen), 47–61. San José, Costa Rica: Universidad de Costa Rica.

Ciach, G. J. and Krajewski, W. F. (1999) On the estimation off radar rainfall error variance. *Adv. Water Resour.*, **22**, 585–595.

Clapp, R. B. and Hornberger, G. M. (1978) Empirical equations for some soil hydraulic properties. *Wat. Resour. Res.*, **14**, 601–604.

Clarke, R. (1973) A review of some mathematical models used in hydrology, with observations on their calibration and use. *J. Hydrol.*, **19**, 1–20.

Costa-Cabral, M. C. and Burges, S. J. (1994) Digital elevation model networks (DEMON): A model of flow over hillslopes for computation of contributing and dispersal areas. *Wat. Resour. Res.*, **30**, 1681–1692.

Crawford, N. and Linsley, R. (1966) Digital Simulation in Hydrology: Stanford Watershed Model IV. *Tech. Rep. 39*, Stanford Univ., Dept. of Civil Engineering.

Daley, R. (1991) *Atmospheric Data Analysis.* Cambridge University Press.

Dawdy, D. and O'Donnell, T. (1965) Mathematical models of catchment behaviour. *J. Hydraul. Div., ASCE.*, **91**, 123–137.

Dekker, L. (1996) *Soil Map Kaibo-V5 Zoundwéogo Burkina Faso, scale 1:10.000.* Master's thesis, Wageningen Agricultural University.

Dingman, S. (1994) *Physical Hydrology*. Englewood Cliffs, N.J.: Prentice-Hall.

Doblas-Reyes, F. J., Déqué, M. and Piedelievre, J.-P. (2000) Multi-model spread and probablistic forecasts in provost. *Q.J.R. Meteorol. Soc.*, **126**, 2069–2087.

Dooge, J. (1973) *Linear theory of hydrologic systems.* Technical bulletin/USDA no. 1468. Washington: USDA.

Duan, Q., Sorooshian, S. and Gupta, V. K. (1992) Effective and efficient global optimization for conceptual rainfall-runoff models. *Wat. Resour. Res.*, **28**, 1015–1031.

Dunne, T. and Black, R. (1970) Partial area contributions to storm runoff in a small New England watershed. *Wat. Resour. Res.*, **6**, 1296–1311.

Dunne, T., Moore, T. R. and Taylor, C. H. (1975) Recognition and prediction of runoff-producing zones in humid regions. *Hydrol. Sci. J.*, **20**, 305–327.

Edelman, M. (1992) *The Logic of Latifundio. The Large States of Northwestern Costa Rica Since the Late XIX Century.* Stanford, California: Stanford University Press.

Emmett, W. W. (1970) The hydraulics of overland flow on hillslopes. *Geological Survey Professional Paper 662-a,* U.S. Dept. of the Interior.

Entekhabi, D. and Eagleson, P. (1989) Land surface hydrology parameterization for atmospheric general circulation models including subgrid scale spatial variability. *Journal of Climate*, **2**, 816–831.

Evensen, G. (1992) Using the extended Kalman filter with a multilayer quasi-geostrophic ocean model. *J. Geophys. Res.*, **97**, 17,905–17,924.

Evensen, G. and van Leeuwen, P. J. (1996) Assimilation of Geosat altimeter data for the Agulhas current using the ensemble Kalman filter with a quasi-geostrophic model. *Monthly Weather Review*, **124**, 85–96.

FAO (1990) *Guidelines for Soil Description.* Rome/Wageningen: FAO/ISRIC.

Fedra, K. (1983) Environmental modeling under uncertainty: Monte carlo simulation. *Tech. Rep. RR-83-28,* International Institute for Applied Systems Analysis (IIASA), Laxenburg, Austria.

Flanagan, D. and Nearing, M. A. (1995) USDA-water erosion prediction project (WEPP). *Tech. Rep. 10*, NSERL, West Lafayette.

Freeman, T. G. (1991) Calculating catchment area with divergent flow based on a regular grid. *Comp. & Geosc.*, **17**, 413–422.

Freeze, R. (1980) A stochastic conceptual analysis of rainfall-runoff processes on a hillslope. *Wat. Resour. Res.*, **16**, 391–408.

Freeze, R. A. and Harlan, R. (1969) Blueprint for a physically-based digitally-simulated hydrologic response model. *J. Hydrol.*, **9**, 237–258.

Gan, T. Y. and Burges, S. J. (1990) An assessment of a conceptual rainfall-runoff model's ability to represent the dynamics of small hypothetical catchments. 1. Models, model properties, and experimental design. *Wat. Resour. Res.*, **26**, 1595–1604.

Gan, T. Y., Dlamini, E. M. and Bifu, G. F. (1997) Effects of model complexity and structure, data quality, and objective functions on hydrologic modeling. *J. Hydrol.*, **192**, 81–103.

Geelhoed, R. (1994) *Les pertes de nutriments dans le ruisellement et le sédiment et l'importance relative d'entraînement.* Master's thesis, Wageningen Agricultural University.

van Genuchten, M. T. (1980) A closed-form equation for predicting the hydraulic conductivity of unsaturated soils. *Soil Sci. Soc. Am. J.*, **44**, 892–898.

Golub, G. H., Heath, M. T. and Wahba, G. (1979) Generalized cross-validation as a method for choosing a good ridge parameter. *Technometrics*, **21**, 215–223.

Grayson, R. B., Moore, I. D. and McMahon, T. A. (1992a) Physically based hydrologic modeling. 1. A terrain-based model for investigative purposes. *Wat. Resour. Res.*, **28**, 2639–2658.

— (1992b) Physically based hydrologic modeling. 2. Is the concept realistic? *Wat. Resour. Res.*, **28**, 2659–2666.

Green, I. R. A. and Stephenson, D. (1986) Criteria for comparison of single event models. *Hydrological Sciences*, **31**, 395–411.

Groot, S. (1996) *Caractérisation Du Terrain Au Moyen Des Transects: Nombre Minimal et Les Endroits Les Plus Qualifiées. Un Test Dans un Petit Bassin Versant Au Burkina Faso.* Master's thesis, Wageningen Agricultural University.

Gupta, H., Sorooshian, S. and Yapo, P. (1998) Toward improved calibration of hydrologic models: multiple and noncommenurable measures of information. *Wat. Resour. Res.*, **34**, 751–763.

Hansen, P. C. (1992) Analysis of discrete ill-posed problems by means of the l-curve. *SIAM Review*, **34**, 561–580.

— (1998) *Rank-Deficient and Discrete Ill-Posed Problems: Numerical Aspects of Linear Inversion.* Philadelphia: SIAM.

Hekman, A. and Wierikx, R. (1998) *Waar blijft het water? Hydrogeologische systeembeschrijving van het stroomgebied Kaibo Sud V5, Burkina Faso.* Master's thesis, Wageningen Agricultural University. (in dutch).

Henderson, F. and Wooding, R. (1964) Overland and groundwater flow from a steady rainfall of finite duration. *Journal of Geophysical Research*, **69**, 1531–1540.

Hendrickson, J., Sorooshian, S. and Brazil, L. E. (1988) Comparison of Newton-type and direct search algorithms for calibration of conceptual rainfall-runoff models. *Wat. Resour. Res.*, **24**, 691–700.

Hillenaar, S. I. (1995) *Infiltration characteristics of some selected sites in Zoundweogo, Burkina Faso.* Master's thesis, Wageningen Agricultural University.

Hogg, S. E. (1982) Sheetflood, sheetwash, or ...? *Earth-Sciences Reviews*, **18**, 59–76.

Holland, J. (1975) *Adaptation in Natural and Artificial Systems.* Univ. of Michigan Press, Minneapolis, MI.

Hoogmoed, W. B. and Stroosnijder, L. (1984) Crust formation on sandy soils in the sahel. I. Rainfall and infiltration. *Soil & Tillage Research*, **4**, 5–23.

Hornberger, G., Beven, K., Cosby, B. and Sappington, D. (1985) Shenandoah watershed study: Calibration of a topography-based, variable contributing area hydrological model to a small forested catchment. *Wat. Resour. Res.*, **21**, 1841–1850.

Hornberger, G. and Boyer, E. (1995) Recent advances in watershed modelling. In *U.S. National Report to the IUGG, 1991-1994, Contributions in Hydrology. Rev. Geophys. Vol. 33 Suppl.* Washington: AGU.

Hoskings, J. R. M. and Clarke, R. T. (1990) Rainfall-runoff relations derived from the probability theory of storage. *Wat. Resour. Res.*, **26**, 1455–1463.

Houtekamer, P. L. and Derome, J. (1994) Methods for enseble prediction. *Monthly Weather Review*, **123**, 2181–2196.

Houtekamer, P. L. and Lefaivre, L. (1997) Using ensemble forecasts for model validation. *Monthly Weather Review*, **125**, 2416–2426.

Houtekamer, P. L. and Mitchell, H. L. (1997) Data assimilation using an ensemble Kalman filter technique. *Monthly Weather Review*, **126**, 796–811.

Jackson, D. (1972) Interpretation of inaccurate, insufficient and inconsistent data. *Geophys. J. R. Astr. Soc*, **28**, 97–109.

Jakeman, A. J. and Hornberger, G. M. (1993) How much complexity is warrented in a rainfall-runoff model? *Wat. Resour. Res.*, **29**, 2637–2649.

Jakeman, A. J., Post, D. and Beck, M. B. (1994) From data and theory to environmental model: The case of rainfall runoff. *Environmetrics*, **5**, 297–314.

Janzen, D. H. (ed.) (1991) *Historia Natural de Costa Rica*. San José, Costa Rica: Universidad de Costa Rica.

Jaynes, E. T. (1963) Information theory and statistical mechanics. In *Statistical Physics* (ed. K. Ford), 181–219. New York, USA: W. A. Benjamin.

— (1982) On the rationale of maximum-entropy methods. *Proc. IEEE*, **9**, 939–952.

Jenson, S. and Domingue, J. (1988) Extracting Topographic Features from Digital Elevation Data for Geographic Information System Analysis. *Photogrammetric Engineering and Remote Sensing*, **54**, 1593–1600.

Johnston, P. R. and Pilgrim, D. H. (1976) Parameter optimization for watershed models. *Wat. Resour. Res.*, **12**, 477–486.

Jolánkai, G. and Rast, W. (1999) The hydrologic cycle and factors affecting the generation, transport and transformation of nonpoint source pollutants. In *Assessment and control of nonpoint source pollution of aquatic ecosystems: a practical approach*. Unesco and The Parthenon Publishing Group, USA.

Julien, P. Y. and Moglen, G. E. (1990) Similarity and length scale for spatially varied overland flow. *Wat. Resour. Res.*, **26**, 1819–1832.

Keesman, K. J. (1989) *A Set-Membership Approach to the Identification and Prediction of Ill-defined Systems: Application to a Water Quality System*. Ph.D. thesis, University of Twente, Netherlands.

Keesman, K. J. and van Straten, G. (1990) Set membership approach to identification and prediction of lake eutrophication. *Wat. Resour. Res.*, **26**, 2643–2652.

Kiepe, P. (1995) *No Runoff, No Soil Loss: Soil and Water Conservation in Hedgerow Barrier Systems*. Ph.D. thesis, Wageningen Agricultural University.

Kim, C., Stricker, J. and Torfs, P. (1996) An analytical framework for the water budget of the unsaturated zone. *Wat. Resour. Res.*, **32**, 3475–3484.

Kim, R. (1995) *The Water Budget of Heterogeneous Areas. Impact of Soil and Rainfall Variability*. Ph.D. thesis, Wageningen Agricultural University.

Klemeš, V. (1983) Conceptualization and scale in hydrology. *J. Hydrol.*, **65**, 1–23.

— (1986) Dilettantism in hydrology: Transition or destiny? *Wat. Resour. Res.*, **22**, 177s–188s.

Koblinsky, C. J., Clarke, R. T., Brenner, A. C. and Frey, H. (1993) Measurement of river level variations with satellite altimetry. *Wat. Resour. Res.*, **29**, 1839–1848.

Krishnamurti, T. N., Kishtawal, C. M., LaRow, T. E., Bachionchi, D. R., Zhang, Z., Willifor, C. E., Gadgil, S. and Surendran, S. (1999) Improved weather and seasonal climate forecasts from multimodel superensemble. *Science*, **285**, 1548–1550.

Lane, L., Hernandez, M. and Nichols, M. (1997) Processes controlling sediment yield from watersheds as functions of spatial scale. *Environmental Modelling and Software*, **12**, 355–369.

de Lima, J. L. M. P. (1989) *Overland Flow Under Rainfall: Some Aspects Related to Modelling and Conditioning Factors*. Ph.D. thesis, Wageningen Agricultural University.

Ljung, L. (1987) *System Identification: Theory for the User*. Englewood Cliffs, N.J.: Prentice Hall.

Loague, K. (1990) R-5 revisited. 2. Reevaluation of a quasi-physically based rainfall-runoff model with supplemental information. *Wat. Resour. Res.*, **26**, 973–987.

Loague, K. and Gander, G. A. (1990) R-5 revisited. 1. Spatial variability of infiltration on a small rangeland catchment. *Wat. Resour. Res.*, **26**, 957–971.

Loague, K. M. and Freeze, R. A. (1985) A comparison of rainfall-runoff modeling techniques on small upland catchments. *Wat. Resour. Res.*, **21**, 229–248.

van Loon, E. E. and Keesman, K. J. (2001) Measurement optimization for model identification. *submitted to Water Resour. Res.*

van Loon, E. E. and Troch, P. A. (2002) Soil moisture data assimilation with a distributed hydrological model: a case study. *Hydrol. Proc., in press.*

Mando, A., L.Stroosnijder and Brussaard, L. (1996) Effects of termites on infiltration on crusted soil. *Geoderma*, **74**, 107–113.

Martz, L. W. and Garbrecht, J. (1992) Numerical definition of drainage network and subcatchment areas from ditital elevation models. *Comp. & Geosc.*, **18**, 747–761.

Massonnet, D. and Rabaute, T. (1993) Radar interferometery: Limits and potential. *IEEE Transactions on Geoscience and Remote Sensing*, **31**, 445–464.

McLaughlin, D. (1995) Recent developments in hydrologic data assimilation. In *U.S. National Report to the IUGG, 1991-1994, Contributions in Hydrology. Rev. Geophys. Vol. 33 Suppl.*, 977–984. Washington: AGU.

Menke, W. (1989) *Geophysical Data Analysis: Discrete Inverse Theory*, vol. 45 of *International Geophysiscs Series*. Academic Press, rev. edn.

Meyer, T., Richards, F. and Packard, N. (1989) Learning algorithm for modeling complex spatial dynamics. *Phys. Rev. Lett.*, **63**, 1735–1738.

Milly, P. C. D. (1993) An analytic solution of the stochastic storage problem applicable to soil water. *Wat. Resour. Res.*, **29**, 3755–3758.

Mitchell, M. (1996) *An Introduction to Genetic Algorithms*. MIT Press.

Molina, M. A. (1994) Propuesta: Consolidación Geográfica del Area de Conservación Guanacaste, y Desarrollo de la Estación Experimental Forestal Horizontes. *Tech. rep.*, MIRENEM, ACG, Liberia, Costa Rica.

Moore, I. D. and Foster, G. R. (1990) Hydraulics and overland flow. In *Process Studies in Hillslope Hydrology* (eds. M. Anderson and T. Burt), chap. 7, 215–254. John Wiley & Sons.

Moore, I. D., Grayson, R. B. and Ladson, A. R. (1991) Digital terrain modelling: A review of hydrological, geomorphological and biological applications. *Hydrol. Proc.*, **5**, 3–30.

Moore, R. and Clarke, R. (1981) A distribution function approach to rainfall runoff modeling. *Wat. Resour. Res.*, **17**, 1367–1382.

Morel-Seytoux, J. (ed.) (1989) *Unsaturated Flow in Hydrologic Modelling*, vol. 275 of *NATO ASI Series C*. Reidel.

Mulders, M. (1996) Soil and land use of the Kaïbo area at medium scale. *Document de project 39*, Antenne Sahélienne de l'Université Agronomique Wageningen Pays-Bas et de l'Université de Ouagaougou Burkina Faso.

Mulders, M. and Zerbo, L. (1997) Explications additives du rapport de Kaïbo Sud V5. *Document de project 42*, Antenne Sahélienne de l'Université Agronomique Wageningen Pays-Bas et de l'Université de Ouagadougou Burkina Faso.

Nash, J. E. and Sutcliffe, J. V. (1970) River flow forecasting through conceptual models part I A discussion of principles. *J. Hydrol.*, **10**, 282–290.

National Research Council (NRC) (1991) *Opportunities in the Hydrologic Sciences.* National Academy Press.

Norton, J. (1986) *An Introduction to Identification.* London: Academic Press.

O'Callaghan, J. F. and Mark, D. M. (1984) The extraction of drainage networks from digital elevation data. *Computer Vision, Graphics and Image Processing*, **28**, 323–344.

O'Connell, P. E. (1991) A historical perspective. In *Recent Advances in the Modeling of Hydrologic Systems. Proceedings of the NATO Advanced Study Institute* (eds. P. E. O'Connell and D. S. Bowles). Kluwer Academic Publishers.

Oficina de hydrologia operativa (1994) Boletin hidrologico. *Tech. Rep. 21*, Instituto Costarricense de Electricidad.

Parsons, A. J. and Abrahams, A. D. (eds.) (1992) *Overland Flow: Hydraulics and Erosion Mechanics.* Chapman & Hall.

Pickup, G. (1977) Testing the efficiencies of algirithms and strategies for automatic calibration of rainfall-runoff models. *Hydrol. Sci. Bull.*, **22**, 257–274.

Pierre, B. (1982) Mapa Geomorfológico del Pacífico Norte de Costa Rica. *Tech. rep.*, Universidad de Costa Rica, Instituto Geografico Nacional, San José, Costa Rica.

Press, W. H., Teukolsky, S. A., Vetterling, W. T. and Flannery, B. P. (1992) *Numerical Recipes in C: The Art of Scientific Computing.* Cambridge University Press, 2nd edn.

Price, W. L. (1979) A controlled random search procedure for global optimisation. *The Computer Journal*, **20**, 367–370.

Proyecto Geotermico de Guanacaste (1976) Informe de Previabilidad Tecnica. Anexo E - Geohidrologia. *Tech. rep.*, Instituto Costarricense de Electricidad.

Quinn, P., Beven, K., Chevallier, P. and Planchon, O. (1991) The prediction of hillslope flow paths for distributed hydrological modelling using digital terrain models. *Hydrol. Proc.*, **5**, 59–79.

Raaphorst, S. (1995) *Digital Surface Modelling and Data Integration in a GIS Using the Global Positioning System.* Master's thesis, Wageningen Agricultural University.

Ramos, J., Mallants, D. and Feyen, J. (1995) State space identification of linear deterministic rainfall-runoff models. *Wat. Resour. Res.*, **31**, 1519–1531.

Rao, C. R. and Mitra, S. K. (1971) *Generalized Inverse of Matrices and its Applications.* John Wiley & Sons.

Refsgaard, J. C., Storm, B. and Abbot, M. B. (1996) Comment on 'a discussion of distributed hydrological modelling' by k. beven. In *Distributed Hydrological Modelling* (eds. M. B. Abbott and J. C. Refsgaard), chap. 13B, 279–287. Kluwer Academic Publishers.

Reggiani, P., Hassanizadeh, M. and Sivapalan, M. (1999) A unifying framework for watershed thermodynamics: constitutive relationships. *Adv. Water Resour.*, **23**, 15–39.

Reggiani, P., Sivapalan, M. and Hassanizadeh, M. (1998) A unifying framework for watershed thermodynamics: balance equations for mass, momentum, energy and entropy and the second law of thermodynamics. *Adv. Water Resour.*, **22**, 367–398.

Reggiani, P., Sivapalan, M. and Hassanizadeh, S. M. (2000) Conservation equations governing hillslope responses: Exploring the physical basis of water balance. *Wat. Resour. Res.*, **37**, 1845–1863.

Reif, K., Sonnemann, F. and Unbehauen, R. (1998) An EKF-Based nonlinear observer with a prescribed degree of stability. *Automatica*, **34**, 1119–1123.

Rering, G. (1997) *Evaluation of the Integrated Transect Method as a Tool for Land Use Characterization in West Africa.* Master's thesis, Wageningen Agricultural University.

Richards, F. C., Meyer, T. P. and Packard, N. H. (1990) Extracting cellular automaton rules directly from experimental data. *Physica D*, **45**, 189–202.

Richards, L. A. (1931) Capillary conduction of liquids through porous mediums. *Physics*, **1**, 318–333.

Robson, A. J., Whitehead, P. G. and Johnson, R. C. (1993) An application of a physically based semi-distributed model to the Balquhidder catchments. *J. Hydrol.*, **145**, 357–370.

Rodier, J. (1982) *Evaluation of Annual Runoff in Tropical African Sahel.* Travaux et documents de l'Orstom No. 145. Paris: ORSTOM. Translated from french by A.Eeles.

Rodier, J. and Auvray, C. (1965) *Estimation des Debits de Crues Decennales pour les Bassins Versants de Superficie Inferieure a 200 km^2 en Afrique Occidentale.* Paris: ORSTOM, Comité Interafricain d'études Hydrauliques.

Rodriguez-Iturbe, I., D'Odorico, P. and adn L. Ridolfi, A. P. (1999) Tree-grass coexistence in savannas: The role of spatial dynamics and climate fluctuations. *Geophysical Research Letters*, **26**, 247.

Scoging, H. (1992a) Application of a dynamic overland flow hydraulic model to a semi arid hillslope, walnut gulch, arizona. In *Overland Flow: Hydraulics and Erosion Mechanics* (eds. A. Parsons and A. D. Abrahams), chap. 6, 105–145. London: UCL Press.

— (1992b) Modelling overland-flow hydrology for dynamic hydraulics. In *Overland Flow: Hydraulics and Erosion Mechanics* (eds. A. Parsons and A. D. Abrahams), chap. 5, 89–103. London: UCL Press.

Šimůnek, J., Vogel, T. and van Genuchten, M. T. (1994) The SWMD-2D code for simulating water flow and solute transport in two-dimensional variably saturated media. version 1.2. *Research Report 132*, U.S. Salinity Laboratory, USDA Riverside, California.

Singh, V. (ed.) (1995) *Computer models of watershed hydrology*. Highlands Ranch, CO: Water Resources Publications.

Sivakumar, M. and Gnoumou, F. (1987) *Agroclimatolgie de l'Afrique de l'Ouest: Le Burkina Faso*. No. 23 in Bulletin d'Information. Niamey, Niger: ICRISAT.

Sivakumar, M., Wallace, M., Renard, J. and Giroux, C. (eds.) (1991) *Soil Water Balance in the Sudano-Sahelian Zone. Proceedings Niamey Workshop*, no. 199 in IAHS Publ. IAHS.

Skinner, B. J. and Porter, S. C. (1992) *The Dynamic Earth: an Introduction to Physical Geology*. John Wiley & Sons, 2nd edn.

Smith, L. C. (1997) Satellite remote sensing of river inundation area, stage, and discharge: A review. *Hydrol. Proc.*, **11**, 1427–1439.

Smith, R. E., Corridini, C. and Melone, F. (1993) Modeling infiltration for multistorm runoff events. *Wat. Resour. Res.*, **29**, 133–144.

Smith, R. E., Goodrich, D. R., Woolhiser, D. A. and Simanton, J. R. (1994) Comment on "pysically based hydrologic modelingg, 2, is the concept realistic?"by R. B. Grayson et al. *Wat. Resour. Res.*, **30**, 851–854.

Some, L. and Sivakumar, M. (1994) *Analyse de la Longeur de la Saison Culturale En Fonction de la Date de Début Des Pluies Au Burkina Faso*. Compte Rendu Des Travaux No1. Division Du Sol et Agroclimatologie. Ouagadougou/Niamey: INERA/ICRISAT.

Sorooshian, S. (1991) Parameter estimation, model identification and model validation: conceptual-type models. In *Recent Advances in the Modeling of Hydrological Syststems* (eds. D. S. Bowles and P. E. O'Connell), chap. 20. Dordrecht, the Netherlands: Kluwer.

Sorooshian, S., Duan, Q. and Gupta, V. (1993) Calibration of rainfall-runoff models: application of global optimization to the sacramento soil moisture accounting model. *Wat. Resour. Res.*, **29**, 1185–1194.

Sorooshian, S. and Gupta, V. (1985) The analysis of structural identifiability: Theory and application to conceptual rainfall-runoff models. *Wat. Resour. Res.*, **21**, 487–495.

van der Steeg, R. (1999) *Factors that Determine the Presence of Enterolobium Cyclocarpum at Estacion Experimental Forestal Horizontes*. Master's thesis, Wageningen Agricultural University.

Stol, W., Rouse, D. I., van Kraalingen, D. W. G. and Klepper, O. (1992) FSEOPT, a FORTRAN program for calibration and uncertainty analysis of simulation models. *CABO-TT 24*, CABO-DLO, Wageningen, the Netherlands.

Stone, J., Renard, K. and Lane, L. J. (1996) Runoff estimation on agricultural fields. In *Soil erosion, conservation and rehabilitation* (ed. M. Agassi), 203–238. New York: Marcel Dekker.

Stroosnijder, L. and Hoogmoed, W. (1984) Crust formation on sandy soils in the sahel. II. tillage and its effect on the water balance. *Soil & Tillage research*, **4**, 321–337.

Tarantola, A. (1987) *Inverse Problem Theory: Methods for Data Fitting and Model Parameter Estimation.* Amsterdam: Elsevier.

Tarboton, D. G. (1997) A new method for the detemination of flow directions and upslope areas in grid digital elevation models. *Wat. Resour. Res.*, **33**, 309–319.

Tarboton, D. G., Bras, R. L. and Rodriguez-Iturbe, I. (1991) On the extraction of channel networks from digital elevation data. *Hydrol. Proc.*, **5**, 81–100.

Troch, P. A., Smith, J. A., Wood, E. F. and de Troch, F. P. (1994) Hydrologic controls of large floods in a small basin: central Appalachian case study. *J. Hydrol.*, **156**.

Vazquez Morear, A. (1991) Suelos. In *Historia natural de Costa Rica* (ed. D. H. Janzen), 47–61. San José, Costa Rica: Universidad de Costa Rica.

Verkleij, J. S. A. (1998) *Integration of Varied Data Sets: an (Im)possible Challange? Case Study of the Watershed Kaibo V5 in Burkina Faso*. Master's thesis, Wageningen Agricultural University.

Wahba, G. (1977) Practical approximate solutions to linear operator equations when the data are noisy. *SIAM J. Numer. Anal.*, **14**, 651–667.

Walker, J. and Willgoose, G. (1999) On the effect of digital elevation model accuracy on hydrology and geomorphology. *Wat. Resour. Res.*, **35**, 2259–2268.

Western, A. W., Blöschl, G. and Grayson, R. B. (1998) Geostatistical characterisation of soil moisture patterns in the Tarrawarra catchment. *J. Hydrol.*, **205**, 20–37.

Western, A. W., Grayson, R. B., Blöschl, G., Willgoose, G. R. and McMahon, T. A. (1999) Observed spatial organization of soil moisture and its relation to terrain indices. *Wat. Resour. Res.*, **35**, 797–810.

Winters, A. F. (1995) *Soil Mapping on the Pleistocene Ignimbritic Bagaces Formation, Guanacaste, Costa Rica: the Construction of a Soil Map, Scaling 1:50.000, in the Estacion Experimental de Reforestation Horizontes, a Sector of Parque Nacional Santa Rosa*. Master's thesis, Wageningen Agricultural University.

Wood, E., Sivapalan, M., Beven, K. and Band, L. (1988) Effects of spatial variability and scale with implications to hydrological modelling. *J. Hydrol.*, **102**, 29–47.

Woolhiser, D., Smith, R. and Giraldez, J.-V. (1996) Effects of spatial variability of saturated hydrolic conductivity on hortonian overland flow. *Wat. Resour. Res.*, **32**, 671–678.

Wu, Y. H., Woolhiser, D. A. and Yevjevic, V. (1982) Effects of spatial variability of hydraulic resistance on runoff hydrographs. *J. Hydrol.*, **59**, 231–248.

Wu, Y. H., Yevjevich, V. and Woolhiser, D. A. (1978) Effects of surface roughness and its spatial distribution on runoff hydrographs. *Hydrology Papers 96*, Colorado State University, Fort Collins, Colorado.

Wubda, M. (1998) *Edtude Pysique Du Micro Bassin Versant de V5 Kaïbo-Sud Province Du Zoundweogo*. Master's thesis, Univeristé de Ouagadougou, Faculté des Lettres, Langues, des Arts des Sciences Humaines et Sociales, Département de Géographie.

Wunsch, C. and Minster, J. F. (1982) Methods for box models and ocean circulation tracers: Mathematical programming and non-linear inverse theory. *Journal of Geophysical Research*, **87**, 5647–5662.

Yameogo, D. (1988) *Hydrogeologie des Formations Fissurees de la Partie sud du Plateau Mossi Entre le Nazino et le Nakambe (Region de Kombissiri-Manga, Burkina Faso)*. Ph.D. thesis, L'Universite Scientifique , Technologique et Medicale de Grenoble.

Young, P. C. and Beven, K. J. (1994) Data-based mechanistic modelling and the rainfall-flow non-linearity. *Environmetrics*, **5**, 335–363.

Zhang, W. and Montgomery, D. R. (1994) Digital elevation model grid size, landscape representation, and hydrologic simulations. *Wat. Resour. Res.*, **30**, 1019–1028.

Curriculum Vitae

Eliza Emiel van Loon, 18 Maart 1971, Ammerzoden

juni 1989
: VWO diploma, Stedelijk Gymnasium ’s Hertogenbosch

november 1993
: ingenieurs-diploma tropisch landgebruik, Landbouwuniversiteit Wageningen
afstudeervakken: Theoretische Productie Ecologie, Wiskunde en Grondbewerking

januari 1994 - juli 1994
: toegevoegd onderzoeker tropische cultuurtechniek

augustus 1994 - juli 1995
: vervulling dienstplicht, medewerker bij ISRIC (International Soil Reference and Information Centre) in Wageningen

augustus 1995 - april 2000
: assistent in opleiding, leerstoelgroep Erosie en Bodem & Waterconservering

mei 2000 -
: onderzoeker, leerstoelgroep Hydrologie en Kwantitatief Waterbeheer